Pontifícia Universidade Católica
do Rio de Janeiro

Mateus Bastos Neiva

3D Numerical Elastoplastic Analysis of Stress and Strain Distributions Around Crack Tips

Dissertação de Mestrado

Dissertation presented to the Programa de Pós–graduação em Engenharia Mecânica, do Departamento de Engenharia Mecânica da PUC-Rio in partial fulfillment of the requirements for the degree of Mestre em Engenharia Mecânica.

Advisor : Prof. Ivan Fabio Mota de Menezes
Co-advisor: Prof. Carlos Alberto de Almeida

Rio de Janeiro
May 2021

Pontifícia Universidade Católica
do Rio de Janeiro

Mateus Bastos Neiva

3D Numerical Elastoplastic Analysis of Stress and Strain Distributions Around Crack Tips

Dissertation presented to the Programa de Pós–graduação em Engenharia Mecânica da PUC-Rio in partial fulfillment of the requirements for the degree of Mestre em Engenharia Mecânica. Approved by the Examination Committee:

Prof. Ivan Fabio Mota de Menezes
Advisor
Departamento de Engenharia Mecânica – PUC-Rio

Prof. Carlos Alberto de Almeida
Co-advisor
Pesquisador Autônomo

Prof. Jaime Tupiassú Pinho de Castro
Departamento de Engenharia Mecânica – PUC-Rio

Prof. Marco Antonio Meggiolaro
Departamento de Engenharia Mecânica – PUC-Rio

Rio de Janeiro, May the 5th, 2021

Mateus Bastos Neiva

Earned B.Sc. in Mechanical Engineering at PUC-Rio in 2018 with minor degree in Mathematics in the same year. Enrolled on the Master Program in Mechanical Engineering at Pontifícia Universidade Católica do Rio de Janeiro, in the area of Solid Mechanics, under scholarship from the CNPq.

Bibliographic data

Neiva, Mateus B.

3D Numerical Elastoplastic Analysis of Stress and Strain Distributions Around Crack Tips / Mateus Bastos Neiva; advisor: Ivan Fabio Mota de Menezes; co-advisor: Carlos Alberto de Almeida. – 2021.

194 f: il. color. ; 30 cm

Dissertação (mestrado) - Pontifícia Universidade Católica do Rio de Janeiro, Departamento de Engenharia Mecânica, 2021.

Inclui bibliografia

1. Mechanical Engineering – Teses. 2. Elementos Finitos. 3. Plasticidade. 4. Mecânica da Fratura. 5. Propagação de trinca por fadiga. I. Menezes, Ivan F. M.. II. Almeida, Carlos A.. III. Pontifícia Universidade Católica do Rio de Janeiro. Departamento de Engenharia Mecânica. IV. Título.

CDD: 620.1

Acknowledgments

Education is not just a matter of capability, but opportunity as well. To my parents, Cláudia Maria Pereira Bastos Neiva and José Antonio Lisbôa Neiva, for providing the best possible education to me; for being a reference to me in love, dedication, intelligence and work.

To my brother and biggest friend, Gustavo Bastos Neiva, for supporting me during all difficult times, for being so attentive and for showing the beauty and the positivity of life.

To my lovely late grandmother Solange Pereira Bastos, an incredible teacher that inspired me to pursue an engineering career, and has taught me the valuable lessons of life as love, knowledge, and courage.

To Colégio de São Bento, a middle-high school, a reference in outstanding education in Brazil, for preparing me for my professional career, with a special thanks to my math teacher Anna Catherina di Gioia Colosimo.

To my professor, Carlos Alberto de Almeida that, even already retired, actively co-advised me on this thesis. His dedication was over any of my expectations; always being available to contribute giving me an incredible opportunity to learn from his high expertise the Mechanical Engineering.

To my professor, Ivan Fabio Mota de Menezes for advising me in this work and providing me with very relevant numerical tools for my work.

To Professor Jaime Tupiassú Pinho de Castro for contributing to such a very interesting topic, the theme of my research.

To my long time friends Henrique Reis Santiago, João Pedro Bezerra da Cunha, Lucas do Nascimento Sagrilo, Murilo Oliveira, Gabriela Wegmann Lima and Thiago Bastos, colleagues in this Master 's program, for the friendship.

To the members of TecGraf Institute, for providing an opportunity to learn and work with such advanced and sophisticated software framework. A special thanks to Leonardo Seperuelo Duarte and to Prof. Waldemar Celes Filho.

To Conselho Nacional de Desenvolvimento Científico e Tecnológico (CNPQ) and PUC-Rio for the scholarships provided.

This study was financed in part by the Coordenação de Aperfeiçoamento de Pessoal de Nível Superior - Brasil (CAPES) - Finance Code 001.

Abstract

Neiva, Mateus B.; Menezes, Ivan F. M. (Advisor); Almeida, Carlos A. (Co-Advisor). **3D Numerical Elastoplastic Analysis of Stress and Strain Distributions Around Crack Tips**. Rio de Janeiro, 2021. 194p. Dissertação de Mestrado – Departamento de Engenharia Mecânica, Pontifícia Universidade Católica do Rio de Janeiro.

In structure life prediction analysis the occurrence of crack defects are of paramount importance to be considered. Basic studies using Linear Elastic Fracture Mechanics approach shows that the Stress Intensity Factor (SIF) parameter controls Fatigue crack growth (FCG). However, overloads may induce material "memory effects" that delay, arrest or accelerate the FCG rate, a behavior that is not described by considering a single elastic parameter. To account for service variable amplitude loadings, the use of a prescribed stress-strain distribution has been proposed in recent research studies, as the driving force of FCG, using the critical damage approach. Due to the assumptions considered in the analytical derivations, important equilibrium and compatibility conditions are violated in the obtained solutions, since an idealized singular stress-strain field at the crack front region is used. In this work a comprehensive review of the recently published analytical results for solutions under the elastic and elastoplastic material behavior regimens are presented: Williams and HRR with singular stress distribution field and Creager-Paris with a non singular stress field, but with the material elastic approach. These solutions are compared, throughout the study, to results obtained from the numerical analysis using a 3D finite element discretization with elastoplastic von Mises yielding criteria employed for the modeling of the crack tip blunt and some comprehensive conclusions are derived regarding application limits of the theoretical models as well as the required extent of the numerical model representation. In addition to monotonic increasing applied loads, unloading conditions were also considered in the numerical analysis, although no reference to this condition is available in the literature, considering the analytical approach. For the numerical simulations presented elastoplastic algorithms were implemented in a plugin based framework.

Keywords

Finite Element Method; Plasticity; Fracture Mechanics; Fatigue Crack Growth.

Resumo

Neiva, Mateus B.; Menezes, Ivan F. M.; Almeida, Carlos A.. **Análise Numérica Elastoplástica 3D da Ditribuição de Tensões e Deformações em Torno de Trincas Passantes**. Rio de Janeiro, 2021. 194p. Dissertação de Mestrado – Departamento de Engenharia Mecânica, Pontifícia Universidade Católica do Rio de Janeiro.

Na análise da predição de vida de estruturas a presença de defeitos por trincas é de fundamental importância. Estudos iniciais utilizando a Mecânica da Fratura Linear Elástica mostram que o Fator de Intensidade de Tensão controla o crescimento de trinca por fadiga. Contudo, sobrecargas podem induzir efeitos de memória no material ao reduzir, parar ou acelerar taxas de propagação, comportamento não previsto considerando-se um único parâmetro elástico. Devido às hipóteses consideradas, as soluções fornecidas pelos métodos analíticos não verificam condições importantes de equilíbrio e compatibilidade, especialmente quando são usados campos singulares idealizados de tensão e de deformação na região da ponta da trinca. Neste trabalho uma extensa revisão dos resultados analíticos recentemente publicados para materiais nos regimes elástico e elastoplástico são apresentadas: Williams e HRR com campo de distribuição singular das tensões e Creager-Paris com campo não-singular das tensões com o material elástico. Neste estudo, estas soluções são comparadas com resultados da análise numérica utilizando a discretização por elementos finitos tridimensionais elastoplásticos com o critério de escoamento do material de von Mises na representação do cegamento da ponta da trinca e importantes conclusões são apresentadas com referência aos limites de aplicação dos modelos teóricos bem como a extensão dos requerimentos para o modelo numérico. Além de carregamentos monotonicamente crescentes, o descarregamento foi também considerado na análise numérica, apesar desta condição não estar presente nas referências consideradas para as soluções analíticas. Para as simulações numéricas consideradas algoritmos de elastoplasticidade foram implementados em um *framework* com arquitetura baseada em *plugins*.

Palavras-chave

Elementos Finitos; Plasticidade; Mecânica da Fratura; Propagação de trinca por fadiga.

Table of contents

List of figures

List of tables

Notation

- All tensors are represented in bold
- $A \rightarrow$ Area
- $a \rightarrow$ Crack size
- $\mathbf{B} \rightarrow$ Deformation matrix
- CTO $\rightarrow$ Consistent Tangent Operator
- $\mathbf{D} \rightarrow$ Constitutive matrix
- $\mathbf{D}^e \rightarrow$ Elastic constitutive matrix
- $\mathbf{D}^{ep} \rightarrow$ Elastoplastic constitutive matrix
- EPFM $\rightarrow$ Elastoplastic fracture mechanics
- $E \rightarrow$ Young's modulus
- $E_P \rightarrow$ Potential energy
- $E_S \rightarrow$ Strain energy
- $E^* \rightarrow$ Complementary energy
- FBD $\rightarrow$ Free-body-diagram
- FCG $\rightarrow$ Fatigue crack growth
- FEM $\rightarrow$ Finite elements method
- $G \rightarrow$ Shear modulus
- $\mathcal{G} \rightarrow$ Griffith's Energy Balance
- $\boldsymbol{I} \rightarrow$ Identity operator
- $\boldsymbol{I}_d \rightarrow$ Deviatoric operator
- $\boldsymbol{I}_S \rightarrow$ Symmetric operator
- $\boldsymbol{I}_T \rightarrow$ Transposition operator
- $J \rightarrow$ J integral
- $J_2 \rightarrow$ Second invariant
- $K \rightarrow$ Bulk's modulus
- $\mathbf{K} \rightarrow$ Stiffness matrix
- $K_t \rightarrow$ Stress concentration factor

- $K_I \rightarrow$ Stress intensity factor in mode I
- $K_{II} \rightarrow$ Stress intensity factor in mode II
- $K_{III} \rightarrow$ Stress intensity factor in mode III
- LEFM $\rightarrow$ Linear elastic fracture mechanics
- $n \rightarrow$ Hardening parameter in Rarberg-Osgood
- $\boldsymbol{n} \rightarrow$ Normal vector
- $p_z \rightarrow$ Plastic zone
- $Q \rightarrow$ Energy dissipation
- $r \rightarrow$ Radius
- $\boldsymbol{R}_B \rightarrow$ Body force
- $\boldsymbol{R}_S \rightarrow$ Surface force
- $\boldsymbol{R}_I \rightarrow$ Concentrated force
- SIF $\rightarrow$ Stress intensity factor
- $\boldsymbol{S} \rightarrow$ Deviatoric stress tensor
- $\boldsymbol{T} \rightarrow$ Stress vector
- $tr \rightarrow$ Trace of a tensor
- $\mathcal{T} \rightarrow$ Toughness $[J/m^2]$
- $U \rightarrow$ Strain energy density
- $\hat{\boldsymbol{u}} \rightarrow$ Nodal displacements
- $V_0 \rightarrow$ Initial volume
- $V_f \rightarrow$ Final volume
- $W \rightarrow$ Work
- $\alpha \rightarrow$ Hardening exponent parameter in Rarberg-Osgood
- $\Delta\gamma \rightarrow$ Plastic multiplier
- $\epsilon^p \rightarrow$ Accumulated plastic strain
- $\epsilon_r \rightarrow$ Radial strain
- $\epsilon_\theta \rightarrow$ Tangential strain
- $\epsilon_{r\theta} \rightarrow$ Shear strain
- $\boldsymbol{\epsilon} \rightarrow$ Strain tensor
- $\boldsymbol{\epsilon}^e \rightarrow$ Elastic strain tensor
- $\boldsymbol{\epsilon}^e_d \rightarrow$ Deviatoric elastic strain tensor
- $\nu \rightarrow$ Poisson's ratio

- $\Pi \rightarrow$ Energy functional
- $\rho \rightarrow$ Curvature radius or Prager's constant
- $\sigma \rightarrow$ Nominal stress
- $\boldsymbol{\sigma} \rightarrow$ Stress tensor
- $\boldsymbol{\sigma}_{\mathrm{v}} \rightarrow$ Volumetric stress tensor
- $\sigma_r \rightarrow$ Radial stress
- $\sigma_\theta \rightarrow$ Tangential stress
- $\sigma_{r\theta} \rightarrow$ Shear stress
- $\sigma_y \rightarrow$ Yield stress
- $\Phi \rightarrow$ Yield function
- $\Psi \rightarrow$ Stress function

1
Introduction

1.1
Motivation

The evaluation of a crack presence is of paramount importance in engineering practice such as the design and life prediction of mechanical components. These tasks are generally achieved by mechanical behavior evaluations using the numerical simulation of crack effects and their growth. For example, in high cycle fatigue crack growth analysis (FCG), the damage extension and integrity of a component are of study considerations, where for material linear elastic behavior stress intensity factor (SIF) is adopted for the prediction of the crack propagation.

Although being an important step in fracture mechanics understanding, the SIF as a single driven force of FCG does not provide all required answers for realistic variable amplitude loadings. For instance, material memory effects can delay, arrest or accelerate a FCG rate after an overload has been reached. Moreover, material local plasticity due to cyclic loading ahead of a crack tip is not well described by a single linear elastic parameter without a somehow adjustment, simply because SIF superposition of solutions is not a possible solution. Some additional methods were then elaborated to predict the appropriate changes in FCG rates.

This work is intended to provide a numerical tool to consider the analysis of crack effects in a mechanical component, including plasticity-induced residual strains in the material behavior. Other phenomena such as oxidation and phase transformations can also affect the FCG rate but are not considered in this study.

One of the first publications to use a simple phenomenological method to estimate the FCG rate in a cracked model was proposed by Willenborg, Engle and Wood in 1971 [14] to treat the overload phenomenon. A similar method was proposed by Wheeler [15]. However, these procedures are too simplistic for not providing accurate mechanical analysis responses.

In 1970 Elber [12, 13] proposed a method to control FCG rate that, instead of using the range of SIF as the driven force, employs the effective

stress intensity factor range (ΔK_{eff}), a parameter dependable on the load that opens the crack (P_{op}).

Later, James Newman proposed, in [7], a FEM formulation for the analysis of 1D structures, using a strip-yield material model to obtain P_{op}, which provides the ΔK_{eff} to perform FCG.

The critical-damage method for FCG prediction provides modeling and numerical representation with stronger physical arguments [8, 9, 10]. It estimates that a volume element breaks whenever the accumulated damage reaches its maximum allowed value. In [11] a model similar to Newman's strip-yield applying 1D elements placed along the plastic zone ahead of the crack tip, as presented in figure 1.1. In this model, every element is represented as a fatigue ϵN specimen, allowing damage calculation for every load event. A mandatory particularity of this model is the use of a non-singular stress field, otherwise the damage would also be singular.

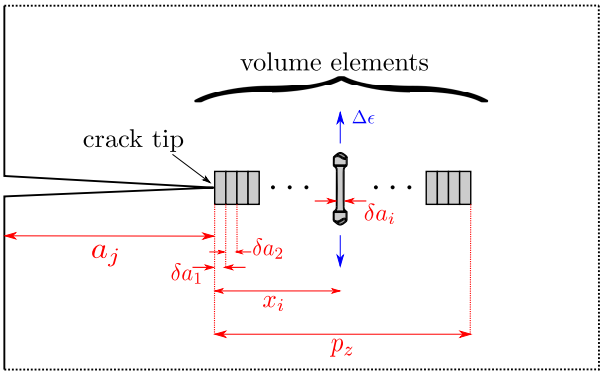

Figure 1.1: Critical-damage representation

1.2 Objectives and main contributions

The purpose of the present dissertation is to obtain appropriate estimates of stresses and strains inside a plastic zone, at the nearby region of a crack tip. To accomplish this a 3D finite element model formulation was developed accounting for stress and strain evaluations with material elastoplastic behavior, especially at the crack tip plastic zone. In the numerical model, mechanical considerations of equilibrium, compatibility and material constitutive conditions are guaranteed to represent the blunt of the crack.

Solutions considering numerical strategies and element model enrichments are discussed and compared to results available in the literature.

As a remark, it should say that this work is not intended to provide a FCG algorithm, but a numerical procedure to evaluate stress and strain distributions under the elastoplastic analysis. However, for FCG simulations

to be considered larger computational efforts would be required to account for its use, for general loadings. In this regard, this dissertation is a step to provide the numerical tools for a possible and more appropriate finite element representation.

This dissertation is organized in seven chapters. In chapter 2 the important aspects of the basics of the Fracture Mechanics Theory are reviewed and discussed. Next, in chapter 3, the elastoplastic formulation with von Mises yielding and aspects of its numerical implementation is presented. The FEM basis needed as a plugin framework for the simulations is considered in chapters 4 and 5, respectively. In chapter 6 details of a numerical simulation are presented and the obtained numerical results are evaluated and discussed. Finally, conclusions and perspectives for future work are treated in chapter 7.

2
Fracture Mechanics Review

Fracture Mechanics is an important area of study in Mechanical Engineering aiming to understand, evaluate, and prevent crack effects in fracture damaged components. Because of major difficulty in making the significant measurements at a cracked region, evaluations of its structural significance in the component integrity have been accomplished by models in two kinds of representations: analytical, in the past, and, at present, numerically. In this chapter the basics of Fracture Mechanics are reviewed and discussed by presenting the features and derivations of earlier analytical models, considering the material linear and elastoplastic behaviors. Analytical solutions are presented for two material conditions: a linear elastic stress field, defining the so-called Linear Elastic Fracture Mechanics (LEFM), and second, the Elastoplastic Fracture Mechanics (EPFM) introduced by considering the material elastoplastic behavior.

2.1
Griffith's Energy Balance

In a pioneering work, Charles Edward Inglis (1875 - 1952)[17] presented a solution for the stress concentration (magnification) factor occurring in elliptical notches (see Appendix A), showing its dependence on the crack's length and radius at the tip as

$$K_t \sim \sqrt{\frac{a}{\rho}} \tag{2-1}$$

Although simple and straightforward to use, this theory fails to explain why a cracked brittle material does not resist positive nominal stress as the tip radius ρ becomes very small, i.e. close to 0 ($K_t \to \infty$). By Inglis derivations, the stress singularity at a crack comes from an idealized crack tip with $\rho = 0$, assumption, employed to simplify the mathematical problem. However, for physical reasons, near to the crack tip, conditions of the singular behavior of stresses or strains, are not sustainable.

In 1920, Griffith [18] proposed, to circumvent stress singularity at the crack tip, a model based on energy conservation which postulates that a crack can only grow if a given work increment δW can deliver enough energy to

increase the crack influence area of a given δA quantity, by a force acting at the crack face which is equal to thickness time crack size increment δa plus an incremental strain energy δE_S stored in the body. Thus, the equation

$$\delta W \geqslant \delta E_S + \mathcal{T} \cdot \delta A \tag{2-2}$$

should hold, $\mathcal{T}$ is the material toughness (J/m^2), the total strain energy is

$$E_S = \int_V U \; dx \; dy \; dz \tag{2-3}$$

with

$$U = \frac{\boldsymbol{\sigma}^V \cdot \boldsymbol{\epsilon}^V}{2} \tag{2-4}$$

written in Voigt notation. For a specimen with a crack and under loading, the stored potential energy (E_P), given by the strain energy (E_S) minus the external work (W), which is released as the crack grows. Thus,

$$E_P = E_S - W \tag{2-5}$$

$$\mathcal{G} = -\frac{\partial E_P}{\partial A} \tag{2-6}$$

The equation in above was defined by Irwin [34] as a crack driving force. Note that this procedure avoids unrestricted energy, as noticed in idealized cracks of $\rho \to 0$ when $K_t \to \infty$, since Griffith's energy is finite by guaranteeing energy conservation.

2.2 Linear Elastic Fracture Mechanics

As previously described, a linear elastic procedure is a basic approach for modeling a fracture problem. In this section, two analytical solutions presented by Williams and Creager-Paris are discussed. Despite every fracture being under an elastoplastic behavior, a LEFM, under some conditions, predicts FCG. This non-intuitive aspect is presented in the following sections as well as the limitations of using a LEFM.

2.2.1 Williams' Solution

In another proposal, Williams'1957 presented a solution for the crack stress distribution problem imposing the crack geometry as described below, having zero radii.

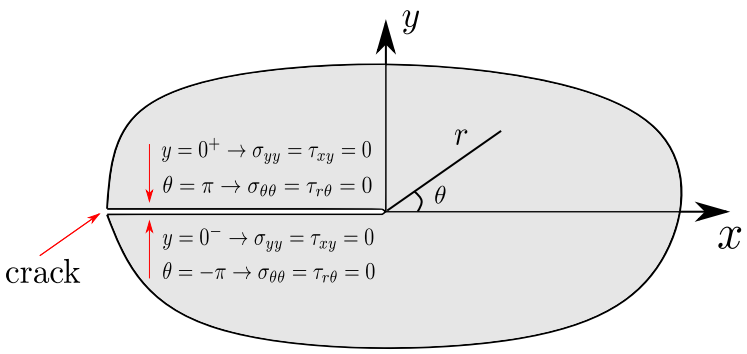

Figure 2.1: Crack coordinates

Using basic stress functions from Theory of Elasticity, associated to a plane stress state, equilibrium, compatibility, and boundary conditions imposed for three different loading conditions what resulted in

$$\begin{bmatrix}\sigma_{xx}\\ \sigma_{yy}\\ \sigma_{xy}\end{bmatrix} = \frac{K_I}{\sqrt{2\pi r}}\cos\left(\frac{\theta}{2}\right)\begin{bmatrix}1-\sin\left(\frac{\theta}{2}\right)\cdot\sin\left(\frac{3\theta}{2}\right)\\ 1+\sin\left(\frac{\theta}{2}\right)\cdot\sin\left(\frac{3\theta}{2}\right)\\ \sin\left(\frac{\theta}{2}\right)\cdot\cos\left(\frac{3\theta}{2}\right)\end{bmatrix} \tag{2-7}$$

$$\begin{bmatrix}\sigma_{xx}\\ \sigma_{yy}\\ \sigma_{xy}\end{bmatrix} = \frac{K_{II}}{\sqrt{2\pi r}}\begin{bmatrix}-\sin\left(\frac{\theta}{2}\right)\left[2+\cos\left(\frac{\theta}{2}\right)\cdot\cos\left(\frac{3\theta}{2}\right)\right]\\ \sin\left(\frac{\theta}{2}\right)\cdot\cos\left(\frac{\theta}{2}\right)\cdot\cos\left(\frac{3\theta}{2}\right)\\ \cos\left(\frac{\theta}{2}\right)\left[1-\sin\left(\frac{\theta}{2}\right)\cdot\sin\left(\frac{3\theta}{2}\right)\right]\end{bmatrix} \tag{2-8}$$

$$\begin{bmatrix}\sigma_{xz}\\ \sigma_{yz}\end{bmatrix} = \frac{K_{III}}{\sqrt{2\pi r}}\begin{bmatrix}-\sin\left(\frac{\theta}{2}\right)\\ \cos\left(\frac{\theta}{2}\right)\end{bmatrix} \tag{2-9}$$

where eqs. (2-7), (2-8) and (2-9) are known as as the stress intensity factor (SIF) for modes I, II and III :

Further information on these equations' analytical derivations is reported in Appendix B, where a complete derivation for K_I is presented.

From a mathematical point of view, SIF is a constant on the stress function solution obtained by Williams, which must hold for a full elastic problem, any crack geometry, and loading. This was certified in an alternative proof also given by Irwin [33], where the stress intensity (SIF) factor comes naturally, obtained for the case of an infinite plate under in-plane biaxial loading, with a centered crack, as compared to nominal Williams solution given in eq. (2-7). Irwin's solution derivations are presented in Appendix C.

It is important to remark that Williams' stress field presumes a linearisation only valid for small values of x. This aspect is clearly observed from Irwin's solution (Appendix C) when the equation below is simplified as following

$$\sigma_{yy} = \frac{\sigma_n(x+a)}{\sqrt{(x+a)^2 - a^2}} \approx \frac{\sigma_n a}{\sqrt{2ax}} = \frac{K_I}{\sqrt{2\pi x}} \tag{2-10}$$

As a consequence, the K_I-induced LE stresses are exact only at a region very close to the crack tip, without verifying boundary and equilibrium conditions.

2.2.1.1 Creager Paris

In a different move, Creager and Paris in [20] and [21] proposed an analytical solution motivated by the study of corrosion on elongated notches, considering the crack as in an elliptical shape. This problem falls into Williams' stress field solution in the case of crack surface radius ρ at the tip goes to 0, being also dependent on an intensity factor. To avoid singularity in the obtained stress distributions at the crack tip, the considered reference coordinate system r and θ was moved to a position inside the notch, as shown in fig. 2.2.

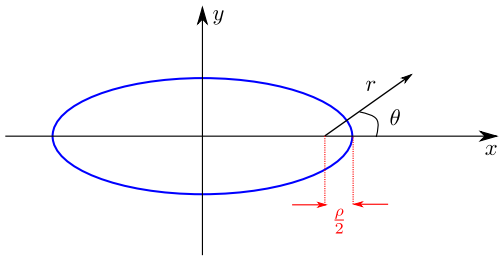

Figure 2.2: Coordinate system used in Creager-Paris model for stress field.

Based on a proposed stress function that satisfies equilibrium, compatibility, and boundary conditions the authors presented an analytical solution for the stress field around the tip as a function of SIF and the tip radius $\frac{\rho}{2}$ as

$$\begin{bmatrix}\sigma_{xx}\\ \sigma_{yy}\\ \sigma_{xy}\end{bmatrix} = \frac{K_I}{\sqrt{2\pi r}}\cos\left(\frac{\theta}{2}\right)\begin{bmatrix}1-\sin\left(\frac{\theta}{2}\right)\cdot\sin\left(\frac{3\theta}{2}\right)\\ 1+\sin\left(\frac{\theta}{2}\right)\cdot\sin\left(\frac{3\theta}{2}\right)\\ \sin\left(\frac{\theta}{2}\right)\cdot\cos\left(\frac{3\theta}{2}\right)\end{bmatrix} + \frac{K_I}{\sqrt{2\pi r}}\frac{\rho}{2r}\begin{bmatrix}-\cos\frac{3\theta}{2}\\ +\cos\frac{3\theta}{2}\\ -\sin\frac{3\theta}{2}\end{bmatrix} \quad (2\text{-}11)$$

$$\begin{bmatrix}\sigma_{xx}\\ \sigma_{yy}\\ \sigma_{xy}\end{bmatrix} = \frac{K_{II}}{\sqrt{2\pi r}}\begin{bmatrix}-\sin\left(\frac{\theta}{2}\right)\left[2+\cos\left(\frac{\theta}{2}\right)\cdot\cos\left(\frac{3\theta}{2}\right)\right]\\ \sin\left(\frac{\theta}{2}\right)\cdot\cos\left(\frac{\theta}{2}\right)\cdot\cos\left(\frac{3\theta}{2}\right)\\ \cos\left(\frac{\theta}{2}\right)\left[1-\sin\left(\frac{\theta}{2}\right)\cdot\sin\left(\frac{3\theta}{2}\right)\right]\end{bmatrix} + \frac{K_{II}}{\sqrt{2\pi r}}\frac{\rho}{2r}\begin{bmatrix}+\sin\frac{3\theta}{2}\\ -\sin\frac{3\theta}{2}\\ -\cos\frac{3\theta}{2}\end{bmatrix} \quad (2\text{-}12)$$

$$\begin{bmatrix}\sigma_{xz}\\ \sigma_{yz}\end{bmatrix} = \frac{K_{III}}{\sqrt{2\pi r}}\begin{bmatrix}-\sin\left(\frac{\theta}{2}\right)\\ \cos\left(\frac{\theta}{2}\right)\end{bmatrix} \quad (2\text{-}13)$$

As observed from eqs. (2-11) to (2-13) the analytically obtained solution for an elliptical shape reduces to Williams' stress distributions presented in eqs. (2-7) to (2-9) as tip radius ρ goes to zero and, conversely, the coordinate system moves to the crack tip as expected in William's solution. Figure 2.3 below illustrates both Williams' and Creager and Paris' coordinate systems used. In Appendix D the derivations related to the results obtained in Creager and Paris' model are presented.

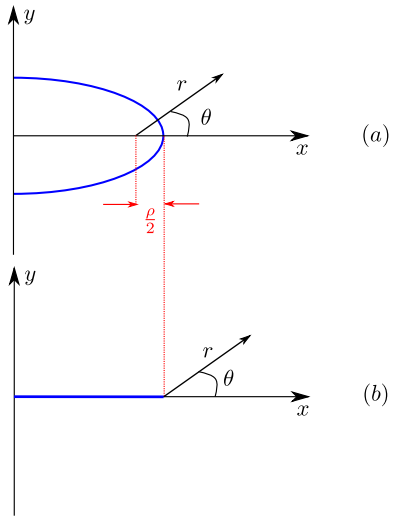

Figure 2.3: a) Creager and Paris' e b) Williams' Coordinate systems used for stress field definitions

2.2.1.2 Stress intensity factor as driving force for fatigue crack growth

As shown in the previous section, the stress intensity factor (SIF) was presented as a single parameter to characterize the stress field in the region ahead of a crack tip. However, in the literature, SIF is commonly defined as an expression to achieve the driven forces of fatigue crack growth (FCG), ΔK and $K_{\max}$, without supporting why they are related, where ΔK is computed, for an increment load, by the variation of SIF and $K_{\max}$ the maximum value of SIF in this interval.

According to [5], Paris, Gomez, and Anderson on [23] stated that the range of stress intensity factors would control the fatigue crack growth (FCG). However, the work was rejected by important scientific journals arguing that a linear elastic parameter could not control a phenomenon caused by cyclic plasticity in brittle failures. Later on, in a more elaborated work, Paris and Erdogan on [24], demonstrated with experimental results that the range of stress intensity factor controls FCG. In reality, FCG is also dependable on $K_{\max}$.

$$\frac{da}{dN} = f(\Delta K) \tag{2-14}$$

Although, the propagation rule, as in eq. (2-14), is a function of the range SIF, because it controls the stress field ahead of a crack tip, Paris and Erdogan did not explain why this linear elastic parameter, a constant on the series of the stress function, could predict a crack growth.

Yielding condition, with von Mises equation, may predict with reasonable accuracy metallic materials as

$$\sigma_{\text{Mises}} = \sqrt{\frac{(\sigma_{xx} - \sigma_{yy})^2 + (\sigma_{yy} - \sigma_{zz})^2 + (\sigma_{zz} - \sigma_{xx})^2 + 6(\sigma_{xy}^2 + \sigma_{xz}^2 + \sigma_{yz}^2)}{2}} \tag{2-15}$$

definition of the stress field, in eq. (2-7), can be expressed in the following generalized form

$$\begin{bmatrix} \sigma_{xx} \\ \sigma_{yy} \\ \sigma_{xy} \end{bmatrix} = \frac{K_I}{\sqrt{2\pi r}} \begin{bmatrix} f_{xx}(\theta) \\ f_{yy}(\theta) \\ f_{xy}(\theta) \end{bmatrix} \tag{2-16}$$

which brought into eq. (2-15) results in

$$\sigma_{\text{Mises}} = \frac{K_I}{\sqrt{2\pi r}} \sqrt{f_{xx}^2(\theta) + f_{yy}^2(\theta) - f_{xx}(\theta) \cdot f_{yy}(\theta) + 3f_{xy}^2(\theta)} \tag{2-17}$$

This equation shows the yield stress in the polar coordinates r and θ by a given K_I, which is the constant that covers the geometric and load contribution to the problem. From this equation, the boundary of the plastic zone (p_z) can be estimated with a simple numerical solver, by fixing a θ parameter to obtain the corresponding r coordinate. Indirectly, SIF also predicts the size of the region with the highest damage in the structure. And, accumulated damage inside the plastic zone is used as an estimation for the FCG which is the basis for the critical-damage method.

Thus, the procedure presented explains why the SIF furnishes a prediction for FCG. However, in an additional consideration, the elastic parameter K_I can control the size of the p_z if the majority of the specimens are under the elastic regimen.

The Linear Elastic Fracture Mechanics is applicable if p_z is small in comparison to the rest of the domain.

2.3 Elastoplastic Fracture Mechanics

In the previous section, it was shown that the SIF parameter, obtained within LEFM, controls FCG whenever the p_z coordinate is sufficiently small when compared to the cracked component dimensions. In what follows, the elastoplastic fracture mechanics (EPFM) procedure presented allows for treatment of stresses and strains occurring ahead of the crack tip and provides a robust tool for the analysis of elastoplasticity in fracture mechanics, under small displacements conditions.

2.3.1 Theory Preliminaries - the J-integral

First presented independently in 1967 by Cherepanov [25] and in 1968 by Rice [26], the J-integral consists of a procedure to evaluate area density of the Potential Energy stored around a crack tip formation in a fractured component under monotonic loading.

Thus, from energy density around a crack, the balance may be stated as $E_p = W - U$, where the external work is given by the integral of the traction vector times the displacement over the boundary

$$W = \oint_S T_i \; u_i \; ds \; t \tag{2-18}$$

with

$$T_i = \sigma_{ij} n_j \tag{2-19}$$

where u_i and T_i are ith-components fo the displacement vector $\boldsymbol{u}$ and traction vector $\boldsymbol{T}$ and n_j the j-th component of $\boldsymbol{n}$ unit vector normal to the boundary (see fig. 2.5).

And U is the strain energy density stored in a ds segment, expressed as

$$U = \int \sigma^V \cdot d\epsilon^V = \int \sigma_{xx} \; d\epsilon_{xx} + \sigma_{yy} \; d\epsilon_{yy} + \tau_{xy} \; d\gamma_{xy} \tag{2-20}$$

In the definition employed, the contour integral J for a x-y plane may be written as

$$J = \oint_S \left[U \; dy - T_i \frac{\partial u_i}{\partial x} \; ds \right] \tag{2-21}$$

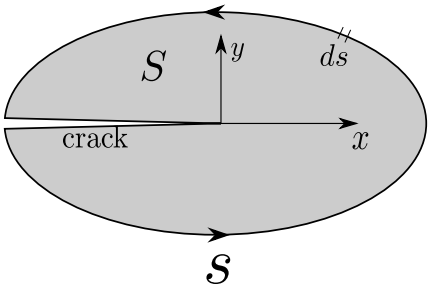

Figure 2.4: J-integral coordinates

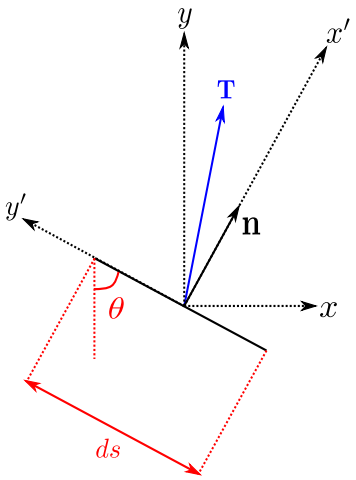

Figure 2.5: Coordinates transformation

where the stress tensor and the normal and displacement vectors should be reduced to the cartesian x-y coordinate system. The traction vector referred to xy coordinates gives

$$\mathbf{T}^{xy} = \begin{bmatrix} T_1^{xy} \\ T_2^{xy} \end{bmatrix} = \begin{bmatrix} \sigma_{xx} & \sigma_{xy} \\ \sigma_{xy} & \sigma_{yy} \end{bmatrix} \cdot \begin{bmatrix} \cos\theta \\ \sin\theta \end{bmatrix} = \begin{bmatrix} \sigma_{xx}\cos\theta + \sigma_{xy}\sin\theta \\ \sigma_{xy}\cos\theta + \sigma_{yy}\sin\theta \end{bmatrix} \tag{2-22}$$

In the case of considering the coordinate system $x'y'$, as presented in fig. 2.5, the displacement vector written in both coordinate systems are

$$\begin{aligned} \boldsymbol{u}^{xy} = \begin{bmatrix} u_1^{xy} \\ u_2^{xy} \end{bmatrix} &= R_z(\theta) \cdot \boldsymbol{u}^{x'y'} \\ &= \begin{bmatrix} \cos\theta & -\sin\theta \\ \sin\theta & \cos\theta \end{bmatrix} \cdot \begin{bmatrix} u_1^{x'y'} \\ u_2^{x'y'} \end{bmatrix} \\ &= \begin{bmatrix} u_1^{x'y'}\cos\theta - u_2^{x'y'}\sin\theta \\ u_1^{x'y'}\sin\theta + u_2^{x'y'}\cos\theta \end{bmatrix} \end{aligned} \tag{2-23}$$

and the same with the traction vector we have,

$$\begin{aligned} \boldsymbol{T}^{x'y'} &= \boldsymbol{\sigma}^{x'y'} \cdot \boldsymbol{n} \\ &= \begin{bmatrix} \sigma_{x'x'} & \sigma_{x'y'} \\ \sigma_{x'y'} & \sigma_{y'y'} \end{bmatrix} \cdot \begin{bmatrix} 1 \\ 0 \end{bmatrix} = \begin{bmatrix} \sigma_{x'x'} \\ \sigma_{x'y'} \end{bmatrix} \end{aligned} \tag{2-24}$$

and

$$\begin{aligned}\boldsymbol{T}^{xy} = \begin{bmatrix} T_1^{xy} \\ T_2^{xy} \end{bmatrix} &= R_z(\theta) \cdot \boldsymbol{T}^{x'y'} \\ &= \begin{bmatrix} \cos\theta & -\sin\theta \\ \sin\theta & \cos\theta \end{bmatrix} \cdot \begin{bmatrix} \sigma_{x'x'} \\ \sigma_{x'y'} \end{bmatrix} \\ &= \begin{bmatrix} \sigma_{x'x'}\cos\theta - \sigma_{x'y'}\sin\theta \\ \sigma_{x'x'}\sin\theta + \sigma_{x'y'}\cos\theta \end{bmatrix}\end{aligned} \tag{2-25}$$

Thus, the J-integral, in both cartesian and polar coordinates is obtained by

$$J = \oint_S \left[U\ dy - \left(T_1^{xy}\ \frac{\partial u_x}{\partial x} + T_2^{xy}\ \frac{\partial u_y}{\partial x} \right) ds \right] \tag{2-26}$$

The use of a polar coordinate system is quite convenient when deriving analytical equations for the HRR field.

2.3.1.1 J-integral properties

J-integrals possess the following three important mathematical [5] properties:

- $J = 0$ only if S is continuous, i.e., the close path does not contain a crack inside.
- Otherwise S includes crack traction free faces and J-integral is path-independent.
- $J = -\frac{\partial E_p}{\partial A} = -\frac{\partial (W - E_D)}{\partial a}$ is the potential energy release rate, so a parameter to represent elastoplastic crack problem, as well as $\mathcal{G}$ is used in LEFM.

The proof of those properties is presented in Appendix E.

2.3.2 The HRR Model

The acronym HRR stands for Hutchinson [27] and Rice and Rosengren [29], who independently developed a model for the stress distribution near to the tip of a crack in an elastoplastic material, with monotonic small strain $\sigma - \epsilon$ hardening.

From Hutchinson's results, which was derived from applying compatibility and equilibrium conditions, a stress function was numerically determined, under the following hypotheses:

- stress and strain singularities at the crack are present;
- small-scale yielding occurs, neglecting elastic behavior near the crack tip;
- non-incremental flow rule condition holds;
- usage as valid, the stress function and compatibility equations are derived for elastic material behavior;

In what follows stress and strain distribution results at the crack front region, with respect to angular coordinates r and θ centered at the crack tip, obtained in [27], are presented, the important parameters are discussed and, finally, the necessary derivations justified. Thus, Hutchinson's equations are as follows,

$$\sigma_{ij} = \sigma_0 \left(\frac{EJ}{\alpha \sigma_0^2 I_n r} \right)^{1/(n+1)} \tilde{\sigma}_{ij}(n, \theta) \tag{2-27}$$

$$\epsilon_{ij} = \frac{\alpha \sigma_0}{E} \left(\frac{EJ}{\alpha \sigma_0^2 I_n r} \right)^{n/(n+1)} \tilde{\epsilon}_{ij}(n, \theta) \tag{2-28}$$

where α and n are two parameters from a simplified form of the Ramberg-Osgood hardening constitutive rule [28]

$$\frac{\epsilon}{\epsilon_0} = \alpha \left(\frac{\sigma}{\sigma_0} \right)^n \tag{2-29}$$

using $\sigma_0 = E \cdot \epsilon_0 = \sigma_y$.

Moreover in eqs. (2-27) and (2-28) the integration constant I_n, which is a function of the type of plane stress state and of the hardening exponent n considered, is as shown in fig. 2.6. A second set of parameters, $\tilde{\sigma}_{ij}$ and $\tilde{\epsilon}_{ij}$, expresses the contribution of the angle θ.

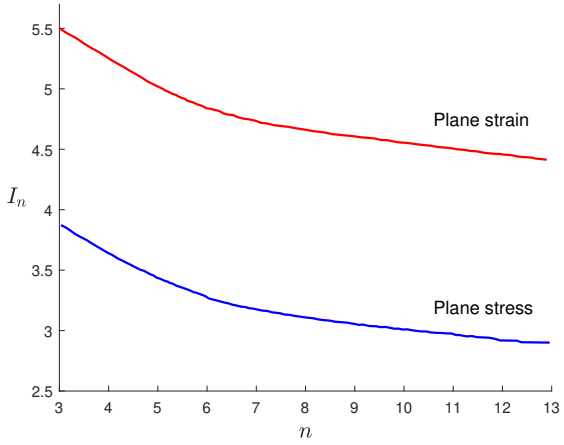

Figure 2.6: The integration constant I_n

Figures 2.7 and 2.8 show distributions for $\tilde{\sigma}_{ij}$ and $\tilde{\epsilon}_{ij}$ parameters, which are function of the angular position theta, for two discrete values of n : $n = 3$ and $n = 13$, respectively.

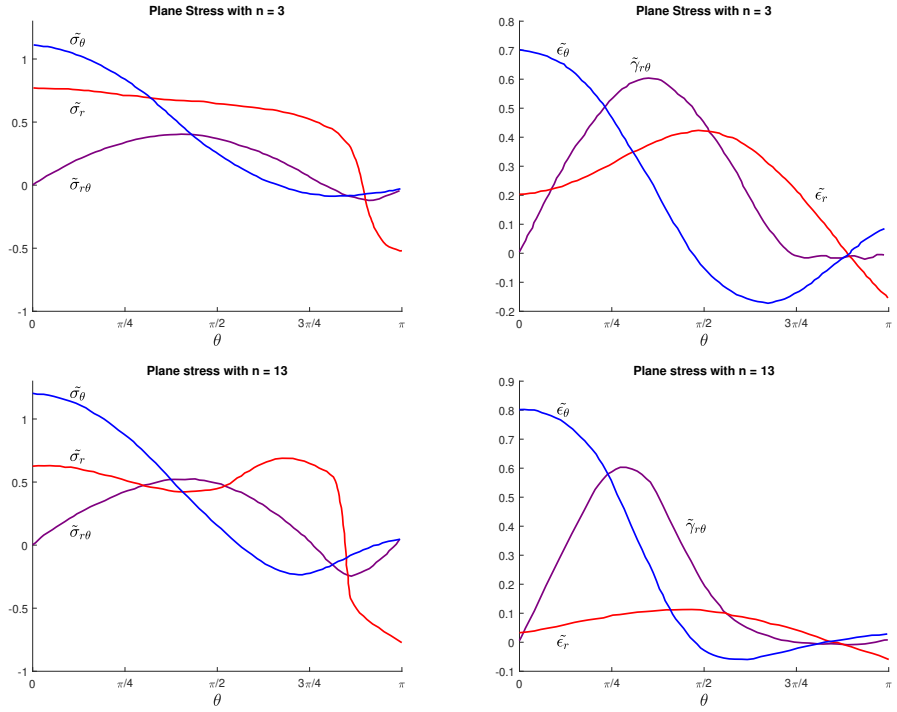

Figure 2.7: Plane stress constants for $n = 3$ and $n = 13$

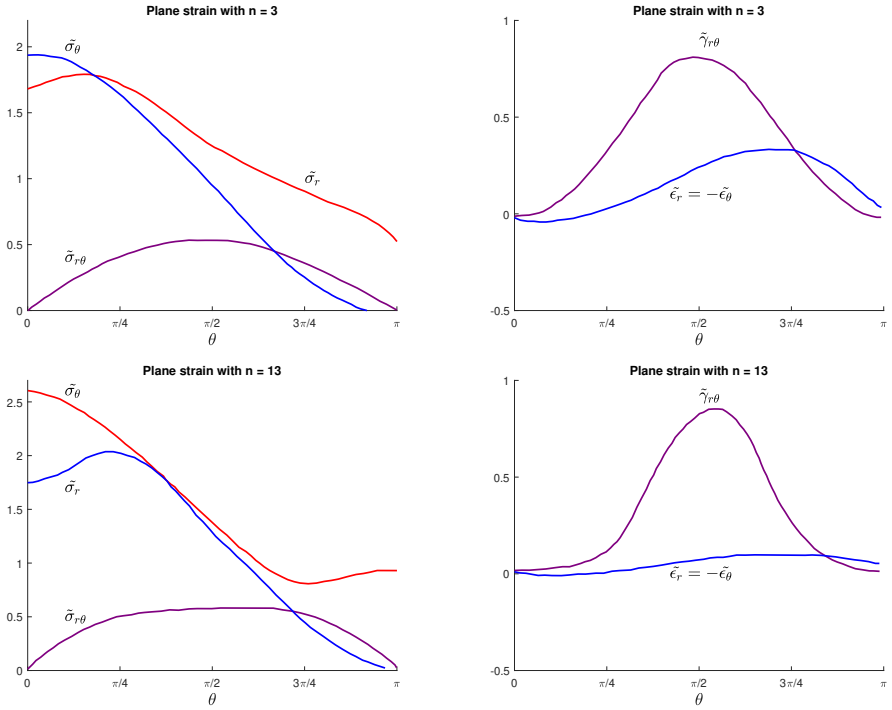

Figure 2.8: Plane strain constants for $n = 3$ and $n = 13$

In addition, the size and shape of plastic zones in plane strain for mode I loading are illustrated in Hutchinson's work as shown in fig. 2.9 below.

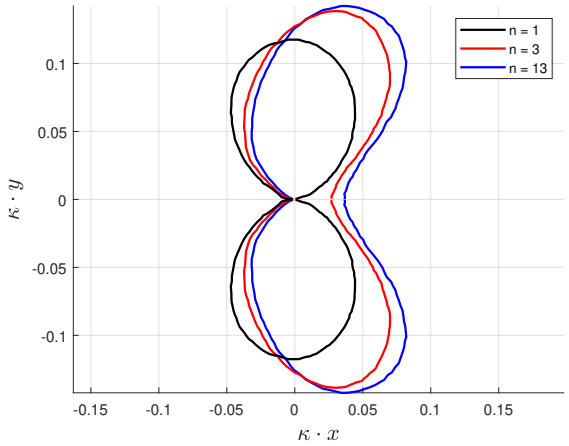

Figure 2.9: p_z for mode I in plane strain

where

$$\kappa := \left(\frac{\sigma_y}{K_I}\right)^2 \tag{2-30}$$

2.3.2.1 Proof for plane stress

As stated previously, Ramberg and Osgood's (1943) hardening condition is employed, which is a scalar condition. Since the problem to be considered is in a 3D state of stresses, the J2-plasticity must be applied in this derivation. Thus the von Mises yield function should be applied, defined as

$$\sigma_e^2 = 3\ J_2 = \frac{3}{2} S_{ij} S_{ij} \tag{2-31}$$

where S_{ij} are components of the deviatoric stress tensor

$$S_{ij} = \sigma_{ij} - \frac{1}{3}\sigma_{kk}\delta_{ij} \tag{2-32}$$

Considering the strain-stress relation in the elastic range

$$\epsilon_{ij}^{el} = \frac{1+\nu}{E}\sigma_{ij} - \frac{\nu}{E}\sigma_{kk}\delta_{ij} \tag{2-33}$$

which results, after substituting the result in eq. (2-32),

$$\epsilon_{ij}^{el} \cdot E = (1+\nu) S_{ij} + \frac{1-2\nu}{3}\sigma_{kk}\delta_{ij} \tag{2-34}$$

From eq. (2-34), rearranging to the definition $\epsilon_0 = \sigma_0/E$ and omitting ϵ_0 and σ_0 from the denominator, one may obtain

$$\epsilon_{ij}^{el} = (1+\nu) S_{ij} + \frac{1-2\nu}{3}\sigma_{kk}\delta_{ij} \tag{2-35}$$

To compute the plastic strain a flow rule must be applied, as shown in chapter 3, in the following differential form:

$$d\boldsymbol{\epsilon}^p = d\bar{\epsilon}^p \cdot \frac{\partial \Phi}{\partial \boldsymbol{\sigma}} \tag{2-36}$$

where $\boldsymbol{\epsilon}^p$ is the plastic strain tensor, $\bar{\epsilon}^p$ is the 1D cumulated strain and is Φ the yield function, as defined in chapter 3. In this same chapter, results from the derivative of the yield function with respect to the von Mises stress tensor are presented. Thus, eq. (2-36) results as,

$$d\boldsymbol{\epsilon}^p = d\epsilon^p \cdot \sqrt{\frac{3}{2}} \frac{\boldsymbol{S}}{\|\boldsymbol{S}\|} \tag{2-37}$$

Considering the normal tensor S as constant, from eq. (2-37) plastic strain components results as

$$\epsilon_{ij}^p = \bar{\epsilon}^p \cdot \sqrt{\frac{3}{2}} \frac{S_{ij}}{\|\boldsymbol{S}\|} \tag{2-38}$$

where from eq. (2-29), $\bar{\epsilon}^p$ is obtained considering the plastic component of the total strain. Substituting into eq. (2-38) results

$$\epsilon_{ij}^p = \sqrt{\frac{3}{2}} \frac{S_{ij}}{\|\boldsymbol{S}\|} \cdot \alpha\sigma^n \tag{2-39}$$

where σ is the von Mises stress, that is defined in eq. (2-31) and brings eq. (2-39) to

$$\epsilon_{ij}^{p} = \frac{3}{2}\alpha\sigma_{e}^{n-1}S_{ij} \tag{2-40}$$

From strain decomposition, the total strain is, by definition, the sum of the elastic strain, in eq. (2-35), and the plastic strain, defined in eq. (2-40). Thus, the generalized elastoplastic strain-stress tensor relation for modeling monotonic increasing load only, under small strain conditions, is:

$$\epsilon_{ij} = (1+\nu)S_{ij} + \frac{1-2\nu}{3}\ \sigma_{kk}\delta_{ij} + \frac{3}{2}\alpha\ \sigma_{e}^{n-1}S_{ij} \tag{2-41}$$

Thus, an expression for the complementary energy functional (E^{*}) for plane stress and plane strain conditions may be obtained, that results is

$$\begin{aligned} E^{*} &= \int \epsilon_{ij}\ d\sigma_{ij} \\ &= \int_{A}\left(\frac{(1+\nu)}{3}\ \sigma_{e}^{2} + \frac{1-2\nu}{6}\ \sigma_{kk}^{2} + \frac{\alpha}{n+1}\ \sigma_{e}^{n+1}\right) dA \end{aligned} \tag{2-42}$$

Derivation of the equation in above is presented in Appendix F.1.

Next, it is assumed that an Airy's stress function Ψ for the problem exists and thus, the stress components written in cylindrical coordinates are expressed by:

$$\begin{cases} \sigma_{r} = r^{-1}\ \Psi_{,r} + r^{-2}\Psi_{,\theta\theta} \\ \sigma_{\theta} = \Psi_{,\theta\theta} \\ \sigma_{r\theta} = -(r^{-1}\Psi_{,\theta})_{,r} \end{cases} \tag{2-43}$$

For plane stress conditions in cylindrical coordinates, the compatibility condition is given by [6] the following equation:

$$r^{-1}(r\epsilon_{\theta})_{,rr} + r^{-2}(\epsilon_{r})_{,\theta\theta} - r^{-1}(\epsilon_{r})_{,r} - 2r^{-2}(r\cdot(\epsilon_{r\theta})_{,\theta})_{,r} = 0 \tag{2-44}$$

Bringing in strain components ϵ_{r}, ϵ_{θ} and $\epsilon_{r\theta}$ obtained in Appendix F.2 with the stress expressions in eq. (2-43), eq. (2-44) results in the following partial differential equation governing the stress function: which is explicitly shown in Appendix F.3.

$$\nabla^4\Psi+\frac{\alpha}{2}\Bigg\{r^{-1}\Bigg[\sigma_e^{n-1}\Big(2r\Psi_{,rr}-\Psi_{,r}-r^{-1}\Psi_{,\theta\theta}\Big)\Bigg]_{,rr}+6r^{-2}\Bigg[\sigma_e^{n-1}\,r\cdot\Big(r^{-1}\Psi_{,\theta}\Big)_{,r}\Bigg]_{,r\theta}$$
$$+r^{-1}\Bigg[\sigma_e^{n-1}\Big(-2r^{-1}\Psi_{,r}-2r^{-2}\Psi_{,\theta\theta}+\Psi_{,rr}\Big)\Bigg]_{,r}$$
$$+r^{-2}\Bigg[\sigma_e^{n-1}\Big(-\Psi_{,rr}+2r^{-1}\Psi_{,r}+2r^{-2}\Psi_{,\theta\theta}\Big)\Bigg]_{,\theta\theta}\Bigg\}=0 \quad (2\text{-}45)$$

with boundary conditions for a stress-free crack on the crack walls as

$$\Psi(\pm\pi)=\Psi_{,\theta}(\pm\pi)=0 \quad (2\text{-}46)$$

The results in eqs. (2-45) and (2-46) are explicitly demonstrated in Appendix F.3.

Solution for the stress function is obtained considering the asymptotic expansion

$$\Psi=r^s\tilde{\Psi}_1(\theta)+r^s\tilde{\Psi}_2(\theta)+\cdots \quad (2\text{-}47)$$

and assuming the first term as dominant, or

$$\Psi=Kr^s\tilde{\Psi}(\theta) \quad (2\text{-}48)$$

where K is the amplitude. Thus, stresses are fully determined from Airy's function definition in eq. (2-43) (see Appendix F.4) as

$$\begin{cases}\sigma_e=Kr^{s-2}\tilde{\sigma}_e(\theta)=Kr^{s-2}(\tilde{\sigma}_r^2+\tilde{\sigma}_\theta^2-\tilde{\sigma}_r\tilde{\sigma}_\theta+3\tilde{\sigma}_{r\theta}^2)^{1/2}\\ \sigma_r=Kr^{s-2}\tilde{\sigma}_r(\theta)=Kr^{s-2}(s\tilde{\Psi}+\tilde{\Psi}_{,\theta\theta})\\ \sigma_\theta=Kr^{s-2}\tilde{\sigma}_\theta(\theta)=Kr^{s-2}s(s-1)\tilde{\Psi}\\ \sigma_{r\theta}=Kr^{s-2}\tilde{\sigma}_{r\theta}(\theta)=Kr^{s-2}(1-s)\tilde{\Psi}_{,\theta}\end{cases} \quad (2\text{-}49)$$

Rewriting eq. (2-45) and substituting the σ_e from eq. (2-49). The derivation is presented in Appendix F.5.

$$\Big[n(s-2)-\frac{\partial^2}{\partial\theta^2}\Big]\cdot\Big[\tilde{\sigma_e}^{n-1}\Big(s(s-3)\tilde{\Psi}-2\tilde{\Psi}_{,\theta\theta}\Big)\Big]$$
$$+\Big(n(s-2)+1\Big)\Big(n(s-2)\Big)\tilde{\sigma_e}^{n-1}\Big(s(2s-3)\tilde{\Psi}-\tilde{\Psi}_{,\theta\theta}\Big)$$
$$+6\Big(n(s-2)+1\Big)(s-1)\Big[\tilde{\sigma_e}^{n-1}\tilde{\Psi}_{,\theta}\Big]_{,\theta}=0 \quad (2\text{-}50)$$

Since the stress values must increase as r decreases, the exponent in

stress eq. (2-49) must be negative what results in $s < 2$. Moreover, since the complementary energy must have a finite value, a chosen sufficiently small neighbourhood of the crack tip the elastic contribution is a small fraction on complementary energy front plastic energy. This results in

$$s > \frac{2n}{n+1} \tag{2-51}$$

which proof is presented in Appendix F.6.

As stated earlier, the HRR is a procedure to obtain the stress-strain fields ahead of a crack tip, and is defined as function of J-integral should evaluated in what follows.

Considering the close path as shown in figure 2.10, $\Gamma = \Gamma_1 - \Gamma_2 + \Gamma_3 + \Gamma_4$ which embraces a region that does not contain the crack tip, the following condition holds

$$J = J_1 - J_2 + J_3 + J_4 = 0 \tag{2-52}$$

from the first J-integral's property, presented in section J-integral. And, due to the traction free condition on path Γ_3 and Γ_4 we have $J_3 = J_4 = 0$.

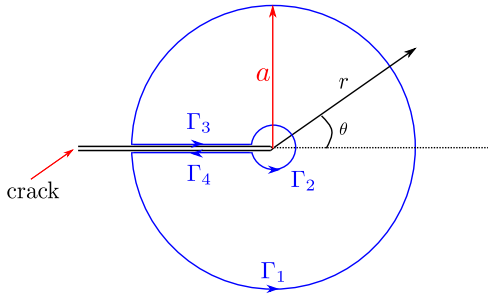

Figure 2.10: Close path integration used

In computing J_1 path integral, Hutchinson initially proposed the use of a linear elastic solution. From [22], the $\mathcal{G}$ is given as following.

$$\mathcal{G} = \frac{K_I^2}{E} \tag{2-53}$$

for plane stress condition, the Griffth's energy rate is associated with the SIF, where, in the case of assuming infinite plate, the SIT is given by eq. (H-1) from Appendix H.

However, assuming LEFM in this step restricts that the size of the plastic zone must be considerably small in comparison to the cracked component dimensions.

Previously proved, J-integral and $\mathcal{G}$ are equal and, as consequence (in dimensionless quantities)

$$\int_{\Gamma_1} (W\ dy + \sigma_{ij}\ n_j\ u_{i,x}\ ds) = \pi\sigma^{\infty\ 2} \tag{2-54}$$

Alternatively, a more accurate version is to consider J integral of the respective specimen, not restricting to small size of plastic zone and covering plastic contribution. Thus, (in dimensionless quantities)

$$\int_{\Gamma_1} (W\ dy + \sigma_{ij}\ n_j\ u_{i,x}\ ds) = J \tag{2-55}$$

For path Γ_2, J_2 is obtained by first considering the work as

$$W = \int_0^{\epsilon_{ij}} \sigma_{ij}\ d\epsilon_{ij} \tag{2-56}$$

where the elastic contribution is neglected compared to plastic strains contributions near the crack tip, resulting (see Appendix F.7)

$$\begin{aligned} W &= \int_0^{\epsilon_{ij}} \sigma_{ij}\ d\epsilon_{ij}^p \\ &= \alpha K^{n+1} \frac{n}{n+1}\ r^{(n+1)(s-2)}\ \tilde{\sigma}_e^{n+1} \end{aligned} \tag{2-57}$$

Secondly, u_r and $u_{\theta_{,\theta}}$ are obtained by integrating the strain equations, in cylindrical coordinates, as shown in Appendix F.8. Thus,

$$\begin{aligned} u_r &= \frac{\alpha\ K^n\ r^{n(s-2)+1}}{n(s-2)+1} \tilde{\sigma}_e^{n-1} \left(\frac{s(3-s)}{2} \tilde{\Psi} + \tilde{\Psi}_{,\theta\theta} \right) \\ &= \alpha\ K^n\ r^{n(s-2)+1}\ \tilde{u}_r(\theta) \end{aligned} \tag{2-58}$$

and

$$\begin{aligned} u_{\theta_{,\theta}} &= \alpha\ K^n\ r^{n(s-2)+1} \left\{ \tilde{\sigma}_e^{n-1} \left[s\left(s - \frac{3}{2} \right) \tilde{\Phi} - \frac{\tilde{\Phi}_{,\theta\theta}}{2} \right] - \tilde{u}_r \right\} \\ &= \alpha\ K^n\ r^{n(s-2)+1}\ \tilde{u}_{\theta_{,\theta}} \end{aligned} \tag{2-59}$$

Therefore, we have

$$\begin{aligned} \sigma_{ij} n_j u_{i,x} = \alpha K^{n+1} r^{(n+1)(s-2)} \{ &\sin\theta [\tilde{\sigma}_r (\tilde{u}_\theta - \tilde{u}_{r_{,\theta}}) - \tilde{\sigma}_{r\theta} (\tilde{u}_r + \tilde{u}_{\theta_{,\theta}})] \\ &+ (n(s-2)+1)\ \cos\theta [\tilde{\sigma}_r \tilde{u}_r + \tilde{\sigma}_{r\theta} \tilde{u}_\theta] \end{aligned} \tag{2-60}$$

with a convenient coordinate transformation being applied in the use of chain rule derivatives.

With eqs. (2-57) and (2-60), obtained in dimensionless form, J_2 in the infinitesimal path $t\ r\ d\theta$ results

$$\int_{\Gamma_2}(W\ dy + \sigma_{ij}\ n_j\ u_{i,x}\ ds) = \alpha\ \sigma_0\ \epsilon_0\ K^{n+1} r_2^{(n+1)(s-2)+1}\ I_n \tag{2-61}$$

where I_n is given by

$$I_n = \int_{-\pi}^{\pi} \left\{ \frac{n}{n+1}\tilde{\sigma}_e^{n+1}\cos\theta - [\sin\theta\tilde{\sigma}_r(\tilde{u}_\theta - \tilde{u}_{r,_\theta}) - \tilde{\sigma}_{r\theta}\ (\tilde{u}_r + \tilde{u}_{\theta,_\theta}) + (n(s-2)+1)(\tilde{\sigma}_r\tilde{u}_r + \tilde{\sigma}_{r\theta}\tilde{u}_\theta)\cos\theta] \right\} d\theta \tag{2-62}$$

For $r_2 \to 0$ condition, J must be finite, resulting in the exponent of r_2 being zero. Therefore,

$$(n+1)(s-2)+1 = 0 \therefore s = \frac{2n+1}{n+1} \tag{2-63}$$

Solving the differential equation for the stress function in eq. (2-50), with boundary conditions in eq. (2-46), and using the relation between r and s being describe as in eq. (2-63), numerical solutions of $\tilde{\Psi}(\theta)$ are obtained as shown in figs. 2.7 and 2.8.

Equalling the J-integral of path Γ_1 to the Γ_2, we have

$$J = \alpha\ \sigma_0\ \epsilon_0\ K^{n+1}\ I_n \tag{2-64}$$

where, from the relation $\sigma_0 = E \cdot \epsilon_0$, amplitude K can be rewritten as

$$K = \left(\frac{EJ}{\alpha\ \sigma_0^2\ I_n}\right)^{\frac{1}{n+1}} \tag{2-65}$$

From eq. (2-49), the stresses are then obtained using the relation of r and s, in eq. (2-63),

$$\begin{aligned}\sigma_{ij} &= K\ r^{-\frac{1}{n+1}}\ \tilde{\sigma}_{ij} \\ &= \left(\frac{K^{n+1}}{r}\right)^{\frac{1}{n+1}}\ \tilde{\sigma}_{ij}\end{aligned} \tag{2-66}$$

Note that K is defined such that K^{n+1} has dimensions of length. Returning to its dimension form and employing the result for the amplitude K obtained in eq. (2-65), one obtains

$$\sigma_{ij} = \sigma_0 \left(\frac{EJ}{\alpha\ \sigma_0^2\ I_n\ r}\right)^{\frac{1}{n+1}}\ \tilde{\sigma}_{ij} \tag{2-67}$$

while, strains are obtained by bringing eq. (2-67) into the Ramberg-Osgood hardening condition, eq. (2-29). Thus,

$$\epsilon_{ij} = \frac{\alpha\ \sigma_0}{E}\ \left(\frac{EJ}{\alpha\ \sigma_0^2\ I_n\ r}\right)^{\frac{n}{n+1}}\ \tilde{\epsilon}_{ij} \tag{2-68}$$

that match the expressions proposed in eqs. (2-27) and (2-28).

2.4 Plastic Zone Estimations in Size and Shape

Due to the high gradient of stress as approaching to the crack tip, the becomes as in its plastic behavior, in a region called plastic zone defined by the sole parameter (p_z) which is associated with damage mechanics.

In the following, plastic region size and shape definitions, through the $p_z(\theta)$ parameter are numerically obtained using stress components from analytical model considered previously. Of a particular interest is to determine the transition of elastic to elastoplastic material behavior, using von Mises condition in the 3D plane state,

$$\sigma_{\text{Mises}} = \sqrt{\sigma_{xx}^2 + \sigma_{yy}^2 - \sigma_{xx}\sigma_{yy} + 3\sigma_{xy}^2} \tag{2-69}$$

2.4.1 Plastic zones estimation for linear elastic stress field

Using Wiliams' stress field summarized by eq. (2-7) with the addition of functions $f_{xx}(\theta)$, $f_{yy}(\theta)$ and $f_{xy}(\theta)$ gives,

$$\begin{bmatrix}\sigma_{xx}\\ \sigma_{yy}\\ \sigma_{xy}\end{bmatrix} = \frac{K_I}{\sqrt{2\pi r}}\ \begin{bmatrix}f_{xx}(\theta)\\ f_{yy}(\theta)\\ f_{xy}(\theta)\end{bmatrix} \tag{2-70}$$

and the von Mises stress measure becomes

$$\sigma_{\text{Mises}}(r,\theta) = \frac{K_I}{\sqrt{2\pi r}}\sqrt{f_{xx}^2(\theta) + f_{yy}^2(\theta) - f_{xx}(\theta)\cdot f_{yy}(\theta) + 3f_{xy}^2(\theta)} \tag{2-71}$$

2.4.2 Influence of nominal stress σ_n on the plastic zone size and shape

Williams' stress derivations present a K_I direct dependence, what provides a correlation when $r \to \infty$ is easily notice that $\sigma_n \to 0$.

Supposing in a infinity plate a nominal stress σ_n in y-direction this limit condition results in

$$\lim_{r\to\infty} \sigma_{yy} = \lim_{r\to\infty} \frac{K_I}{\sqrt{2\pi r}} f_{yy}(\theta) = 0 \neq \sigma_n \tag{2-72}$$

where the boundary condition is not considered and indicating the dependence of σ_n/σ_y in the shape and size of the p_z.

Considering the nominal stress, σ_n can be add into y component to enforce the boundary condition. Thus

$$\sigma_{\text{Mises}}(r,\theta) = \sqrt{(\kappa \cdot f_{xx})^2 + (\kappa \cdot f_{yy} + \sigma_n)^2 - (\kappa \cdot f_{xx})(\kappa \cdot f_{yy} + \sigma_n) + 3(\kappa \cdot f_{xy})^2} \tag{2-73}$$

where κ:

$$\kappa \coloneqq \frac{K_I}{\sqrt{2\pi r}} \tag{2-74}$$

Despite this procedure being simplistic for not presenting a rigorous stress analyses, this approach obey the correct far field boundary condition.

2.4.3 LE plastic zone estimate that considers the equilibrium requirements

Irwin's estimation of p_z size partially considering equilibrium. When Williams' stress field is applied, the stress distribution due to singularity of the model inside p_z, without rearranging along residual ligament violates equilibrium. In Irwin's model a constant stress is assumed in the plastic zone $\sigma_{yy}(0 \leqslant r \leqslant p_z) = \kappa \cdot \sigma_y$, neglecting strain hardening, where κ depends on the stress state ahead of the crack tip.

Irwin redistributed the stress field outside the p_z, by shifting Williams' stress field. In figure 2.11 a new translated radius defined as $r_{\text{new}} = r - r_{_P}$ where $r_{_P}$ is the coordinate that reaches $\sigma_{yy} = \kappa \cdot \sigma_y$ at point P, creates a second translated curve with point P', as long as $r \geqslant p_z$.

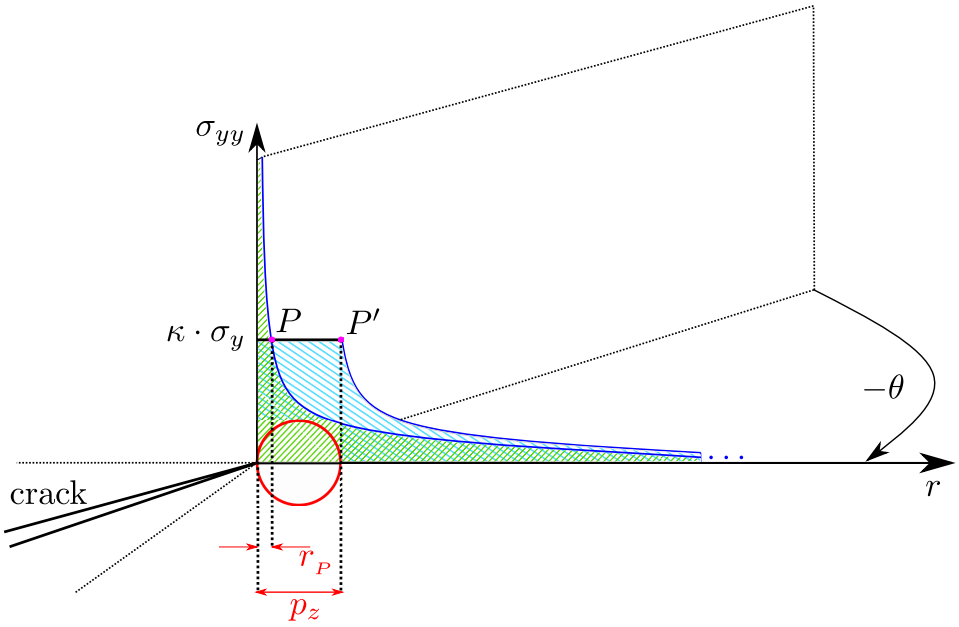

Figure 2.11: Irwin's stress redistribution

To determine the size of p_z that represents the assumed stress field redistribution, the integral of Williams' stress field, green hatch area must be equal to the blue hatch area in the graph, which defines the stress distribution resulting in, mathematically,

$$\int_0^{\infty} \sigma_{yy}(r,\theta)dr = \int_0^{pz(\theta)} \underbrace{\sigma_{yy}(r = r_{_P},\theta)}_{\text{constant in r}} dr + \int_{r_{_P}(\theta)}^{\infty} \sigma_{yy}(r,\theta)dr \tag{2-75}$$

or

$$pz(\theta) = \frac{1}{\sigma_{yy}(r = r_{_P},\theta)} \int_0^{r_{_P}(\theta)} \sigma_{yy}(r,\theta)dr \tag{2-76}$$

that is p_z, and verifying the equilibrium condition.

3
Plasticity

In this chapter, elements for the complete definition of a formulation that represents the nonlinear behavior of materials beyond its linear elastic regimen are presented. Some basic plasticity equations with the von Mises criteria formulation are presented.

3.1
Basic Plastic Equations

As in a general case, it must provide (from reference [2]):

- the elastoplastic strain decomposition
- an elastic law
- a yield criterion, stated with the use of a yield function
- a plastic flow rule defining the evolution of the plastic strain
- a hardening law, which characterises the evolution of the material yield limit

Considering the evolution of strains, at each loading total strains may be decomposed into two addictive quantities: elastic and plastic strains - each presenting different behaviors under loading and unloading conditions. Thus,

$$\boldsymbol{\epsilon} = \boldsymbol{\epsilon}^e + \boldsymbol{\epsilon}^p \tag{3-1}$$

where $\boldsymbol{\epsilon}$, $\boldsymbol{\epsilon}_e$ and $\boldsymbol{\epsilon}^p$ are the total strains tensor, elastic strain tensor and plastic strain tensor, respectively. This equation can incrementally be represented as:

$$\boldsymbol{\Delta\epsilon} = \boldsymbol{\Delta\epsilon}^e + \boldsymbol{\Delta\epsilon}^p \tag{3-2}$$

Throughout this study, a linear constitutive relation is considered, in the form

$$\boldsymbol{\sigma} = \boldsymbol{D}^e : \boldsymbol{\epsilon}^e \tag{3-3}$$

where $\boldsymbol{D}^e$ is the standard isotropic constitutive elastic tensor.

The Yield function sets an expression for the stress state conditions of material in plasticity. In general, the yield function is as following:

$$\Phi(\boldsymbol{\sigma}, \boldsymbol{\epsilon}, \boldsymbol{\epsilon}^p, \bar{\epsilon}^p, \alpha, \cdots) = \begin{cases} \leqslant 0 \rightarrow \text{elastic state} \\ > 0 \rightarrow \text{elastoplastic state} \end{cases} \tag{3-4}$$

where α is an internal variable. It also depends on stress tensor state $\boldsymbol{\sigma}$, strain state tensor $\boldsymbol{\epsilon}$, plastic strain tensor $\boldsymbol{\epsilon}^p$ and the accumulated plastic strain $\bar{\epsilon}^p$ from the uniaxial test, in a correlation of 3D stress state with the uniaxial constitutive stress-strain relation.

Moreover, the hardening law is incorporated in the equation above, since the evolution of accumulated plastic strain ϵ^p affects Yield function Φ. The evolution law for the internal variables is defined by the Flow Rule which, in associative plasticity we use:

$$\dot{\boldsymbol{\epsilon}}^p = \dot{\gamma}\frac{\partial \Phi}{\partial \boldsymbol{\sigma}} \tag{3-5}$$

which, applying Backward Euler for incremental plasticity reduces to:

$$\boldsymbol{\Delta\epsilon}^p = \Delta\gamma \, \frac{\partial \Phi}{\partial \boldsymbol{\sigma}} \tag{3-6}$$

where $\Delta\boldsymbol{\epsilon}^p$ is the incremental plastic strain tensor.

3.1.1 Stress Decomposition

The stress tensor additive decomposition in hydrostatic (or also called volumetric) and deviatoric tensors consists of, in the matrix form.

$$\begin{bmatrix} \sigma_{xx} & \sigma_{xy} & \sigma_{xz} \\ \sigma_{yx} & \sigma_{yy} & \sigma_{yz} \\ \sigma_{zx} & \sigma_{zy} & \sigma_{zz} \end{bmatrix} = \begin{bmatrix} p & 0 & 0 \\ 0 & p & 0 \\ 0 & 0 & p \end{bmatrix} + \begin{bmatrix} \sigma_{xx} - p & \sigma_{xy} & \sigma_{xz} \\ \sigma_{yx} & \sigma_{yy} - p & \sigma_{yz} \\ \sigma_{zx} & \sigma_{zy} & \sigma_{zz} - p \end{bmatrix} \tag{3-7}$$

This decomposition allows reducing the hydrostatic effects, which does not cause material plasticity, from the total stress tensor, or

$$\begin{cases} \boldsymbol{\sigma} = \boldsymbol{\sigma}_{\mathrm{v}} + \boldsymbol{S} \\ \boldsymbol{S} = \boldsymbol{\sigma} - \boldsymbol{\sigma}_{\mathrm{v}} \end{cases} \tag{3-8}$$

In eq. (3-8) p is any real value. However, to establish a fixed p in order to the deviatoric tensor preserves the volumetric deformation, we consider a cube with initial side lengths l_1, l_2 and l_3 and final side lengths $l_1^{'}$, $l_2^{'}$ and $l_3^{'}$. Initial volume V_o and the final volume V_f are

$$\begin{cases} V_0 = l_1 \cdot l_2 \cdot l_3 \\ V_f = l_1^{'} \cdot l_2^{'} \cdot l_3^{'} \end{cases} \tag{3-9}$$

respectively. Since only large deformations are assumed to occur linear strains are, as defined,

$$\begin{cases} \epsilon_{xx} = \ln \frac{l_1^{'}}{l_1} \therefore l_1^{'} = l_1 \cdot e^{\epsilon_{xx}} \\ \epsilon_{yy} = \ln \frac{l_2^{'}}{l_2} \therefore l_2^{'} = l_2 \cdot e^{\epsilon_{yy}} \\ \epsilon_{zz} = \ln \frac{l_3^{'}}{l_3} \therefore l_3^{'} = l_3 \cdot e^{\epsilon_{zz}} \end{cases} \tag{3-10}$$

Substituting results in eq. (3-10) into V_f results

$$\frac{V_f}{V_0} = e^{\epsilon_{xx}+\epsilon_{yy}+\epsilon_{zz}} \tag{3-11}$$

Defining ΔV as the variation of volume V:

$$\Delta V = \ln \frac{V_f}{V_0} = \epsilon_{xx} + \epsilon_{yy} + \epsilon_{zz} \tag{3-12}$$

Considering the constitutive linear relations, from continuum mechanics, we have:

$$\begin{cases} \epsilon_{xx} = \frac{1}{E}[\sigma_{xx} - \nu(\sigma_{yy} + \sigma_{zz})] \\ \epsilon_{yy} = \frac{1}{E}[\sigma_{yy} - \nu(\sigma_{xx} + \sigma_{zz})] \\ \epsilon_{zz} = \frac{1}{E}[\sigma_{zz} - \nu(\sigma_{xx} + \sigma_{yy})] \end{cases} \tag{3-13}$$

that brought into eq. (3-12), it results in

$$\Delta V = \frac{3(1-2\nu)}{E}\left(\frac{\sigma_{xx} + \sigma_{yy} + \sigma_{zz}}{3}\right) \tag{3-14}$$

Equation (3-14) shows that for $\nu \neq 0.5$ volume is preserved only if:

$$\sigma_{xx} + \sigma_{yy} + \sigma_{zz} = 0 \tag{3-15}$$

Since volume preservation must be verified on deviatoric tensor $\boldsymbol{S}$, from eq. (3-15) this condition results in

$$tr(\boldsymbol{S}) = (\sigma_{xx} - p) + (\sigma_{yy} - p) + (\sigma_{zz} - p) = 0 \tag{3-16}$$

or

$$p = \frac{\sigma_{xx} + \sigma_{yy} + \sigma_{zz}}{3} = \frac{tr(\boldsymbol{\sigma})}{3} \tag{3-17}$$

Also defining p as function of strain tensor, requires that eqs. (3-13) are added, resulting

$$E \cdot (\epsilon_1 + \epsilon_2 + \epsilon_3) = \sigma_1 + \sigma_2 + \sigma_3 - 2\nu(\sigma_1 + \sigma_2 + \sigma_3)$$

$$E \cdot tr(\epsilon^e) = 3 \cdot \frac{\sigma_1 + \sigma_2 + \sigma_3}{3} - 2\nu \cdot 3\left(\frac{\sigma_1 + \sigma_2 + \sigma_3}{3}\right)$$

$$E \cdot tr(\boldsymbol{\epsilon}^e) = 3p - 2\nu \cdot 3p$$

$$tr(\boldsymbol{\epsilon}^e) = p\frac{3(1-2\nu)}{E} \tag{3-18}$$

or

$$p = K \cdot tr(\boldsymbol{\epsilon}^e) \tag{3-19}$$

where $K = E/(3(1-2\nu))$ is the Bulk modulus.

Thus, in short , we have

$$\begin{cases} \boldsymbol{\sigma}_{\mathrm{v}} = p\boldsymbol{I} \\ \boldsymbol{S} = \boldsymbol{\sigma} - p\boldsymbol{I} \end{cases} \tag{3-20}$$

where

$$\begin{cases} p = \frac{tr(\boldsymbol{\sigma})}{3} \\ p = K \cdot tr(\boldsymbol{\epsilon}^e) \end{cases} \tag{3-21}$$

3.1.2 Deviatoric stress

To obtain the deviatoric stress tensor as function of the strain tensor let start with strain definition from elasticity in index notation

$$\epsilon_{ij} = \frac{1+\nu}{E} \cdot \sigma_{ij} - \frac{\nu}{E}\sigma_{kk}\delta_{ij} \tag{3-22}$$

The deviatoric strain tensor is obtained from ($\boldsymbol{\epsilon}^d$) as:

$$\boldsymbol{\epsilon}_d = \boldsymbol{\epsilon} - \frac{tr(\boldsymbol{\epsilon})}{3}\boldsymbol{I} \tag{3-23}$$

and the volumetric strain tensor is

$$\boldsymbol{\epsilon}_{\mathrm{v}} = \frac{tr(\boldsymbol{\epsilon})}{3}\boldsymbol{I} \tag{3-24}$$

Using the definition 3-23

$$\begin{aligned} tr(\boldsymbol{\epsilon}) &= \epsilon_{ij}\delta_{ij} \\ &= \left(\frac{1+\nu}{E} \cdot \sigma_{ij} - \frac{\nu}{E}\sigma_{kk}\delta_{ij}\right)\delta_{ij} \\ &= \frac{1+\nu}{E} \cdot \sigma_{kk} - \frac{\nu}{E}\sigma_{kk}\underbrace{\delta_{ij}\delta_{ij}}_{3} \\ &= \frac{1-2\nu}{E}\sigma_{kk} \end{aligned} \tag{3-25}$$

deviatoric strain tensor in eq. (3-23) can be expressed as:

$$\begin{aligned}\epsilon_{ij_d} &= \epsilon_{ij} - \frac{1-2\nu}{3E}\sigma_{kk}\delta_{ij} \\ &= \frac{1+\nu}{E}\sigma_{ij} - \frac{\nu}{E}\sigma_{kk}\delta_{ij} - \frac{1-2\nu}{3E}\sigma_{kk}\delta_{ij} \\ &= \frac{1+\nu}{E}\sigma_{ij} - \frac{1+\nu}{3E}\sigma_{kk}\delta_{ij} \\ &= \frac{1+\nu}{E}\left(S_{ij} + \frac{1}{3}\sigma_{kk}\delta_{ij}\right) - \frac{1+\nu}{3E}\sigma_{kk}\delta_{ij} \\ &= \frac{1+\nu}{E}\cdot S_{ij} \\ &= \frac{S_{ij}}{2G}\end{aligned} \tag{3-26}$$

resulting

$$\boldsymbol{S} = 2G\cdot\boldsymbol{\epsilon}_d \tag{3-27}$$

3.1.3 Deviatoric operator

The deviatoric projection tensor is a fourth-order tensor that projects a symmetric second-order tensor into the deviatoric subspace, [2].

$$\boldsymbol{I}_d \coloneqq \boldsymbol{I}_S - \frac{1}{3}\,\boldsymbol{I}\otimes\boldsymbol{I} \tag{3-28}$$

where $\boldsymbol{I}_S$ is a fourth-order operator tensor that maps any second-order tensor into its symmetric. The definition of symmetric operator of a symmetric tensor $\boldsymbol{\sigma}$ is given by, [2]

$$\boldsymbol{I}_S : \boldsymbol{\sigma} = \boldsymbol{\sigma} \tag{3-29}$$

The definition of symmetric operator is given by

$$(I_S)_{ijkl} = \frac{1}{2}(\delta_{ik}\delta_{jl} + \delta_{il}\delta_{jk}) \tag{3-30}$$

or,

$$\boldsymbol{I}_S = \frac{1}{2}(\boldsymbol{I} + \boldsymbol{I}_T) \tag{3-31}$$

where $\boldsymbol{I}_T$ is the transposition tensor that provides

$$\boldsymbol{I}_T : \boldsymbol{\sigma} = \boldsymbol{\sigma} : \boldsymbol{I}_T = \boldsymbol{\sigma}^T \tag{3-32}$$

The definition, in index notation, for transposition tensor is

$$(I_T)_{ijkl} = \delta_{il}\delta_{jk} \tag{3-33}$$

Below the proof of the deviatoric projection tensor is presented. Assuming a symmetric tensor $\boldsymbol{\sigma}$, we have

$$\begin{aligned} \boldsymbol{I}_d : \boldsymbol{\sigma} = (I_d)_{ijkl}\, \boldsymbol{\sigma}_{ij} &= \left[\frac{1}{2}(\delta_{ik}\delta_{jl} + \delta_{il}\delta_{jk}) - \frac{1}{3}\,\delta_{ij}\delta_{kl}\right]\sigma_{ij} \\ &= \frac{1}{2}\,(\sigma_{kl} + \sigma_{lk}) - \frac{1}{3}\,tr(\boldsymbol{\sigma})\delta_{kl} \\ &= \sigma_{kl} - \frac{1}{3}\,tr(\boldsymbol{\sigma})\delta_{kl} \end{aligned} \tag{3-34}$$

Therefore, from eqs. (3-20) and (3-21) we have

$$\boldsymbol{S} = \boldsymbol{I}_d : \boldsymbol{\sigma} \tag{3-35}$$

3.2 The von Mises Isotropic 3D Plasticity

This work considers the 3D isotropic plasticity model with von Mises yield surface, appropriate to represent most metallic materials that only stretch in the radial direction of the yield surface.

In the numerical simulation presented a mathematical model is employed to predict the material physical behavior. Plasticity occurs due to dislocations whose driven forces are the deviatoric stresses. Moreover, for metal materials, we expect a plasticity model that should be invariant regardless of the coordinate system used.

In our study the yield function is defined as [2]:

$$\Phi(\boldsymbol{\sigma}, \sigma_y) = \sqrt{3J_2(\boldsymbol{S}(\boldsymbol{\sigma}))} - \sigma_y \tag{3-36}$$

where $\sigma_y = \sigma_y(\bar{\epsilon}^p)$ is a function of the accumulated plastic strain in the uniaxial load.

In eq. (3-36) J_2 is the second invariant of stress tensor for the deviatoric tensor is used.

$$J_2(\boldsymbol{S}) \equiv \frac{1}{2}\,\|\boldsymbol{S}\|^2 = \frac{1}{2}\,\boldsymbol{S} : \boldsymbol{S} = \frac{1}{2}S_{ij}S_{ij} \tag{3-37}$$

In an algorithm procedure, the derivative of the yield function with respect to the stress tensor, generally referred as the normal tensor,

$$\begin{aligned} \boldsymbol{N} \equiv \frac{\partial \Phi}{\partial \boldsymbol{\sigma}} &= \sqrt{3}\frac{\partial}{\partial \boldsymbol{\sigma}}(J_2)^{1/2} - \frac{\partial \sigma_y}{\partial \boldsymbol{\sigma}} \\ &= \sqrt{\frac{3}{2}}\frac{\partial \|\boldsymbol{S}\|}{\partial \boldsymbol{\sigma}} \end{aligned} \tag{3-38}$$

or, using the chain rule derivative,

$$N_{ij} = \sqrt{\frac{3}{2}}\frac{\partial \|\boldsymbol{S}\|}{\partial S_{kl}}\frac{\partial S_{kl}}{\partial \sigma_{ij}} \tag{3-39}$$

where, the first fraction from equation in above is rewritten considering that a norm of a tensor $\boldsymbol{T}$ is $\|\boldsymbol{T}\| = (T_{ij}T_{ij})^{1/2}$. Therefore,

$$\frac{\partial\|\boldsymbol{S}\|}{\partial S_{kl}} = \frac{1}{2}(S_{ij}S_{ij})^{-1/2}\frac{\partial}{\partial S_{kl}}(S_{ij}S_{ij}) \tag{3-40}$$

and

$$\begin{aligned}\frac{\partial}{\partial S_{kl}}(S_{ij}S_{ij}) &= \frac{\partial S_{ij}}{\partial S_{kl}}S_{ij} + S_{ij}\frac{\partial S_{ij}}{\partial S_{kl}} \\ &= \delta_{ik}\delta_{jl}S_{ij} + S_{ij}\delta_{ik}\delta_{jl} \\ &= 2S_{kl}\end{aligned} \tag{3-41}$$

Thus, plugging this in eq. (3-40) results

$$\frac{\partial\|\boldsymbol{S}\|}{\partial S_{kl}} = \frac{S_{kl}}{(S_{ij}S_{ij})^{1/2}} = \frac{S_{kl}}{\|\boldsymbol{S}\|} \tag{3-42}$$

or

$$\frac{\partial\|\boldsymbol{S}\|}{\partial \boldsymbol{S}} = \frac{\boldsymbol{S}}{\|\boldsymbol{S}\|} \tag{3-43}$$

Moreover, in eq. (3-39) we may also consider from eq. (3-20)

$$\begin{aligned}\frac{\partial S_{ij}}{\partial\sigma_{kl}} &= \frac{\partial}{\partial\sigma_{kl}}(\sigma_{ij} - p\delta_{ij}) \\ &= I_{ijkl} - \frac{\partial p}{\partial\sigma_{kl}}\delta_{ij}\end{aligned} \tag{3-44}$$

that using index contraction, gives

$$\frac{\partial p}{\partial\sigma_{kl}} = \frac{1}{3}\frac{\partial\sigma_{mm}}{\partial\sigma_{kl}} = \frac{1}{3}\delta_{mk}\delta_{ml} = \frac{1}{3}\delta_{kl} \tag{3-45}$$

Substituting the results in eq. (3-43), (3-44) into eq. (3-39) we may obtain

$$\begin{aligned}\boldsymbol{N} &= \sqrt{\frac{3}{2}}\frac{\partial\|\boldsymbol{S}\|}{\partial\boldsymbol{S}} : \frac{\partial\boldsymbol{S}}{\partial\boldsymbol{\sigma}} \\ &= \sqrt{\frac{3}{2}}\frac{\boldsymbol{S}}{\|\boldsymbol{S}\|} : \left(\boldsymbol{I} - \frac{1}{3}\delta\otimes\delta\right) \\ &= \sqrt{\frac{3}{2}}\frac{\boldsymbol{S}}{\|\boldsymbol{S}\|}\end{aligned} \tag{3-46}$$

the normal tensor as a function of the deviatoric stress $\boldsymbol{\sigma}$ tensor.

3.2.1 The plasticity model considered

Since material plasticity is a non-linear phenomena, its numerical model representation requires procedures with loading and state variable increments under linear assumptions and, as a consequence, the use of iterative techniques in order to obtain a numerical solution. In this section an incremental form of plasticity analysis procedure is presented, assuming small linearised increments.

First, the incremental strains ($\boldsymbol{\Delta\epsilon}$), from a time increment n to $n+1$, is considered in tensor form:

$$\boldsymbol{\Delta\epsilon} = \boldsymbol{\epsilon}_{n+1} - \boldsymbol{\epsilon}_n \tag{3-47}$$

where is initially computated considering an elastic problem, by this reason, the concept of a *trial* state must be introduced.

$$\boldsymbol{\epsilon}^{e\ trial}_{n+1} = \boldsymbol{\epsilon}^{e}_{n} + \boldsymbol{\Delta\epsilon} \tag{3-48}$$

The trial accumulated plastic strain in t_{n+1} is defined as being:

$$\bar{\epsilon}^{p\ trial}_{n+1} = \bar{\epsilon}^{p}_{n} \tag{3-49}$$

The corresponding trial stress in obtained by:

$$\boldsymbol{\sigma}^{trial}_{n+1} = \boldsymbol{D}^{e} : \boldsymbol{\epsilon}^{e\ trial}_{n+1} \tag{3-50}$$

or, alternatively, the use of the stress decomposition. From eq. (3-27):

$$\boldsymbol{S}^{trial}_{n+1} = 2G \cdot \boldsymbol{\epsilon}^{e\ trial}_{d\ n+1} \tag{3-51}$$

and from eq. (3-19):

$$p^{trial}_{n+1} = K \cdot tr(\boldsymbol{\epsilon}^{e\ trial}_{v\ n+1}) \tag{3-52}$$

The trial yield stress can also be computed as a function of the accumulated plastic strains:

$$\sigma^{trial}_{y\ n+1} = \sigma_y(\bar{\epsilon}^{p}_{n}) = \sigma_{y_n} \tag{3-53}$$

At this point, plastic admissibility should be checked for the trial stress ($\boldsymbol{\sigma}^{trial}_{n+1}$) being inside the trial yield surface or outside of it:

– In the case, lying inside (see eq. 3-4), we have:

$$\Phi(\boldsymbol{\sigma}^{trial}_{n+1}, \sigma_{y_n}) \leqslant 0 \tag{3-54}$$

In this case, the obtained trial tensor is the elastic solution at $n+1$:

$$\begin{aligned} \boldsymbol{\epsilon}^e_{n+1} &= \boldsymbol{\epsilon}^{e\ trial}_{n+1} \\ \boldsymbol{\sigma}_{n+1} &= \boldsymbol{\sigma}^{trial}_{n+1} \\ \bar{\epsilon}^p_{n+1} &= \bar{\epsilon}^{p\ trial}_{n+1} = \bar{\epsilon}^p_n \\ \sigma_{y\ n+1} &= \sigma^{trial}_{y\ n+1} = \sigma_{y\ n} \end{aligned} \tag{3-55}$$

– Otherwise, $\boldsymbol{\sigma}^{trial}_{n+1}$ representation lies outside the yield surface and a *return-mapping* procedure must be performed in order to obtain the correct state. This is accomplished by forcing $\boldsymbol{\sigma}^{trial}_{n+1}$ to lie on the surface.

Under this condition, correct elastic strain state ($\boldsymbol{\epsilon}^e_{n+1}$) is no longer the trial elastic strain tensor ($\boldsymbol{\epsilon}^{e\ trial}_{n+1}$), but modifying by subtracting it with the plastic increment ($\Delta\boldsymbol{\epsilon}^p_{n+1}$), resulting in

$$\boldsymbol{\epsilon}^e_{n+1} = \boldsymbol{\epsilon}^{e\ trial}_{n+1} - \boldsymbol{\Delta\epsilon}^p_{n+1} \tag{3-56}$$

substituting the incremental plastic strain ($\boldsymbol{\Delta\epsilon}^p_{n+1}$) with the flow rule from eq. (3-6) and the derivative of the yield function with respect to the stress from eq. (3-46) gives:

$$\boldsymbol{\epsilon}^e_{n+1} = \boldsymbol{\epsilon}^{e\ \text{trial}}_{n+1} - \Delta\gamma\sqrt{\frac{3}{2}}\frac{\boldsymbol{S}_{n+1}}{\|\boldsymbol{S}_{n+1}\|} \tag{3-57}$$

moreover, the new cumulative strain must be updated in the form

$$\bar{\epsilon}^p_{n+1} = \bar{\epsilon}^p_n + \Delta\gamma \tag{3-58}$$

where $\Delta\gamma$ is obtained by forcing the stress representation to belong to the yield surface. Therefore, the following condition must hold

$$\sqrt{3J_2(\boldsymbol{S}_{n+1})} - \sigma_y(\bar{\epsilon}^p_{n+1}) = 0 \tag{3-59}$$

This is a nonlinear equation since $\boldsymbol{S}_{n+1}$ and σ_y are functions of $\Delta\gamma$. In order to obtain the explicit relation between $\boldsymbol{S}_{n+1}$ and $\Delta\gamma$, we make use of eq. (3-27) and (3-57) by imposing the deviatoric operator and multiplying for $2G$. Note that the second term of the right-hand-side of eq. (3-57) is already deviatoric. Thus we have

$$\left(1 + \sqrt{\frac{3}{2}}\frac{\Delta\gamma\ 2G}{\|\boldsymbol{S}_{n+1}\|}\right)\boldsymbol{S}_{n+1} = \boldsymbol{S}^{trial}_{n+1} \tag{3-60}$$

resulting that $\boldsymbol{S}_{n+1}$ and $\boldsymbol{S}^{trial}_{n+1}$ are collinear, what implies in

$$\frac{\boldsymbol{S}_{n+1}}{\|\boldsymbol{S}_{n+1}\|} = \frac{\boldsymbol{S}^{trial}_{n+1}}{\|\boldsymbol{S}^{trial}_{n+1}\|} \tag{3-61}$$

Bringing the above results into eq. (3-60) stress tensor at time $n+1$ may explicitly be written as

$$\boldsymbol{S}_{n+1} = \left(1 - \sqrt{\frac{3}{2}}\frac{\Delta\gamma\ 2G}{\|\boldsymbol{S}^{trial}_{n+1}\|}\right)\boldsymbol{S}^{trial}_{n+1} \tag{3-62}$$

Defying q^{trial}_{n+1} and using eq. (3-37):

$$q^{trial}_{n+1} \coloneqq \sqrt{3\ J_2(\boldsymbol{S}^{trial}_{n+1})} = \sqrt{\frac{3}{2}}\left\|\boldsymbol{S}^{trial}_{n+1}\right\| \tag{3-63}$$

the eq. (3-62) can be rewritten as:

$$\boldsymbol{S}_{n+1} = \left(1 - \frac{\Delta\gamma\ 3G}{q^{\text{trial}}_{n+1}}\right)\boldsymbol{S}^{trial}_{n+1} \tag{3-64}$$

and the yield function can also be rewritten with the explicit relation with $\Delta\gamma$, substituting eq. (3-64) and (3-58) into (3-59):

$$\begin{aligned}
\tilde{\Phi}(\Delta\lambda) &= \sqrt{3J_2(\boldsymbol{S}_{n+1})} - \sigma_y(\bar{\epsilon}^p_{n+1}) = 0 \\
&= \sqrt{\frac{3}{2}}\|\boldsymbol{S}_{n+1}\| - \sigma_y(\bar{\epsilon}^p_n + \Delta\gamma) = 0 \\
&= \left(1 - \frac{\Delta\gamma\ 3G}{q^{\text{trial}}_{n+1}}\right)\cdot \underbrace{\sqrt{\frac{3}{2}}\left\|\boldsymbol{S}^{trial}_{n+1}\right\|}_{q^{trial}_{n+1}} - \sigma_y(\bar{\epsilon}^p_n + \Delta\gamma) = 0 \\
&= q^{\text{trial}}_{n+1} - 3G\Delta\lambda - \sigma_y(\bar{\epsilon}^p_n + \Delta\gamma) = 0
\end{aligned} \tag{3-65}$$

Finally, the above scalar (non-linear) equation is solved for the plastic multiplier $\Delta\gamma$ by using the Newton-Raphson iterative technique. For this, the hardening slope H, derivative of σ_y with respect to $\bar{\epsilon}^p$ is defined as following

$$H = \left.\frac{\partial\sigma_y}{\partial\bar{\epsilon}^p}\right|_{\bar{\epsilon}^p_n + \Delta\gamma} \tag{3-66}$$

It is important to point out that since the non-linearity in eq. (3-65) is due to σ_y only, for a bilinear hardening law no numerical algorithm is needed. From $\Delta\gamma$ obtained value, state variables are updated using the corrected deviatoric stress tensor, resulting

$$\boldsymbol{\sigma}_{n+1} = \boldsymbol{S}_{n+1} + p^{trial}_{n+1}\,\boldsymbol{I} \tag{3-67}$$

Thus, the correct elastic strain tensor results from the addition of the hydrostatic and deviatoric elastic strain, in eqs. (3-27) and (3-24), respectively,

$$\boldsymbol{\epsilon}^e_{n+1} = \frac{1}{2G}\,\boldsymbol{S}_{n+1} + \frac{1}{3}\,tr(\boldsymbol{\epsilon}^{e\ trial}_{n+1})\,\boldsymbol{I} \tag{3-68}$$

These last eqs. (3-67) and (3-68) define stress and strain tensors in plasticity evolution, resulting in zero value for the yield function considered.

The flowchart that follows presents a step-by-step sequence for the algorithm numerical implementation as considered in this study.

Return-mapping Algorithm

– Given a $\boldsymbol{\Delta\epsilon}$

$$\boldsymbol{\epsilon}^{e\ trial}_{n+1} = \boldsymbol{\epsilon}^{e}_{n} + \boldsymbol{\Delta\epsilon}$$

$$\bar{\epsilon}^{p\ \text{trial}}_{n+1} = \bar{\epsilon}^{p}_{n}$$

$$p^{\text{trial}}_{n+1} = K \cdot tr(\boldsymbol{\epsilon}^{e\ trial}_{v\ n+1}) \qquad \boldsymbol{S}^{trial}_{n+1} = 2G \cdot \boldsymbol{\epsilon}^{e\ trial}_{d\ n+1} \tag{3-69}$$

$$q^{\text{trial}}_{n+1} = \sqrt{\frac{3}{2}\, \boldsymbol{S}^{trial}_{n+1} : \boldsymbol{S}^{trial}_{n+1}} \tag{3-70}$$

– Check plastic admissibility
if ($q^{\text{trial}}_{n+1} - \sigma_y(\bar{\epsilon}^{p\ \text{trial}}_{n+1}) \leqslant 0$) {

$$\boldsymbol{\epsilon}^{e}_{n+1} = \boldsymbol{\epsilon}^{e\ trial}_{n+1} \tag{3-71}$$

$$\boldsymbol{\sigma}_{n+1} = \boldsymbol{\sigma}^{trial}_{n+1} \tag{3-72}$$

$$\bar{\epsilon}^{p}_{n+1} = \bar{\epsilon}^{p\ \text{trial}}_{n+1} = \bar{\epsilon}^{p}_{n} \tag{3-73}$$

} else {
Return mapping. Solve the equation

$$\Phi(\Delta\gamma) = q^{trial}_{n+1} - 3G\ \Delta\gamma - \sigma_y(\bar{\epsilon}^{p}_{n} + \Delta\gamma) = 0 \tag{3-74}$$

for $\Delta\gamma$ using the Newton-Raphson.

$$p_{n+1} = p^{trial}_{n+1} \qquad \boldsymbol{S}_{n+1} = \left(1 - \frac{\Delta\gamma\ 3G}{q^{trial}_{n+1}}\right)\boldsymbol{S}^{trial}_{n+1} \tag{3-75}$$

$$\boldsymbol{\sigma}_{n+1} = \boldsymbol{S}_{n+1} + p_{n+1}\ \boldsymbol{I} \tag{3-76}$$

$$\boldsymbol{\epsilon}^{e}_{n+1} = \frac{1}{2G}\ \boldsymbol{S}_{n+1} + \frac{1}{3}\ tr(\boldsymbol{\epsilon}^{e\ trial}_{n+1})\ \boldsymbol{I} \tag{3-77}$$

$$\bar{\epsilon}^{p}_{n+1} = \bar{\epsilon}^{p}_{n} + \Delta\gamma \tag{3-78}$$

}

– Exit

The iterative procedure was considered as follows,

Newton-Raphson Algorithm

– Set initial guess for $\Delta\gamma$:

$$\Delta\gamma^{(0)} = 0 \tag{3-79}$$

and calculate the residual (in this case the Yield Function):

$$\tilde{\Phi} = q_{n+1}^{trial} - \sigma_y(\bar{\epsilon}_n^p) \tag{3-80}$$

– Do the Newton-Raphson iteration

$$H = \frac{\partial \sigma_y}{\partial \bar{\epsilon}^p}\Big|_{\bar{\epsilon}_n^p + \Delta\gamma} \quad \text{(hardening slope)} \tag{3-81}$$

$$d = \frac{\partial \tilde{\Phi}}{\partial \Delta\gamma} = -3G - H \quad \text{(residual derivative)} \tag{3-82}$$

$$\Delta\gamma = \Delta\gamma - \frac{\tilde{\Phi}}{d} \quad \text{(new guess)} \tag{3-83}$$

– Check for convergence

3.2.2 Geometric interpretation

Under the algebraic point of view, the theory presented so far is established on a robust mathematical support with no insight on the geometric considerations. Nonetheless, visualizing each procedure can give a clear view to the understanding on how the procedure is performed in solving a plasticity problem.

The yield function is geometrically represented by a 3D convex surface in the principal stress components defined space. To von Mises pressure-insensitive materials, which hydrostatic stresses do not cause plasticity the yielding function is geometrically represented by a cylindrical surface which axis is equally apart from reference axis, along with no restriction in plasticity occurs.

To obtain the equation representing the surface, a rotation from the principal stress tensor $\boldsymbol{\sigma}$, to $\boldsymbol{\sigma}''$ lies in a special coordinate system known in literature, composed by the hydrostatic axis and the π-plane. According to [3], between the principal coordinate axis and the rotated ones we have

$$\boldsymbol{\sigma} = AB\boldsymbol{\sigma}'' \tag{3-84}$$

where A and B are matrix transformations given by:

$$A = \begin{bmatrix} \frac{\sqrt{2}}{2} & 0 & \frac{\sqrt{2}}{2} \\ 0 & 1 & 0 \\ -\frac{\sqrt{2}}{2} & 0 & \frac{\sqrt{2}}{2} \end{bmatrix} \ , \ B = \begin{bmatrix} 1 & 0 & 0 \\ 0 & \sqrt{\frac{2}{3}} & \frac{1}{\sqrt{3}} \\ 0 & -\frac{1}{\sqrt{3}} & \sqrt{\frac{2}{3}} \end{bmatrix} \tag{3-85}$$

Considering shear stress, since J_2 is invariant, the norm of the deviatoric stress tensor referred to the principal coordinate axis is

$$\|\boldsymbol{S}\| = \frac{1}{\sqrt{3}}\left[(\sigma_1 - \sigma_2)^2 + (\sigma_2 - \sigma_3)^2 + (\sigma_1 - \sigma_3)^2\right] \tag{3-86}$$

Applying the transformation defined in eq. (3-84) between normal stress and plugging in the result in eq. (3-86) results

$$\|\boldsymbol{S}\| = (\sigma_1''^2 + \sigma_2''^2)^{1/2} \tag{3-87}$$

The corresponding yield surface (function) equation is

$$\begin{aligned} \Phi &= \sqrt{\frac{3}{2}\|\boldsymbol{S}\|^2} - \sigma_y = 0 \\ &= \sqrt{\frac{3}{2}}(\sigma_1''^2 + \sigma_2''^2)^{1/2} - \sigma_y = 0 \end{aligned} \tag{3-88}$$

which geometrically describes a cylindrical surface of radius $\sqrt{\frac{2}{3}}\sigma_y$ which axis is equally apart from the σ_1'', σ_2'' and σ_3'' coordinate axis.

Figure 3.1 summarizes the return mapping algorithm used. As shown, the cylindrical yield surface with hydrostatic axis expands in the radial direction, depending on σ_y value. Thus, considering a stress tensor σ_n, that lies on the initial yield surface, it can be achieved under two different circumstances. First, a fully elastic behavior that reaches the maximum admissible value before yielding or a previous plastic stress state is already corrected by the return-mapping.

Imposing a $\boldsymbol{\Delta\epsilon}$ strain increment, the trial stress tensor ($\boldsymbol{\sigma}_{n+1}^{trial}$) can be obtained and is verified if it lies outside the yield surface. In this case, a return mapping is required. After a new stretched surface is found using the plastic multiplier ($\Delta\gamma$) as well as the correction of the stress in eq. (3-65) by recapping to lie on the surface. In the case of a bilinear material, the plastic multiplier can be obtained in a closed formula and no need for the Newton-Raphson iteration algorithm and the radial return mapping, as geometrically described in fig. 3.1.

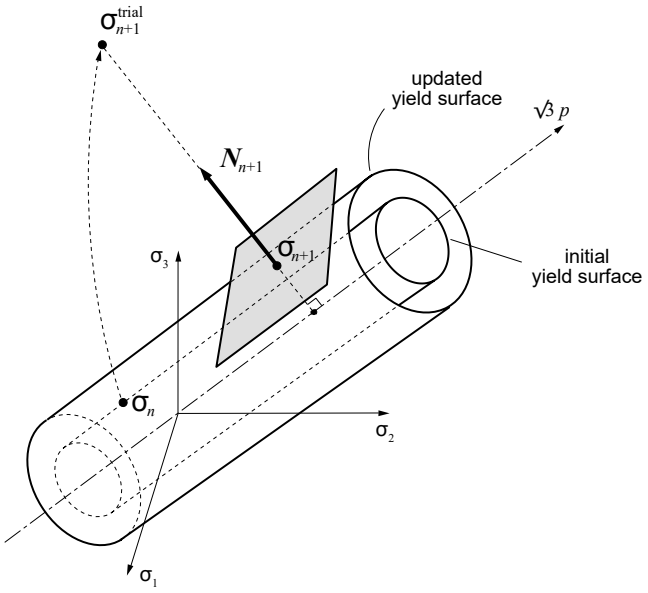

Figure 3.1: The implicit elastic predictor,return-mapping scheme for the von Mises model. Geometric interpretation is in principal stress space. Figure from [2]

Considering this same geometric procedure, seeing in the π-plane representation, the plastic multiplier $\Delta\gamma$ factor for a constant H is observed, as shown in fig. 3.2.

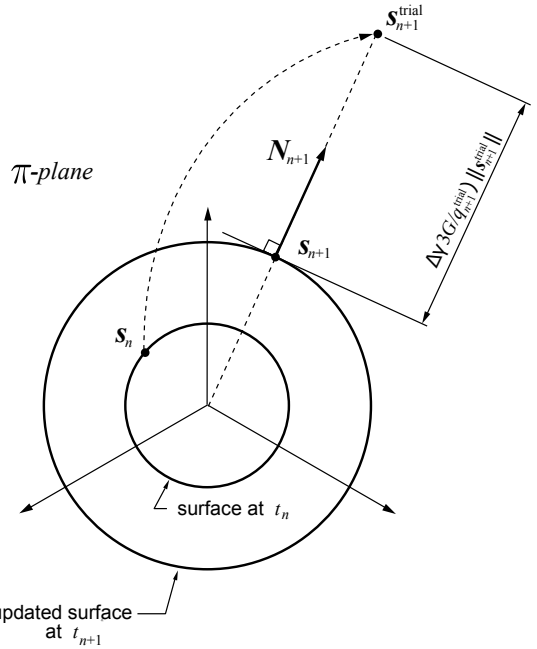

Figure 3.2: The implicit elastic predictor,return-mapping scheme considering the von Mises model. Geometric interpretation in principal stress space. Figure from [2]

3.2.3 Consistent Tangent Operator

To evaluate the constitutive relation, that varies in an elastoplastic problem, the Consistent Tangent Operator(CTO) [2] is a suitable numerical procedure that derives the analytical expression of the algorithm constitutive relation.

Recalling the stress tensor decomposition in eq. (3-8), rewriting it for both the corrected and *trial* states one obtains

$$\begin{cases} \boldsymbol{\sigma}_{n+1} = \boldsymbol{S}_{n+1} + \boldsymbol{\sigma}_{\mathrm{v}} \\ \boldsymbol{\sigma}^{trial}_{n+1} = \boldsymbol{S}^{trial}_{n+1} + \boldsymbol{\sigma}_{\mathrm{v}} \end{cases} \tag{3-89}$$

and substituting the unchanged hydrostatic tensor from eq. (3-89), the result is

$$\boldsymbol{\sigma}_{n+1} = \boldsymbol{S}_{n+1} - \boldsymbol{S}^{trial}_{n+1} + \boldsymbol{\sigma}^{trial}_{n+1} \tag{3-90}$$

Bringing in, $\boldsymbol{S}_{n+1}$ from eq. (3-64), $\boldsymbol{S}^{trial}_{n+1}$, from eq. (3-51) and using the deviatoric identity operator into eq. (3-90) one ends to

$$\begin{aligned} \boldsymbol{\sigma}_{n+1} &= -\frac{\Delta\gamma\ 3G}{q^{trial}_{n+1}} 2G \underbrace{\boldsymbol{\epsilon}^{e\ trial}_{d\ n+1}}_{\boldsymbol{I}_d : \boldsymbol{\epsilon}^{e\ trial}_{n+1}} + \boldsymbol{D}^e : \boldsymbol{\epsilon}^{e\ trial}_{n+1} \\ &= \left(\boldsymbol{D}^e - \frac{\Delta\gamma\ 6G^2}{q^{trial}_{n+1}} \boldsymbol{I}_d \right) : \boldsymbol{\epsilon}^{e\ trial}_{n+1} \end{aligned} \tag{3-91}$$

which is the constitutive relation between the corrected stress tensor in respect to the trial elastic strain tensor. In the return-mapping algorithm the predicted strain remains unchanged while the stress tensor is adjusted to the correct state. Thus, the algebraically derivation of CTO is obtained from

$$\frac{\partial \boldsymbol{\sigma}_{n+1}}{\partial \boldsymbol{\epsilon}^{e\ trial}_{n+1}} = \frac{\partial}{\partial \boldsymbol{\epsilon}^{e\ trial}_{n+1}} \left[\left(\boldsymbol{D}^e - \frac{\Delta\gamma\ 6G^2}{q^{trial}_{n+1}} \boldsymbol{I}_d \right) : \boldsymbol{\epsilon}^{e\ trial}_{n+1} \right] \tag{3-92}$$

which results in, since $\Delta\gamma$ and q^{trial}_{n+1} are dependable of $\boldsymbol{\epsilon}^{e\ trial}_{n+1}$, after applying the chain rule,

$$\begin{aligned} \frac{\partial \boldsymbol{\sigma}_{n+1}}{\partial \boldsymbol{\epsilon}^{e\ trial}_{n+1}} = \boldsymbol{D}^e - \frac{\Delta\gamma\ 6G^2}{q^{trial}_{n+1}} \boldsymbol{I}_d - \frac{6G^2}{q^{trial}_{n+1}} \left(\frac{\partial \Delta\gamma}{\partial \boldsymbol{\epsilon}^{e\ trial}_{n+1}} \boldsymbol{I}_d \otimes \boldsymbol{\epsilon}^{e\ trial}_{n+1} \right) \\ + 6G^2 \Delta\gamma\ (q^{trial}_{n+1})^{-2} \frac{\partial q^{trial}_{n+1}}{\partial \boldsymbol{\epsilon}^{e\ trial}_{n+1}} \boldsymbol{I}_d \otimes \boldsymbol{\epsilon}^{e\ trial}_{n+1} \end{aligned} \tag{3-93}$$

In eq. (3-93) two derivatives need to be computed. First, considering q^{trial}_{n+1} with respect to $\boldsymbol{\epsilon}^{e\ trial}_{n+1}$. From the definition of q^{trial}_{n+1} on eq. (3-63) into eq. (3-27)

gives

$$q_{n+1}^{trial} = 2G\sqrt{\frac{3}{2}}\left\|\boldsymbol{\epsilon}_{d\ n+1}^{e\ trial}\right\| \tag{3-94}$$

and its required derivative is:

$$\begin{aligned}\frac{\partial q_{n+1}^{trial}}{\partial \boldsymbol{\epsilon}_{n+1}^{e\ trial}} &= 2G\sqrt{\frac{3}{2}}(\boldsymbol{\epsilon}_{d\ n+1}^{e\ trial} : \boldsymbol{\epsilon}_{d\ n+1}^{e\ trial})^{1/2} \\ &= 2G\sqrt{\frac{3}{2}}\cdot\frac{1}{2}(\boldsymbol{\epsilon}_{d\ n+1}^{e\ trial} : \boldsymbol{\epsilon}_{d\ n+1}^{e\ trial})^{-1/2}\left(\frac{\partial \boldsymbol{\epsilon}_{d\ n+1}^{e\ trial}}{\partial \boldsymbol{\epsilon}_{n+1}^{e\ trial}} : \boldsymbol{\epsilon}_{d\ n+1}^{e\ trial} + \boldsymbol{\epsilon}_{d\ n+1}^{e\ trial} : \frac{\partial \boldsymbol{\epsilon}_{d\ n+1}^{e\ trial}}{\partial \boldsymbol{\epsilon}_{n+1}^{e\ trial}}\right) \\ &= 2G\sqrt{\frac{3}{2}}\cdot\frac{1}{2}\frac{1}{\left\|\boldsymbol{\epsilon}_{d\ n+1}^{e\ trial}\right\|}2\left(\boldsymbol{\epsilon}_{d\ n+1}^{e\ trial} : \frac{\partial \boldsymbol{\epsilon}_{d\ n+1}^{e\ trial}}{\partial \boldsymbol{\epsilon}_{n+1}^{e\ trial}}\right)\end{aligned} \tag{3-95}$$

Moreover, eq. (3-95) still requires the following explicit derivative. Thus, using the definition of deviatoric identity as presented in section 3.1.3

$$\begin{aligned}\frac{\partial \boldsymbol{\epsilon}_{d\ n+1}^{e\ trial}}{\partial \boldsymbol{\epsilon}_{n+1}^{e\ trial}} &= \frac{\partial}{\partial \boldsymbol{\epsilon}_{n+1}^{e\ trial}}(\boldsymbol{I}_d : \boldsymbol{\epsilon}_{n+1}^{e\ trial}) \\ &= \left(\frac{\partial \boldsymbol{I}_d}{\partial \boldsymbol{\epsilon}_{n+1}^{e\ trial}} : \boldsymbol{\epsilon}_{n+1}^{e\ trial} + \boldsymbol{I}_d : \underbrace{\frac{\partial \boldsymbol{\epsilon}_{n+1}^{e\ trial}}{\partial \boldsymbol{\epsilon}_{n+1}^{e\ trial}}}_{\boldsymbol{I}}\right) \\ &= \boldsymbol{I}_d\end{aligned} \tag{3-96}$$

that brought to eq. (3-95) gives

$$\begin{aligned}\frac{\partial q_{n+1}^{trial}}{\partial \boldsymbol{\epsilon}_{n+1}^{e\ trial}} &= 2G\sqrt{\frac{3}{2}}\frac{1}{\left\|\boldsymbol{\epsilon}_{d\ n+1}^{e\ trial}\right\|}(\boldsymbol{\epsilon}_{d\ n+1}^{e\ trial} : \boldsymbol{I}_d) \\ &= 2G\sqrt{\frac{3}{2}}\frac{\boldsymbol{\epsilon}_{d\ n+1}^{e\ trial}}{\left\|\boldsymbol{\epsilon}_{d\ n+1}^{e\ trial}\right\|}\end{aligned} \tag{3-97}$$

Recalling from eqs. (3-46) and (3-61) that the normal tensor $\boldsymbol{N}_{n+1}$ is also a function of the deviatoric *trial* state and, moreover, that from eq. (3-27) the deviatoric *trial* state can be expressed as a function of the deviatoric strain, the following is then observed.

$$\boldsymbol{N}_{n+1} = \sqrt{\frac{3}{2}}\frac{\boldsymbol{S}_{n+1}^{trial}}{\|\boldsymbol{S}_{n+1}^{trial}\|} = \sqrt{\frac{3}{2}}\frac{\boldsymbol{\epsilon}_{d\ n+1}^{e\ trial}}{\left\|\boldsymbol{\epsilon}_{d\ n+1}^{e\ trial}\right\|} \tag{3-98}$$

Since the above normal tensor $\boldsymbol{N}_{n+1}$ is not a unit vector a convenient definition can be used.

$$\bar{\boldsymbol{N}}_{n+1} = \sqrt{\frac{2}{3}}\boldsymbol{N}_{n+1} = \frac{\boldsymbol{S}^{trial}_{n+1}}{\|\boldsymbol{S}^{trial}_{n+1}\|} = \frac{\boldsymbol{\epsilon}^{e\ trial}_{d\ n+1}}{\left\|\boldsymbol{\epsilon}^{e\ trial}_{d\ n+1}\right\|} \tag{3-99}$$

and eq. (3-97) is rewritten as function of $\bar{\boldsymbol{N}}_{n+1}$ as

$$\frac{\partial q^{trial}_{n+1}}{\partial \boldsymbol{\epsilon}^{e\ trial}_{n+1}} = 2G\sqrt{\frac{3}{2}}\bar{\boldsymbol{N}}_{n+1} \tag{3-100}$$

Also, in eq. (3-93) the derivative of $\frac{\partial \Delta\gamma}{\partial \boldsymbol{\epsilon}^{e\ trial}_{n+1}}$ should be evaluated. As in eq. (3-65), $\Delta\gamma$ results from the solution of the return-mapping algorithm as

$$\Phi = q^{trial}_{n+1} - 3G\Delta\gamma - \sigma_y(\bar{\epsilon}^p_n + \Delta\gamma) \tag{3-101}$$

linearising the curve σ_y in each iteration, using the hardening slope H, defined in eq. (3-66), we have

$$\Phi = q^{trial}_{n+1} - 3G\Delta\gamma - \sigma_y(\bar{\epsilon}^p_n) - H\Delta\gamma = 0 \tag{3-102}$$

As a result, isolating $\Delta\gamma$ from the linearised eq. (3-102) gives:

$$\begin{aligned}
\frac{\partial \Delta\gamma}{\partial \boldsymbol{\epsilon}^{e\ trial}_{n+1}} &= \frac{\partial}{\partial \boldsymbol{\epsilon}^{e\ trial}_{n+1}}\left(\frac{q^{trial}_{n+1} - \sigma_y(\bar{\epsilon}^p_n)}{3G + H}\right) \\
&= \frac{1}{3G + H}\frac{\partial q^{trial}_{n+1}}{\partial \boldsymbol{\epsilon}^{e\ trial}_{n+1}} \\
&= \frac{2G}{3G + H}\sqrt{\frac{3}{2}}\bar{\boldsymbol{N}}_{n+1}
\end{aligned} \tag{3-103}$$

Finaling binging in the results from eqs. (3-100) and (3-103), and substituting the definition of $\bar{\boldsymbol{N}}_{n+1}$ from eq. (3-99), eq. (3-93) results

$$\begin{aligned}
\frac{\partial \boldsymbol{\sigma}_{n+1}}{\partial \boldsymbol{\epsilon}^{e\ trial}_{n+1}} = \boldsymbol{D}^e - \frac{\Delta\gamma 6G^2}{q^{trial}_{n+1}}\boldsymbol{I}_d - 6G^2\Bigg(\frac{2\cancel{G}}{3G + H}\sqrt{\frac{\cancel{3}}{2}}\bar{\boldsymbol{N}}_{n+1} \otimes \frac{1}{2\cancel{G}\sqrt{\frac{\cancel{3}}{2}}} \cdot \frac{\overbrace{\boldsymbol{\epsilon}^{e\ trial}_{d\ n+1}}^{\bar{\boldsymbol{N}}_{n+1}}}{\left\|\boldsymbol{\epsilon}^{e\ trial}_{d\ n+1}\right\|}\Bigg) \\
+ \frac{6G^2\Delta\gamma}{q^{trial}_{n+1}}\Bigg(2\cancel{G}\sqrt{\frac{\cancel{3}}{2}}\bar{\boldsymbol{N}}_{n+1} \otimes \frac{1}{2\cancel{G}\sqrt{\frac{\cancel{3}}{2}}} \cdot \underbrace{\frac{\boldsymbol{\epsilon}^{e\ trial}_{d\ n+1}}{\left\|\boldsymbol{\epsilon}^{e\ trial}_{d\ n+1}\right\|}}_{\bar{\boldsymbol{N}}_{n+1}}\Bigg)
\end{aligned} \tag{3-104}$$

which after proper simplifications gives the algorithm for the elastoplastic constitutive relation, considering softening of the material, in its final and formal form:

$$\boldsymbol{D}^{ep} = \boldsymbol{D}^{e} - \frac{\Delta\gamma\ 6G^2}{q_{n+1}^{trial}}\boldsymbol{I}_d + 6G^2\left(\frac{\Delta\gamma}{q_{n+1}^{trial}} - \frac{1}{3G+H}\right)\bar{\boldsymbol{N}}_{n+1}\otimes\bar{\boldsymbol{N}}_{n+1} \tag{3-105}$$

4
The Finite Element Method

Finite elements is a numerical procedure, widely used in structural analysis, to evaluate and represent an structure capacity to support loading under prescribed support conditions. Mathematically, the method results from applying the partial differential equation from elasticity into the Galerkin method [1]. Alternatively, a simpler and effective derivation can be achieved by applying the Principle of Virtual (or infinitesimal variation) Displacements, that states

$$\delta U = \delta W + \delta Q \tag{4-1}$$

where U is the system internal energy Q the energy dissipation and W the work on the system by external loadings. Considering a system with no energy dissipation, eq. (4-1) reduces to

$$\delta U = \delta W \therefore \delta(U - W) = 0 \tag{4-2}$$

From the above equation, an energy functional Π may be defined as

$$\Pi = U - W \quad / \quad \delta\Pi = 0 \tag{4-3}$$

In a structural problem where body, surface and concentrated forces are present, the variation of the energy functional can be written as, [1]

$$\int \delta\boldsymbol{\epsilon}^T \cdot \boldsymbol{\sigma}\ dV - \underbrace{\int_V \delta\boldsymbol{u}^T \cdot \boldsymbol{f}^B\ dV}_{\text{body force work}} - \underbrace{\int_S \delta\boldsymbol{u}^T \cdot \boldsymbol{f}^S\ dv}_{\text{surface force work}} - \underbrace{\sum_{i=1}^{n} \delta\boldsymbol{u}_i^T \cdot \boldsymbol{R}_i^C}_{\text{concentrated force work}} = 0 \tag{4-4}$$

In the equation above a continuum domain is considered. However, to solve it numerically, the state variable should no longer be continuum but discretized. In Finite Elements Methods (FEM) discrete displacements are solved in the nodes of each element m ($\hat{\boldsymbol{u}}^{(m)}$) which are interpolated for a continuum displacement vector ($\boldsymbol{u}^{(m)}$). Thus,

$$\boldsymbol{u}^{(m)} = \boldsymbol{H}^{(m)} \cdot \hat{\boldsymbol{u}}^{(m)} \tag{4-5}$$

where $\boldsymbol{H}^{(m)}$ is, in this particular study, the Lagrange's functions defined in a given coordinate system.

From small strain definitions, strain vectors result from the derivatives of continuum displacements with respect to the system coordinates. As a result we have

$$\boldsymbol{\epsilon}^{(m)} = \boldsymbol{B}^{(m)} \cdot \hat{\boldsymbol{u}}^{(m)} \tag{4-6}$$

where $\boldsymbol{B}^{(m)}$ is a transformation matrix obtained from derivatives of Lagrange's functions interpolation.

For the constitutive stress-strain relation, established from elasticity, $\boldsymbol{\sigma} = \boldsymbol{D} \cdot \boldsymbol{\epsilon}$ rewritten by considering the discretization in eq. (4-6) and initial residual stress as ($\boldsymbol{\sigma}_I$) we have.

$$\boldsymbol{\sigma}^{(m)} = \boldsymbol{\sigma}_I^{(m)} + \boldsymbol{D}^{(m)}\ \boldsymbol{B}^{(m)}\ \hat{\boldsymbol{u}} \tag{4-7}$$

Taking the variational after transposing eqs. (4-5), (4-6) and considering the constitutive eq. (4-7); functional Π in eq. (4-4) is rewritten in elements contribution as

$$\begin{aligned}\sum_{m=1}^{M} \int_{V^{(m)}} \delta\hat{\boldsymbol{u}}^T\ \boldsymbol{B}^{(m)\ T}(\boldsymbol{\sigma}_I^{(m)} + \boldsymbol{D}^{(m)}\ \boldsymbol{B}^{(m)}\ \hat{\boldsymbol{u}})\ dV^{(m)} = \\ \sum_{m=1}^{M} \int_{V^{(m)}} \delta\hat{\boldsymbol{u}}^T \boldsymbol{H}^{(m)\ T}\ \boldsymbol{f}^B dV^{(m)} + \sum_{m=1}^{M} \int_{S^{(m)}} \delta\hat{\boldsymbol{u}}^T \boldsymbol{H}^{(m)\ T}\ \boldsymbol{f}^S dS^{(m)} \\ + \sum_i \delta\hat{\boldsymbol{u}}^T\ \boldsymbol{R}_C^i\end{aligned} \tag{4-8}$$

that provides the stiffness matrix, body forces, surface forces, concentrated forces and initial internal forces.

$$\begin{aligned}\left[\sum_{m=1}^{M} \underbrace{\int_{V^{(m)}} \boldsymbol{B}^{(m)\ T}\ \boldsymbol{D}^{(m)}\ \boldsymbol{B}^{(m)\ T}\ dV^{(m)}}_{\boldsymbol{K}^{(m)}}\right] \hat{\boldsymbol{u}} = \\ \sum_{m=1}^{M} \underbrace{\int_{V^{(m)}} \boldsymbol{H}^{(m)\ T}\ \boldsymbol{f}^B\ dV^{(m)}}_{\boldsymbol{R}_B^{(m)}} + \sum_{m=1}^{M} \underbrace{\int_{S^{(m)}} \boldsymbol{H}^{(m)\ T}\ \boldsymbol{f}^S\ dS^{(m)}}_{\boldsymbol{R}_S^{(m)}} + \sum_i \boldsymbol{R}_C^i \\ - \sum_{m=1}^{M} \underbrace{\int_{V^{(m)}} \boldsymbol{B}^{(m)\ T}\ \boldsymbol{\tau}_I^{(m)}\ dV^{(m)}}_{\boldsymbol{R}_I^{(m)}}\end{aligned} \tag{4-9}$$

After assemblage of all element contribution, the global problem results in

$$\boldsymbol{K} \cdot \hat{\boldsymbol{u}} = \boldsymbol{R}_B + \boldsymbol{R}_S + \boldsymbol{R}_C - \boldsymbol{R}_I \tag{4-10}$$

where the nodal displacements are state variables to be solved for.

4.1 Small strain plasticity

In the previous section the FEM formulation for a linear elastic problem was presented and the numerical solution obtained by solving a linear system of equations.

In this work, the procedure for small strain plasticity in the FEM is added to the infinitesimal approach, without considering the non-linearities due to geometry change. In this case, the global stiffness matrix in the structural discretization remains constant as in linear FEM.

The resulting equilibrium equation to solve presents a constitutive stress dependent matrix that requires, the use of an iterative algorithm. For this application, the most popular is the Newton-Raphson algorithm with load control, which was used throughout this work.

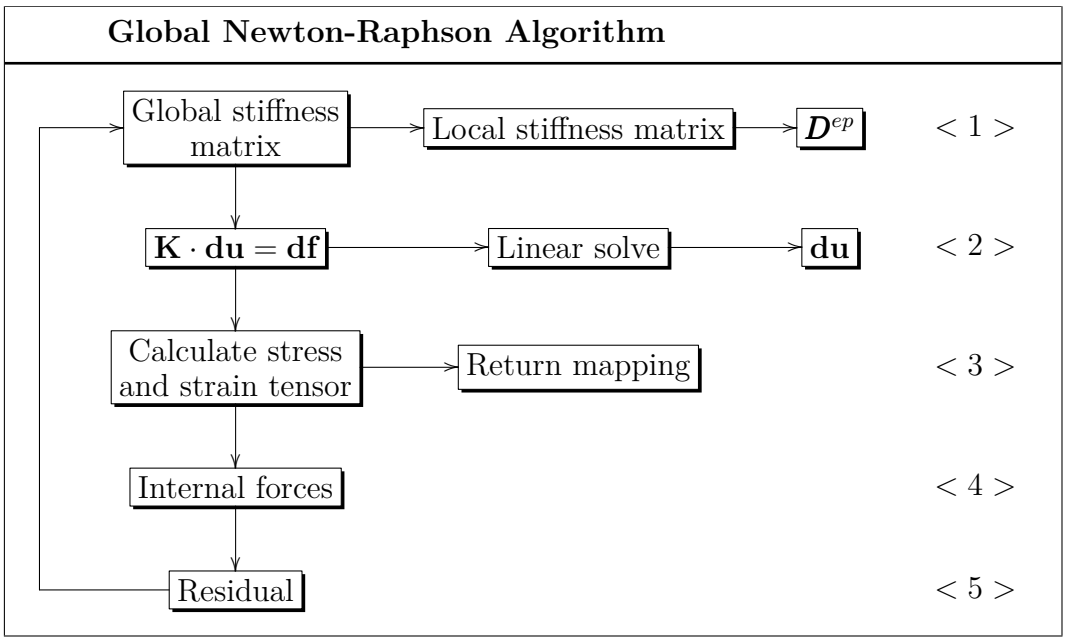

Similarly, the schematic overview presented in flowchart shows how the cycle of the iterations is performed. In step $< 1 >$, the structure global stiffness matrix is obtained by the regular local element stiffness matrix assemblage. As already discussed in section 3.2.3, during the material hardening evolution the constitutive stress-strain relation changes and the derivation of a Consistent Tangent Operator is required.

In large scale simulations, the efficiency of employed numerical algorithms must be of consideration in this regard, the modified Newton-Raphson iteration procedure is preferable because of large computer efforts required in the assemblage of the total stiffness matrix. However, the use of the CTO significantly reduces the number of iterations.

Therefore, for a given external load increment and the obtained global stiffness matrix, the displacement incremental vector **du** is obtained by using a linear solver as in step $< 2 >$ in the flowchart.

Using **du** vector, strain and stress tensors are obtained. However, as in this step $< 3 >$, resides main difference from the elastoplastic analysis when compared to the regular linear FEM; an additional feature is added in the algorithm to "correct" the obtained stress and strain tensors - the return-mapping as described in section 3.2.1.

After the stress tensor compatible with the plasticity theory is obtained, convergence must be verified by verifying the obtained internal forces as to applied the external forces. This procedure is explicitly shown in steps $< 4 >$ and $< 5 >$. In case of non convergence, a new iteration procedure should be performed until convergence conditions are satisfied.

4.2 Consistent Tangent Operator

Although the CTO matrix transformation in eq. (3-105) is of a quite simple implementation, some numerical difficulties related to the return-mapping and the unloading, since interferes directly in the elastic predictor and the unload must recover original elastic relation.

To illustrate this difficulty, considering a bilinear $\sigma - \epsilon$ relation shown the the stress after applied first load increment is higher than the material yield stress a stress correction is required and a new stress-strain slope can be computed, by using CTO. However, as indicated in fig. 4.1, for the next load increment, the constitutive relation is parallel to the material hardening and there is no need for the return-mapping to modify the stress tensor. From eq. (3-65) the dependence on the elastic parameter G, which is a function of E and ν, causes failure on imposing $\Delta\gamma = 0$, since the CTO is no longer proportional to E. Moreover, in using the return-mapping, the CTO inclination also provides no accumulated plastic strains, making the change of return-mapping non-trivial since $\Delta\gamma = 0$ is expected but accumulated plastic strain still need to be computed, see eq. (3-58). These are considerations in the loading case.

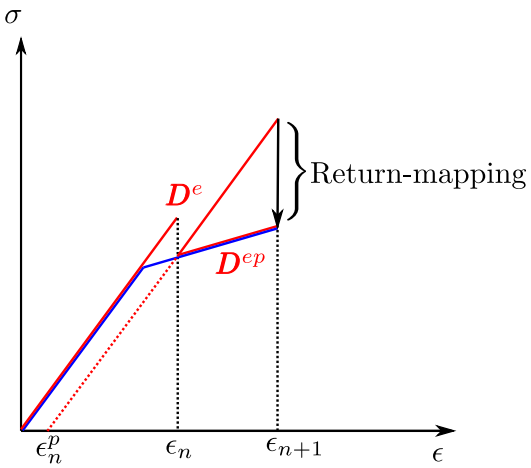

Figure 4.1: Unload recovering elastic inclination

On the other hand, when unloading is considered, the slope must be recovered as in the initial elastic; using the usual CTO procedure as defined, it results in wrong estimation as shown in fig. 4.2. If for instance, the simple example of a bar is under uni-axial traction loading and subsequent unloading, the use of a incorrect constitutive relation may result in a negative remaining residual strain, fact not physically expected.

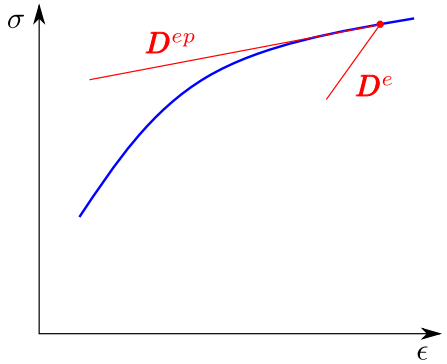

Figure 4.2: Unload recovering elastic inclination

To circumvent this difficulty, a check to verify if the stress state reached inside the yield surface can be carried out confirming if the appropriated elastic constitutive relation is used. However, this strategy is not computationally efficient because it must be performed at each evaluation point (integration points) as required. A more elegant and effective procedure is to use a two step strategy as follows. In first, the global stiffness matrix with the modified Newton-Raphson procedure is obtained from the use of CTO, and second, while computing the internal stresses from the obtained strains to use the elastic constitutive relation.

With this strategy trial stress tensor components are obtained from an elastic predictor, being consistent to the projection of the return-mapping.

This is shown in Figure 4.3 where a trial stress is computed from the elastic predictions and from the CTO, avoiding changes on the return-mapping.

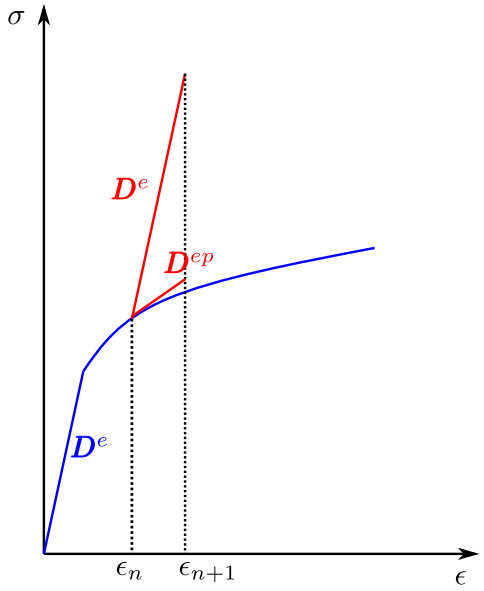

Figure 4.3: Trial stress

In case of unloading presented in fig. 4.4 the recovery of the elastic constitutive relation is naturally described. Although global stiffness is dependent of the CTO, the return-mapping is able to adjust to the expected stress value due to the elastic predictor when computing internal stresses.

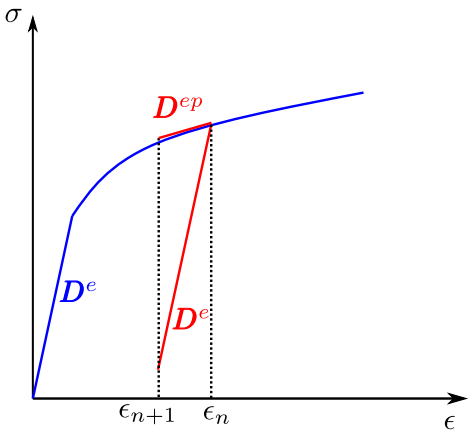

Figure 4.4: Unload recovering elastic inclination

The procedure here presented includes the use of CTO in the return-mapping presented in chapter 3 and the elastic unloading as expected in plasticity.

It is important to remark that the use of CTO is not mandatory in an elastoplastic FEM algorithm. However, it drastically reduces the computational effort involved in performing Newton-Raphson's required iterative procedure.

5
TopSim Programming Details

TopSim, developed for Topology Simulation, is a plugin based numerical simulation tool developed by the TecGraf Institute of PUC-Rio.

Plugins are software components that allow addictions of new specific features to an existing computer program. Each plug-in is itself a separate project, individually compiled, that, in executing time, the TopSim's kernel, manages the connections by the use of an interface protocol.

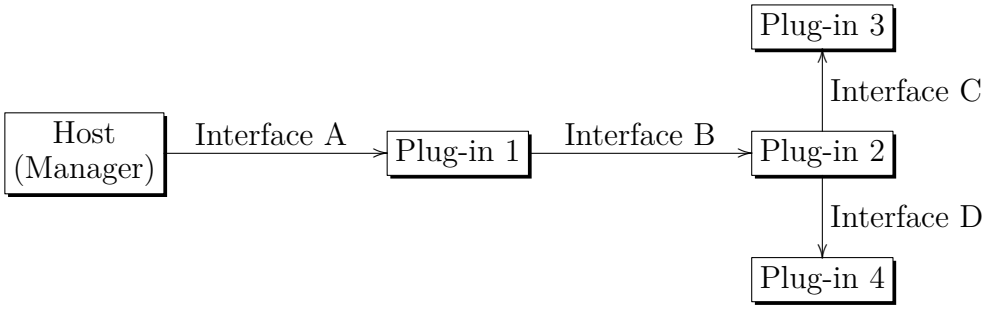

The flowchart above gives an insight into how the structure of the software works. Each plug-in, whenever an interface is loaded, can connect to the next plugin passing attributes to a new algorithm.

Applications within the use of plug-in programs are enormous. However, TopSim has its focus on numerical simulation and in this chapter, their advantages focused on structural analysis, in particular Finite Elements Method, are presented.

Complex FEM programs for all sorts of different analyses, such as large deformations, thermal analysis, and a variety of plasticity and hyperelasticity models all end up having some difficulties in arranging the application. Usually, there are two possible solutions. The first is a neutral file setting parameters to the analysis, which requires pre-existing processing in the reader that must be able to read all the necessary conditions. Moreover, in every new implementation, the reader must be adjusted according to the new condition. Another possibility, very inefficient let say, is the use of a general case that covers a simple one. A linear elastic problem can be modeled as a large strain whenever the nonlinear portion is numerically insignificant. Similarly, plasticity can be removed from the simulation by defining yield stress bigger enough to

never be reached, as well as imposing a change of temperature being zero in a thermal problem. Although the results do not present numerical changes, irrelevant calculations must be performed such as the contribution of large deformation, the check of plasticity, and a contribution that is zero due to the temperature change, increasing the time of the simulation.

The Plugin structure allows, in a very simple but elegant way, to organize a numerical simulation. There is no need for a reader previously to know the analysis, since a load of a plugin, in execution time, solves the calling of the respective plug-in through interfaces. Because plugin must be independent, this allows others to implement new features without having the source code. When it comes to the second solution, from the paragraph above, a simple linear FEM case can be run by not linking more complex plug-ins like large deformations, plasticity, and thermal in the analysis.

The focus of this dissertation is on the implementation and testing of an additional plugin for the 3D Isotropic von Mises Plasticity. Originally, any material nonlinearity was implemented in the TopSim. In this work, the Return-Mapping algorithm and Consistent Tangent Operator are implemented as previously illustrated in the flow chart of section 4.1. It is important to remark that other important features are already available on TopSim, such as large displacement and large deformation analysis compatibilities.

Traceability is an important feature in a large simulation program, in which every step of an additional model must be validated. In Appendix G several FEM solutions are presented and evaluated with the corresponding analytical solutions including the linear elasticity, strain energy calculations, and elastoplastic problem analysis.

6
Numerical Results

In this chapter, the simulation of a cracked specimen using the procedures presented in chapter 4 and employing the finite element modeling discussed is presented. Details of the implemented model are also discussed to achieve better and realistic stress and strain fields occurring at the region ahead of the crack tip.

Regarding the material constitutive behavior in Fracture Mechanics, in the literature concerning analytical solutions, two approaches are concerned: the Linear Elastic Fracture Mechanics (LEFM) with theoretical solutions offered in Williams, sec. 2.2.1 and Creager-Paris, sec. 2.2.1.1, and the Elasto-plastic Fracture Mechanics (EPFM) HRR solutions, published in sec. 2.3.2.

The important hypothesis of each analytical solution has already been discussed in the respective section over verifying equilibrium, boundary condition, singularity, and non-singularity and neglecting elastic contribution.

The finite element model employed in the numerical analysis considered: a) no enrichment in the element's interpolation function subspace, a procedure used to represent a possible stress singularity occurrence at the crack tip where plasticity occurs due to blunting, as loading increases; and b) the use of material models including plasticity effects to obtain a realistic specimen's mechanical behavior, by considering the material peculiarities close to the tip of the crack.

Due to the occurrence of high-stress component values (stress concentration) at a short region of the cracked specimen, the material ought to have a plastic behavior in a plastic zone. The high-stress gradient in this region, required, in the present analysis discretization, the use of second-order 10-node tetrahedron elements ($T10$).

The specimen geometry considered is shown in fig. 6.1. Due to symmetry, only one-fourth is represented, consisting of a tensioned central cracked plate under a self-equilibrated, distributed, loading applied in the direction normal to the crack. Thus, in this case, K_I and J are well-known parameters, as shown in Appendix H and I.

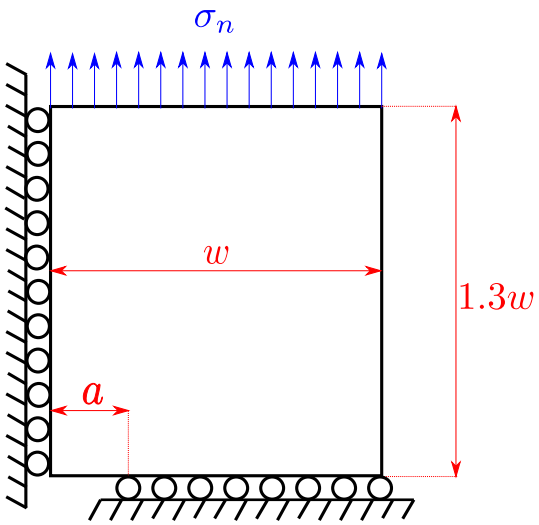

Figure 6.1: Geometric and physical parameters used in the numerical analysis. 1/4 of the model was considered with thickness t.

The material hardening law employed is described by dimensionless Ramberg-Osgood, as in eq. (2-29), same as in HRR derivations. Numerical parameters for this simulation are presented in table 6.1.

Parameters		
Variables	**Num. Values**	**Units**
σ_n	$180 \cdot 10^6$	Pa
E	$210 \cdot 10^9$	Pa
σ_y	$300 \cdot 10^6$	Pa
α	$0.02 \cdot 10^9$	Pa
n	13	–
a	0.025	m
w	0.1	m
t	0.01	m

Table 6.1: Geometric, material and load parameters

In the next sections, different approaches to the problem solution are presented and the results compared to the classical formulation whenever applicable. The finite element model employed 51.310 elements with 77.468 nodes resulting in 228.361 active degrees-of-freedoms.

The result presentation comprises three main objectives: first, the distribution of σ_{yy} along the specimen residual ligament is evaluated by comparing to various other proposed methods; second, the prediction of the plastic zone shape is evaluated; and, third a plot the $\sigma\epsilon$ relation, under monotonic loading and under cyclic loadings are presented and discussed.

For the analysis result presentation points ahead of the crack, located at distances from the tip in multiples of the plastic zone length, are considered. The following fig. 6.2 presents these point locations showing by different colors the material in two regimens, plastic or elastic. Notice that the mid-section plastic zone length is used as the reference length of the plastic zone. Thus, in this regard, as shown in fig. 6.2, point $80\%p_z$ on the upper surface is, in fact, under the elastic regime due to the parabolic-like shape of the plastic zone throughout the cross-section.

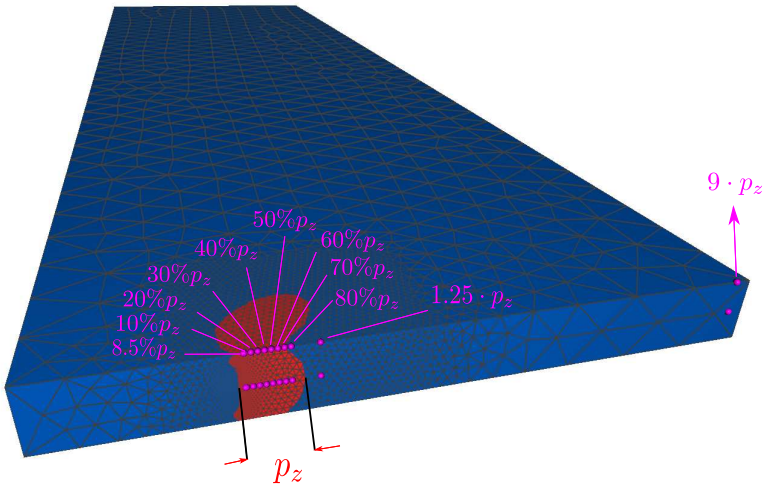

Figure 6.2: Points multiples of the length of plastic zone. Blue elastic and red plastic

6.1 Residual Ligament Evaluation

In this section, the numerically obtained stresses and strains varying along the specimen residual ligament are evaluated considering: at full ligament, at the plastic zone, and, finally, close to the crack tip. Over the length of full ligament, where the material is in the elastic regime since the

$$p_z = 8.06 \cdot 10^{-3}\ m \tag{6-1}$$

the specimen bound is roughly $9 \cdot p_z$, fig. 6.2. Besides the elastoplastic HRR field, William and Creager-Paris, linear elastic solution, are also present in the

comparison.

Concerning Creager-Paris analytical model, the curvature of the blunted crack is obtained from the finite element analysis considering y-direction displacements along the length of the crack stress-free face, as in fig. 6.3

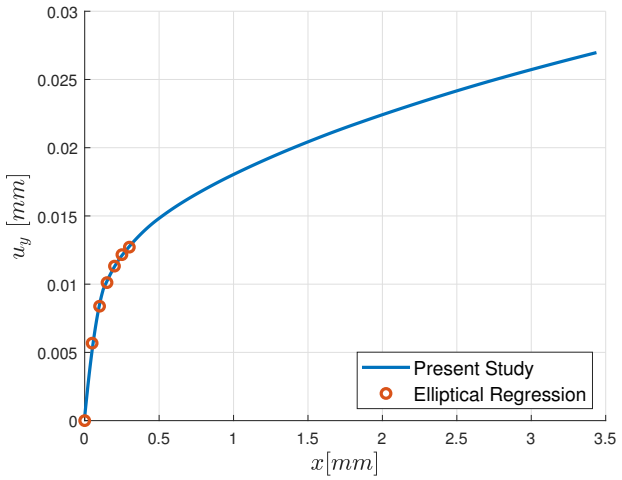

Figure 6.3: Path plot of σ_{yy} as function of the residual ligament

From the results close to the crack tip, a regression is performed by applying an optimization algorithm, a nonlinear least-squares solver, to reduce the error between FEM data and the equation of an ellipse which obtained geometric parameters are in the table 6.2.

Ellipse Parameters		
Geometric parameters	**Value**	**Unit**
a	$3.7401 \cdot 10^{-4}$	m
b	$1.3070 \cdot 10^{-5}$	m
c	$3.7378 \cdot 10^{-4}$	m
ρ	$4.5675 \cdot 10^{-7}$	m

Table 6.2: Geometric parameters of the ellipse

Thus, a comparison of numerically obtained results with the solutions from Williams, eq. (2-7), Creager-Paris, eq. (2-11) and HRR, eq.(2-27) for stress σ_{yy}, in plane-stress conditions, is presented in fig. 6.4

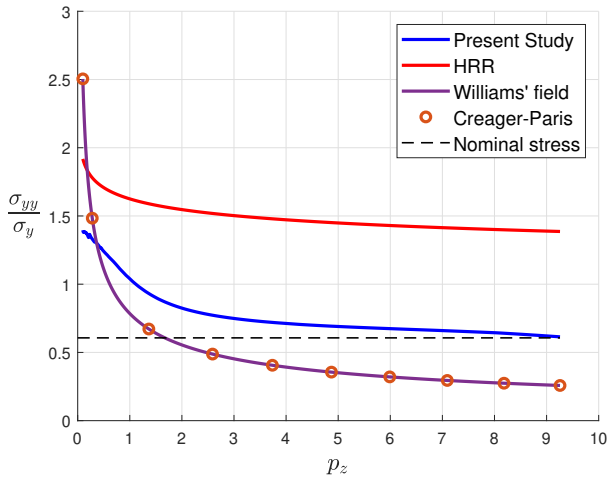

Figure 6.4: Path plot of σ_{yy}/σ_y as function of the residual ligament

From these results, it may be observed that all three analytical solutions do not guarantee the correct boundary condition at $9 \cdot p_z$, as expected by the applied stress nominal value, indicated the dashed line. On the other hand, this same condition is adequately satisfied by the FEM solution, with validation of Saint-Venant's principle.

As discussed earlier in section 2.2.1, equilibrium is no longer guaranteed by the analytical solutions once it is only valid at a region close to the crack tip. From graph 6.4, it can be inferred that the Williams solution is exact to the numerical in $0.36 \cdot p_z$. In the case of the HRR field, which uses elasticity formulation, the solution along the residual ligament is quite different from what is expected from the numerical analysis, predicting plastic collapse over the cross-section.

Although the Creager-Paris model provides a non-singular analytical solution because of the assumed curvature at the crack tip, significant differences to Williams' solution are observed, reinforcing the use of an elastoplastic behaviour, since not only a non-singular approach is necessary.

Restricting our observation of the results in fig. 6.4 to the region about the plastic zone where FEM and HRR solutions are of significance, which is shown in fig. 6.5

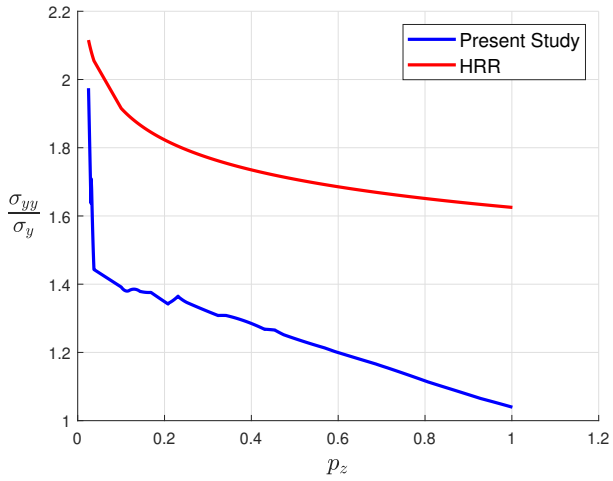

Figure 6.5: Path plot of σ_{yy} as function of the residual ligament

As shown, discrepancies between the results are quite large in this region, with an error difference even though elastic contributions have been neglected in the analytical solution presented.

In evaluating the numerical results very close to the crack tip, solutions by McMeeking and Parks [30] were used, which presents numerical results using 2D elastoplastic FEM with small and large scale yielding for both stress and strain plane conditions. As a reference, the geometric and material parameters for this simulation were adapted for the respective value of the paper [30]. In this case, only, new geometric and material parameters are present in the table above.

Parameters		
Variables	**Num. Values**	**Units**
σ_n	$180 \cdot 10^6$	Pa
E	$120 \cdot 10^9$	Pa
σ_y	$400 \cdot 10^6$	Pa
α	$0.02 \cdot 10^9$	Pa
n	10	–
a	0.05	m
w	0.1	m
t	0.01	m

Table 6.3: Geometric, material and load parameters

Figure 6.6 presents a comparison of normalized stresses as a function of the normalized position along the residual ligament for three model solutions: the HRR, the FEM, and the numerical results obtained by McMeeking and Parks [30], which legends are on table 6.4. The curve in green is a case when considering small-scale yielding.

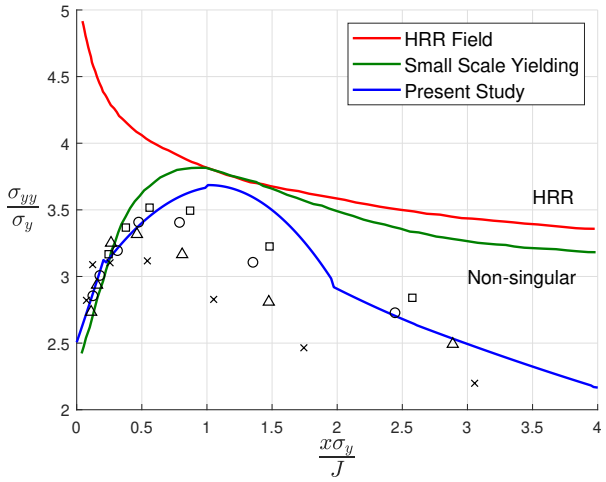

Figure 6.6: Normal stress on plane ahead of crack tip versus distance for center-cracked panel with $\sigma_y/E = 1/300$ and $a/w = 0.5$

Numerical Parameters	
Symbol	$\frac{w-a}{J/\sigma_y}$
□	537
○	286
△	177
×	64

Table 6.4: Legend of graph 6.6 with numerical points from Parks [30]

The curve in blue presents FEM elastoplastic solution in 3D FEM simulation. Because this 3D solution assumes straining restrictions in the direction transverse to the specimen plane this results in higher plasticity but does not smooth stresses as much as a large strain approach. Moreover, the blue curve has its peak approximately in the same coordinate as the green curve.

These numerical results are compatible with the dispersed numerical data from the graph and predict a high error when comparing to HRR at the bottom right of graph 6.6, also previously noticed in fig. 6.5.

6.2 The Plastic Zone Identification

Plastic zones (p_z) in cracked specimens are associated with damage mechanics. In this section analytical estimations of shape and size are presented and compared to the FEM numerical results.

As discussed earlier in chapter 2, section 2.4.1, the material elastoplastic frontier Williams obtained, using polar coordinates to define the space upfront the crack tip, a pair of functions r and θ that defines the material in plastic regime.

The second proposal [5] is partially considered the boundary condition, by the addition of the nominal stress in y direction into the original Williams' field. Despite this procedure being simplistic for not presenting a rigorous stress analysis, this approach obeys the far-field boundary.

When considering a plastic zone by defining the elastoplastic frontier, the stress inside p_z remains unchanged with both procedures above, differently from a classical perfectly plastic approach that defines a maximum value of stress. To consider a constant value of stress inside, the stress field must be rearranged to verify equilibrium. In this case, applying Irwin's integral, section 2.4.3, a new p_z may be defined.

In the fig. 6.7 that follows, these proposed solutions are compared to obtained finite element results. The material and geometric parameters are in the original table 6.1 presented.

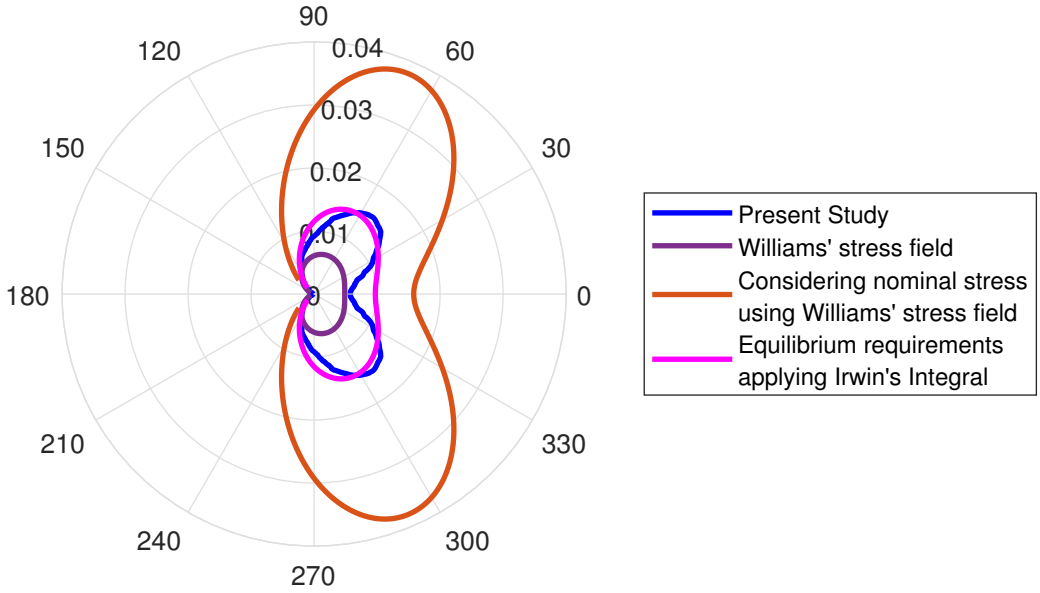

Figure 6.7: Plastic zone estimation

Analyzing the graph above, it is noticed that neither Williams nor nominal correction predicts p_z size and shape well. Although considering nomi-

nal stress is an attempt to enforce the boundary conditions, it automatically causes disequilibrium. Assuming the FEM solution as a reference, the equilibrium requirement predicts quite well the size of p_z, besides θ close to zero, while considering the nominal stress the shape of p_z. The only solution that covers simultaneously both of these corrections and prevents singular fields is the FEM.

An interesting topic that must be pointed out is the use of HRR for p_z prediction. Since the size of the thickness in this 3D simulation is small in comparison to other dimensions of the specimen, plane stress is assumed. Combining stresses σ_{yy}, σ_{xx} and σ_{xy} from HRR, it is possible to estimate the size and shape of p_z. However, the high-stress prediction due to plasticity consideration with the assumption of no transversal stress estimates unrealistic p_z. From fig. 6.4, it is noticed that HRR predicts, along all residual ligament, σ_{yy} bigger than the yield stress. Thus, when bringing the stresses into von Mises equation, assuming $\sigma_{zz} = 0$, all residual ligament is considered part of p_z.

In fact, plane stresses are idealization that differs from a realistic 3D analysis, since, due to plasticity, strain restrictions create residual stress compression transversal to the cross-section.

6.3 Stress-strain relation in Monotonic Loading

In this section, stress-strain relations are considered, measured at specific points along the residual ligament. Obtained results for the finite element numerical solutions and the analytical HRR model solutions, for measurements at the specimen upper plane and mid surface, are presented in figs. 6.8 and 6.9, respectively. Plot 6.8 corresponds to the results at the specimen surface where σ_{zz} is zero, while plot 6.9 is to the mid surface. In both figures, eleven point positions are indicated, corresponding to distances to the crack tip as percentages of the plastic region length p_z.

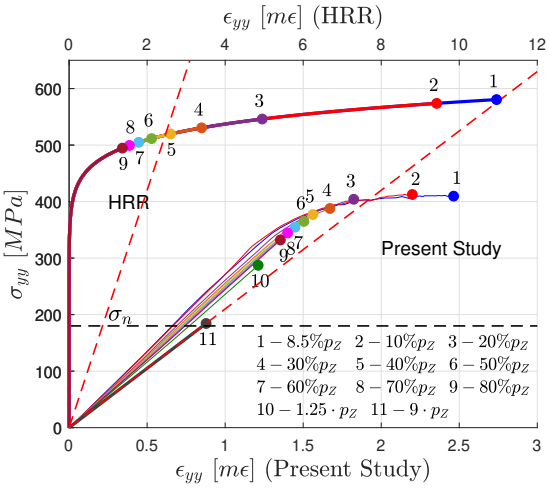

Figure 6.8: σ_{yy} *vs* ϵ_{yy} in surface section in different points ahead of the crack tip

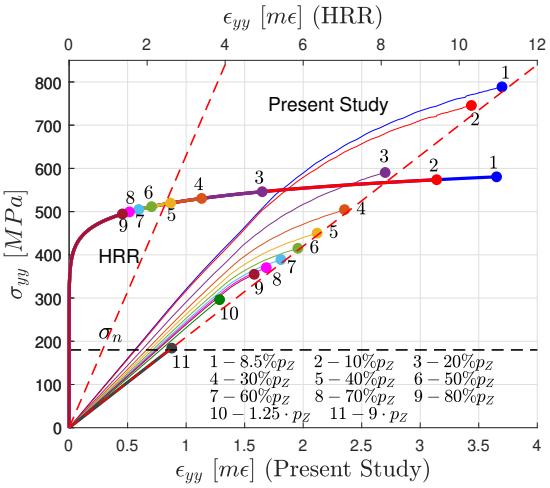

Figure 6.9: σ_{yy} *vs* ϵ_{yy} in middle section in different points ahead of the crack tip

A comparison of these results show significant differences in ϵ_{yy} and stress σ_{yy} values. However, as previously indicated, with the HRR model results a singular field in the stresses distribution and a constant tensor normal to the yield surface in principal coordinates during the loading is assumed. These conditions quite interfere in the cumulative plastic strain accounted for the material flow rule, resulting in ϵ_{yy} results with severe distortions when compared to the numerically obtained solutions.

For instance, close to the crack tip as in point 1 the HRR model predicts strains three times larger than FEM solutions, compatible with singular approach solutions when compared to non-singular formulation results. However, considering the predictions up to the frontier of the p_z strain, at points $9-80\%p_z$, for example, they are compatible with the error presented in graph

6.5 for the stresses.

In all plots show classical stress-strain relations are indicated, starting with the linear elasticity when the pair of stress and strain tensor correlates σ_{yy} and ϵ_{yy} are also proportional. Depending on the stress concentration factor, afterward, the material response is non-linear whenever plasticity is required.

Although it may sound surprising, the derivative of the curve from plots 6.8 and 6.9 (E_y) varies along x-axis or multiples of p_z and the behavior can not be predicted in a simple uniaxial tensile test.

In what follows this phenomenon is illustrated, we establish a linear relation between y-direction in 3D analysis, where the stress and strain tensor are linearly related as

$$\sigma_{yy} = E_y \cdot \epsilon_{yy} \tag{6-2}$$

In 1D analysis, ϵ and σ are related by the material Young's Modulus E_y ,in the form,

$$\sigma_{yy} = E_y \cdot \left[\frac{\sigma_{yy}}{E}\right] \tag{6-3}$$

$$E_y = E \tag{6-4}$$

Considering a multiaxial problem, this relation becomes

$$\sigma_{yy} = E_y \cdot \left[\frac{\sigma_{yy}}{E} - \frac{\nu}{E}\sigma_{xx} - \frac{\nu}{E}\sigma_{zz}\right] \tag{6-5}$$

or

$$E_y = \frac{\sigma_{yy}}{\frac{\sigma_{yy}}{E} - \frac{\nu}{E}\sigma_{xx} - \frac{\nu}{E}\sigma_{zz}} \tag{6-6}$$

with E_y as a function of normal stress components. Consequently, a change in one of these parameters causes changes in the E_y which varies with x position along the cross-section. This fact is illustrated by the simple example shown in Table 6.5. Here numerically obtained stress components for $0.7p_z$ and $1.25p_z$ positions in the upper plane are presented with the material still in the linear elastic regime:

Stresses			
p_z	σ_{xx} $[Pa]$	σ_{yy} $[Pa]$	σ_{zz} $[Pa]$
70%	$6.9456 \cdot 10^6$	$1.6248 \cdot 10^7$	$-1.4838 \cdot 10^4$
1.25	$4.3984 \cdot 10^6$	$1.4171 \cdot 10^7$	$2.9245 \cdot 10^3$

Table 6.5: Stress components in normal direction for $0.7\%p_z$ and $1.25p_z$

From the plot:

$$E_y^{0.7p_z} = \left.\frac{\partial \sigma_{yy}}{\partial \epsilon_{yy}}\right|_{\text{elastic}} = 240.82\ GPa \tag{6-7}$$

$$E_y^{1.25p_z} = \left.\frac{\partial \sigma_{yy}}{\partial \epsilon_{yy}}\right|_{\text{elastic}} = 231.58\ GPa \tag{6-8}$$

and, these results match the obtained values from eq. (6-6), using the numerical values in table 6.5.

Some comparisons on neglecting elastic contribution in HRR may now be made. Due to Saint-Venant's principle and besides the nominal stress being verified (black dashed line) at point 11 far from the crack tip, the parameter E_y converges to E value in the same point in the red dashed line, since other stress components are approximately zero. The same evaluation with the plot for HRR furnishes that the elastic contribution is neglected.

Also comparing figs. 6.8 and 6.9 the condition of strain restriction along the thickness is observed, as dispersed values of E_y in the middle section occurs. As a consequence, since the elastoplastic stress depends on elastic contribution, the middle section it is noticed a large difference in the stresses between the curves.

Although the numerical results in both (upper and mid) surface present considerable differences, the section solutions were employed in comparison to the HRR results (under plane stress condition).

6.4 Stress-strain Relation in Load and Unloading

Considering the unloading process in a numerical crack problem two additional features must be considered: firstly, the procedure used for the nonlinear monotonic incremental elasticity can no longer be used because plastic residual strains must be continuously evaluated and, secondly, the numerical procedure shall recognize the plasticity state when in unloading.

In loading conditions, the stress-strain relation is represented by a monotonically increasing curve which should return to the original linear constitutive relation as unloading.

In the previous section, the monotonic curve was divided into two stages: elastic and elastoplastic. Continuing the same procedure as before, when the specimen unloads, stage three initiates with a linear elastic regime. Next, in the last stage of this analysis, stage four starts when, during the unload, the material behaves non-linearly under the plasticity regime.

In figs. 6.10 and 6.11 the unload is performed to a zero nominal stress, to avoid contact between crack faces.

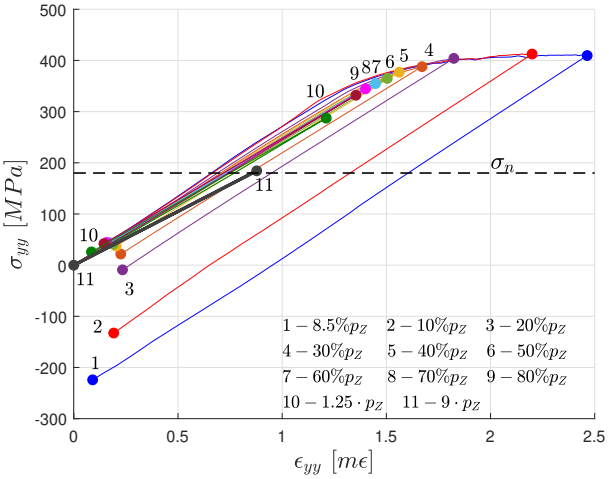

Figure 6.10: σ_{yy} vs ϵ_{yy} in surface section in different points ahead of the crack tip considering unload

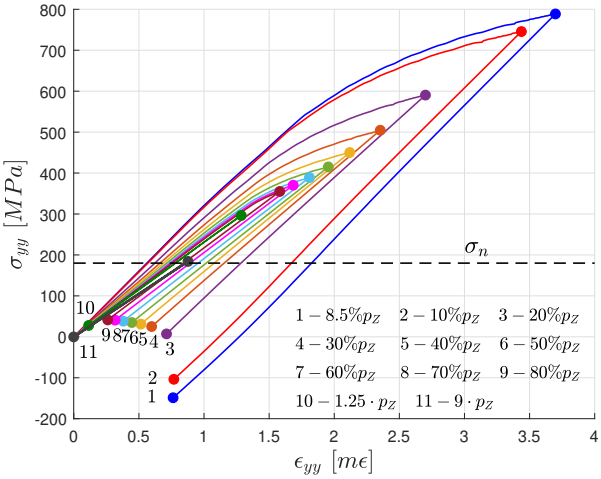

Figure 6.11: σ_{yy} vs ϵ_{yy} in middle section in different points ahead of the crack tip considering unload

A very relevant aspect is that linear elastic stress-strain curves may end up having residual strain, as shown in point 10 in the graphs 6.10 and 6.11. A solution to a 3D problem depends on the stress field over the full domain. In the case of point 10, the constitutive relation $\frac{\partial \sigma}{\partial \epsilon}$ depends on the residual compression stress and strains, making a coupling problem. In Appendix J, a simple example of elasticity shows how coupling effects may interfere the derivative $\frac{\partial \sigma}{\partial \epsilon}$ in one specific direction.

Compared to the 1D isotropic plastic model, when unloading, the regime remains elastic until stress reaches $-\sigma_y$ crossing the stress axis. However, this behavior does not occur in 3D models. The yield function in 3D depends on the norm of the deviatoric stress, a result that is not unique, since multiple

deviatoric stress tensors may have the same norm; differently, in 1D the stress applied in the yield function, a scalar, is unique. Due to the complexity of the 3D yield condition, a stress component of the tensor is not guaranteed to be the same that starts plastic behavior in load or unload.

From the previous analysis, it was presented that a residual stress-strain relation may appear under elasticity. However, this phenomenon only occurs when plasticity is required. In graph 6.12 a subsequential load and unload, preventing plasticity, was performed. In this case, it is possible to see that coupling will not be noticed since at any point the derivative $\frac{\partial \sigma}{\partial \epsilon}$ changed.

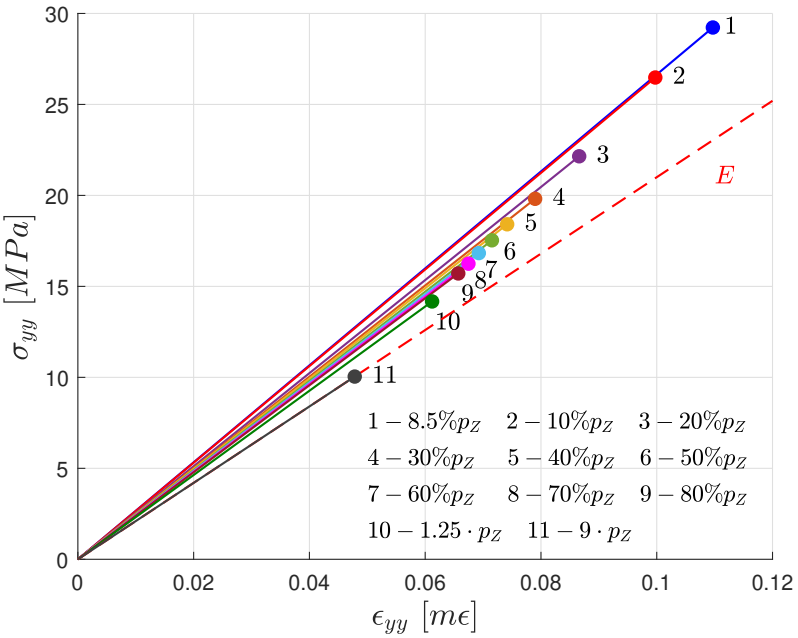

Figure 6.12: σ_{yy} *vs* ϵ_{yy} in surface section in different points ahead of the crack tip considering load and unload under elastic regime

7
Conclusion

This thesis aims for an evaluation and comparison of classical analytical procedures available in Fracture Mechanics' literature to a fully numerical FEM simulation for predicting material stress and strain distributions around a specimen crack tip. Linear elastic approaches by Williams, section 2.2.1, and Creager-Paris, section 2.2.1.1, while the well known HRR field theory for the elastoplasticity, section 2.3.2, were adopted as main references.

To perform the simulation in this work, a plugin framework called TopSim, originally with no plasticity model is adopted as a FEM numerical tool. To consider elastoplasticity, the Return-mapping algorithm with von Mises yield criterion is implemented, and as a result, the global Newton-Raphson adapted to take into account this new nonlinearity. Moreover, variable loads were also considered, especially unload in elastoplastic problems. To provide efficiency, the variable constitutive relation, CTO, is computed in the simulation.

A comparison between the numerical and analytical stresses along the residual ligament ahead of the crack tip was presented and discussed. As expected, close to the crack tip analytical solutions fail on reproducing the appropriate numerical results, since boundary and equilibrium conditions are not verified. McMeeking and Parks [30] elastoplastic numerical solution considering plane stress state, were used as validation for stress analysis close to the crack tip.

In addition, a study on the size and shape of the plastic zone (p_z) is presented and discussed. The qualitative analysis of these results enforced the importance of considering the equilibrium and the appropriate boundary conditions in the proposed solution analysis.

Finally, the analysis of stress-strain curve relation in the stress y component, which is paramount in fatigue analysis. Under loading and unloading, obtained results at different points along the residual ligament, in the surface and middle section planes, have shown that the HRR model is not an appropriate analytical solution tool, significantly differing from the numerically obtained results.

This thesis work provided, with solid arguments, that Williams, Creager-

Paris, and HRR are inaccurate theoretical models to represent the stresses and strains fields. Although Thermodynamics' first law is guaranteed by the Williams stress field model, equilibrium and boundary conditions are not verified since the solution is only valid close to the crack tip. Moreover, the assumption of elastic distribution is of limited value because of the high-stress concentration factor around crack tips. The same assumptions are followed by Creager-Paris except that the stress solution may not be singular as approaching the crack tip.

In the elastoplastic behavior, the HRR model for the stress field assumes equilibrium and compatibility equation, both derived directly from the Theory of Elasticity. In addition, the assumed stress function is singular at the crack tip and, despite considering small range plasticity, the derivations neglect elastic contributions to obtain stress and strain distributions. As a result, even inside the p_z, region of confidence, HRR models provide solutions with significant differences when compared to numerical procedure solutions.

7.1 Future Work Proposals

The Material hardening considered for the 3D elastoplastic von Mises model was assumed isotropic since yield surface stretches occur in the radial direction only. However, after a large number of load steps, significant loads may not be considered in the elastoplastic range. To exemplify this fact, in an isotropic model the step after an overload will only cause plasticity only for higher loading. As natural progress of the work, the implementation of a kinematic hardening rule in the numerical procedure should now be considered.

When it comes to modeling solutions where the stress distribution presents a too steep variation, the finite element procedure requires the use of domain discretization enrichments by the addition of a significantly large number of elements. In the present study, this condition arised in the region around the tip of the crack, making the problem to a large-scale simulation that for realistic and variable amplitude loads, numerically inefficient. To overcome this condition an enrichment of the finite element model' function subspace considering a nonsingular function could be proposed, similarly as used in Creager-Paris analytical solutions.

Moreover, an analytical/numerical analysis may be proposed by adapting the HRR field inspired by the Creager-Paris solution. Translating the singular field into the crack and rewriting the differential equation in elliptical coordinates, instead of the cylindrical coordinate system, the stress function may be numerically defined depending on the position angle. Therefore, an elasto-

plastic nonsingular solution may result and can be used as a reference for the numerical solution obtained by using the FEM.

References

[1] Bathe, K. J. *Finite Element Procedures*, 2nd edition 2015

[2] Neto, E. S.; Peric, D.; Owens, D.; *Computational methods for plasticity : theory and applications*, 2008 John Wiley & Sons Ltd

[3] Borja, R.I.; *Plasticity: Modeling & Computing*, 2013 Springer

[4] Castro, J.T.P.; Meggiolaro, M.A.; *Fatigue Design Techniques Under Real Service Loads - Volume I - High-Cycle Fatigue*, 2016

[5] Castro, J.T.P.; Meggiolaro, M.A.; *Fatigue Design Techniques Under Real Service Loads - Volume III - Crack Propagation, Temperature and Statistical Effects*, 2016

[6] S. Timoshenko and J. N. Goodier, *Theory of Elasticity*, McGraw-Hill Book Company, Inc., New York, 1951

[7] Newman Jr, JC.; *A crack-closure model for predicting fatigue crack growth under aircraft spectrum loading.* ASTM STP 748:53-84, 1981

[8] Durán, J.A.R.; Castro, J.T.P.; Payão Filho, J.C.; *Fatigue crack propagation prediction by plasticity damage accumulation models.* Fatigue Fract Eng Mater Struct 26:137-150

[9] Castro, J.T.P.; Meggiolaro, M.A.; Miranda, A.C.O.; *A note on fatigue crack growth predictions based on damage accumulation ahead of the crack tip.* Solid Mechanics in Brazil 2007, Alves & Mattos ed., p.133-146, ABCM, 2007

[10] Castro, J.T.P.; Meggiolaro, M.A.; Miranda, A.C.O.; *Fatigue crack growth predictions based on damage accumulation calculations ahead of the vrack tip.* Comput Mat Sci 46:115-123, 2009

[11] Ferreira, S. E.; *Modelagem da Propagação da Trinca de Fadiga Através do Dano Acumulado na Zona Plástica*, Tese de Doutorado, Pontifícia Universidade Católica do Rio de Janeiro, 2018

[12] Elber, W.; *Fatigue crack closure under cyclic tension.* Eng Fract Mech 2:37-45, 1970

[13] Elber, W.; *The significance of fatigue crack closure.* ASTM STP 486:230-242, 1971

[14] Willenborg, J; Engle, RM; Wood, HA; *Crack growth retardation model using an effective stress concept.* Wright Patterson Air Force Laboratory, 1971

[15] Wheeler, OE. *Spectrum loading and crack growth.* J Basic Eng 94:181-186, 1972

[16] Tada, H; Paris, PC; Irwin, GR. *The Stress Analysis of Cracks Handbook*, del Research 1985

[17] Inglis, CE. *Stress in a plate due to the presence of cracks and sharp corners.* Philos Trans Royal Soc A 215:119-223, 1913

[18] Griffith, A.A.; *The Phenomenon of rupture and flow in solids.* Philos T Roy Soc A 221: 163-198, 1920

[19] Williams, M.L.; *On the stress distribution at the base of a stationary crack.* J App Mech 24:109-114, 1957

[20] Creager, M.; Paris, P.C.; *Elastic field equations for blunt cracks with reference to stress corrosion cracking.* Int J Fract Mech 3:247-252, 1967

[21] Creager, M.; *The Elastic Stress Field Near the Tip of a Blunt Crack*, Master's Thesis, Lehigh University 1966

[22] Anderson, T.L.; *Fracture Mechanics.* 3^{rd} ed. CRC 2005.

[23] Paris, P.C.; Gomez, M. P.; Anderson, W. E., *A rational analytic theory of fatigue.* The Trend in Engineering 13:9-14, 1961

[24] Paris, P. C.; Erdogan, F.; *A critical analysis of crack propagation laws.* J Basic Eng 85:528-534, 1963

[25] Cherepanov, G. P.; *The propagation of cracks in a continuous medium* J App Math Mech 31:503-512, 1967

[26] Rice, J. R.; *A path independent integral and the approximate analysis of strain concentration by notches and cracks*, J App Mech 35:379-386, 1968

[27] Hutchinson, JW. *Singular behaviour at the end of a tensile crack tip in a hardening material.* J Mech Phys Solids 16:13-31, 1968.

[28] Ramberg, W., & Osgood, W. R.; Description of stress–strain curves by three parameters. Technical Note No. 902, National Advisory Committee For Aeronautics, Washington DC, 1943

[29] Rice, JR; Rosengrn, GF. *Plane strain deformation near a crack tip in a power-law hardening material.* J Mech Phys Solids 16:1-12, 1968.

[30] McMeeking, RM; Parks, DM. *A criterion for J-dominance of crack-tip fields in a large scale yielding.* ASTM STP 668:175-194, 1979

[31] Prager, W.; Hodge, P. G., Jr. *Theory of Perfectly Plastic Solids.* Dover, New York, 1968

[32] Milne-Thomson, L.M.; *Theoretical Hydrodynamics*, The MacMillan Company, New York, 1950

[33] Irwin, G.R.; *Analysis of stresses and strains near the end of a crack transversing a plate.* J App Mech 24:361-370, 1957

[34] Irwin, GR.; *Onset of fast crack propagation in high strength steel and aluminum alloys.* Sagamore Research Conf P 2:289-305, 1956

[35] Gere, J. M.; Goodno, B. J.; *Mecânica dos Materiais*, Cengage Learning, Tradução da 7ł edição norte-americana, 2013

A
Inglis Problem

In 1913, Inglis [17] proposed an analytical solution for the stress concentration factor

$$K_t = 1 + \frac{2a}{b} = 1 + 2\sqrt{\frac{a}{\rho}} \tag{A-1}$$

occurring in an infinite plate, with an elliptical hole and under a traction loading as illustrated in figure A.1.

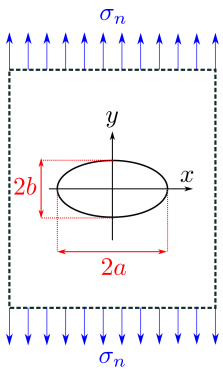

Figure A.1: Ellipse

Beginning from the general theory of curvilinear coordinates, cartesian x and y are written as function of ξ and η

$$\begin{cases} x = c\cosh\xi\cos\eta \\ y = c\sinh\xi\sin\eta \end{cases} \tag{A-2}$$

which, by eliminating variable η, reduces to :

$$\frac{x^2}{c^2\cosh^2\xi} + \frac{y^2}{c^2\sinh^2\xi} = 1 \tag{A-3}$$

For a fixed value of η, the equation in above describes an ellipse in cartesian coordinates with the geometric parameters shown in fig. A.2

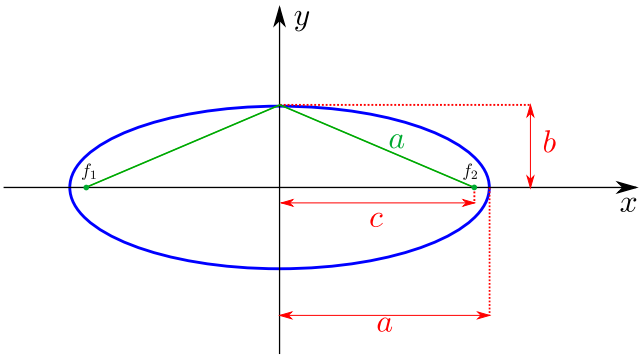

Figure A.2: Ellipse

where a and b are half axis lengths and c is half of focal distance. Therefore we have,

$$\begin{cases} a = c\cosh\xi_0 \\ b = c\sinh\xi_0 \end{cases} \tag{A-4}$$

and the radius of curvature ρ, a mathematical simplification, define as:

$$\rho := \frac{b^2}{a} \tag{A-5}$$

For a general bi-axial load, Inglis proposed an infinite series expansion for the stresses as

$$\begin{aligned}\sigma_{\xi\xi} = {} & \frac{1}{[\cosh(2\xi)-\cos(2\eta)]^2}\sum_n A_n\Big\{(n+1)e^{(1-n)\xi}\cos((n+3)\eta) \\ & + (n-1)e^{-(n+1)\xi}\cos((n-3)\eta) - \Big[4e^{-(n+1)\xi} + (n+3)e^{(3-n)\xi}\Big]\cos((n+1)\eta) \\ & + \Big[4e^{(1-n)\xi} + (3-n)e^{-(n+3)\xi}\Big]\cos((n-1)\eta)\Big\} + B_n\Big\{e^{-(n+1)\xi}\Big[n\cos((n+3)\eta) \\ & + (n+2)\cos((n-1)\eta)\Big] - \Big[(n+2)e^{(1-n)\xi} + ne^{-(n+3)\xi}\Big]\cos((n+1)\eta)\Big\}\end{aligned} \tag{A-6}$$

$$\begin{aligned}\sigma_{\eta\eta} = {} & \frac{1}{[\cosh(2\xi)-\cos(2\eta)]^2}\sum_n A_n\Big\{(3-n)e^{(1-n)\xi}\cos((n+3)\eta) \\ & - (n+3)e^{-(n+1)\xi}\cos((n-3)\eta) - \Big[4e^{-(n+1)\xi} - (n-1)e^{(3-n)\xi}\Big]\cos((n+1)\eta) \\ & + \Big[4e^{(1-n)\xi} + (n+1)e^{-(n+3)\xi}\Big]\cos((n-1)\eta)\Big\} + B_n\Big\{e^{-(n+1)\xi}\Big[n\cos((n+3)\eta) \\ & + (n+2)\cos((n-1)\eta)\Big] - \Big[(n+2)e^{(1-n)\xi} + ne^{-(n+3)\xi}\Big]\cos((n+1)\eta)\Big\}\end{aligned} \tag{A-7}$$

$$\sigma_{\xi\eta} = \frac{1}{[\cosh(2\xi) - \cos(2\eta)]^2} \sum_n A_n \Big\{ (n-1)e^{(1-n)\xi} \sin(n+3)\eta + (n+1)e^{-(n+1)\xi} \sin(n-3)\eta - (n+1)e^{(3-n)\xi} \sin(n+1)\eta - (n-1)e^{-(n+3)\xi} \sin(n-1)\eta \Big\} + B_n \Big\{ e^{-(n+1)\xi} \Big[n \sin(n+3)\eta + (n+2)\sin(n-1)\eta \Big] - \Big[(n+2)e^{(1-n)\xi} + ne^{-(n+3)\xi} \Big] \sin(n+1)\eta \Big\} \quad \text{(A-8)}$$

where constants A_n and B_n are constants obtained from boundary condition verifications. If the case of uniaxial tension σ_n in y direction, as presented in figure A.1, the only non-zero constants are as following

$$\begin{cases} A_1 = -\frac{\sigma_n(1+2e^{2\xi_0})}{16} \\ B_1 = \frac{\sigma_n e^{4\xi_0}}{8} \\ A_{-1} = -\frac{\sigma_n}{16} \\ B_{-1} = \frac{\sigma_n(1+\cosh(2\xi_0))}{4} \\ B_{-3} = -\frac{\sigma_n}{8} \end{cases} \quad \text{(A-9)}$$

corresponding to zero stresses on the ellipse free surface as $\xi = \xi_0$.

$$\begin{cases} \sigma_{\xi\xi}(\xi = \xi_0) = 0 \\ \sigma_{\xi\eta}(\xi = \xi_0) = 0 \end{cases} \quad \text{(A-10)}$$

Thus $\sigma_{\eta\eta}$ in eq. (A-7) yields to

$$\sigma_{\eta\eta}(\xi = \xi_0) = \sigma_n e^{2\xi_0} \left[\frac{(1 + e^{-2\xi_0}) \sinh(2\xi_0)}{\cosh(2\xi_0) - \cos(2\eta)} - 1 \right] \quad \text{(A-11)}$$

and the maximum value of $\sigma_{\eta\eta}$ results from the smallest denominator value of denominator with $\cos(2\eta) = 1$. Thus, from eq. (A-11), the stress concentration factor results in

$$\frac{\sigma_{\beta\beta}^{\text{Max}}}{\sigma_n} = e^{2\xi_0} \left[\frac{(1 + e^{-2\xi_0}) \sinh(2\xi_0)}{\cosh(2\xi_0) - 1} - 1 \right] \quad \text{(A-12)}$$

From eqs. (A-2) we have

$$\frac{b}{a} = \tanh \xi_0 = \frac{e^{\xi_0} - e^{-\xi_0}}{e^{\xi_0} + e^{-\xi_0}} = \frac{\frac{e^{2\xi_0}-1}{e^{2\xi_0}}}{\frac{e^{2\xi_0}+1}{e^{2\xi_0}}} = \frac{e^{2\xi_0} - 1}{e^{2\xi_0} + 1} \quad \text{(A-13)}$$

or

$$e^{2\xi_0} = \frac{a+b}{a-b} \quad \text{(A-14)}$$

Combining the terms of eq. (A-12) on the hyperbolic function basic definitions with eq. (A-14), after few algebraic manipulations, results in:

$$\begin{aligned}\frac{\sigma_{\beta\beta}^{\text{Max}}}{\sigma_n} &= \frac{a+b}{a-b}\left[\frac{\left(1+\frac{a-b}{a+b}\right)\cdot\left(\frac{a+b}{a-b}-\frac{a-b}{a+b}\right)^{\frac{1}{2}}}{\left(\frac{a+b}{a-b}-\frac{a-b}{a+b}\right)^{\frac{1}{2}}-1}-1\right] \\ &= 1+\frac{2a}{b}\end{aligned} \tag{A-15}$$

which is Ingris' result, presented in eq. (A-1), for the stress concentration factor occurring in an elliptical hole, in an infinite plate with an elliptical hole, under traction.

B
William Solution

In this Appendix equations for plane stress distributions due to a crack, in a plate loaded for mode I failure are derived, according to Wiliams' solutions in

$$\nabla^4\Psi(r,\theta) = \left(\frac{\partial^2}{\partial r^2} + \frac{1}{r}\frac{\partial}{\partial r} + \frac{1}{r^2}\frac{\partial^2}{\partial\theta^2}\right)\left(\frac{\partial^2\Psi}{\partial r^2} + \frac{1}{r}\frac{\partial\Psi}{\partial r} + \frac{1}{r^2}\frac{\partial^2\Psi}{\partial\theta^2}\right) = 0 \quad \text{(B-1)}$$

with the following stress component expressions

$$\sigma_r(r,\theta) = \frac{1}{r}\frac{\partial\Psi}{\partial r} + \frac{1}{r^2}\frac{\partial^2\Psi}{\partial\theta^2} \quad \text{(B-2)}$$

$$\sigma_\theta(r,\theta) = \frac{\partial^2\Psi}{\partial r^2} \quad \text{(B-3)}$$

$$\sigma_{r\theta}(r,\theta) = -\frac{\partial}{\partial r}\left(\frac{1}{r}\frac{\partial\Psi}{\partial\theta}\right) \quad \text{(B-4)}$$

In addition, proper boundary conditions must be satisfied as shown in fig. B.1

For the solution of Ψ it was proposed the following infinite periodic series expansion function

$$\Psi(r,\theta) = r^2\ f(r,\theta) + g(r,\theta) \quad \text{(B-5)}$$

with

$$f = \sum_n A_n r^n \cos(n\theta) + C_n r^n \sin(n\theta) \quad \text{(B-6)}$$

$$g = \sum_n B_n r^{n+2} \cos\Big[(n+2)\theta\Big] + D_n r^{n+2} \sin\Big[(n+2)\theta\Big] \quad \text{(B-7)}$$

where A_n, B_n, C_n and D_n are constants to be defined.

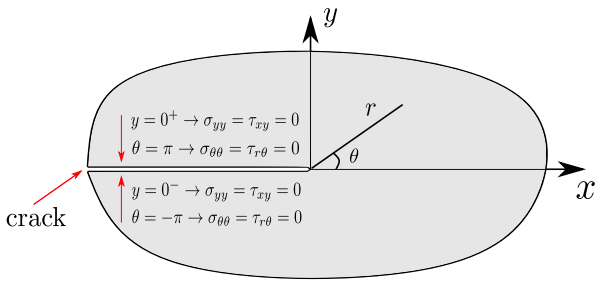

Figure B.1: Crack coordinates

For mode I type of fracture, symmetry on σ_θ, imposes the following condition

$$\sigma_\theta(\theta) = \sigma_\theta(-\theta) \tag{B-8}$$

Using Airy's equation proposed in eq. (B-5) σ_θ is obtained as follows

$$\begin{aligned} \sigma_\theta = \frac{\partial^2 \Psi}{\partial r^2} &= \frac{\partial}{\partial r}\left[\frac{\partial}{\partial r}\left(r^2 f + g\right)\right] \\ &= 2f + 4r\frac{\partial f}{\partial r} + r^2\frac{\partial^2 f}{\partial r^2} + \frac{\partial^2 g}{\partial r^2} \end{aligned} \tag{B-9}$$

where using f and g defined in eqs. (B-6) and (B-7) we have

$$\frac{\partial f}{\partial r} = \sum_n A_n n r^{n-1}\cos(n\theta) + C_n n r^{n-1}\sin(n\theta) \tag{B-10}$$

$$\frac{\partial^2 f}{\partial r^2} = \sum_n A_n n(n-1) r^{n-2}\cos(n\theta) + C_n n(n-1) r^{n-2}\sin(n\theta) \tag{B-11}$$

$$\frac{\partial g}{\partial r} = \sum_n B_n(n+2) r^{n+1}\cos\Big[(n+2)\theta\Big] + D_n(n+2) r^{n+1}\sin\Big[(n+2)\theta\Big] \tag{B-12}$$

$$\frac{\partial^2 g}{\partial r^2} = \sum_n B_n(n+2)(n+1) r^{n}\cos\Big[(n+2)\theta\Big] + D_n(n+2)(n+1) r^{n}\sin\Big[(n+2)\theta\Big] \tag{B-13}$$

Thus, resulting in

$$\begin{aligned}\sigma_\theta = 2\sum_n A_n r^n \cos(n\theta) + C_n r^n \sin(n\theta) \\ + 4\sum_n A_n n r^n \cos(n\theta) + C_n n r^n \sin(n\theta) \\ + \sum_n A_n n(n-1) r^n \cos(n\theta) + C_n n(n-1) r^n \sin(n\theta) \\ + \sum_n B_n (n+2)(n+1) r^n \cos\Big[(n+2)\theta\Big] + D_n (n+2)(n+1) r^n \sin\Big[(n+2)\theta\Big]\end{aligned} \tag{B-14}$$

From the condition of symmetry in eq. (B-8)

$$C_n = D_n = 0 \tag{B-15}$$

Resulting f and g, from eqs. (B-6) and (B-7) as

$$\begin{cases} f = \sum_n A_n r^n \cos(n\theta) \\ g = \sum_n B_n r^{n+2} \cos\Big[(n+2)\theta\Big] \end{cases} \tag{B-16}$$

and the stress function Ψ as

$$\Psi_I = r^2 \sum_n A_n r^n \cos(n\theta) + \sum_n B_n r^{n+2} \cos\Big[(n+2)\theta\Big] \tag{B-17}$$

Finally, back to eq. (B-14), with the result in eq. (B-15), reduces to

$$\sigma_\theta = \sum_n (n+2)(n+1) r^n \left[A_n \cos(n\theta) + B_n \cos\Big[(n+2)\theta\Big] \right] \tag{B-18}$$

Similarly, bringing into σ_r, the Airy's function as in eq. (B-2), we have

$$\begin{aligned}\sigma_r &= \frac{1}{r}\cdot\frac{\partial \Psi}{\partial r} + \frac{1}{r^2}\cdot\frac{\partial^2 \Psi}{\partial \theta^2} \\ &= 2f + r\cdot\frac{\partial f}{\partial r} + \frac{1}{r}\cdot\frac{\partial g}{\partial r} + \frac{\partial^2 f}{\partial \theta^2} + \frac{1}{r^2}\frac{\partial^2 g}{\partial \theta^2}\end{aligned} \tag{B-19}$$

that from eq. (B-16) provides

$$\sigma_r = \sum_n r^n \left\{ A_n (n+2-n^2)\cos(n\theta) + B_n \Big[(n+2) - (n+2)^2\Big] \cos\Big[(n+2)\theta\Big] \right\} \tag{B-20}$$

Using the same procedure as before, for $\sigma_{r\theta}$, we have

$$\begin{aligned}\sigma_{r\theta} &= -\frac{\partial}{\partial r}\left(\frac{1}{r}\cdot\frac{\partial\psi}{\partial\theta}\right)\\ &= -\frac{\partial f}{\partial\theta} - r\cdot\frac{\partial^2 f}{\partial\theta\partial r} + \frac{1}{r^2}\cdot\frac{\partial g}{\partial\theta} - \frac{1}{r}\cdot\frac{\partial^2 g}{\partial\theta\partial r}\end{aligned} \tag{B-21}$$

that, from eq. (B-16), gives

$$\begin{aligned}\sigma_{r\theta} &= \sum_n A_n(n+n^2)r^n\sin(n\theta) + \sum_n B_n r^n\Big[-(n+2)+(n+2)^2\Big]\sin\Big[(n+2)\theta\Big]\\ &= \sum_n (n+1)r^n\Big[nA_n\sin(n\theta) + (n+2)B_n\sin[(n+2)\theta]\Big]\end{aligned} \tag{B-22}$$

From eqs. (B-18), (B-20) and (B-22)

$$\begin{cases}\sigma_\theta = \sum_n (n+2)(n+1)r^n\Big[A_n\cos(n\theta) + B_n\cos\Big[(n+2)\theta\Big]\Big]\\ \sigma_r = \sum_n r^n\Big\{A_n(n+2-n^2)\cos(n\theta) + B_n\Big[(n+2)-(n+2)^2\Big]\cos\Big[(n+2)\theta\Big]\Big\}\\ \sigma_{r\theta} = \sum_n (n+1)r^n\Big[nA_n\sin(n\theta) + (n+2)B_n\sin[(n+2)\theta]\Big]\end{cases} \tag{B-23}$$

Boundary conditions at the crack faces state that normal and shear stresses are zero

$$\sigma_\theta(\theta=\pm\pi) = \sigma_{r\theta}(\theta=\pm\pi) = 0 \tag{B-24}$$

what implies, considering the equation for σ_θ at eq. (B-23).

$$A_n\cos(n\pi) + B_n\cos[(n+2)\pi] = 0$$

$$A_n\cos(n\pi) + B_n\cos[n\pi+2\pi] = 0$$

From cos addictive property

$$(A_n + B_n)\cos(n\pi) = 0$$

and, as well for $\sigma_{r\theta}$:

$$nA_n\sin(n\pi) + (n+2)B_n\sin[(n+2)\pi] = 0$$

$$nA_n\sin(n\pi) + (n+2)B_n\sin[n\pi+2\pi] = 0$$

From sin addictive property

$$[nA_n + (n+2)B_n]\sin(n\pi) = 0$$

As a consequence, from eq. (B-24) we have

$$\begin{cases} (A_n + B_n)\cos(n\pi) = 0 \\ [nA_n + (n+2)B_n]\sin(n\pi) = 0 \end{cases} \tag{B-25}$$

From the first equation in above, at least one of the products must be zero. So,

$$\begin{cases} n = \cdots, -3/2, -1/2,\ 1/2,\ 3/2, \cdots \\ A_n = -B_n \end{cases} \tag{B-26}$$

and, the same for the second equation

$$\begin{cases} n = \cdots, -2, -1,\ 0,\ 1,\ 2 \cdots \\ nA_n = -(n+2)B_n \end{cases} \tag{B-27}$$

In this case some additional conditions must also be verified:

- n must be non-positive $n < 0$, otherwise the solution gives stress singularity far from the crack tip. It is expected that higher stresses occur as approaching to the crack tip.
- On the other hand, $n = 0$ implies in constant stress values not correct for stress concentrations, physically expected, nearby to a crack tip.
- thus negative value of n reproduces stress singularity.

Applying the first law of thermodynamics, with finite and positive strain energy (E_S), thus

$$E_S \approx \int \sigma\epsilon \; dA = \int \frac{\sigma^2}{E} \; dA \tag{B-28}$$

from eq. (B-23), the stress can be represented as a geometric portion dependable of θ and a portion of r^n

$$\sigma = f(\theta) \cdot r^n \tag{B-29}$$

rewriting eq. (B-28):

$$E_S = \int_{-\pi}^{\pi} f^2(\theta) \; d\theta \int_0^R r^{2n} r \; dr \tag{B-30}$$

where R is the radius of the circular area centered in the crack. So:

$$0 < \int_{-\pi}^{\pi} f^2(\theta) \; d\theta \int_0^R r^{2n} r \; dr < \infty \tag{B-31}$$

Note that, since $f(\theta)$ has sines and cosines, that are bounded function, then

$$0 < \int_{-\pi}^{\pi} f^2(\theta)\ d\theta < \infty \tag{B-32}$$

The condition of finite and positivity lies on the second part of the eq. (B-31)

$$0 < \int_0^R r^{2n} r\ dr = \frac{R^{2n+2}}{2n+2} < \infty \therefore n > -1 \tag{B-33}$$

From the first law of thermodynamics that provides $n > -1$ and physical meaning coverage of $n < 0$, the only n that verify boundary condition from eqs. (B-26) and (B-27) is

$$n = -\frac{1}{2} \tag{B-34}$$

that verifies (B-26). For the second case, eq. (B-27), we have

$$nA_n = -(n+2)B_n \tag{B-35}$$

Therefore, assuming $A_{-1/2}$ function of a constant K_I we have

$$\begin{cases} A_{-1/2} = K_I/\sqrt{2\pi} \\ B_{-1/2} = A_{-1/2}/3 = K_I/3\sqrt{2\pi} \end{cases} \tag{B-36}$$

that substituting into eq. (B-23) gives

$$\begin{bmatrix} \sigma_{xx} \\ \sigma_{yy} \\ \sigma_{xy} \end{bmatrix} = \frac{K_I}{\sqrt{2\pi r}}\ \cos\left(\frac{\theta}{2}\right) \begin{bmatrix} 1 - \sin\left(\frac{\theta}{2}\right) \cdot \sin\left(\frac{3\theta}{2}\right) \\ 1 + \sin\left(\frac{\theta}{2}\right) \cdot \sin\left(\frac{3\theta}{2}\right) \\ \sin\left(\frac{\theta}{2}\right) \cdot \cos\left(\frac{3\theta}{2}\right) \end{bmatrix} \tag{B-37}$$

C
Irwin's Solution

Using the Westergaard stress function [6] - which is a complex analytical function that represents a stress function, provided the problem boundary conditions are satisfied - George Rankin Irwin [33] characterized the SIF for an infinite plate loaded under biaxial nominal stresses σ_n.

The box in below presents a proof of of this important mathematical property of Westergaard stress functions

Basically we start with the general form definition of a complex function in cartesian coordinates

$$Z(z) = f(x,y) + i \cdot g(x,y) \tag{C-1}$$

where $z = x + i\ y$ and $Z(z) = Re(z) + i \cdot Im(z)$ is an analytical form if Z' is unique. Thus, for $Z(z)$ be derivable, it must obey the Cauchy-Riemann condition, given by:

$$\begin{cases} \frac{\partial Re(Z)}{\partial x} = \frac{\partial Im(Z)}{\partial y} = Re(Z') \\ \frac{\partial Im(Z)}{\partial x} = \frac{\partial Re(Z)}{\partial y} = Im(Z') \end{cases} \tag{C-2}$$

or using eq. (C-1) definitions

$$\begin{cases} \frac{\partial f}{\partial x} = \frac{\partial g}{\partial y} \\ \frac{\partial f}{\partial y} = -\frac{\partial g}{\partial x} \end{cases} \tag{C-3}$$

Applying the Laplace operator ($\nabla^2 = \partial^2/\partial x^2 + \partial^2/\partial y^2$) in f and g, we have

$$\begin{cases} \nabla^2 f = \frac{\partial^2 f}{\partial x^2} - \frac{\partial^2 g}{\partial x \partial y} + \frac{\partial^2 f}{\partial y^2} + \frac{\partial^2 g}{\partial x \partial y} = 0 \\ \nabla^2 g = -\frac{\partial^2 f}{\partial x \partial y} + \frac{\partial^2 g}{\partial y^2} + \frac{\partial^2 f}{\partial x \partial y} + \frac{\partial^2 g}{\partial x^2} = 0 \end{cases} \tag{C-4}$$

Therefore for a given complex analytical function, Re and Im are harmonic (obey Laplace equation) and conjugate (for a given f, g is obtained less than a constant, and vice versa).

$$\nabla^4 Z = \nabla^2(\underbrace{\nabla^2 f}_{=0}) + i \cdot \nabla^2(\underbrace{\nabla^2 g}_{=0}) = 0 \tag{C-5}$$

that concludes the proof sought.

Thus, Westergaard stress function's in its general format is:

$$\Psi(z) = Re(\bar{\bar{Z}}) + y\ Im(\bar{Z}) \tag{C-6}$$

where

$$Z = \frac{\partial \bar{Z}}{\partial z} \quad , \quad \bar{Z} = \frac{\partial \bar{\bar{Z}}}{\partial z} \tag{C-7}$$

Applying Airy's formulation, the stresses are the following

$$\begin{aligned} \sigma_{xx} &= \frac{\partial^2 \phi}{\partial y^2} \\ &= \frac{\partial}{\partial y}\left(\frac{Re(\bar{\bar{Z}})}{\partial y} + \frac{\partial(y\ Im(\bar{Z}))}{\partial y}\right) \\ &= \frac{\partial(-Im(\bar{Z}) + Im(\bar{Z}) + y\ Re(Z))}{\partial y} \\ &= Re(Z) - y\ Im(Z') \end{aligned} \tag{C-8}$$

$$\begin{aligned} \sigma_{yy} &= \frac{\partial^2 \phi}{\partial x^2} \\ &= \frac{\partial}{\partial x}\left(\frac{Re(\bar{\bar{Z}})}{\partial x} + \frac{\partial(y\ Im(\bar{Z}))}{\partial x}\right) \\ &= \frac{\partial(Re(\bar{Z}) + y\ Im(Z))}{\partial x} \\ &= Re(Z) + y\ Im(Z') \end{aligned} \tag{C-9}$$

$$\begin{aligned} \tau_{xy} &= \frac{\partial^2 \phi}{\partial x \partial y} \\ &= -\frac{\partial}{\partial x}\left(\frac{Re(\bar{\bar{Z}})}{\partial y} + \frac{\partial(y\ Im(\bar{Z}))}{\partial y}\right) \\ &= \frac{\partial(y\ Re(Z))}{\partial x} \\ &= -y\ Re(Z') \end{aligned} \tag{C-10}$$

Considering a crack with $2a$ in size centered in an infinite plate loaded under nominal σ_n biaxial stresses , as proposed by Irwin,, a stress function Z to solve the stress field around the crack tip is given by

$$Z = \frac{z\ \sigma}{\sqrt{z^2 - a^2}} \Rightarrow Z' = -\frac{\sigma\ a^2}{(z^2 - a^2)^{3/2}} \tag{C-11}$$

with the following boundary conditions, in cartesian coordinates,

– $\sigma_{yy} = \sigma_{xy} = 0$ for $-a < x < a$ and $y = 0$;

– $\sigma_{xx} = \sigma_{yy} = \frac{\sigma_n\ x}{\sqrt{x^2-a^2}}$ and $\sigma_{xy} = 0$. with $y = 0$. As $x \to \infty$, therefore $\sigma_{xx} = \sigma_{yy} = \sigma_n$

By using polar coordinates centered at the crack tip in the complex plane representation we have

$$z = r\ e^{i\theta} + a \tag{C-12}$$

where

$$r^2 = (x-a)^2 + y^2 \tag{C-13}$$

Rewriting eq. (C-11) one may obtain

$$\begin{aligned} Z &= \frac{\sigma_n\ (r\ e^{i\theta} + a)}{\sqrt{(r\ e^{i\theta} + a)^2 - a^2}} \\ &= \frac{\sigma_n \Big(\overbrace{\frac{r}{a}}^{\approx 0}\ e^{i\theta} + 1 \Big) a}{\sqrt{r^2\ e^{i\theta} + 2a\ r\ e^{i\theta} + \cancel{a^2} - \cancel{a^2}}} \\ &= \frac{\sigma_n\ \sqrt{a}\ \cancel{\sqrt{a}}}{\cancel{\sqrt{a}} \Big(\underbrace{\frac{r}{a}}_{\approx 0}\ r\ e^{i\theta} + \frac{2\cancel{a}\ r}{\cancel{a}} e^{i\theta} \Big)} \\ &= \frac{\sigma_n\ \sqrt{a}}{\sqrt{2re^{i\theta}}} \end{aligned} \tag{C-14}$$

$$Z(z_t) = \frac{\sigma_n\ \sqrt{a}}{\sqrt{2}}\ e^{-i\theta} = \frac{\sigma_n\ \sqrt{a}}{\sqrt{2r}} \left[\cos\frac{\theta}{2} - i \sin\frac{\theta}{2} \right] \tag{C-15}$$

where

$$z_t = r\ e^{i\theta} \tag{C-16}$$

and

$$Z'(z_t) = -\frac{\sigma_n\ \sqrt{a}}{\sqrt{2}}\ z_t^{-3/2} = \frac{\sigma_n\ \sqrt{a}}{2r\sqrt{2r}} \left[-\cos\frac{3\theta}{2} + i \sin\frac{3\theta}{2} \right] \tag{C-17}$$

Thus expressions for plane stress components are readily obtained

$$\begin{aligned} \sigma_{yy} &= Re(Z) + yIm(Z') \\ &= \frac{\sigma_n\ \sqrt{a}}{\sqrt{2r}} \cdot \cos\frac{\theta}{2} \left[1 + \sin\frac{\theta}{2} \sin\frac{3\theta}{2} \right] \end{aligned} \tag{C-18}$$

$$\begin{aligned}\sigma_{xx} &= Re(Z) - y\ Im(Z') \\ &= \frac{\sigma_n\ \sqrt{a}}{\sqrt{2r}} \cdot \cos\frac{\theta}{2}\left[1 - \sin\frac{\theta}{2}\sin\frac{3\theta}{2}\right]\end{aligned} \tag{C-19}$$

$$\begin{aligned}\sigma_{xy} &= -y\ Re(Z') \\ &= \frac{\sigma_n\ \sqrt{a}}{\sqrt{2r}} \cdot \cos\frac{\theta}{2}\sin\frac{\theta}{2}\cos\frac{3\theta}{2}\end{aligned} \tag{C-20}$$

Multiplying eqs. (C-18), (C-19) and (C-20) for $\frac{\sqrt{\pi}}{\sqrt{\pi}}$, factor K_I (SIF) results as obtained for William's stress field in eq. (2-7),

$$K_I = \sigma_n\sqrt{\pi a} \tag{C-21}$$

D
Creager-Paris Solution

The proof of the following problem requires additional knowledge of continuum mechanics and theory of elasticity that will not be fully demonstrated in this chapter.

Stress functions can be separated into two parts. The harmonic terms (Ω) and the complex function (χ)

$$\Psi = Re[\bar{Z}\Omega(Z) + \chi(Z)] \tag{D-1}$$

what implies in (see [6] section 58):

$$\sigma_{xx} + \sigma_{yy} = 4Re[\Omega'(Z)] \tag{D-2}$$

$$\sigma_{yy} - \sigma_{xx} + 2i\sigma_{xy} = 2[\bar{Z}\Omega''(Z) + \chi''(Z)] \tag{D-3}$$

From The general theory of curvilinear coordinates (section in [6]), cartesian x and y coordinates relate to

$$\begin{cases} x = c\cosh\xi\cos\eta \\ y = c\sinh\xi\sin\eta \end{cases} \tag{D-4}$$

In complex coordinates one may have:

$$\begin{aligned} Z &= x + iy \\ &= c\cosh\xi\cos\eta + i\cdot c\sinh\xi\sin\eta \\ &= c\cosh(\xi + i\eta) \\ &= c\cosh(\zeta) \end{aligned} \tag{D-5}$$

that, by eliminating η, yields:

$$\frac{x^2}{c^2\cosh^2\xi} + \frac{y^2}{c^2\sinh^2\xi} = 1 \tag{D-6}$$

which, for a fixed value of ξ, describes an ellipse of focal distance $2c$ and semi-axis dimensions $2a$ and $2b$, as

$$\begin{cases} a = c\cosh\xi_0 \\ b = c\sinh\xi_0 \end{cases} \tag{D-7}$$

and curvature radius ρ is mathematically defined by

$$\rho := \frac{b^2}{a} \tag{D-8}$$

These geometric parameters are also related as

$$\begin{aligned} c^2 &= a^2 - b^2 \\ &= a^2\left(1 - \frac{1}{a}\frac{b^2}{a}\right) \\ &= a^2\left(1 - \frac{\rho}{a}\right) \end{aligned} \tag{D-9}$$

Stress components in curvilinear coordinates are set for a rotation angle γ in the original cartesian coordinates xy to the new curvilinear system $\xi\eta$. In [6], section 61 presents

$$\begin{cases} \sigma_{\xi\xi} + \sigma_{\eta\eta} = \sigma_{xx} + \sigma_{yy} \\ \sigma_{\eta\eta} - \sigma_{\xi\xi} + 2i\sigma_{\xi\eta} = e^{2i\gamma}(\sigma_{yy} - \sigma_{xx} + 2i\sigma_{xy}) \end{cases} \tag{D-10}$$

Timoshenko proposed a solution for an elliptic hole in an infinite plate under simple tensile stress σ_n at rotated with an angle of γ above x axis. (see reference [6] in section number 63).

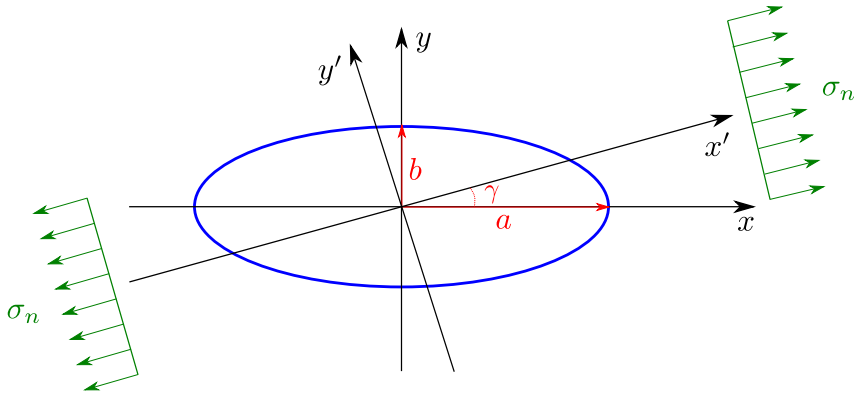

Figure D.1: Ellipse coordinates for the problem considered

In fig. D.1 the coordinate system xy and the rotated coordinate system is presented as well as the external load. For this case, the stresses in the rotated configuration is:

$$\begin{cases} \sigma_{x'x'} = \sigma_n \\ \sigma_{y'y'} = \sigma_{x'y'} = 0 \end{cases} \tag{D-11}$$

and the stress function to this problem is

$$4\Omega(Z) = \sigma_n c[e^{2\xi_0}\cos(2\gamma)\cosh(\zeta) + (1 - e^{2\xi_0 + 2i\gamma})\sinh(\zeta)] \tag{D-12}$$

$$4\chi(Z) = -\sigma_n c^2 \left[\left(\cosh(2\xi_0) - \cos(2\gamma) \right) \zeta + \frac{1}{2} e^{2\xi_0} \cosh[2(\zeta - \xi_0 - i\gamma)] \right] \quad \text{(D-13)}$$

Rewriting both stress function above with the explicit dependency of variable Z, from eq. (D-5), gives:

$$4\Omega(Z) = \sigma_n \left[e^{2\xi_0} Z \cos(2\gamma) + (1 - e^{2\xi_0 + 2i\gamma}) \sqrt{Z^2 - c^2} \right] \quad \text{(D-14)}$$

and

$$\begin{aligned} 4\chi(Z) = -\sigma_n c^2 \Bigg[& [\cosh(2\xi_0) - \cos(2\gamma)] \cosh^{-1}\left(\frac{Z}{c}\right) \\ & + \frac{1}{2} e^{2\xi_0} \Bigg(\cosh[2(\xi_0 + i\gamma)] \frac{2Z^2 - c^2}{c^2} \\ & - 2\sinh[2(\xi_0 + i\gamma)] \frac{Z\sqrt{Z^2 - c^2}}{c^2} \Bigg) \Bigg] \end{aligned} \quad \text{(D-15)}$$

The full derivation is presented in section D.5.

$\Omega'(Z)$ and $\chi''(Z)$ are obtained from eqs. (D-2) and (D-3). After some algebraic manipulations (see section D.6)

$$\Omega'(Z) = \frac{d\Omega}{dZ} = \frac{1}{4}\sigma_n \left[e^{2\xi_0} \cos(2\gamma) + (1 - e^{2\xi_0 + 2i\gamma}) \cdot \frac{Z}{\sqrt{Z^2 - c^2}} \right] \quad \text{(D-16)}$$

and

$$\begin{aligned} \chi''(Z) = \frac{\sigma_n}{4\ (Z^2 - c^2)^{3/2}} \Bigg[& [\cosh(2\xi_0) - \cos(2\gamma)]\ Zc^2 \\ & + e^{2\xi_0}\ \sinh[2(\xi_0 + i\gamma)]\ (2Z^3 - 3Zc^2) \Bigg] \\ & - \frac{\sigma_n}{2}\ e^{2\xi_0}\ \cosh[2(\xi_0 + i\gamma)] \end{aligned} \quad \text{(D-17)}$$

Later, $\bar{Z}\Omega''(Z)$ will be presented.

To obtain the position of a point in relation to the ellipse crack, two non-dimensional parameters are presented: α and β. In the x axis the distance is given by the product $\alpha\rho$ while in the y axis the product $\beta\rho$ in reference to the point of the crack tip. Figure above shows the definition of α and β

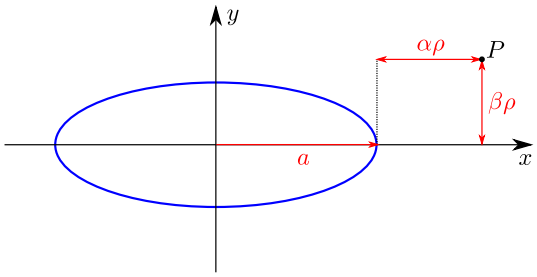

Figure D.2: Plastic zone estimation based on Williams' field

In complex coordinates, Z is defined as function of α and β as:

$$Z = a\left(1 + \alpha\frac{\rho}{a} + \beta\frac{\rho}{a}i\right) \tag{D-18}$$

For a crack $\frac{\rho}{a} << 1$ and only the region near to the crack tip is an area of interest. Thus,

$$\alpha\frac{\rho}{a} << 1 \quad \beta\frac{\rho}{a} << 1 \tag{D-19}$$

resulting in a simplified definition of Z^2, highly accurate approximation, as

$$Z^2 = a^2\left(1 + 2\alpha\frac{\rho}{a} + 2\beta\frac{\rho}{a}i\right) \tag{D-20}$$

and

$$\begin{aligned} Z^2 - c^2 &= a^2\left(1 + 2\alpha\frac{\rho}{a} + 2\beta\frac{\rho}{a}i\right) - a^2\left(1 - \frac{\rho}{a}\right) \\ &= 2a^2\left(\alpha + \frac{1}{2} + \beta i\right)\frac{\rho}{a} \end{aligned} \tag{D-21}$$

As proposed by Creager-Paris, a polar coordinate system is set from the focus of the ellipse moving $\rho/2$ the axis r and θ, to inside the notch (see fig. 2.2).

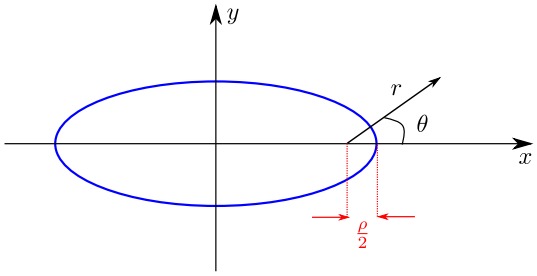

Figure D.3: Plastic

In the cases of using the definition of α and β above, this new coordinates is obtained by

$$\alpha = -\frac{1}{2} \quad \beta = 0 \tag{D-22}$$

Splitting variable Z into the complex coordinate x and y and rewriting for cylindrical coordinate provides:

$$r\cos\theta = \left(\alpha + \frac{1}{2}\right)\rho \tag{D-23}$$

$$r\sin\theta = \beta\rho \tag{D-24}$$

Moreover, rewriting $Z^2 - c^2$, from eq. (D-21), with the new coordinate system

$$\begin{aligned} Z^2 - c^2 &= 2a^2\left(\alpha + \frac{1}{2} + \beta i\right)\frac{\rho}{a} \\ &= 2a^2\left[\underbrace{\left(\alpha + \frac{1}{2}\right)\rho}_{r\cos\theta} + \underbrace{\beta\rho}_{r\sin\theta}\ i\right]\frac{1}{a} \\ &= 2a^2\underbrace{\left(\cos\theta + i\sin\theta\right)}_{e^{i\theta}}\frac{r}{a} \\ &= 2a^2 e^{i\theta}\ \frac{r}{a} \end{aligned} \tag{D-25}$$

Back to the derivation of eqs, (D-2) and (D-3), linearisation of variable $e^{2\xi_0}$ is considered, given by (see section D.7):

$$e^{2\xi_0} = \frac{(a+b)^2}{c^2} = 1 + 2\sqrt{\frac{\rho}{a}} + 2\frac{\rho}{a} + \cdots \tag{D-26}$$

Another assumption, in the case of $\Psi'(Z)$, is to neglect the term $e^{2\xi_0}$ in comparison to $\sqrt{\frac{a}{r}}$, since

$$e^{2\xi_0} = \frac{(a+b)^2}{c^2} = 1 + 2\left(\frac{\rho}{a}\right)^{\frac{1}{2}} + \cdots << \left(\frac{a}{r}\right)^{\frac{1}{2}} \tag{D-27}$$

Replacing variable Z, applying eqs. (D-26) and (D-27) and neglecting higher order then $\frac{\rho}{a}$ provides:

$$\begin{aligned} \Omega'(Z) = \frac{\sigma_n}{4}\sqrt{\frac{a}{2r}}\Bigg[&(1-\cos 2\gamma)\cos\frac{\theta}{2} - \sin\frac{\theta}{2} \\ &+ i\left(\sin\frac{\theta}{2} - \sin\frac{\theta}{2}\cos 2\gamma - \sin 2\gamma\cos\frac{\theta}{2}\right)\Bigg] \end{aligned} \tag{D-28}$$

$$\bar{Z}\Omega''(Z) = -\frac{\sigma_n a^3}{4\cdot(Z^2-c^2)^{3/2}}\Bigg[1+(\alpha-1)\frac{\rho}{a}-\beta\frac{\rho}{a}i-\cos 2\gamma\Bigg(1+2\sqrt{\frac{\rho}{a}} + (\alpha+1)\frac{\rho}{a}-\beta\frac{\rho}{a}i\Bigg) - i\sin 2\gamma\Bigg(1+2\sqrt{\frac{\rho}{a}}+(\alpha+1)\frac{\rho}{a}-\beta\frac{\rho}{a}i\Bigg) \quad \text{(D-29)}$$

$$\chi''(Z) = \frac{\sigma_n a^3}{4\ (Z^2-c^2)^{3/2}}\Bigg[1+(\alpha+1)\frac{\rho}{a}+\beta\frac{\rho}{a}i - \cos 2\gamma\Bigg(1+2\sqrt{\frac{\rho}{a}}+(\alpha+3)\frac{\rho}{a}+\beta\frac{\rho}{a}i\Bigg) - i\sin 2\gamma\Bigg(1+2\sqrt{\frac{\rho}{a}}+(1-3\alpha)\frac{\rho}{a}-3\beta\frac{\rho}{a}i\Bigg)\Bigg] \quad \text{(D-30)}$$

For the additional proof, see section D.8.

Substituting equations above into conditions from eqs. (D-2) and (D-3) we have

$$\sigma_{xx}+\sigma_{yy} = \sigma_n\sqrt{\frac{a}{2r}}\Bigg[(1-\cos 2\gamma)\cos\frac{\theta}{2}-\sin 2\gamma\sin\frac{\theta}{2}\Bigg] \quad \text{(D-31)}$$

$$\sigma_{yy}-\sigma_{xx}+2i\ \sigma_{xy} = \frac{\sigma_n a^{\frac{3}{2}}\ e^{-\frac{3}{2}i\theta}}{2\sqrt{2}\ r^{\frac{3}{2}}}\Bigg[1+\beta i-\cos 2\gamma\Bigg(1+\beta i\Bigg)+ i\sin 2\gamma\Bigg(2\alpha+\beta i\Bigg)\Bigg]\frac{\rho}{a} \quad \text{(D-32)}$$

Derived in section D.9.

D.1
Fracture under Mode I

For mode I problem, as loading is perpendicular to the crack face, angle γ is equal to $\frac{\pi}{2}$. Rewriting eq. (D-31) and comparing to Williams' solution from eq. (2-7) provides:

$$K_I = \sigma_n\sqrt{\pi a} \quad \text{(D-33)}$$

and

$$\sigma_{xx}+\sigma_{yy} = \frac{2K_I}{\sqrt{2\pi r}}\cos\frac{\theta}{2} \quad \text{(D-34)}$$

Similarly, for eq. (D-32), imposing $\gamma = \frac{\pi}{2}$ and replacing the definition of K_I gives

$$\sigma_{yy} - \sigma_{xx} + 2i\ \sigma_{xy} = \frac{K_I\ e^{-\frac{3}{2}i\theta}}{\sqrt{2\pi r}}\left[\frac{\rho}{r} + 2i\ \sin\frac{\theta}{2}\cos\frac{\theta}{2}\right] \tag{D-35}$$

Solving the system of equations for three unknown variables, eq. (D-34) provides one equation while eq. (D-35) two equations, by splitting real and complex portions results.

$$\sigma_{xx} = \frac{K_I}{\sqrt{2\pi r}}\cos\frac{\theta}{2}\left[1 - \sin\frac{\theta}{2}\sin\frac{3\theta}{2}\right] - \frac{K_I}{\sqrt{2\pi r}}\left[\frac{\rho}{2r}\cos\frac{3\theta}{2}\right] \tag{D-36}$$

$$\sigma_{yy} = \frac{K_I}{\sqrt{2\pi r}}\cos\frac{\theta}{2}\left[1 + \sin\frac{3\theta}{2}\sin\frac{\theta}{2}\right] + \frac{K_I}{\sqrt{2\pi r}}\left[\frac{\rho}{2r}\cos\frac{3\theta}{2}\right] \tag{D-37}$$

$$\sigma_{xy} = \frac{K_I}{\sqrt{2\pi r}}\left[\sin\frac{\theta}{2}\cos\frac{\theta}{2}\cos\frac{3\theta}{2}\right] - \frac{K_I}{\sqrt{2\pi r}}\left[\frac{\rho}{r}\sin\frac{3\theta}{2}\right] \tag{D-38}$$

The full derivation is presented in section D.10.

D.2
Fracture under Mode II

For mode II case, resultant stresses are obtained by combining the superposition of a positive load σ_n in an angle $\gamma = \frac{\pi}{4}$ and a negative load $-\sigma_n$ in $\gamma = \frac{3\pi}{4}$. Rewriting eq. (D-31) and comparing to Williams' solution in eq. (2-8) provides:

$$K_{II} = \sigma_n\sqrt{\pi a} \tag{D-39}$$

and

$$\sigma_{xx} + \sigma_{yy} = -2\sigma_n\sqrt{\frac{a}{2r}}\cdot\sin\frac{\theta}{2} \tag{D-40}$$

For eq. (D-32):

$$\sigma_{yy} - \sigma_{xx} + 2i\ \sigma_{xy} = \frac{K_{II}\ e^{-\frac{3}{2}i\theta}}{2\sqrt{2\pi r}\ r}\cdot 2i[2\alpha + \beta i]\rho \tag{D-41}$$

substituting definition from eqs. (D-23) and (D-24) we have

$$\sigma_{yy} - \sigma_{xx} + 2i\ \sigma_{xy} = \frac{K_{II}\ e^{-\frac{3}{2}i\theta}}{\sqrt{2\pi r}}\cdot\left[2i\ \cos\theta - \sin\theta - i\frac{\rho}{r}\right] \tag{D-42}$$

Solving system of eqs. (D-40) and (D-42) for σ_{xx}, σ_{yy} and σ_{xy} results

$$\sigma_{xx} = -\frac{K_{II}}{\sqrt{2\pi r}}\cdot\sin\frac{\theta}{2}\left[2 + \cos\frac{\theta}{2}\cos\frac{3\theta}{2}\right] + \frac{K_{II}}{\sqrt{2\pi r}}\cdot\left[\frac{\rho}{2r}\sin\frac{3\theta}{2}\right] \tag{D-43}$$

$$\sigma_{yy} = \frac{K_{II}}{\sqrt{2\pi r}} \cdot \left[\sin\frac{\theta}{2} \cos\frac{\theta}{2} \cos\frac{3\theta}{2} \right] - \frac{K_{II}}{\sqrt{2\pi r}} \cdot \left[\frac{\rho}{2r} \sin\frac{3\theta}{2} \right] \tag{D-44}$$

$$\sigma_{xy} = \frac{K_{II}}{\sqrt{2\pi r}} \cdot \cos\frac{\theta}{2} \left[1 - \sin\frac{\theta}{2} \sin\frac{3\theta}{2} \right] - \frac{K_{II}}{\sqrt{2\pi r}} \cdot \left[\frac{\rho}{2r} \cos\frac{3\theta}{2} \right] \tag{D-45}$$

Full derivation is presented in section D.11.

D.3
Fracture under Mode III

The Mode III solution is obtained by subjecting a shear stress $\pm S_n$ loading in z-direction, at $y = \pm\infty$. Using the hydrodynamic analogy to torsion and considering the flow past an elliptical cylinder, from [32], we have

$$\sigma_{xz} - i\ \sigma_{yz} = \frac{S_n(a+b)}{c} \left[\frac{\sinh\left(\zeta - \xi_0 - \frac{i\pi}{2}\right)}{\sinh\zeta} \right] \tag{D-46}$$

that, by proceeding some algebraic manipulation, yields on

$$\sigma_{xz} - i\ \sigma_{yz} = S_n \frac{1 + \sqrt{\frac{\rho}{a}}}{\sqrt{1 - \frac{\rho}{a}}} \cdot \frac{i}{\sqrt{1 - \frac{\rho}{a}}} \left[\sqrt{\frac{\rho}{a}} - \frac{\cosh\zeta}{\sinh\zeta} \right] \tag{D-47}$$

where

$$\frac{\cosh\zeta}{\sinh\zeta} = \frac{(1 + \alpha\frac{\rho}{a} + \beta\frac{\rho}{a}i)e^{-\frac{i\theta}{2}}}{\sqrt{2\frac{r}{a}}} \tag{D-48}$$

Neglecting the higher order terms in $\frac{\rho}{a}$, eq. (D-46) gives

$$\sigma_{xz} - i\ \sigma_{yz} = -\frac{S_n\ i}{\sqrt{2}} \sqrt{\frac{a}{r}}\ e^{-\frac{i\theta}{2}} \tag{D-49}$$

Comparing σ_{xz} and σ_{yz} from Williams' stress field, in eq. (2-9), K_{III} results in

$$K_{III} = S_n\sqrt{\pi a} \tag{D-50}$$

As a result, the stresses for mode III are as

$$\sigma_{xz} = -\frac{K_{III}}{\sqrt{2\pi r}} \cdot \sin\frac{\theta}{2} \tag{D-51}$$

$$\sigma_{yz} = \frac{K_{III}}{\sqrt{2\pi r}} \cdot \cos\frac{\theta}{2} \tag{D-52}$$

Full derivation is presented in section D.11.

D.4
Part 1

In this section some basic trigonometric equations are presented for further use in the problem derivation.

$$\sin -x = -\sin x \tag{D-53}$$

$$\cos -x = \cos x \tag{D-54}$$

$$\sin 2x = 2\sin x \cos x \tag{D-55}$$

$$e^{ix} = \cos x + i \sin x \tag{D-56}$$

$$\cos(x - y) = \cos x \cos y + \sin x \sin y \tag{D-57}$$

$$\sin(x - y) = \sin x \cos y - \cos x \sin y \tag{D-58}$$

$$\sinh(-x) = -\sinh x \tag{D-59}$$

$$\cosh(-x) = \cosh x \tag{D-60}$$

$$\cosh^2 x - \sinh^2 x = 1 \tag{D-61}$$

$$\cosh(x + y) = \cosh x \cosh y + \sinh x \sinh y \tag{D-62}$$

$$\sinh(x + y) = \sinh x \cosh y + \cosh x \sinh y \tag{D-63}$$

$$\sinh(x + iy) = \sinh x \cos y + i \cosh x \sin y \tag{D-64}$$

$$\cosh(x + iy) = \cosh x \cos y + i \sinh x \sin y \tag{D-65}$$

$$\sinh 2x = 2\sinh x \cdot \cosh x \tag{D-66}$$

$$\cosh 2x = \cosh^2 x + \sinh^2 x \tag{D-67}$$

$$\sinh x = \frac{e^x - e^{-x}}{2} \tag{D-68}$$

$$\cosh x = \frac{e^x + e^{-x}}{2} \tag{D-69}$$

$$\frac{d}{dx}\cosh^{-1} x = \frac{1}{\sqrt{x^2 - 1}} \tag{D-70}$$

D.5
Part 2

Considering the hyperbolic eq. (D-61) and substituting definition from eq. (D-7), we have:

$$\underbrace{c\cosh^2\zeta}_{Z} - c\sinh^2\zeta = c \therefore c\sinh\zeta = \sqrt{Z^2-c^2} \tag{D-71}$$

Therefore, rewriting $4\Omega(Z)$ with results from equation in above and (D-5)

$$\begin{aligned} 4\Omega(Z) &= \sigma_n[e^{2\xi_0}\cos(2\gamma)\underbrace{c\cosh(\zeta)}_{Z} + (1-e^{2\xi_0+2i\gamma})\underbrace{c\sinh(\zeta)}_{\sqrt{Z^2-c^2}}] \\ &= \sigma_n\left[e^{2\xi_0}Z\cos(2\gamma) + (1-e^{2\xi_0+2i\gamma})\sqrt{Z^2-c^2}\right] \end{aligned} \tag{D-72}$$

For the second stress function $4\chi(Z)$, it is convinient to derive some equations for future use. Applying eqs. (D-66), (D-67) and (D-65)

$$\sinh 2\zeta = 2\underbrace{\sinh\zeta}_{\frac{\sqrt{Z^2-c^2}}{c}}\cdot\underbrace{\cosh\zeta}_{\frac{Z}{c}} = \frac{2Z\sqrt{Z^2-c^2}}{c^2} \tag{D-73}$$

$$\cosh 2\zeta = (\underbrace{\cosh\zeta}_{\frac{Z}{c}})^2 + (\underbrace{\sinh\zeta}_{\frac{\sqrt{Z^2-c^2}}{c}})^2 = \frac{2Z^2-c^2}{c^2} \tag{D-74}$$

$$\cosh 2(\zeta-\xi_0-i\gamma) = \cosh 2\zeta\cdot\cosh 2(-\xi_0-i\gamma) + \sinh 2\zeta\cdot\sinh 2(-\xi_0-i\gamma) \tag{D-75}$$

simplifying equation in above with properties (D-59) and (D-60)

$$\cosh 2(\zeta-\xi_0-i\gamma) = \cosh 2\zeta\cdot\cosh 2(\xi_0+i\gamma) - \sinh 2\zeta\cdot\sinh 2(\xi_0+i\gamma) \tag{D-76}$$

and substituting eqs. (D-73) and (D-74) into equation in above results in

$$\cosh 2(\zeta-\xi_0-i\gamma) = \cosh 2(\xi_0+i\gamma)\cdot\frac{2Z^2-c^2}{c^2} - 2\sinh 2(\xi_0+i\gamma)\cdot\frac{Z\sqrt{Z^2-c^2}}{c^2} \tag{D-77}$$

In addition, from eq. (D-5), ζ is isolated as

$$\zeta = \cosh^{-1}\frac{Z}{c} \tag{D-78}$$

By substituting eqs. (D-77), (D-78) into eq. (D-13)

$$4\chi(Z) = -\sigma_n c^2 \Bigg[[\cosh(2\xi_0) - \cos(2\gamma)] \cosh^{-1}\left(\frac{Z}{c}\right) + \frac{1}{2} e^{2\xi_0} \Bigg(\cosh[2(\xi_0 + i\gamma)] \frac{2Z^2 - c^2}{c^2} - 2\sinh[2(\xi_0 + i\gamma)] \frac{Z\sqrt{Z^2 - c^2}}{c^2} \Bigg) \Bigg] \quad \text{(D-79)}$$

D.6
Part 3

Taking the derivative of eq. (D-14), we have:

$$\Omega'(Z) = \frac{d\Omega}{dZ} = \frac{1}{4}\sigma_n\left[e^{2\xi_0}\cos(2\gamma) + (1 - e^{2\xi_0+2i\gamma})\cdot\frac{Z}{\sqrt{Z^2-c^2}}\right] \tag{D-80}$$

For the second stress function, taking the first and second derivative of eq. (D-79) provides

$$\begin{aligned}\chi'(Z) = &-\frac{\sigma_n c^2}{4}\Bigg\{[\cosh(2\xi_0)-\cos(2\gamma)]\frac{1}{\sqrt{\frac{Z^2}{c^2}-1}}\frac{1}{c} + \frac{1}{2}e^{2\xi_0}\Bigg[\cosh[2(\xi_0+i\gamma)]\frac{4Z}{c^2} \\ &- 2\sinh[2(\xi_0+i\gamma)]\left(\frac{\sqrt{Z^2-c^2}}{c^2} + \frac{Z}{c^2}\frac{1}{2}(Z^2-c^2)^{-1/2}\,2Z\right)\Bigg]\Bigg\}\end{aligned} \tag{D-81}$$

$$\begin{aligned}\chi''(Z) = &-\frac{\sigma_n c^2}{4}\Bigg\{[\cosh(2\xi_0)-\cos(2\gamma)]\left(-\frac{1}{2}\frac{c^3}{(Z^2-c^2)^{3/2}}\frac{2Z}{c^3}\right) \\ &+ \frac{1}{2}e^{2\xi_0}\Bigg[\cosh[2(\xi_0+i\gamma)]\frac{4}{c^2} \\ &- 2\sinh[2(\xi_0+i\gamma)]\left(\frac{1}{2c^2}(Z^2-c^2)^{-1/2}\,2Z + \frac{2Z}{c^2}(Z^2-c^2)^{-1/2}\right. \\ &\left.- \frac{1}{2}\frac{Z^2}{c^2}(Z^2-c^2)^{-3/2}\,2Z\right)\Bigg]\Bigg\} \\ = &\frac{\sigma_n}{4}\left\{[\cosh(2\xi_0)-\cos(2\gamma)]\cdot\frac{Zc^2}{(Z^2-c^2)^{3/2}}\right\} - \frac{\sigma_n}{2}e^{2\xi_0}\cosh[2(\xi_0+i\gamma)] \\ &+ \frac{\sigma_n c^2}{4}e^{2\xi_0}\sinh[2(\xi_0+i\gamma)]\cdot(Z^2-c^2)^{-3/2}\,\frac{1}{c^2}\cdot \\ &\cdot\underbrace{\Big[Z\,(Z^2-c^2)+2Z\,(Z^2-c^2)-Z^3\Big]}_{2Z^3-3Zc^2} \\ = &\frac{\sigma_n}{4\,(Z^2-c^2)^{3/2}}\Bigg[[\cosh(2\xi_0)-\cos(2\gamma)]\;Zc^2 \\ &+ e^{2\xi_0}\;\sinh[2(\xi_0+i\gamma)]\;(2Z^3-3Zc^2)\Bigg] - \frac{\sigma_n}{2}\;e^{2\xi_0}\;\cosh[2(\xi_0+i\gamma)]\end{aligned} \tag{D-82}$$

D.7
Part 4

From a basic math, $e^{2\xi_0}$ may be written as

$$e^{2\xi_0} = \frac{e^{2\xi_0} - e^{2\xi_0}}{2} + \frac{e^{2\xi_0} + e^{2\xi_0}}{2} \tag{D-83}$$

or, from eqs. (D-68) and (D-69)

$$e^{2\xi_0} = \sinh 2\xi_0 + \cosh 2\xi_0 \tag{D-84}$$

expanding equation above as function of half of the angle, as presented in eqs. (D-66) and (D-67)

$$e^{2\xi_0} = 2\sinh\xi_0\cosh\xi_0 + \cosh^2\xi_0 + \sinh^2\xi_0 \tag{D-85}$$

Rewriting equation in above by replacing definition of $\sinh\xi_0$ and $\cosh\xi_0$ from eq. (D-7), we have

$$e^{2\xi_0} = 2\frac{b}{c}\frac{a}{c} + \frac{a^2}{c^2} + \frac{b^2}{c^2} = \frac{(a+b)^2}{c^2} \tag{D-86}$$

Substituting c^2 from eq. (D-9)

$$\begin{aligned} e^{2\xi_0} &= \frac{a^2 + 2ab + b^2}{a^2(1-\frac{\rho}{a})} \\ &= \left(1 + \frac{2\cancel{a}}{\cancel{a}}\overbrace{\frac{b}{a}}^{\sqrt{\frac{\rho}{a}}} + \frac{1}{a}\overbrace{\frac{b^2}{a}}^{\rho}\right)\cdot\frac{1}{1-\frac{\rho}{a}} \\ &= \frac{1 + 2\sqrt{\frac{\rho}{a}} + \frac{\rho}{a}}{1-\frac{\rho}{a}} \end{aligned} \tag{D-87}$$

$e^{2\xi_0}$ is written as function of $\sqrt{\frac{\rho}{a}}$. Defining λ as

$$\lambda \coloneqq \sqrt{\frac{\rho}{a}} \tag{D-88}$$

and assuming f being the analytical function equal to $e^{2\xi_0}$, we have

$$f = \frac{1 + 2\lambda + \lambda^2}{1 - \lambda^2} \tag{D-89}$$

that, by using Taylor's series expansion, function f may be approximated as

$$f = f(\lambda = 0) + f'(\lambda = 0)(\lambda - 0) + \frac{f''(\lambda = 0)}{2!}(\lambda - 0)^2 + \cdots \tag{D-90}$$

where the derivatives are

$$f' = \frac{2 + 2\lambda}{1 - \lambda^2} + \frac{2\lambda(1 + 2\lambda + \lambda^2)}{(1-\lambda)^2} \tag{D-91}$$

$$f'' = \frac{2}{1-\lambda^2} + \frac{2(\lambda^2+2\lambda+1)}{(\lambda^2-1)^2} + \frac{4\lambda(2\lambda+2)}{(\lambda^2-1)^2} - \frac{8\lambda^2(\lambda^2+2\lambda+1)}{(\lambda^2-1)^3} \tag{D-92}$$

Therefore, substituting eqs. (D-91) and (D-92) into (D-90)

$$e^{2\xi_0} = 1 + 2\sqrt{\frac{\rho}{a}} + 2\frac{\rho}{a} + \cdots \tag{D-93}$$

Following the same procedure, it is convenient to prove the expansion of the above function for future use

$$f = \left(1 - \frac{\rho}{a}\right)^{-1} \tag{D-94}$$

using λ as

$$\lambda \coloneqq \frac{\rho}{a} \tag{D-95}$$

function f, is rewritten as

$$f = (1-\lambda)^{-1} \tag{D-96}$$

Since only higher order terms in $\frac{\rho}{a}$, we have

$$f = f(\lambda = 0) + f'(\lambda = 0)(\lambda - 0) + \cdots \tag{D-97}$$

where

$$f' = (1-\lambda)^{-2} \tag{D-98}$$

Therefore,

$$\left(1 - \frac{\rho}{a}\right)^{-1} \approx 1 + \frac{\rho}{a} \tag{D-99}$$

D.8
Part 5

Replacing variable Z, defined in eq. (D-18), and result from eq. (D-25), provides

$$\begin{aligned}\Omega'(Z) &= \frac{1}{4}\sigma_n\left[e^{2\xi_0}\cos(2\gamma) + (1-e^{2\xi_0+2i\gamma})\cdot\cancel{a}\left(1+\alpha\frac{\rho}{a}+\beta\frac{\rho}{a}i\right)\cdot\frac{1}{\sqrt{2\cancel{a}^2 e^{i\theta}\,\frac{r}{\cancel{a}}}}\right] \\ &= \frac{1}{4}\sigma_n\left[e^{2\xi_0}\cos(2\gamma) + \frac{(1-e^{2\xi_0+2i\gamma})}{\sqrt{2}}\left(1+\alpha\frac{\rho}{a}+\beta\frac{\rho}{a}i\right)e^{-\frac{i\theta}{2}}\sqrt{\frac{a}{r}}\right]\end{aligned} \tag{D-100}$$

As previously presented in eq. (D-27), the first term may be neglected. Although the first term also depends on $\cos 2\gamma$, since cosine is a limited function, it does not affect in our simplification. Thus, replacing the expansion from D-26, we have

$$\begin{aligned}\Omega'(Z) &= \frac{1}{4}\sigma_n\left[\frac{(1-e^{2\xi_0+2i\gamma})}{\sqrt{2}}\left(1+\alpha\frac{\rho}{a}+\beta\frac{\rho}{a}i\right)e^{-\frac{i\theta}{2}}\sqrt{\frac{a}{r}}\right] \\ &= \frac{\sigma_n}{4}\sqrt{\frac{a}{2r}}\left(1-e^{2\xi_0}\cdot e^{2i\gamma}\right)\left(1+\alpha\frac{\rho}{a}+\beta\frac{\rho}{a}i\right)\left(\cos\frac{\theta}{2}+i\sin\frac{\theta}{2}\right) \\ &= \frac{\sigma_n}{4}\sqrt{\frac{a}{2r}}\left[1-\left(1+2\sqrt{\frac{\rho}{a}}+2\frac{\rho}{a}\right)\cdot(\cos 2\gamma+i\sin 2\gamma)\right]\cdot \\ &\qquad\cdot\left[\cos\frac{\theta}{2}+i\sin\frac{\theta}{2}+\left(\alpha\frac{\rho}{a}+i\beta\frac{\rho}{a}\right)\cdot\left(\cos\frac{\theta}{2}+i\sin\frac{\theta}{2}\right)\right] \\ &= \frac{\sigma_n}{4}\sqrt{\frac{a}{2r}}\left[1-\cos 2\gamma-i\sin 2\gamma-\underbrace{\left(2\sqrt{\frac{\rho}{a}}+2\frac{\rho}{a}\right)\cdot(\cos 2\gamma+i\sin 2\gamma)}_{*}\right]\cdot \\ &\qquad\cdot\left[\cos\frac{\theta}{2}+i\sin\frac{\theta}{2}+\underbrace{\left(\alpha\frac{\rho}{a}+i\beta\frac{\rho}{a}\right)\cdot\left(\cos\frac{\theta}{2}+i\sin\frac{\theta}{2}\right)}_{*}\right]\end{aligned} \tag{D-101}$$

Note that, from the same reason as presented before (eq. D-27), terms $*$ can be neglected since they are irrelevant in comparison to $\sqrt{\frac{a}{r}}$. Rewriting equation in above and splitting the real and complex portions, we have

$$\begin{aligned}\Omega'(Z) &= \frac{\sigma_n}{4}\sqrt{\frac{a}{2r}}\left(1-\cos 2\gamma - i\sin 2\gamma\right)\cdot\left(\cos\frac{\theta}{2}+i\sin\frac{\theta}{2}\right)\\ &= \frac{\sigma_n}{4}\sqrt{\frac{a}{2r}}\Bigg(\cos\frac{\theta}{2}-\cos 2\gamma\cos\frac{\theta}{2}-\sin 2\gamma\sin\frac{\theta}{2}\underbrace{i^2}_{-1}+i\sin\frac{\theta}{2}\\ &\qquad\qquad -i\sin\frac{\theta}{2}\cos 2\gamma - i\sin 2\gamma\cos\frac{\theta}{2}\Bigg)\\ &= \frac{\sigma_n}{4}\sqrt{\frac{a}{2r}}\Bigg[(1-\cos 2\gamma)\cos\frac{\theta}{2}-\sin\frac{\theta}{2}\\ &\qquad + i\left(\sin\frac{\theta}{2}-\sin\frac{\theta}{2}\cos 2\gamma-\sin 2\gamma\cos\frac{\theta}{2}\right)\Bigg]\end{aligned} \tag{D-102}$$

Taking the derivative of $\Omega'(Z)$, from eq. (D-16), and expanding $e^{2\xi_0}$ as presented on eq. (D-26), we obtain

$$\begin{aligned}\Omega''(Z) &= \frac{1}{4}\sigma_n(1-e^{2i\gamma}\cdot e^{2\xi_0})\left[-\frac{1}{2}(Z^2-c^2)^{-3/2}\cdot Z^2+(Z^2-c^2)^{1/2}\right]\\ &= \frac{1}{4}\sigma_n\left[1-e^{2i\gamma}\cdot\left(1+2\sqrt{\frac{\rho}{a}}+2\frac{\rho}{a}\right)\right]\cdot(Z^2-c^2)^{-3/2}\left[-\cancel{Z^2}+(\cancel{Z^2}-\underbrace{c^2}_{a^2(1-\frac{\rho}{a})})\right]\\ &= -\frac{\sigma_n a^2}{4}\left(1-\frac{\rho}{a}\right)\left[1-e^{2i\gamma}\cdot\left(1+2\sqrt{\frac{\rho}{a}}+2\frac{\rho}{a}\right)\right]\cdot(Z^2-c^2)^{-3/2}\end{aligned} \tag{D-103}$$

From eq. (D-5), the conjugate of Z, $\bar{Z}$, is easily obtained as

$$\bar{Z} = a\left(1+\alpha\frac{\rho}{a}-\beta\frac{\rho}{a}i\right) \tag{D-104}$$

that, multiplied by $\Omega''(Z)$, substituting eqs. (D-9), (D-26) and ignoring higher order terms in $\frac{\rho}{a}$

$$\begin{aligned}
\bar{Z}\Omega''(Z) &= -\frac{\sigma_n a^2}{4\cdot(Z^2-c^2)^{3/2}}\cdot\overbrace{a\left(1+\alpha\frac{\rho}{a}-\beta\frac{\rho}{a}i\right)}^{\bar{Z}}\cdot\left(1-\frac{\rho}{a}\right)\left[1-e^{2i\gamma}\cdot\left(1+2\sqrt{\frac{\rho}{a}}+2\frac{\rho}{a}\right)\right] \\
&= -\frac{\sigma_n a^3}{4\cdot(Z^2-c^2)^{3/2}}\left(1-\frac{\rho}{a}+\alpha\frac{\rho}{a}-\alpha\underbrace{\left(\frac{\rho}{a}\right)^2}_{\approx 0}-\beta\frac{\rho}{a}i+\beta\underbrace{\left(\frac{\rho}{a}\right)^2}_{\approx 0}i\right)\cdot \\
&\qquad\qquad\left[1-(\cos 2\gamma+i\sin 2\gamma)\cdot\left(1+2\sqrt{\frac{\rho}{a}}+2\frac{\rho}{a}\right)\right] \\
&= -\frac{\sigma_n a^3}{4\cdot(Z^2-c^2)^{3/2}}\left[1+(\alpha-1)\frac{\rho}{a}-\beta\frac{\rho}{a}i-(\cos 2\gamma+i\sin 2\gamma)\cdot\right. \\
&\qquad\qquad\left.\cdot\left(1+(\alpha-1)\frac{\rho}{a}-\beta\frac{\rho}{a}i\right)\cdot\left(1+2\sqrt{\frac{\rho}{a}}+2\frac{\rho}{a}\right)\right] \\
&= -\frac{\sigma_n a^3}{4\cdot(Z^2-c^2)^{3/2}}\left[1+(\alpha-1)\frac{\rho}{a}-\beta\frac{\rho}{a}i-\cos 2\gamma\left(1+2\sqrt{\frac{\rho}{a}}\right.\right. \\
&\quad\left.\left.+(\alpha+1)\frac{\rho}{a}-\beta\frac{\rho}{a}i\right)-i\sin 2\gamma\left(1+2\sqrt{\frac{\rho}{a}}+(\alpha+1)\frac{\rho}{a}-\beta\frac{\rho}{a}i\right)\right.
\end{aligned} \tag{D-105}$$

From eq. (D-15)

$$\begin{aligned}
\chi''(Z) &= \frac{\sigma_n}{4\ (Z^2-c^2)^{3/2}}\Big[[\cosh(2\xi_0)-\cos(2\gamma)]\ Zc^2 \\
&+ e^{2\xi_0}\ \sinh[2(\xi_0+i\gamma)]\ (2Z^3-3Zc^2)\Big]\underbrace{-\frac{\sigma_n}{2}\ e^{2\xi_0}\ \cosh[2(\xi_0+i\gamma)]}_{\text{insignificant}}
\end{aligned} \tag{D-106}$$

Note that the last term from equation above is considered negligible in comparison to the rest of equation.

Expanding Z^3, from eq. (D-18), we have

$$\begin{aligned}
Z^3 &= \left(1+\alpha\frac{\rho}{a}+\beta\frac{\rho}{a}\right)\cdot\left(1+\alpha\frac{\rho}{a}+\beta\frac{\rho}{a}\right)\cdot\left(1+\alpha\frac{\rho}{a}+\beta\frac{\rho}{a}\right) \\
&= \left[1+2\alpha\frac{\rho}{a}+2\beta\frac{\rho}{a}+\underbrace{\left(\alpha\frac{\rho}{a}+\beta\frac{\rho}{a}\right)^2}_{\approx 0}\right]\cdot\left(1+\alpha\frac{\rho}{a}+\beta\frac{\rho}{a}\right) \\
&= 1+3\alpha\frac{\rho}{a}+3\beta\frac{\rho}{a}+\underbrace{2\left(\alpha\frac{\rho}{a}+\beta\frac{\rho}{a}\right)^2}_{\approx 0}
\end{aligned} \tag{D-107}$$

Resulting in

$$\chi''(Z) = \frac{\sigma_n}{4\ (Z^2 - c^2)^{3/2}} \Bigg\{ [\cosh(2\xi_0) - \cos(2\gamma)]\ a\left(1 + \alpha\frac{\rho}{a} + \beta\frac{\rho}{a}i\right)c^2 + \left(1 + 2\sqrt{\frac{\rho}{a}}\right)\ \sinh[2(\xi_0 + i\gamma)]\ \left[2a^3\left(1 + 3\alpha\frac{\rho}{a} + 3\beta\frac{\rho}{a}i\right) - 3a\left(1 + \alpha\frac{\rho}{a} + \beta\frac{\rho}{a}i\right)\ c^2\right]\Bigg\} \tag{D-108}$$

From eq. (D-64) we have

$$\sinh[2(\xi_0 + i\gamma)] = \sinh 2\xi_0 \cos 2\gamma + i \cosh 2\xi_0 \sin 2\gamma \tag{D-109}$$

from definition of c^2 (eq. D-9) and ρ (eq. D-8) eqs. (D-67) and (D-68) are derived as following

$$\cosh(2\xi_0) = \underbrace{(\cosh\xi_0)}_{\frac{a}{c}}^2 + \underbrace{(\sinh\xi_0)}_{\frac{b}{c}}^2 = \frac{a^2 + b^2}{c^2} = \frac{a^2}{c^2}\left(1 + \underbrace{\frac{b^2}{a}}_{\rho}\frac{1}{a}\right) = \frac{a^2}{c^2}\left(1 + \frac{\rho}{a}\right) \tag{D-110}$$

$$\sinh(2\xi_0) = 2\underbrace{\sinh\xi_0}_{\frac{b}{c}} \cdot \underbrace{\cosh\xi_0}_{\frac{a}{c}} = \frac{2ab}{c^2} = \frac{2a^2}{c^2}\sqrt{\underbrace{\frac{b^2}{a}}_{\rho}\frac{1}{a}} = \frac{2a^2}{c^2}\sqrt{\frac{\rho}{a}} \tag{D-111}$$

Substituting eqs. (D-109), (D-110) and (D-111) into (D-108) provides

$$\begin{aligned}
\chi''(Z) = \frac{\sigma_n}{4\,(Z^2-c^2)^{3/2}}\Bigg\{ & \left[\frac{a^2}{c^2}\left(1+\frac{\rho}{a}\right) - \cos(2\gamma)\right]\, a\left(1+\alpha\frac{\rho}{a}+\beta\frac{\rho}{a}i\right)c^2 + \\
& \left(1+2\sqrt{\frac{\rho}{a}}+2\frac{\rho}{a}\right)\left[\frac{2a^2}{c^2}\sqrt{\frac{\rho}{a}}\cdot\cos 2\gamma + i\frac{a^2}{c^2}\left(1+\frac{\rho}{a}\right)\cdot\sin 2\gamma\right]\cdot \\
& \cdot\left[2a^3\left(1+3\alpha\frac{\rho}{a}+3\beta\frac{\rho}{a}i\right) - 3a\left(1+\alpha\frac{\rho}{a}+\beta\frac{\rho}{a}i\right)\,c^2\right]\Bigg\} \\
= \frac{\sigma_n}{4\,(Z^2-c^2)^{3/2}}\Bigg\{ & \underbrace{\frac{a^3}{\cancel{c^2}}\left(1+\frac{\rho}{a}\right)\left(1+\alpha\frac{\rho}{a}+\beta\frac{\rho}{a}i\right)\cancel{c^2}}_{I} \\
& - \cos 2\gamma\,\underbrace{a\left(1+\alpha\frac{\rho}{a}+\beta\frac{\rho}{a}i\right)\overbrace{c^2}^{a^2(1-\frac{\rho}{a})}}_{II} \\
& + \cos 2\gamma\,\underbrace{\left[\frac{2a^2}{c^2}\sqrt{\frac{\rho}{a}}\left(1+2\sqrt{\frac{\rho}{a}}+2\frac{\rho}{a}\right)\cdot\left(2a^3\left(1+3\alpha\frac{\rho}{a}+3\beta\frac{\rho}{a}i\right)\right.\right.}_{III} \\
& \underbrace{\left.\left. -3a\left(1+\alpha\frac{\rho}{a}+\beta\frac{\rho}{a}i\right)\,c^2\right)\right]}_{} \\
& + i\sin 2\gamma\,\underbrace{\left[\frac{a^2}{c^2}\left(1+\frac{\rho}{a}\right)\cdot\left(1+2\sqrt{\frac{\rho}{a}}+2\frac{\rho}{a}\right)\cdot\left(2a^3\left(1+3\alpha\frac{\rho}{a}+3\beta\frac{\rho}{a}i\right)\right.\right.}_{IV} \\
& \underbrace{\left.\left. -3a\left(1+\alpha\frac{\rho}{a}+\beta\frac{\rho}{a}i\right)\,c^2\right)\right]}_{}\Bigg\}
\end{aligned} \tag{D-112}$$

Due to its size of equation in above, four efferents parts (I, II, III and IV) will be derived in bellow. Higher order terms in $\frac{\rho}{a}$ are neglected.

$$\begin{aligned}
I &= a^3\left(1+\frac{\rho}{a}+\alpha\frac{\rho}{a}+\alpha\underbrace{\left(\frac{\rho}{a}\right)^2}_{\approx 0}+\beta\frac{\rho}{a}i+\beta\underbrace{\left(\frac{\rho}{a}\right)^2}_{\approx 0}i\right) \\
&= a^3\left(1+\frac{\rho}{a}+\alpha\frac{\rho}{a}+\beta\frac{\rho}{a}i\right)
\end{aligned} \tag{D-113}$$

$$\begin{aligned}
II &= a^3\left(1-\frac{\rho}{a}+\alpha\frac{\rho}{a}-\alpha\underbrace{\left(\frac{\rho}{a}\right)^2}_{\approx 0}+\beta\frac{\rho}{a}i-\beta\underbrace{\left(\frac{\rho}{a}\right)^2}_{\approx 0}i\right) \\
&= a^3\left(1-\frac{\rho}{a}+\alpha\frac{\rho}{a}+\beta\frac{\rho}{a}i\right)
\end{aligned} \tag{D-114}$$

In parts III and IV, an additional approximation must be considered, by applying eq. (D-99) gives

$$\begin{aligned}
III &= \frac{2a^2}{c^2}\left(\sqrt{\frac{\rho}{a}} + 2\frac{\rho}{a} + \underbrace{2\frac{\rho}{a}\sqrt{\frac{\rho}{a}}}_{\approx 0}\right)\cdot\left[2a^3\left(1 + 3\alpha\frac{\rho}{a} + 3\beta\frac{\rho}{a}i\right)\right. \\
&\qquad\qquad\qquad\qquad\qquad\qquad\qquad\qquad \left. - 3a\left(1 + \alpha\frac{\rho}{a} + \beta\frac{\rho}{a}i\right)\, c^2\right] \\
&= \frac{4a^2}{c^2}\left(\sqrt{\frac{\rho}{a}} + 2\frac{\rho}{a}\right)\cdot\left(1 + 3\alpha\frac{\rho}{a} + 3\beta\frac{\rho}{a}i\right)a^3 \\
&\quad - \frac{6a^3}{\cancel{c^2}}\left(\sqrt{\frac{\rho}{a}} + 2\frac{\rho}{a}\right)\cdot\left(1 + \alpha\frac{\rho}{a} + \beta\frac{\rho}{a}i\right)\cancel{c^2} \\
&= \frac{4\cancel{a^2}}{\cancel{a^2}}\underbrace{\left(1 - \frac{\rho}{a}\right)^{-1}}_{\approx(1+\frac{\rho}{a})}\left[\sqrt{\frac{\rho}{a}} + 2\frac{\rho}{a} + \underbrace{\left(\sqrt{\frac{\rho}{a}} + 2\frac{\rho}{a}\right)\cdot\left(3\alpha\frac{\rho}{a} + 3\beta\frac{\rho}{a}i\right)}_{\approx 0}\right]a^3 \\
&\qquad\qquad - 6a^3\left[\sqrt{\frac{\rho}{a}} + 2\frac{\rho}{a} + \underbrace{\left(\sqrt{\frac{\rho}{a}} + 2\frac{\rho}{a}\right)\cdot\left(\alpha\frac{\rho}{a} + \beta\frac{\rho}{a}i\right)}_{\approx 0}\right] \\
&= 4a^3\left[\sqrt{\frac{\rho}{a}} + 2\frac{\rho}{a} + \underbrace{\frac{\rho}{a}\left(\sqrt{\frac{\rho}{a}} + 2\frac{\rho}{a}\right)}_{\approx 0}\right] - 6a^3\left(\sqrt{\frac{\rho}{a}} + 2\frac{\rho}{a}\right) \\
&= 4a^3\sqrt{\frac{\rho}{a}} + 8a^3\frac{\rho}{a} - 6a^3\sqrt{\frac{\rho}{a}} - 12a^3\frac{\rho}{a} \\
&= -2a^3\sqrt{\frac{\rho}{a}} - 4a^3\frac{\rho}{a}
\end{aligned} \tag{D-115}$$

$$
\begin{aligned}
IV = \frac{a^2}{c^2}\left(1+\frac{\rho}{a}\right)\cdot\left(1+2\sqrt{\frac{\rho}{a}}+2\frac{\rho}{a}\right)\cdot\Bigg[2a^3\left(1+3\alpha\frac{\rho}{a}+3\beta\frac{\rho}{a}i\right) \\
-3a\left(1+\alpha\frac{\rho}{a}+\beta\frac{\rho}{a}i\right)c^2\Bigg] \\
= \frac{a^2}{c^2}\Bigg[1+2\sqrt{\frac{\rho}{a}}+3\frac{\rho}{a}+\underbrace{\frac{\rho}{a}\left(2\sqrt{\frac{\rho}{a}}+2\frac{\rho}{a}\right)}_{\approx 0}\Bigg]\cdot\Bigg[2a^3\left(1+3\alpha\frac{\rho}{a}+3\beta\frac{\rho}{a}i\right) \\
-3a\left(1+\alpha\frac{\rho}{a}+\beta\frac{\rho}{a}i\right)c^2\Bigg] \\
= \frac{a^2}{c^2}\Bigg[1+3\alpha\frac{\rho}{a}+3\beta\frac{\rho}{a}i+2\sqrt{\frac{\rho}{a}}+3\frac{\rho}{a}+\underbrace{\left(2\sqrt{\frac{\rho}{a}}+3\frac{\rho}{a}\right)\cdot\left(3\alpha\frac{\rho}{a}+3\beta\frac{\rho}{a}i\right)}_{\approx 0}\Bigg]2a^3 \\
-\frac{3a^3}{\cancel{c^2}}\Bigg[1+\alpha\frac{\rho}{a}+\beta\frac{\rho}{a}i+2\sqrt{\frac{\rho}{a}}+3\frac{\rho}{a}+\underbrace{\left(2\sqrt{\frac{\rho}{a}}+3\frac{\rho}{a}\right)\cdot\left(\alpha\frac{\rho}{a}+\beta\frac{\rho}{a}i\right)}_{\approx 0}\Bigg]\cancel{c^2} \\
= 2a^3\,\frac{\cancel{a^2}}{\cancel{a^2}}\underbrace{\left(1-\frac{\rho}{a}\right)^{-1}}_{\approx(1+\frac{\rho}{a})}\left(1+3\alpha\frac{\rho}{a}+3\beta\frac{\rho}{a}i+2\sqrt{\frac{\rho}{a}}+3\frac{\rho}{a}\right) \\
-3a^3\left(1+\alpha\frac{\rho}{a}+\beta\frac{\rho}{a}i+2\sqrt{\frac{\rho}{a}}+3\frac{\rho}{a}\right) \\
= 2a^3\Bigg[1+3\alpha\frac{\rho}{a}+3\beta\frac{\rho}{a}i+2\sqrt{\frac{\rho}{a}}+4\frac{\rho}{a}+\underbrace{\frac{\rho}{a}\left(3\alpha\frac{\rho}{a}+3\beta\frac{\rho}{a}i+2\sqrt{\frac{\rho}{a}}+3\frac{\rho}{a}\right)}_{\approx 0}\Bigg] \\
-3a^3\left(1+\alpha\frac{\rho}{a}+\beta\frac{\rho}{a}i+2\sqrt{\frac{\rho}{a}}+3\frac{\rho}{a}\right) \\
= -a^3\left(1-3\alpha\frac{\rho}{a}-3\beta\frac{\rho}{a}+2\sqrt{\frac{\rho}{a}}+\frac{\rho}{a}\right)
\end{aligned}
\tag{D-116}
$$

Finally, combining the four variables above, we have

$$
\begin{aligned}
\chi''(Z) = \frac{\sigma_n a^3}{4\,(Z^2-c^2)^{3/2}}\Bigg[1+(\alpha+1)\frac{\rho}{a}+\beta\frac{\rho}{a}i \\
-\cos 2\gamma\left(1+2\sqrt{\frac{\rho}{a}}+(\alpha+3)\frac{\rho}{a}+\beta\frac{\rho}{a}i\right) \\
-i\sin 2\gamma\left(1+2\sqrt{\frac{\rho}{a}}+(1-3\alpha)\frac{\rho}{a}-3\beta\frac{\rho}{a}i\right)\Bigg]
\end{aligned}
\tag{D-117}
$$

D.9
Part 6

Combining eqs. (D-29) and (D-30) to the format of eq. (D-3)

$$
\begin{aligned}
2[\bar{Z}\Psi''(Z)+\chi''(Z)] = & -\frac{\sigma_n a^3}{2\cdot(Z^2-c^2)^{3/2}}\Bigg[1+(\alpha-1)\frac{\rho}{a}-\beta\frac{\rho}{a}i-\cos 2\gamma\Bigg(1+2\sqrt{\frac{\rho}{a}} \\
& +(\alpha+1)\frac{\rho}{a}-\beta\frac{\rho}{a}i\Bigg)-i\sin 2\gamma\Bigg(1+2\sqrt{\frac{\rho}{a}}+(\alpha+1)\frac{\rho}{a}-\beta\frac{\rho}{a}i\Bigg) \\
& +\frac{\sigma_n a^3}{4\ (Z^2-c^2)^{3/2}}\Bigg[1+(\alpha+1)\frac{\rho}{a}+\beta\frac{\rho}{a}i \\
& -\cos 2\gamma\Bigg(1+2\sqrt{\frac{\rho}{a}}+(\alpha+3)\frac{\rho}{a}+\beta\frac{\rho}{a}i\Bigg) \\
& -i\sin 2\gamma\Bigg(1+2\sqrt{\frac{\rho}{a}}+(1-3\alpha)\frac{\rho}{a}-3\beta\frac{\rho}{a}i\Bigg)\Bigg] \\
= & \frac{\sigma_n a^3}{2\cdot(Z^2-c^2)^{3/2}}\Bigg[\cancel{-1}-\cancel{\alpha}\frac{\rho}{a}+\frac{\rho}{a}+\beta\frac{\rho}{a}i+\cancel{1}+\cancel{\alpha}\frac{\rho}{a}+\frac{\rho}{a}+\beta\frac{\rho}{a}i \\
& -\cos 2\gamma\Bigg(\cancel{-1}-2\cancel{\sqrt{\frac{\rho}{a}}}-\cancel{\alpha}\frac{\rho}{a}-\frac{\rho}{a}+\beta\frac{\rho}{a}i \\
& +\cancel{1}+2\cancel{\sqrt{\frac{\rho}{a}}}+\cancel{\alpha}\frac{\rho}{a}+3\frac{\rho}{a}+\beta\frac{\rho}{a}i\Bigg) \\
& +i\sin 2\gamma\Bigg(\cancel{1}+2\cancel{\sqrt{\frac{\rho}{a}}}+\alpha\frac{\rho}{a}+\frac{\rho}{a}-\beta\frac{\rho}{a}i \\
& -\cancel{1}-2\cancel{\sqrt{\frac{\rho}{a}}}-\frac{\rho}{a}+3\alpha\frac{\rho}{a}+3\beta\frac{\rho}{a}i\Bigg)\Bigg]
\end{aligned}
\tag{D-118}
$$

Substituting eq. (D-25) into equation in above

$$
\begin{aligned}
2[\bar{Z}\Psi''(Z)+\chi''(Z)] = & \frac{\sigma_n a^3}{\cancel{2}\cdot(\cancel{2}a^{\cancel{2}}e^{i\theta}\frac{r}{\cancel{a}})^{3/2}}\Bigg[\cancel{2}\frac{\rho}{a}+\cancel{2}\beta\frac{\rho}{a}i-\cos 2\gamma\Bigg(\cancel{2}\frac{\rho}{a}+\cancel{2}\beta\frac{\rho}{a}i\Bigg)+ \\
& i\sin 2\gamma\Bigg(\cancel{2}\ 2\alpha\frac{\rho}{a}+\cancel{2}\beta\frac{\rho}{a}i\Bigg)\Bigg] \\
= & \frac{\sigma_n a^{\frac{3}{2}}\ e^{-\frac{3}{2}i\theta}}{2\sqrt{2}r^{\frac{3}{2}}}\Bigg[1+\beta i-\cos 2\gamma\Bigg(1+\beta i\Bigg)+ \\
& i\sin 2\gamma\Bigg(2\alpha+\beta i\Bigg)\Bigg]\frac{\rho}{a}
\end{aligned}
\tag{D-119}
$$

Therefore, substituting this equation into (D-3) provides

$$\sigma_{yy} - \sigma_{xx} + 2i\sigma_{xy} = \frac{\sigma_n a^{\frac{3}{2}}\ e^{-\frac{3}{2}i\theta}}{2\sqrt{2}r^{\frac{3}{2}}}\Bigg[1 + \beta i - \cos 2\gamma\bigg(1 + \beta i\bigg) + i\sin 2\gamma\bigg(2\alpha + \beta i\bigg)\Bigg]\frac{\rho}{a} \tag{D-120}$$

D.10
Part 7

For fracture under mode I, the angle is

$$\gamma = \frac{\pi}{2} \tag{D-121}$$

substituting into eq. (D-31)

$$\begin{aligned}\sigma_{xx} + \sigma_{yy} &= \sigma_n\sqrt{\frac{a}{2r}}\left[(1 - \overbrace{\cos\pi}^{-1})\cos\frac{\theta}{2} - \overbrace{\sin\pi}^{0}\sin\frac{\theta}{2}\right] \\ &= \frac{2\sigma_n\sqrt{\pi a}}{\sqrt{2\pi r}}\cos\frac{\theta}{2}\end{aligned} \tag{D-122}$$

Comparing the equation in above with σ_{xx} and σ_{yy} from William's stress field, eq. (2-7), K_I is defined as

$$K_I = \sigma_n\sqrt{\pi a} \tag{D-123}$$

Therefore,

$$\sigma_{xx} + \sigma_{yy} = \frac{2K_I}{\sqrt{2\pi r}}\cos\frac{\theta}{2} \tag{D-124}$$

Substituting the angle into the second condition for the stress function, eq. (D-32), we have

$$\begin{aligned}\sigma_{yy} - \sigma_{xx} + 2i\ \sigma_{xy} &= \frac{\sigma_n\sqrt{a}\ a\ \ e^{-\frac{3}{2}i\theta}}{2\sqrt{2}\ r\sqrt{r}}\frac{\sqrt{\pi}}{\sqrt{\pi}}\left[1 + \beta i - \overbrace{\cos\pi}^{-1}\left(1 + \beta i\right) + \right. \\ &\qquad \left. i\overbrace{\sin\pi}^{0}\left(2\alpha + \beta i\right)\right]\frac{\rho}{a} \\ &= \frac{\overbrace{\sigma_n\sqrt{\pi a}}^{K_I}\ \cancel{a}\ e^{-\frac{3}{2}i\theta}}{\cancel{2}\sqrt{2\pi r}\ r}\cdot\cancel{2}[1 + \beta i]\ \frac{\rho}{\cancel{a}} \\ &= \frac{K_I\ e^{-\frac{3}{2}i\theta}}{\sqrt{2\pi r}}\left[\frac{\rho}{r} + \frac{i}{\cancel{r}}\overbrace{\beta\rho}^{\cancel{r}\sin\theta}\right]\end{aligned} \tag{D-125}$$

Rewriting (D-125) as function of half of the angle gives

$$\sigma_{yy} - \sigma_{xx} + 2i\ \sigma_{xy} = \frac{K_I\ e^{-\frac{3}{2}i\theta}}{\sqrt{2\pi r}}\left[\frac{\rho}{r} + 2i\ \sin\frac{\theta}{2}\cos\frac{\theta}{2}\right] \tag{D-126}$$

Splitting by using Euler's formula, eq. (D-56)

$$\sigma_{yy} - \sigma_{xx} + 2i\ \sigma_{xy} = \frac{K_I}{\sqrt{2\pi r}}\left[\cos\left(-\frac{3\theta}{2}\right) + i\sin\left(-\frac{3\theta}{2}\right)\right]\cdot\left[\frac{\rho}{r} + 2i\ \sin\frac{\theta}{2}\cos\frac{\theta}{2}\right] \tag{D-127}$$

and applying sin and cos properties, from eqs. (D-53) and (D-54)

$$\begin{aligned}\sigma_{yy} - \sigma_{xx} + 2i\ \sigma_{xy} &= \frac{K_I}{\sqrt{2\pi r}}\left[\cos\frac{3\theta}{2} - i\sin\frac{3\theta}{2}\right]\cdot\left[\frac{\rho}{r} + 2i\ \sin\frac{\theta}{2}\cos\frac{\theta}{2}\right] \\ &= \frac{K_I}{\sqrt{2\pi r}}\left[\frac{\rho}{r}\cos\frac{3\theta}{2} + 2\sin\frac{3\theta}{2}\sin\frac{\theta}{2}\cos\frac{\theta}{2}\right. \\ &\qquad \left. + i\left(2\sin\frac{\theta}{2}\cos\frac{\theta}{2}\cos\frac{3\theta}{2} - \frac{\rho}{r}\sin\frac{3\theta}{2}\right)\right]\end{aligned} \tag{D-128}$$

where the complex portion provides

$$\sigma_{xy} = \frac{K_I}{\sqrt{2\pi r}}\left[\sin\frac{\theta}{2}\cos\frac{\theta}{2}\cos\frac{3\theta}{2}\right] - \frac{K_I}{\sqrt{2\pi r}}\left[\frac{\rho}{r}\sin\frac{3\theta}{2}\right] \tag{D-129}$$

while the real portion

$$\sigma_{yy} - \sigma_{xx} = \frac{K_I}{\sqrt{2\pi r}}\left[\frac{\rho}{r}\cos\frac{3\theta}{2} + 2\sin\frac{3\theta}{2}\sin\frac{\theta}{2}\cos\frac{\theta}{2}\right] \tag{D-130}$$

Adding eqs. (D-124) and (D-130), we have

$$2\sigma_{yy} = \frac{K_I}{\sqrt{2\pi r}}\left[2\cos\frac{\theta}{2} + 2\sin\frac{3\theta}{2}\sin\frac{\theta}{2}\cos\frac{\theta}{2}\right] + \frac{K_I}{\sqrt{2\pi r}}\left[\frac{\rho}{r}\cos\frac{3\theta}{2}\right] \tag{D-131}$$

Thus, σ_{yy} is given by

$$\sigma_{yy} = \frac{K_I}{\sqrt{2\pi r}}\cos\frac{\theta}{2}\left[1 + \sin\frac{3\theta}{2}\sin\frac{\theta}{2}\right] + \frac{K_I}{\sqrt{2\pi r}}\left[\frac{\rho}{2r}\cos\frac{3\theta}{2}\right] \tag{D-132}$$

Multiplying eq. (D-130) with -1 and adding to eq. (D-124) provides

$$2\sigma_{xx} = \frac{K_I}{\sqrt{2\pi r}}\left[2\cos\frac{\theta}{2} - 2\sin\frac{3\theta}{2}\sin\frac{\theta}{2}\cos\frac{\theta}{2} - \frac{\rho}{r}\cos\frac{3\theta}{2}\right] \tag{D-133}$$

Thus, σ_{xx} is given by

$$\sigma_{xx} = \frac{K_I}{\sqrt{2\pi r}}\cos\frac{\theta}{2}\left[1 - \sin\frac{\theta}{2}\sin\frac{3\theta}{2}\right] - \frac{K_I}{\sqrt{2\pi r}}\left[\frac{\rho}{2r}\cos\frac{3\theta}{2}\right] \tag{D-134}$$

D.11
Part 8

For fracture under mode II, the solution is achieved by superposing a positive load σ_n in an angle $\gamma = \frac{\pi}{4}$ (first solution) and a negative load $-\sigma_n$ in $\gamma = \frac{3\pi}{4}$ (second solution). Rewriting eq. (D-31) for the first solution

$$\begin{aligned}\sigma_{xx} + \sigma_{yy}\Big|_{\gamma=\frac{\pi}{4}} &= \sigma_n\sqrt{\frac{a}{2r}}\left[\left(1 - \overbrace{\cos\frac{\pi}{2}}^{0}\right)\cos\frac{\theta}{2} - \overbrace{\sin\frac{\pi}{2}}^{1}\sin\frac{\theta}{2}\right] \\ &= \sigma_n\sqrt{\frac{a}{2r}}\left[\cos\frac{\theta}{2} - \sin\frac{\theta}{2}\right]\end{aligned} \tag{D-135}$$

and for the second solution,

$$\begin{aligned}\sigma_{xx} + \sigma_{yy}\Big|_{\gamma=\frac{3\pi}{4}} &= (-\sigma_n)\sqrt{\frac{a}{2r}}\left[\left(1 - \overbrace{\cos\frac{3\pi}{2}}^{0}\right)\cos\frac{\theta}{2} - \overbrace{\sin\frac{3\pi}{2}}^{-1}\sin\frac{\theta}{2}\right] \\ &= (-\sigma_n)\sqrt{\frac{a}{2r}}\left[\cos\frac{\theta}{2} + \sin\frac{\theta}{2}\right]\end{aligned} \tag{D-136}$$

Adding eqs. (D-135) and (D-136) results in

$$\begin{aligned}\sigma_{xx} + \sigma_{yy} &= \sigma_n\sqrt{\frac{a}{2r}}\left[\cancel{\cos\frac{\theta}{2}} - \sin\frac{\theta}{2} - \cancel{\cos\frac{\theta}{2}} - \sin\frac{\theta}{2}\right] \\ &= -2\sigma_n\sqrt{\frac{a}{2r}}\cdot\sin\frac{\theta}{2}\end{aligned} \tag{D-137}$$

that, when comparing to σ_{xx} and σ_{yy} from William's stress field, on eq. (2-8), provides

$$K_{II} = \sigma_n\sqrt{\pi a} \tag{D-138}$$

Therefore,

$$\sigma_{xx} + \sigma_{yy} = -\frac{2K_{II}}{\sqrt{2\pi r}}\cdot\sin\frac{\theta}{2} \tag{D-139}$$

For condition second condition of the stress function, eq. (D-32), the first solution provides

$$\sigma_{yy} - \sigma_{xx} + 2i\ \sigma_{xy}\Big|_{\gamma=\frac{\pi}{4}} = \frac{\sigma_n\sqrt{a}\,\cancel{\alpha}\ e^{-\frac{3}{2}i\theta}}{2\sqrt{2}\ r\sqrt{r}}\frac{\sqrt{\pi}}{\sqrt{\pi}}\left[1+\beta i - \overbrace{\cos\frac{\pi}{2}}^{0}\left(1+\beta i\right)+ i\overbrace{\sin\frac{\pi}{2}}^{1}\left(2\alpha+\beta i\right)\right]\frac{\rho}{\cancel{\alpha}}$$
$$= \frac{\overbrace{\sigma_n\sqrt{\pi a}}^{K_{II}}\ e^{-\frac{3}{2}i\theta}}{2\sqrt{2\pi r}\ r}\left[1+\beta i + i(2\alpha+\beta i)\right]\rho \tag{D-140}$$

while, for the second solution, we have

$$\sigma_{yy} - \sigma_{xx} + 2i\ \sigma_{xy}\Big|_{\gamma=\frac{3\pi}{4}} = \frac{(-\sigma_n)\sqrt{a}\,\cancel{\alpha}\ e^{-\frac{3}{2}i\theta}}{2\sqrt{2}\ r\sqrt{r}}\frac{\sqrt{\pi}}{\sqrt{\pi}}\left[1+\beta i - \overbrace{\cos\frac{3\pi}{2}}^{0}\left(1+\beta i\right)+ i\overbrace{\sin\frac{3\pi}{2}}^{-1}\left(2\alpha+\beta i\right)\right]\frac{\rho}{\cancel{\alpha}}$$
$$= -\frac{\overbrace{\sigma_n\sqrt{\pi a}}^{K_{II}}\ e^{-\frac{3}{2}i\theta}}{2\sqrt{2\pi r}\ r}\left[1+\beta i - i(2\alpha+\beta i)\right]\rho \tag{D-141}$$

Adding eqs. (D-140) and (D-141) provides

$$\sigma_{yy} - \sigma_{xx} + 2i\ \sigma_{xy} = \frac{K_{II}\ e^{-\frac{3}{2}i\theta}}{2\sqrt{2\pi r}\ r}\cdot 2i[2\alpha+\beta i]\rho \tag{D-142}$$

Isolating α from eq. (D-23)

$$\alpha = \frac{r\cos\theta}{\rho} - \frac{1}{2} \tag{D-143}$$

and substituting into eq. (D-142)

$$\begin{aligned}\sigma_{yy} - \sigma_{xx} + 2i\ \sigma_{xy} &= \frac{K_{II}\ e^{-\frac{3}{2}i\theta}}{\cancel{2}\sqrt{2\pi r}\ r}\cdot\cancel{2}i\left[2\left(\frac{r\cos\theta}{\rho}-\frac{1}{2}\right)+\beta i\right]\rho \\ &= \frac{K_{II}\ e^{-\frac{3}{2}i\theta}}{\sqrt{2\pi r}}\cdot\left[\frac{2i\ \cancel{r}\cancel{\rho}\cos\theta}{\cancel{r}\ \cancel{\rho}} - \frac{\cancel{2}i\rho}{\cancel{2}r} - \frac{\beta\rho}{r}\right] \\ &= \frac{K_{II}\ e^{-\frac{3}{2}i\theta}}{\sqrt{2\pi r}}\cdot\left[2i\ \cos\theta - i\frac{\rho}{r} - \frac{\cancel{r}\sin\theta}{\cancel{r}}\right] \\ &= \frac{K_{II}\ e^{-\frac{3}{2}i\theta}}{\sqrt{2\pi r}}\cdot\left[2i\ \cos\theta - \sin\theta - i\frac{\rho}{r}\right]\end{aligned} \tag{D-144}$$

Splitting by using Euler's formula, eq. (D-56)

$$\sigma_{yy}-\sigma_{xx}+2i\ \sigma_{xy}=\frac{K_{II}}{\sqrt{2\pi r}}\cdot\left[\cos\left(-\frac{3\theta}{2}\right)+i\sin\left(-\frac{3\theta}{2}\right)\right]\cdot\left[2i\ \cos\theta-\sin\theta-i\frac{\rho}{r}\right] \tag{D-145}$$

and applying sin and cos properties, from eq. (D-53) and (D-54)

$$\begin{aligned}\sigma_{yy}-\sigma_{xx}+2i\ \sigma_{xy}&=\frac{K_{II}}{\sqrt{2\pi r}}\cdot\left[\cos\frac{3\theta}{2}-i\sin\frac{3\theta}{2}\right]\cdot\left[2i\ \cos\theta-\sin\theta-i\frac{\rho}{r}\right]\\&=\frac{K_{II}}{\sqrt{2\pi r}}\cdot\left[-\sin\theta\cos\frac{3\theta}{2}+2\sin\frac{3\theta}{2}\cos\theta-\frac{\rho}{r}\sin\frac{3\theta}{2}\right.\\&\qquad\left.+2i\ \cos\frac{3\theta}{2}\cos\theta+i\sin\theta\sin\frac{3\theta}{2}-i\frac{\rho}{r}\cos\frac{3\theta}{2}\right]\end{aligned} \tag{D-146}$$

where the complex portion provides

$$2\sigma_{xy}=\frac{K_{II}}{\sqrt{2\pi r}}\cdot\left[2\ \cos\frac{3\theta}{2}\cos\theta+\sin\theta\sin\frac{3\theta}{2}-\frac{\rho}{r}\cos\frac{3\theta}{2}\right] \tag{D-147}$$

Rewriting equation above and applying properties (D-57) gives

$$\begin{aligned}2\sigma_{xy}&=\frac{K_{II}}{\sqrt{2\pi r}}\cdot\left[\underbrace{2\ \cos\frac{3\theta}{2}\cos\theta+2\ \sin\theta\sin\frac{3\theta}{2}}_{2\cos\frac{\theta}{2}}-\sin\theta\sin\frac{3\theta}{2}-\frac{\rho}{r}\cos\frac{3\theta}{2}\right]\\&=\frac{K_{II}}{\sqrt{2\pi r}}\cdot\left[2\cos\frac{\theta}{2}-2\sin\frac{\theta}{2}\cos\frac{\theta}{2}\sin\frac{3\theta}{2}-\frac{\rho}{r}\cos\frac{3\theta}{2}\right]\end{aligned} \tag{D-148}$$

Therefore, σ_{xy} is

$$\sigma_{xy}=\frac{K_{II}}{\sqrt{2\pi r}}\cdot\cos\frac{\theta}{2}\left[1-\sin\frac{\theta}{2}\sin\frac{3\theta}{2}\right]-\frac{K_{II}}{\sqrt{2\pi r}}\cdot\left[\frac{\rho}{2r}\cos\frac{3\theta}{2}\right] \tag{D-149}$$

The real portion of eq. (D-146) provides

$$\sigma_{yy}-\sigma_{xx}=\frac{K_{II}}{\sqrt{2\pi r}}\cdot\left[-\sin\theta\cos\frac{3\theta}{2}+2\sin\frac{3\theta}{2}\cos\theta-\frac{\rho}{r}\sin\frac{3\theta}{2}\right] \tag{D-150}$$

Rewriting equation in above and applying properties (D-58) gives

$$\sigma_{yy} - \sigma_{xx} = \frac{K_{II}}{\sqrt{2\pi r}} \cdot \left[\underbrace{2\sin\frac{3\theta}{2}\cos\theta - 2\sin\theta\cos\frac{3\theta}{2}}_{2\sin\frac{\theta}{2}} + \sin\theta\cos\frac{3\theta}{2} - \frac{\rho}{r}\sin\frac{3\theta}{2} \right]$$
$$= \frac{K_{II}}{\sqrt{2\pi r}} \cdot \left[2\sin\frac{\theta}{2} + 2\sin\frac{\theta}{2}\cos\frac{\theta}{2}\cos\frac{3\theta}{2} - \frac{\rho}{r}\sin\frac{3\theta}{2} \right] \tag{D-151}$$

Adding eqs. (D-137) and (D-151), we have

$$2\sigma_{yy} = \frac{K_{II}}{\sqrt{2\pi r}} \cdot \left[-2\sin\frac{\theta}{2} + 2\sin\frac{\theta}{2} + 2\sin\frac{\theta}{2}\cos\frac{\theta}{2}\cos\frac{3\theta}{2} - \frac{\rho}{r}\sin\frac{3\theta}{2} \right] \tag{D-152}$$

Thus, σ_{yy} is given by

$$\sigma_{yy} = \frac{K_{II}}{\sqrt{2\pi r}} \cdot \left[\sin\frac{\theta}{2}\cos\frac{\theta}{2}\cos\frac{3\theta}{2} \right] - \frac{K_{II}}{\sqrt{2\pi r}} \cdot \left[\frac{\rho}{2r}\sin\frac{3\theta}{2} \right] \tag{D-153}$$

Multiplying eq. (D-151) with -1 and adding to eq. (D-137) provides

$$2\sigma_{xx} = \frac{K_{II}}{\sqrt{2\pi r}} \cdot \left[-2\sin\frac{\theta}{2} - 2\sin\frac{\theta}{2} - 2\sin\frac{\theta}{2}\cos\frac{\theta}{2}\cos\frac{3\theta}{2} + \frac{\rho}{r}\sin\frac{3\theta}{2} \right] \tag{D-154}$$

Thus, σ_{xx} is given by

$$\sigma_{xx} = -\frac{K_{II}}{\sqrt{2\pi r}} \cdot \sin\frac{\theta}{2}\left[2 + \cos\frac{\theta}{2}\cos\frac{3\theta}{2} \right] + \frac{K_{II}}{\sqrt{2\pi r}} \cdot \left[\frac{\rho}{2r}\sin\frac{3\theta}{2} \right] \tag{D-155}$$

D.12
Part 9

From eq. (D-46), expanding the sin term using properties from eqs. (D-64), (D-59) and (D-60)

$$\begin{aligned}\sinh\left(\zeta-\xi_0-\frac{i\pi}{2}\right) &= \sinh(\zeta-\xi_0)\overbrace{\cos\left(-\frac{\pi}{2}\right)}^{0}+i\cosh(\zeta-\xi_0)\overbrace{\sin\left(-\frac{\pi}{2}\right)}^{-1}\\ &= -i\cosh(\zeta-\xi_0)\\ &= -i\Big[\cosh\zeta\cosh(-\xi_0)+\sinh\zeta\sinh(-\xi_0)\Big]\\ &= -i\Big[\cosh\zeta\cosh\xi_0-\sinh\zeta\sinh\xi_0\Big]\end{aligned} \tag{D-156}$$

Substituting eqs. (D-7) and (D-8) into equation above gives

$$\begin{aligned}\sinh\left(\zeta-\xi_0-\frac{i\pi}{2}\right) &= -i\left[\frac{a}{c}\cosh\zeta-\frac{b}{c}\sinh\zeta\right]\\ &= \frac{i}{c}\Big[b\sinh\zeta-a\cosh\zeta\Big]\\ &= \frac{i}{a\sqrt{1-\frac{\rho}{a}}}\Big[b\sinh\zeta-a\cosh\zeta\Big]\\ &= \frac{i}{\sqrt{1-\frac{\rho}{a}}}\Big[\overbrace{\frac{b}{a}}^{\sqrt{\frac{\rho}{a}}}\sinh\zeta-\frac{\cancel{a}}{\cancel{a}}\cosh\zeta\Big]\\ &= \frac{i}{\sqrt{1-\frac{\rho}{a}}}\left[\sqrt{\frac{\rho}{a}}\sinh\zeta-\cosh\zeta\right]\end{aligned} \tag{D-157}$$

From eqs. (D-9) and (D-8)

$$\begin{aligned}\frac{a+b}{c} &= \frac{a+b}{\sqrt{a^2(1-\frac{\rho}{a})}} = \frac{a+b}{a\sqrt{1-\frac{\rho}{a}}}\\ &= \frac{1}{\sqrt{1-\frac{\rho}{a}}}\left[1+\frac{b}{a}\right]\end{aligned} \tag{D-158}$$

$$\frac{a+b}{c} = \frac{1+\sqrt{\frac{\rho}{a}}}{\sqrt{1-\frac{\rho}{a}}} \tag{D-159}$$

Therefore, rewriting eq. (D-46) by substituting into eqs. (D-157) and (D-159) provides

$$\sigma_{xz} - i\ \sigma_{yz} = S_n \frac{1+\sqrt{\frac{\rho}{a}}}{\sqrt{1-\frac{\rho}{a}}} \cdot \frac{i}{\sqrt{1-\frac{\rho}{a}}} \left[\sqrt{\frac{\rho}{a}} \frac{\sinh\zeta}{\sinh\zeta} - \frac{\cosh\zeta}{\sinh\zeta} \right] \tag{D-160}$$

where, from eq. (D-5) and (D-71) gives

$$\frac{\cosh\zeta}{\sinh\zeta} = \frac{Z}{\sqrt{Z^2 - c^2}} \tag{D-161}$$

that from eqs. (D-18) and (D-25) is rewritten as function of $\frac{\rho}{a}$ as

$$\frac{\cosh\zeta}{\sinh\zeta} = \frac{(1+\alpha\frac{\rho}{a}+\beta\frac{\rho}{a}i)e^{-\frac{i\theta}{2}}}{\sqrt{2\frac{r}{a}}} \tag{D-162}$$

As a result, with algebraic manipulation and considering higher order terms in $\frac{\rho}{a}$

$$\begin{aligned}
\sigma_{xz} - i\ \sigma_{yz} &= \sigma_n \frac{1+\sqrt{\frac{\rho}{a}}}{\sqrt{1-\frac{\rho}{a}}} \cdot \frac{i}{\sqrt{1-\frac{\rho}{a}}} \left[\sqrt{\frac{\rho}{a}} - \frac{(1+\alpha\frac{\rho}{a}+\beta\frac{\rho}{a}i)e^{-\frac{i\theta}{2}}}{\sqrt{2\frac{r}{a}}} \right] \\
&= i\sigma_n \frac{1+\sqrt{\frac{\rho}{a}}}{1-\frac{\rho}{a}} \left[\underbrace{\sqrt{\frac{\rho}{a}}}_{\text{neglect}} - \frac{(1+\alpha\frac{\rho}{a}+\beta\frac{\rho}{a}i)e^{-\frac{i\theta}{2}}}{\sqrt{2}} \sqrt{\frac{a}{r}} \right] \\
&= -i\sigma_n \frac{\cancel{1+\sqrt{\frac{\rho}{a}}}}{(1-\sqrt{\frac{\rho}{a}})\cancel{(1+\sqrt{\frac{\rho}{a}})}} \left[\frac{(1+\alpha\frac{\rho}{a}+\beta\frac{\rho}{a}i)e^{-\frac{i\theta}{2}}}{\sqrt{2}} \sqrt{\frac{a}{r}} \right] \\
&= -\frac{\sigma_n\ i}{\sqrt{2}} \sqrt{\frac{a}{r}}\ e^{-\frac{i\theta}{2}} \cdot \overbrace{\left(1-\sqrt{\frac{\rho}{a}}\right)^{-1} \cdot \left(1+\alpha\frac{\rho}{a}+\beta\frac{\rho}{a}i\right)}^{\approx 1}
\end{aligned} \tag{D-163}$$

provides

$$\sigma_{xz} - i\ \sigma_{yz} = -\frac{\sigma_n\ i}{\sqrt{2}} \sqrt{\frac{a}{r}}\ e^{-\frac{i\theta}{2}} \tag{D-164}$$

Expanding the exponential term

$$\begin{aligned}
\sigma_{xz} - i\ \sigma_{yz} &= -\frac{\sigma_n}{\sqrt{2}} \sqrt{\frac{a}{r}} \cdot i \left[\cos\left(-\frac{\theta}{2}\right) + i\sin\left(-\frac{\theta}{2}\right) \right] \\
&= -\frac{\sigma_n}{\sqrt{2}} \sqrt{\frac{a}{r}} \cdot i \left[\cos\frac{\theta}{2} - i\sin\frac{\theta}{2} \right] \\
&= -\frac{\sigma_n}{\sqrt{2}} \sqrt{\frac{a}{r}} \cdot \left[i\ \cos\frac{\theta}{2} + \sin\frac{\theta}{2} \right]
\end{aligned} \tag{D-165}$$

that when taking the real part of the above equation provides

$$\begin{aligned}\sigma_{xz} &= -\frac{\sigma_n}{\sqrt{2}}\sqrt{\frac{a}{r}} \cdot \sin\frac{\theta}{2} \\ &= -\frac{\overbrace{\sigma_n\sqrt{\pi a}}^{K_{III}}}{\sqrt{2\pi r}} \cdot \sin\frac{\theta}{2} \\ &= -\frac{K_{III}}{\sqrt{2\pi r}} \cdot \sin\frac{\theta}{2}\end{aligned} \tag{D-166}$$

while from the complex term

$$\begin{aligned}\sigma_{yz} &= \frac{\sigma_n}{\sqrt{2}}\sqrt{\frac{a}{r}} \cdot \cos\frac{\theta}{2} \\ &= \frac{\overbrace{\sigma_n\sqrt{\pi a}}^{K_{III}}}{\sqrt{2\pi r}} \cdot \cos\frac{\theta}{2} \\ &= \frac{K_{III}}{\sqrt{2\pi r}} \cdot \cos\frac{\theta}{2}\end{aligned} \tag{D-167}$$

E
J Properties

First: $J = 0$ in any closed contour path that does not contain a crack (first bullet), From the first The Kelvin-Stokes's theorem a line integral can be converted into an equivalent area integral. The box in bellow presents a recap of the theorem.

Recap on Kelvin-Stoke's theorem:
The formula bellow converts an area integral to a line integral in a vectorial field $\boldsymbol{F}$

$$\int_A (\nabla \times \boldsymbol{F})\ dA = \int_S \boldsymbol{F}\ ds$$

where

$$\nabla \times \boldsymbol{F} = \left(\frac{\partial F_z}{\partial y} - \frac{\partial F_y}{\partial z}\right)\hat{i} + \left(\frac{\partial F_x}{\partial z} - \frac{\partial F_z}{\partial x}\right)\hat{j} + \left(\frac{\partial F_y}{\partial x} - \frac{\partial F_x}{\partial y}\right)\hat{k} \qquad \text{(E-1)}$$

More explicitly, the equality says that

$$\int_A \left[\left(\frac{\partial F_z}{\partial y} - \frac{\partial F_y}{\partial z}\right) dy\ dz + \left(\frac{\partial F_x}{\partial z} - \frac{\partial F_z}{\partial x}\right) dz\ dx + \left(\frac{\partial F_y}{\partial x} - \frac{\partial F_x}{\partial y}\right) dx\ dy\right] = \int_S (F_x\ dx + F_y\ dy + F_z\ dz) \qquad \text{(E-2)}$$

J integral can be decomposed by the addition of the following two line integrals.

$$\begin{cases} J_1 = \oint_S U\ dy \\ J_2 = \oint_S T_i \frac{\partial u_i}{\partial x}\ ds \end{cases} \qquad \text{(E-3)}$$

As to J_1, imposing $\boldsymbol{F}$ having just y component equal to U, eq. (E-2) provides:

$$J_1 = \oint_S U\ dy = \int_A \frac{\partial U}{\partial x}\ dA \qquad \text{(E-4)}$$

As to J_2, can be rewritten as:

$$J_2 = \oint_S T_i \frac{\partial u_i}{\partial x}\, ds = \oint_S \sigma_{ij} n_j \frac{\partial u_i}{\partial x}\, ds = \oint_S \sigma_{i1} \frac{\partial u_i}{\partial x}\, \underbrace{n_1\, ds}_{dy} + \int_S \sigma_{i2} \frac{\partial u_i}{\partial x}\, \underbrace{n_2\, ds}_{-dx} \tag{E-5}$$

where $\boldsymbol{F}$, in eq. (E-2), is

$$\boldsymbol{F} = \begin{bmatrix} -\sigma_{i2} \frac{\partial u_i}{\partial x} \\ \sigma_{i1} \frac{\partial u_i}{\partial x} \end{bmatrix} \tag{E-6}$$

Applying the Kelvin-Stokes's theorem on eq. (E-5) results

$$J_2 = \oint_S T_i \frac{\partial u_i}{\partial x}\, ds = \int_A \frac{\partial}{\partial x_1}\left(\sigma_{i1} \frac{\partial u_i}{\partial x}\right) dA + \int_A \frac{\partial}{\partial x_2}\left(\sigma_{i2} \frac{\partial u_i}{\partial x}\right) dA \tag{E-7}$$

that simplifies to

$$J_2 = \oint_S T_i \frac{\partial u_i}{\partial x}\, ds = \int_A \frac{\partial}{\partial x_j}\left(\sigma_{ij} \frac{\partial u_i}{\partial x}\right) dA \tag{E-8}$$

Then, combining eqs. (E-4) and (E-8) J integral results

$$J = \int_S \left[U\, dy - T_i \frac{\partial u_i}{\partial x}\, ds \right] = \int_A \left[\frac{\partial U}{\partial x} - \frac{\partial}{\partial x_j}\left(\sigma_{ij} \frac{\partial u_i}{\partial x}\right) \right] dA \tag{E-9}$$

where

$$\frac{\partial U}{\partial x} = \underbrace{\frac{\partial U}{\partial \epsilon_{ij}}}_{\sigma_{ij}} \frac{\partial \epsilon_{ij}}{\partial x} = \sigma_{ij} \frac{\partial \epsilon_{ij}}{\partial x} \tag{E-10}$$

Moreover, from elasticity, the Green-Lagrange strain tensor is given by:

$$\begin{aligned} \boldsymbol{E} &= \frac{1}{2}(\boldsymbol{C} - \boldsymbol{I}) \\ &= \frac{1}{2}\left[\frac{\partial \boldsymbol{u}}{\partial \boldsymbol{X}} + \left(\frac{\partial \boldsymbol{u}}{\partial \boldsymbol{X}} \right)^T \right] + \frac{1}{2}\left[\left(\frac{\partial \boldsymbol{u}}{\partial \boldsymbol{X}} \right)^T \cdot \left(\frac{\partial \boldsymbol{u}}{\partial \boldsymbol{X}} \right) \right] \end{aligned} \tag{E-11}$$

which, considering small strains only, reduces to

$$\epsilon_{ij} = \frac{1}{2}\left[\frac{\partial u_i}{\partial x_j} + \frac{\partial u_j}{\partial x_i} \right] \tag{E-12}$$

because the non-linear term is irrelevant.

Substituting eq. (E-12) into eq. (E-10) and imposing symmetry condition on the stress tensor we have:

$$\begin{aligned}\frac{\partial U}{\partial x} &= \frac{1}{2}\,\sigma_{ij}\left[\frac{\partial}{\partial x}\left(\frac{\partial u_i}{\partial x_j}\right)+\frac{\partial}{\partial x}\left(\frac{\partial u_j}{\partial x_i}\right)\right]\\ &= \frac{1}{2}\left[\sigma_{ij}\frac{\partial}{\partial x}\left(\frac{\partial u_i}{\partial x_j}\right)+\underbrace{\sigma_{ji}}_{\sigma_{ij}}\frac{\partial}{\partial x}\left(\frac{\partial u_j}{\partial x_i}\right)\right]\\ &= \sigma_{ij}\frac{\partial}{\partial x}\left(\frac{\partial u_i}{\partial x_j}\right)\end{aligned} \tag{E-13}$$

Substituting eq. (E-13) into eq. (E-9), results

$$J=\int_A\left\{\sigma_{ij}\frac{\partial}{\partial x}\left(\frac{\partial u_i}{\partial x_j}\right)-\left[\sigma_{ij}\frac{\partial}{\partial x_j}\left(\frac{\partial u_i}{\partial x}\right)+\frac{\partial\sigma_{ij}}{\partial x_j}\frac{\partial u_i}{\partial x_j}\right]\right\}dA \tag{E-14}$$

where from equilibrium $\frac{\partial\sigma_{ij}}{\partial x_j}=0$, resulting in eq. (E-14) being zero. Notice that, small strain (linear or non-linear) is assumed inside the contour path S for the proof above.

Second: J is path-independent if the contour path includes traction-free faces. Considering the figure below E.1 the close contour path is composed by $S=S_1\to S_2\to S_3\to S_4$ where the J integral, using the proof presents above, is $J=J_1+J_2+J_3+J_4=0$.

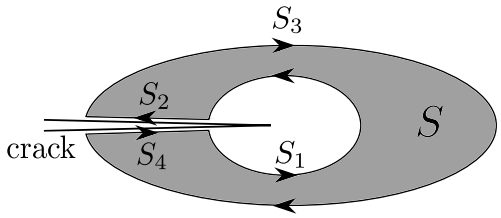

Figure E.1: Closed path that does not contain the crack

For the two traction-free crack faces $J_2=J_4=0$ because $T_i=dy=0$. So, $J_1=-J_3$, proving a non-dependency, where any (anti-clockwise) path has the same value of J.

As previously stated, J is defined as being equal to Griffith's Energy with a much more complex form, see eq. (2-21). Here It is convenient to prove how to achieve eq. (2-21) through Griffith's Energy (last bullet).

First, starting with Griffith's Energy definition in eq. (2-6), J

$$J=-\frac{\partial E_P}{\partial A}=-\frac{\partial(E_S-W)}{\partial A} \tag{E-15}$$

where potential energy E_p is dependable on the strain energy and external work. The strain energy is given by eq. (2-3) while the external work is given by the integral of the traction vector times the displacement over the boundary. Therefore,

$$\begin{aligned} E_P &= E_S - W \\ &= \iint_A U \; dx \; dy \; t - \oint_S T_i \; u_i \; ds \; t \end{aligned} \tag{E-16}$$

The total derivative with respect to the area, in a plane problem with thickness t is:

$$\frac{d}{dA} = \frac{1}{t} \cdot \frac{d}{da} = \frac{1}{t}\left(\frac{\partial}{\partial a} + \frac{\partial}{\partial x} \cdot \underbrace{\frac{\partial x}{\partial a}}_{-1}\right) = \frac{1}{t}\left(\frac{\partial}{\partial a} - \frac{\partial}{\partial x}\right) \tag{E-17}$$

Noticed that the crack increment da is associated with the decrement in $dx = -da$. The derivative of eq. (E-16) with respect to the crack length a results in

$$\frac{dE_P}{da} = \iint_A \left[\frac{\partial U}{\partial a} - \frac{\partial U}{\partial x}\right] dx\, dy - \oint_S T_i \left[\frac{\partial u_i}{\partial a} - \frac{\partial u_i}{\partial x}\right] ds \tag{E-18}$$

where applying small strain in Green-Lagrange strain tensor and symmetry conditions, already discussed, gives:

$$\begin{aligned} \frac{\partial U}{\partial a} &= \underbrace{\frac{\partial U}{\partial \epsilon_{ij}}}_{\sigma_{ij}} \cdot \frac{\partial \epsilon_{ij}}{\partial a} = \frac{1}{2}\sigma_{ij}\frac{\partial}{\partial a}\left(\frac{\partial u_i}{\partial x_j} + \frac{\partial u_j}{\partial x_i}\right) \\ &= \frac{1}{2}\frac{\partial}{\partial a}\left(\sigma_{ij}\frac{\partial u_i}{\partial x_j} + \sigma_{ji}\frac{\partial u_j}{\partial x_i}\right) \\ &= \sigma_{ij}\frac{\partial}{\partial x_j}\left(\frac{\partial u_i}{\partial a}\right) \end{aligned} \tag{E-19}$$

Substituting eq. (E-19) into eq. (E-18) provides

$$\frac{dE_P}{da} = \iint_A \left[\sigma_{ij}\frac{\partial}{\partial x_j}\left(\frac{\partial u_i}{\partial a}\right) - \frac{\partial U}{\partial x}\right] dx\, dy - \oint_S T_i \left[\frac{\partial u_i}{\partial a} - \frac{\partial u_i}{\partial x}\right] ds \tag{E-20}$$

Moreover, from the virtual work theorem we have

$$\iint_A \sigma_{ij}\frac{\partial}{\partial x_j}\left(\frac{\partial u_i}{\partial a}\right) dx\, dy = \oint_S T_i \frac{\partial u_i}{\partial a}\, ds \tag{E-21}$$

and, substituting the virtual work theorem in eq. (E-21) into eq. (E-20) gives

$$\begin{aligned}\frac{dE_P}{da} &= \cancel{\oint_S T_i \frac{\partial u_i}{\partial a}\, ds} - \iint_A \frac{\partial U}{\partial x}\, dx\, dy - \cancel{\oint_S T_i \frac{\partial u_i}{\partial a}\, ds} + \oint_S T_i \frac{\partial u_i}{\partial x}\, ds \\ &= \oint_S T_i \frac{\partial u_i}{\partial a}\, ds - \iint_A \frac{\partial U}{\partial x}\, dx\, dy\end{aligned} \tag{E-22}$$

Finally, applying the Stoke's Theorem to the second term of eq. (E-22), results

$$-\frac{dE_P}{da} = \int_S \left[U\ dy - T_i \frac{\partial u_i}{\partial x}\ ds \right] = J \tag{E-23}$$

F
HRR Solution

F.1
Part 1 - Complementary energy

The complementary energy, in eq. (2-42), is evaluated by changing the coordinates to deviatoric stress tensor $\boldsymbol{S}$, since the strain eq. (2-41) is also a function of $\boldsymbol{S}$. Thus, using eq. (2-32):

$$\begin{aligned} d\sigma_{ij} &= \frac{\partial}{\partial S_{pq}}\left(S_{pq} + \frac{1}{3}\overbrace{\sigma_{kk}}^{\text{constant}}\,\delta_{pq}\right) dS_{ij} \\ &= \frac{\partial S_{pq}}{\partial S_{pq}}\, dS_{ij} \\ &= dS_{ij} \end{aligned} \tag{F-1}$$

and Replacing the definition of the strain tensor, from eq. (2-41), into the complementary energy and changing the coordinates result

$$\begin{aligned} E^* &= \int \epsilon_{ij}\, dS_{ij} \\ &= \int \left[(1+\nu)\, S_{ij} + \frac{1-2\nu}{3}\, \sigma_{kk}\, \delta_{ij} + \frac{3}{2}\, \alpha\, \sigma_e^{n-1} S_{ij}\right] dS_{ij} \\ &= \frac{(1+\nu)}{2}\, \underbrace{S_{ij}S_{ij}}_{\frac{2}{3}\,\sigma_e^2} + \int \frac{\partial}{\partial S_{ij}}\left(\frac{1-2\nu}{6}\sigma_{kk}^2\right) dS_{ij} + \int \frac{\partial}{\partial S_{ij}}\left(\frac{\alpha}{n+1}\sigma_e^{n+1}\right) dS_{ij} \\ &= \frac{(1+\nu)}{3}\, \sigma_e^2 + \frac{1-2\nu}{6}\, \sigma_{kk}^2 + \frac{\alpha}{n+1}\, \sigma_e^{n+1} \end{aligned} \tag{F-2}$$

where the integrand in the above integral may be expressed as

$$\begin{aligned}\frac{\partial}{\partial S_{ij}}\left(\frac{1-2\nu}{6}\sigma_{kk}^2\right) &= \frac{1-2\nu}{6}\ 2\sigma_{kk}\ \frac{\partial\sigma_{pp}}{\partial S_{ij}} \\ &= \frac{1-2\nu}{3}\sigma_{kk}\ \frac{\partial\sigma_{pp}}{\partial S_{ij}} \\ &= \frac{1-2\nu}{3}\sigma_{kk}\ \underbrace{\frac{\partial\sigma_{pp}}{\partial\sigma_{ij}}}_{\delta_{ip}\delta_{jp}=\delta_{ij}} \\ &= \frac{1-2\nu}{3}\ \sigma_{kk}\ \delta_{ij}\end{aligned} \tag{F-3}$$

and

$$\begin{aligned}\frac{\partial}{\partial S_{ij}}\left(\frac{\alpha}{n+1}\sigma_e^{n+1}\right) &= \frac{\alpha}{n+1}\frac{\partial}{\partial S_{ij}}\left(\frac{3}{2}\ S_{pq}S_{pq}\right)^{\frac{n+1}{2}} \\ &= \frac{\alpha}{\cancel{n+1}}\frac{\cancel{n+1}}{2}\underbrace{\left(\frac{3}{2}\ S_{pq}S_{pq}\right)^{\frac{n-1}{2}}}_{\sigma_e^{n-1}}\ \frac{\partial}{\partial S_{ij}}\left(\frac{3}{2}\ S_{pq}S_{pq}\right) \\ &= \frac{\alpha}{\cancel{2}}\sigma_e^{n-1}\frac{3}{2}\left(\cancel{2}\underbrace{\frac{\partial S_{pq}}{\partial S_{ij}}}_{\delta_{ip}\delta_{jq}}\ S_{pq}\right) \\ &= \frac{3}{2}\alpha\sigma_e^{n-1}S_{ij}\end{aligned} \tag{F-4}$$

completing the derivation of the complementary energy functional.

F.2
Part 2 - Strains

Since the cylindrical coordinate system has orthogonal bases, the index notation of eq. (2-41) is maintained, but using stress in polar coordinates. Assuming the radial axis r as 1 and θ as 2.

For the radial strain the corresponding index notation is

$$\epsilon_r = \epsilon_{11} \tag{F-5}$$

from eq. (2-41)

$$\epsilon_r = (1+\nu)S_r + \frac{1-2\nu}{3}(\sigma_r + \sigma_\theta) + \frac{3}{2}\alpha\ \sigma_e^{n-1}\ S_r \tag{F-6}$$

where the deviatoric tensor, from eq. (2-32) is

$$S_r = \sigma_r - \frac{1}{3}(\sigma_r + \sigma_\theta) = \frac{2}{3}\sigma_r - \frac{\sigma_\theta}{3} \tag{F-7}$$

Thus

$$\begin{aligned}\epsilon_r &= (1+\nu)\left(\frac{2}{3}\sigma_r - \frac{\sigma_\theta}{3}\right) + \frac{1-2\nu}{3}(\sigma_r + \sigma_\theta) + \frac{3}{2}\alpha\ \sigma_e^{n-1}\left(\frac{2}{3}\sigma_r - \frac{\sigma_\theta}{3}\right) \\ &= \frac{2(1+\nu)+1-2\nu}{3\sigma_0}\cdot\sigma_r + \frac{1-2\nu-1-\nu}{3\sigma_0}\cdot\sigma_\theta + \alpha\ \sigma_e^{n-1}\left(\sigma_r - \frac{1}{2}\sigma_\theta\right) \\ &= \sigma_r - \nu\sigma_\theta + \alpha\ \sigma_e^{n-1}\cdot\left(\sigma_r - \frac{1}{2}\sigma_\theta\right)\end{aligned} \tag{F-8}$$

For the tangential strain, similarly from procedure above

$$\epsilon_\theta = (1+\nu)S_\theta + \frac{1-2\nu}{3}(\sigma_r + \sigma_\theta) + \frac{3}{2}\alpha\ \sigma_e^{n-1}\ S_\theta \tag{F-9}$$

where:

$$S_\theta = \sigma_\theta - \frac{1}{3}(\sigma_r + \sigma_\theta) = \frac{2}{3}\sigma_\theta - \frac{\sigma_r}{3} \tag{F-10}$$

So:

$$\epsilon_\theta = \sigma_{r\theta} - \nu\sigma_r + \alpha\ \sigma_e^{n-1}\cdot\left(\sigma_\theta - \frac{1}{2}\sigma_r\right) \tag{F-11}$$

For the shear strain:

$$\epsilon_{r\theta} = (1+\nu)S_\theta + \frac{1-2\nu}{3}(\sigma_r + \sigma_\theta)\cdot 0 + \frac{3}{2}\alpha\ \sigma_e^{n-1}\ S_{r\theta} \tag{F-12}$$

where:

$$S_{r\theta} = \sigma_{r\theta} \tag{F-13}$$

As a result

$$\epsilon_{r\theta} = (1+\nu)\sigma_{r\theta} + \frac{3}{2}\alpha\ \sigma_e^{n-1}\sigma_{r\theta} \tag{F-14}$$

Finally,

$$\begin{cases} \epsilon_r = \sigma_r - \nu\sigma_\theta + \alpha\ \sigma_e^{n-1} \cdot (\sigma_r - \frac{1}{2}\sigma_\theta) \\ \epsilon_\theta = \sigma_{r\theta} - \nu\sigma_r + \alpha\ \sigma_e^{n-1} \cdot (\sigma_\theta - \frac{1}{2}\sigma_r) \\ \epsilon_{r\theta} = (1+\nu)\sigma_{r\theta} + \frac{3}{2}\alpha\ \sigma_e^{n-1}\ \sigma_{r\theta} \end{cases} \tag{F-15}$$

F.3
Part 3 - Compatibility

From the compatibility eq. (2-44), some parts are derived by substituting eqs. (2-43) and (F-15). So,

$$\begin{aligned}(r\epsilon_\theta)_{,rr} &= \left[r\sigma_\theta - \nu r\sigma_r + \alpha\sigma_e^{n+1} r\left(\sigma_\theta - \frac{1}{2}\sigma_r\right)\right]_{,rr} \\ &= \left[r\Psi_{,rr} - \nu r(r^{-1}\Psi_{,r} + r^{-2}\Psi_{,\theta\theta}) + \alpha\sigma_e^{n+1} r\left(\Psi_{,\theta\theta} - \frac{r^{-1}\Psi_{,r}}{2} - \frac{r^{-2}\Psi_{,\theta\theta}}{2}\right)\right]_{,rr} \\ &= \left(r\Psi_{,rr} - \nu\Psi_{,r} - \nu r^{-1}\Psi_{,\theta\theta}\right)_{,rr} + \frac{\alpha}{2}\left[\sigma_e^{n+1}\left(2r\Psi_{,\theta\theta} - \Psi_{,r} - r^{-1}\Psi_{,\theta\theta}\right)\right]_{,rr}\end{aligned} \tag{F-16}$$

$$\begin{aligned}(\epsilon_r)_{,\theta\theta} &= \left[\sigma_r - \nu\sigma_\theta + \alpha\sigma_e^{n+1}\left(\sigma_r - \frac{1}{2}\sigma_\theta\right)\right]_{,\theta\theta} \\ &= \left(r^{-1}\Psi_{,r} + r^{-2}\Psi_{,\theta\theta} - \nu\Psi_{,rr}\right)_{,\theta\theta} + \frac{\alpha}{2}\left[\sigma_e^{n+1}\left(2r^{-1}\Psi_{,r} + 2r^{-2}\Psi_{,\theta\theta} - \Psi_{,rr}\right)\right]_{,\theta\theta}\end{aligned} \tag{F-17}$$

$$(\epsilon_r)_{,r} = \left(r^{-1}\Psi_{,r} + r^{-2}\Psi_{,\theta\theta} - \nu\Psi_{,rr}\right)_{,r} + \frac{\alpha}{2}\left[\sigma_e^{n+1}\left(2r^{-1}\Psi_{,r} + 2r^{-2}\Psi_{,\theta\theta} - \Psi_{,rr}\right)\right]_{,r} \tag{F-18}$$

$$\begin{aligned}(r\cdot(\epsilon_{r\theta})_{,\theta})_{,r} &= \left\{r\cdot\left[(1+\nu)\sigma_{r\theta} + \frac{3}{2}\alpha\sigma_e^{n+1}\sigma_{r\theta}\right]_{,\theta}\right\}_{,r} \\ &= \left\{\left[-(1+\nu)r(r^{-1}\Psi_{,\theta})_{,r} - \frac{3}{2}\alpha\sigma_e^{n+1} r(r^{-1}\Psi_{,\theta})_{,r}\right]_{,\theta}\right\}_{,r} \\ &= -(1+\nu)\left[r(r^{-1}\Psi_{,\theta})_{,r}\right]_{,r\theta} - \frac{3}{2}\alpha\left[\sigma_e^{n+1} r(r^{-1}\Psi_{,\theta})_{,r}\right]_{,r\theta}\end{aligned} \tag{F-19}$$

Combining the equations in above into the compatibility equation, we have:

$$r^{-1}\left\{\left(r\Psi_{,rr}-\nu\Psi_{,r}-\nu r^{-1}\Psi_{,\theta\theta}\right)_{,rr}+\frac{\alpha}{2}\left[\sigma_e^{n+1}\left(2r\Psi_{,\theta\theta}-\Psi_{,r}-r^{-1}\Psi_{,\theta\theta}\right)\right]_{,rr}\right\}+$$
$$r^{-2}\left\{\left(r^{-1}\Psi_{,r}+r^{-2}\Psi_{,\theta\theta}-\nu\Psi_{,rr}\right)_{,\theta\theta}+\frac{\alpha}{2}\left[\sigma_e^{n+1}\left(2r^{-1}\Psi_{,r}+2r^{-2}\Psi_{,\theta\theta}-\Psi_{,rr}\right)\right]_{,\theta\theta}\right\}$$
$$-r^{-1}\left\{\left(r^{-1}\Psi_{,r}+r^{-2}\Psi_{,\theta\theta}-\nu\Psi_{,rr}\right)_{,r}+\frac{\alpha}{2}\left[\sigma_e^{n+1}\left(2r^{-1}\Psi_{,r}+2r^{-2}\Psi_{,\theta\theta}-\Psi_{,rr}\right)\right]_{,r}\right\}$$
$$-2r^{-2}\left\{-(1+\nu)\left[r(r^{-1}\Psi_{,\theta})_{,r}\right]_{,r\theta}-\frac{3}{2}\alpha\left[\sigma_e^{n+1}r(r^{-1}\Psi_{,\theta})_{,r}\right]_{,r\theta}\right\}=0 \quad \text{(F-20)}$$

that, by expanding, simplify to:

$$r^{-1}(r\Psi_{,rr})_{,rr}\cancel{-\nu r^{-1}(\Psi_{,r})_{,rr}}-\nu r^{-1}(r^{-1}\Psi_{,\theta\theta})_{,rr}+\frac{\alpha}{2}r^{-1}\left[\sigma_e^{n-1}\left(2r\Phi_{,rr}-\Psi_{,r}-r^{-1}\Psi_{,\theta\theta}\right)\right]_{,rr}$$
$$+r^{-2}(r^{-1}\Psi_{,r})_{,\theta\theta}+r^{-2}(r^{-2}\Psi_{,\theta\theta})_{,\theta\theta}-\nu r^{-2}(\Psi_{,rr})_{,\theta\theta}+\frac{\alpha}{2}r^{-2}\left[\sigma_e^{n+1}\left(2r^{-1}\Psi_{,r}+2r^{-2}\Psi_{,\theta\theta}-\Psi_{,rr}\right)\right]_{,\theta\theta}$$
$$-r^{-1}(r^{-1}\Psi_{,r})_{,r}-r^{-1}(r^{-2}\Psi_{,\theta\theta})_{,r}\cancel{+\nu r^{-1}(\Psi_{,rr})_{,r}}+\frac{\alpha}{2}r^{-2}\left[\sigma_e^{n+1}\left(-2r^{-1}\Psi_{,r}-2r^{-2}\Psi_{,\theta\theta}+\Psi_{,rr}\right)\right]_{,r}$$
$$+2r^{-2}(1+\nu)\left[r(r^{-1}\Psi_{,\theta})_{,r}\right]_{,r\theta}+3r^{-2}\alpha\left[\sigma_e^{n+1}r(r^{-1}\Psi_{,\theta})_{,r}\right]_{,r\theta}=0 \quad \text{(F-21)}$$

Splitting the compatibility equation into elastic (C_{el}) and plastic (C_p), we have

$$C_{el}=r^{-1}(r\Psi_{,rr})_{,rr}-\nu r^{-1}(r^{-1}\Psi_{,\theta\theta})_{,rr}+r^{-2}(r^{-1}\Psi_{,r})_{,\theta\theta}+r^{-2}(r^{-2}\Psi_{,\theta\theta})_{,\theta\theta}$$
$$-\nu r^{-2}(\Psi_{,rr})_{,\theta\theta}-r^{-1}(r^{-1}\Psi_{,r})_{,r}-r^{-1}(r^{-2}\Psi_{,\theta\theta})_{,r}$$
$$\underbrace{+2r^{-2}(1+\nu)\left[r(r^{-1}\Psi_{,\theta})_{,r}\right]_{,r\theta}}_{*} \quad \text{(F-22)}$$

$$C_p=\frac{\alpha}{2}\left\{r^{-1}\left[\sigma_e^{n-1}\left(2r\Psi_{,rr}-\Psi_{,r}-r^{-1}\Psi_{,\theta\theta}\right)\right]_{,rr}+6r^{-2}\left[\sigma_e^{n-1}\ r\cdot\left(r^{-1}\Psi_{,\theta}\right)_{,r}\right]_{,r\theta}\right.$$
$$+r^{-1}\left[\sigma_e^{n-1}\left(-2r^{-1}\Psi_{,r}-2r^{-2}\Psi_{,\theta\theta}+\Psi_{,rr}\right)\right]_{,r}$$
$$\left.+r^{-2}\left[\sigma_e^{n-1}\left(-\Psi_{,rr}+2r^{-1}\Psi_{,r}+2r^{-2}\Psi_{,\theta\theta}\right)\right]_{,\theta\theta}\right\} \quad \text{(F-23)}$$

Note that, C_p is already in its final form. Exploring the elastic contribu-

tion, $*$ is expanded as following

$$\begin{aligned}
* &= 2r^{-2}(1+\nu)\Big[r(r^{-1}\Psi_{,\theta})_{,r}\Big]_{,r\theta} \\
&= 2r^{-2}(1+\nu)\Big[r(r^{-1}\Psi_{,\theta\theta})_{,r}\Big]_{,r} \\
&= 2r^{-2}(1+\nu)\Big[(r^{-1}\Psi_{,\theta\theta})_{,r} + r(r^{-1}\Psi_{,\theta\theta})_{,rr}\Big] \\
&= 2r^{-2}(1+\nu)(r^{-1}\Psi_{,\theta\theta})_{,r} + 2r^{-1}(1+\nu)(r^{-1}\Psi_{,\theta\theta})_{,rr} \\
&= 2r^{-2}(r^{-1}\Psi_{,\theta\theta})_{,r} + \underbrace{2\nu r^{-2}(r^{-1}\Psi_{,\theta\theta})_{,r}}_{**} + 2r^{-1}(r^{-1}\Psi_{,\theta\theta})_{,rr} + 2\nu r^{-1}(r^{-1}\Psi_{,\theta\theta})_{,rr}
\end{aligned} \tag{F-24}$$

Manipulating $**$, we have

$$\begin{aligned}
** &= 2\nu r^{-2}(r^{-1}\Psi_{,\theta\theta})_{,r} \\
&= 2\nu r^{-2}(-r^{-2}\Psi_{,\theta\theta} + r^{-1}\Psi_{,r\theta\theta}) \\
&= -2\nu r^{-4}\Psi_{,\theta\theta} + 2\nu r^{-3}\Psi_{,r\theta\theta}
\end{aligned} \tag{F-25}$$

and, back in $*$, the last portion is rewritten as following

$$\begin{aligned}
\nu r^{-1}(r^{-1}\Psi_{,\theta\theta})_{,rr} &= \nu r^{-1}(-r^{-2}\Psi_{,\theta\theta} + r^{-1}\Psi_{,\theta\theta r})_{,r} \\
&= \nu r^{-1}(2r^{-3}\Psi_{,\theta\theta} - r^{-2}\Psi_{,\theta\theta r} - r^{-2}\Psi_{,r\theta\theta} + r^{-1}\Psi_{,\theta\theta rr}) \\
&= 2\nu r^{-4}\Psi_{,\theta\theta} - 2\nu r^{-3}\Psi_{,\theta\theta r} + \nu r^{-2}\Psi_{,\theta\theta rr}
\end{aligned} \tag{F-26}$$

As a result, substituting eqs. (F-25) and (F-26) into (F-24)

$$\begin{aligned}
* = 2r^{-2}(r^{-1}\Psi_{,\theta\theta})_{,r} &\cancel{-2\nu r^{-4}\Psi_{,\theta\theta}} \cancel{+2\nu r^{-3}\Psi_{,r\theta\theta}} + 2r^{-1}(r^{-1}\Psi_{,\theta\theta})_{,rr} + \\
&\nu r^{-1}(r^{-1}\Psi_{,\theta\theta})_{,rr} \cancel{+2\nu r^{-4}\Psi_{,\theta\theta}} \cancel{-2\nu r^{-3}\Psi_{,\theta\theta r}} + \nu r^{-2}\Psi_{,\theta\theta rr}
\end{aligned} \tag{F-27}$$

The elastic contribution is

$$\begin{aligned}
C_{el} = r^{-1}(r\Psi_{,rr})_{,rr} &\cancel{-\nu r^{-1}(r^{-1}\Psi_{,\theta\theta})_{,rr}} + r^{-2}(r^{-1}\Psi_{,r})_{,\theta\theta} + r^{-2}(r^{-2}\Psi_{,\theta\theta})_{,\theta\theta} \\
&\cancel{-\nu r^{-2}(\Psi_{,rr})_{,\theta\theta}} - r^{-1}(r^{-1}\Psi_{,r})_{,r} - r^{-1}(r^{-2}\Psi_{,\theta\theta})_{,r} + 2r^{-2}(r^{-1}\Psi_{,\theta\theta})_{,r} \\
&+ 2r^{-1}(r^{-1}\Psi_{,\theta\theta})_{,rr} \cancel{+\nu r^{-1}(r^{-1}\Psi_{,\theta\theta})_{,rr}} \cancel{+\nu r^{-2}\Phi_{,\theta\theta rr}}
\end{aligned} \tag{F-28}$$

simplifying, we have

$$C_{el} = r^{-1}(r\Psi_{,rr})_{,rr} + r^{-2}(r^{-1}\Psi_{,r})_{,\theta\theta} + r^{-2}(r^{-2}\Psi_{,\theta\theta})_{,\theta\theta} - r^{-1}(r^{-1}\Psi_{,r})_{,r} \\ - r^{-1}(r^{-2}\Psi_{,\theta\theta})_{,r} + 2r^{-2}(r^{-1}\Psi_{,\theta\theta})_{,r} + 2r^{-1}(r^{-1}\Psi_{,\theta\theta})_{,rr} \quad \text{(F-29)}$$

where, manipulating portions of the equation in above we have

$$\begin{aligned} r^{-1}(r\Psi_{,rr})_{,rr} &= r^{-1}(\Psi_{,rr} + r\Psi_{,rrr})_{,r} \\ &= r^{-1}\Psi_{,rrr} + r^{-1}(\Psi_{,rrr} + r\Psi_{,rrrr}) \\ &= 2r^{-1}\Psi_{,rrr} + \Psi_{,rrrr} \end{aligned} \quad \text{(F-30)}$$

$$\begin{aligned} 2r^{-2}(r^{-1}\Psi_{,\theta\theta})_{,r} &= 2r^{-1}(-r^{-2}\Psi_{,\theta\theta} + r^{-1}\Psi_{,\theta\theta r})_{,r} \\ &= -2r^{-4}\Psi_{\theta\theta} + 2r^{-3}\Psi_{\theta\theta r} \end{aligned} \quad \text{(F-31)}$$

$$\begin{aligned} 2r^{-1}(r^{-1}\Psi_{,\theta\theta})_{,rr} &= 2r^{-1}(-r^{-2}\Psi_{\theta\theta} + r^{-1}\Psi_{,\theta\theta r})_{,r} \\ &= 2r^{-1}(2r^{-3}\Psi_{,\theta\theta} - r^{-2}\Psi_{,\theta\theta r} - r^{-2}\Psi_{,\theta\theta r} + r^{-1}\Psi_{,\theta\theta rr}) \\ &= 4r^{-4}\Psi_{,\theta\theta} - 2r^{-3}\Psi_{\theta\theta r} - 2r^{-3}\Psi_{,\theta\theta r} + 2r^{-2}\Psi_{,\theta\theta rr} \end{aligned} \quad \text{(F-32)}$$

Rewriting eq. (F-29) by substituting eqs. (F-30), (F-31) and (F-32)

$$C_{el} = 2r^{-1}\Psi_{,rrr} + \Psi_{,rrrr} + r^{-2}(r^{-1}\Psi_{,r})_{,\theta\theta} + r^{-2}(r^{-2}\Psi_{,\theta\theta})_{,\theta\theta} + r^{-1}(r^{-1}\Psi_{,r})_{,r} \\ - 2r^{-1}(r^{-1}\Psi_{,r})_{,r} + r^{-1}(r^{-2}\Psi_{,\theta\theta})_{,r} - 2r^{-1}(r^{-2}\Psi_{,\theta\theta})_{,r} - 2r^{-4}\Psi_{\theta\theta} + \\ 2r^{-3}\Psi_{\theta\theta r} + 4r^{-4}\Psi_{,\theta\theta} - 2r^{-3}\Psi_{\theta\theta r} - 2r^{-3}\Psi_{,\theta\theta r} + 2r^{-2}\Psi_{,\theta\theta rr} \quad \text{(F-33)}$$

As previously done before, two portions of the equation in above are derived as

$$\begin{aligned} -2r^{-1}(r^{-1}\Psi_{,r})_{,r} &= -2r^{-1}(-r^{-2}\Psi_{,r} + r^{-1}\Psi_{,rr}) \\ &= 2r^{-3}\Psi_{,r} - 2r^{-2}\Psi_{,rr} \end{aligned} \quad \text{(F-34)}$$

$$\begin{aligned} -2r^{-1}(r^{-2}\Psi_{,\theta\theta})_{,r} &= -2r^{-1}(-2r^{-3}\Psi_{,\theta\theta} + r^{-2}\Psi_{,\theta\theta r}) \\ &= 4r^{-4}\Psi_{,\theta\theta} - 2r^{-3}\Psi_{,\theta\theta r} \end{aligned} \quad \text{(F-35)}$$

that, with some mathematical manipulation, yields on

$$C_{el} = 2r^{-1}\Psi_{,rrr} + \Psi_{,rrrr} + r^{-2}(r^{-1}\Psi_{,r})_{,\theta\theta} + r^{-2}(r^{-2}\Psi_{,\theta\theta})_{,\theta\theta} + r^{-1}(r^{-1}\Psi_{,r})_{,r}$$
$$2r^{-3}\Psi_{,r} - 2r^{-2}\Psi_{,rr} + r^{-1}(r^{-2}\Psi_{,\theta\theta})_{,r} + 4r^{-4}\Psi_{,\theta\theta} \cancel{-2r^{-3}\Psi_{,\theta\theta r}}$$
$$- 2r^{-4}\Psi_{\theta\theta} \cancel{+2r^{-3}\Psi_{\theta\theta r}} + 4r^{-4}\Psi_{,\theta\theta} - 2r^{-3}\Psi_{\theta\theta r} - 2r^{-3}\Psi_{,\theta\theta r} + 2r^{-2}\Psi_{,\theta\theta rr} \quad \text{(F-36)}$$

$$C_{el} = \Psi_{,rrrr} + r^{-1}\Psi_{,rrr} + \underbrace{r^{-1}\Psi_{,rrr} + 2r^{-3}\Psi_{,r} - 2r^{-2}\Psi_{,rr}}_{(r^{-1}\Psi_{,r})_{,rr}} + r^{-2}(r^{-1}\Psi_{,r})_{,\theta\theta}$$
$$+ r^{-2}(r^{-2}\Psi_{,\theta\theta})_{,\theta\theta} + r^{-1}(r^{-1}\Psi_{,r})_{,r} + r^{-1}(r^{-2}\Psi_{,\theta\theta})_{,r}$$
$$+ \underbrace{6r^{-4}\Psi_{,\theta\theta} - 4r^{-3}\Psi_{\theta\theta r} + r^{-2}\Psi_{,\theta\theta rr}}_{(r^{-2}\Psi_{,\theta\theta})_{,rr}} + r^{-2}\Psi_{,\theta\theta rr} \quad \text{(F-37)}$$

$$C_{el} = \Psi_{,rrrr} + (r^{-1}\Psi_{,r})_{,rr}(r^{-2}\Psi_{,\theta\theta})_{,rr} + r^{-1}\Psi_{,rrr} + r^{-1}(r^{-1}\Psi_{,r})_{,r}$$
$$+ r^{-1}(r^{-2}\Psi_{,\theta\theta})_{,r} + r^{-2}\Psi_{,\theta\theta rr} + r^{-2}(r^{-1}\Psi_{,r})_{,\theta\theta} + r^{-2}(r^{-2}\Psi_{,\theta\theta})_{,\theta\theta} \quad \text{(F-38)}$$

$$C_{el} = \nabla^4\Psi \quad \text{(F-39)}$$

This equation express the compatibility in the elastic case.

F.4
Part 4 - Stresses

The equations for stress definitions are derived using Airy's function, eq. (2-43), from the assumed stress function, eq. (2-48).

For the radial stress,

$$\begin{aligned}\sigma_r &= \frac{1}{r}\frac{\partial\Psi}{\partial r} + \frac{1}{r^2}\frac{\partial^2\Psi}{\partial\theta^2} \\ &= \frac{1}{r}\left(sKr^{s-1}\tilde{\Psi}\right) + \frac{1}{r^2}\left(Kr^s\tilde{\Psi}_{,\theta\theta}\right) \\ &= Kr^{s-2}s\tilde{\Psi} + Kr^{s-2}\tilde{\Psi}_{,\theta\theta} \\ &= Kr^{s-2}\cdot\left(s\tilde{\Psi} + \tilde{\Psi}_{,\theta\theta}\right) \\ &= Kr^{s-2}\cdot\tilde{\sigma_r}\end{aligned} \tag{F-40}$$

while, the tangential stress

$$\begin{aligned}\sigma_\theta &= \frac{\partial^2\Psi}{\partial r^2} \\ &= Kr^{s-2}s(s-1)\tilde{\Psi} \\ &= Kr^{s-2}\tilde{\sigma_\theta}\end{aligned} \tag{F-41}$$

and for shear stress

$$\begin{aligned}\sigma_{r\theta} &= -\frac{\partial}{\partial r}\left(\frac{1}{r}\frac{\partial\Psi}{\partial\theta}\right) \\ &= -\frac{\partial}{\partial r}\left(\frac{1}{r}Kr^s\tilde{\Phi}_{,\theta}\right) \\ &= -\frac{\partial}{\partial r}\left(Kr^{s-1}\tilde{\Psi}_{,\theta}\right) \\ &= -K(s-1)r^{s-2}\tilde{\Psi}_{,\theta} \\ &= Kr^{s-2}(1-s)\tilde{\Psi}_{,\theta} \\ &= Kr^{s-2}\tilde{\sigma_{r\theta}}\end{aligned} \tag{F-42}$$

F.5
Part 5

From obtained stress function in eq. (2-48), compatibility and von Mises equations can be rewrite. Due to the need of extensive algebraic manipulation, four individual terms were considered in the compatibility equation as shown below:

$$\underbrace{r^{-1}\left[\sigma_e^{n-1}\left(2r\Psi_{,rr}-\Psi_{,r}-r^{-1}\Psi_{,\theta\theta}\right)\right]_{,rr}}_{I}+\underbrace{6r^{-2}\left[\sigma_e^{n-1}\ r\cdot\left(r^{-1}\Psi_{,\theta}\right)_{,r}\right]_{,r\theta}}_{II}$$
$$+\underbrace{r^{-1}\left[\sigma_e^{n-1}\left(-2r^{-1}\Psi_{,r}-2r^{-2}\Psi_{,\theta\theta}+\Psi_{,rr}\right)\right]_{,r}}_{III}$$
$$+\underbrace{r^{-2}\left[\sigma_e^{n-1}\left(-\Psi_{,rr}+2r^{-1}\Psi_{,r}+2r^{-2}\Psi_{,\theta\theta}\right)\right]_{,\theta\theta}}_{IV}=0 \quad \text{(F-43)}$$

where I, II, III and IV, expanded using the definitions in eqs. (2-48) and (2-49) results in

$$\begin{aligned}
I &= r^{-1}\left[K^{n-1}r^{(s-2)(n-1)}\tilde{\sigma_e}^{n-1}\left(2Ks(s-1)r^{s-1}\tilde{\Psi}-Ksr^{s-1}\tilde{\Psi}-r^{-1}Kr^{s}\tilde{\Psi}_{,\theta\theta}\right)\right]_{,rr}\\
&= r^{-1}\left[K^{n}r^{(s-2)(n-1)+s-1}\tilde{\sigma_e}^{n-1}\left(2s(s-1)\tilde{\Psi}-s\tilde{\Psi}-\tilde{\Psi}_{,\theta\theta}\right)\right]_{,rr}\\
&= r^{-1}K^{n}\tilde{\sigma_e}^{n-1}\left[r^{(s-2)(n-1)+s-1}\left(s(2s-3)\tilde{\Psi}-\tilde{\Psi}_{,\theta\theta}\right)\right]_{,rr}\\
&= r^{-1}K^{n}\tilde{\sigma_e}^{n-1}\left(s(2s-3)\tilde{\Psi}-\tilde{\Psi}_{,\theta\theta}\right)[(s-2)(n-1)+s-1]\left(r^{(s-2)(n-1)+s-2}\right)_{,r}\\
&= r^{-1}K^{n}\tilde{\sigma_e}^{n-1}\left(s(2s-3)\tilde{\Psi}-\tilde{\Psi}_{,\theta\theta}\right)[(s-2)(n-1)+s-1]\cdot\\
&\qquad\qquad [(s-2)(n-1)+s-2]r^{(s-2)(n-1)+s-3}\\
&= r^{(s-2)(n-1)+s-4}K^{n}\tilde{\sigma_e}^{n-1}\left(s(2s-3)\tilde{\Psi}-\tilde{\Psi}_{,\theta\theta}\right)[n(s-2)+1][n(s-2)]
\end{aligned} \quad \text{(F-44)}$$

$$
\begin{aligned}
II &= 6r^{-2}\left[K^{n-1}r^{(s-2)(n-1)}\tilde{\sigma_e}^{n-1}r\left(r^{-1}Kr^{s}\tilde{\Psi}_{,\theta}\right)_{,r}\right]_{,r\theta} \\
&= 6r^{-2}K^{n}\left[r^{(s-2)(n-1)+1}\tilde{\sigma_e}^{n-1}\left((s-1)r^{s-2}\tilde{\Psi}_{,\theta}\right)\right]_{,r\theta} \\
&= 6r^{-2}K^{n}(s-1)\left[r^{(s-2)(n-1)+s-1}\tilde{\sigma_e}^{n-1}\tilde{\Psi}_{,\theta}\right]_{,r\theta} \\
&= 6r^{-2}K^{n}(s-1)\left[\tilde{\sigma_e}^{n-1}[(s-2)(n-1)+s-1]r^{(s-2)(n-1)+s-2}\tilde{\Psi}_{,\theta}\right]_{,\theta} \\
&= 6r^{(s-2)(n-1)+s-4}K^{n}(s-1)[n(s-2)+1]\left[\tilde{\sigma_e}^{n-1}\tilde{\Psi}_{,\theta}\right]_{,\theta}
\end{aligned}
\tag{F-45}
$$

$$
\begin{aligned}
III &= r^{-1}\left[K^{n-1}r^{(s-2)(n-1)}\tilde{\sigma_e}^{n-1}\Big(-2r^{-1}sKr^{s-1}\tilde{\Psi}-2r^{-2}Kr^{s}\tilde{\Psi}_{,\theta\theta}\right. \\
&\qquad\qquad \left.+Ks(s-1)r^{s-2}\tilde{\Psi}\Big)\right]_{,r} \\
&= r^{-1}\left[K^{n}r^{(s-2)(n-1)+s-2}\tilde{\sigma_e}^{n-1}\Big(-2s\tilde{\Psi}-2\tilde{\Psi}_{,\theta\theta}+s(s-1)\tilde{\Psi}\Big)\right]_{,r} \\
&= r^{-1}K^{n}\tilde{\sigma_e}^{n-1}[s(s-3)\tilde{\Psi}-2\tilde{\Psi}_{,\theta\theta}]\left[r^{(s-2)(n-1)+s-2}\right]_{,r} \\
&= r^{-1}K^{n}\tilde{\sigma_e}^{n-1}[s(s-3)\tilde{\Psi}-2\tilde{\Psi}_{,\theta\theta}][(s-2)(n-1)+s-2]r^{(s-2)(n-1)+s-3} \\
&= r^{(s-2)(n-1)+s-4}K^{n}\tilde{\sigma_e}^{n-1}n(s-2)[s(s-3)\tilde{\Psi}-2\tilde{\Psi}_{,\theta\theta}]
\end{aligned}
\tag{F-46}
$$

$$
\begin{aligned}
IV &= r^{-2}\left[K^{n-1}r^{(s-2)(n-1)}\tilde{\sigma_e}^{n-1}\Big(-Ks(s-1)r^{s-2}\tilde{\Psi}+2r^{-1}Ksr^{s-1}\tilde{\Psi}\right. \\
&\qquad\qquad \left.+2r^{-2}Kr^{s}\tilde{\Psi}_{,\theta\theta}\Big)\right]_{,\theta\theta} \\
&= r^{-2}\left[K^{n}r^{(s-2)(n-1)+s-2}\tilde{\sigma_e}^{n-1}\Big(-s(s-1)\tilde{\Psi}+2s\tilde{\Psi}+2\tilde{\Psi}_{,\theta\theta}\Big)\right]_{,\theta\theta} \\
&= -r^{(s-2)(n-1)+s-4}K^{n}\left[\tilde{\sigma_e}^{n-1}\Big(s(s-3)\tilde{\Psi}-2\tilde{\Psi}_{,\theta\theta}\Big)\right]_{,\theta\theta}
\end{aligned}
\tag{F-47}
$$

Substituting the results in above into compatibility condition in eq. (F-43) we have

$$\left[n(s-2)-\frac{\partial^2}{\partial\theta^2}\right]\cdot\left[\tilde{\sigma_e}^{n-1}\left(s(s-3)\tilde{\Psi}-2\tilde{\Psi}_{,\theta\theta}\right)\right]$$
$$+\left(n(s-2)+1\right)\left(n(s-2)\right)\tilde{\sigma_e}^{n-1}\left(s(2s-3)\tilde{\Psi}-\tilde{\Psi}_{,\theta\theta}\right)$$
$$+6\left(n(s-2)+1\right)(s-1)\left[\tilde{\sigma_e}^{n-1}\tilde{\Psi}_{,\theta}\right]_{,\theta}=0 \quad \text{(F-48)}$$

F.6
Part 6 - Inequality

At the crack tip neighbourhood, only the plastic contribution on the complementary energy is assumed relevant for stress calculations. Substituting the definition of σ_e, from eq. (2-49), into the simplified equation for the complementary energy we have

$$\begin{aligned} E_p^* &= \int_A \frac{\alpha}{n+1} (\overbrace{Kr^{s-2}\tilde{\sigma}_e}^{\sigma_e})^{n+1} \overbrace{dA}^{t\ r\ d\theta} \\ &= \frac{\alpha}{n+1} K^{n+1} \int r^{(s-2)(n+1)+1}\ \tilde{\sigma}_e^{n+1}\ d\theta \\ &= \frac{\alpha}{n+1} \frac{K^{n+1}}{(s-2)(n+1)+2}\ r^{(s-2)(n+1)+2}\ \int \tilde{\sigma}_e^{n+1}\ d\theta \end{aligned} \tag{F-49}$$

Different from the stresses that increase as r decreases the energy increases as the area of interest increases. As a result, r exponent in equation above must be larger than zero. Thus,

$$(s-2)(n+1)+2 > 0 \tag{F-50}$$

or

$$s > \frac{2n}{n+1} \tag{F-51}$$

F.7
Part 7 - Work

Neglecting the elastic contributions, the work integral is

$$W = \int_0^{\epsilon_{ij}} \sigma_{ij}\ d\epsilon_{ij}^p \tag{F-52}$$

where the infinitesimal plastic strains, in eq. (2-41) results in

$$\begin{aligned}
d\epsilon_{ij}^p &= \frac{3}{2}\alpha\ \frac{\partial}{\partial S_{pq}}\left(\sigma_e^{n-1}\ S_{pq}\right)\ dS_{ij} \\
&= \frac{3}{2}\alpha\ \left[\frac{\partial}{\partial S_{pq}}(\sigma_e^{n-1})\ S_{pq} + \sigma_e^{n-1}\ \underbrace{\frac{\partial S_{pq}}{\partial S_{pq}}}_{1}\right] dS_{ij} \\
&= \frac{3}{2}\alpha\ \left[\frac{\partial}{\partial S_{pq}}\left(\frac{3}{2}\ S_{rs}S_{rs}\right)^{\frac{n-1}{2}}\ S_{pq} + \sigma_e^{n-1}\right] dS_{ij} \\
&= \frac{3}{2}\alpha\ \left[\frac{n-1}{2}\ \underbrace{\left(\frac{3}{2}\ S_{rs}S_{rs}\right)^{\frac{n-3}{2}}}_{\sigma_e^{n-3}}\ \frac{\partial}{\partial S_{pq}}\left(\frac{3}{2}\ S_{rs}S_{rs}\right)\ S_{pq} + \sigma_e^{n-1}\right] dS_{ij} \\
&= \frac{3}{2}\alpha\ \left[\frac{n-1}{\cancel{2}}\ \sigma_e^{n-3}\ \frac{3}{2}\left(\cancel{2}\ \underbrace{\frac{\partial S_{rs}}{\partial S_{pq}}}_{\delta_{pr}\delta_{qs}}\ S_{rs}\right)\ S_{pq} + \sigma_e^{n-1}\right] dS_{ij} \\
&= \frac{3}{2}\alpha\ \left[(n-1)\ \sigma_e^{n-3}\ \underbrace{\frac{3}{2}\ S_{pq}S_{pq}}_{\sigma_e^2} + \sigma_e^{n-1}\right] dS_{ij} \\
&= \frac{3}{2}\alpha\ n\ \sigma_e^{n-1}\ dS_{ij}
\end{aligned} \tag{F-53}$$

or

$$\begin{aligned}
W &= \int \left(S_{ij} + \frac{1}{3}\ \sigma_{kk}\delta_{ij}\right)\ \frac{3}{2}\alpha\ n\ \sigma_e^{n-1}\ dS_{ij} \\
&= \int \frac{3}{2}\alpha\ n\ \sigma_e^{n-1}\ S_{ij}\ dS_{ij} + \int \frac{1}{2}\ \alpha\ n\ \sigma_{kk}\delta_{ij}\ \sigma_e^{n-1}\ dS_{ij} \\
&= \int \frac{\partial}{\partial S_{ij}}\left(\alpha\ \frac{n}{n+1}\ \sigma_e^{n+1}\right) dS_{ij} + 0
\end{aligned} \tag{F-54}$$

where the integrand in the above integral may be expressed as

$$\begin{aligned}
\frac{\partial}{\partial S_{ij}}\left(\alpha\ \frac{n}{n+1}\ \sigma_e^{n+1}\right) &= \alpha\ \frac{n}{n+1}\ \frac{\partial}{\partial S_{ij}}\left(\frac{3}{2}S_{pq}S_{pq}\right)^{\frac{n+1}{2}} \\
&= \alpha\ \frac{n}{\cancel{n+1}}\ \frac{\cancel{n+1}}{2}\left(\frac{3}{2}S_{pq}S_{pq}\right)^{\frac{n-1}{2}}\ \frac{\partial}{\partial S_{ij}}\left(\frac{3}{2}S_{pq}S_{pq}\right) \\
&= \alpha\ \frac{n}{\cancel{2}}\ \sigma_e^{n-1}\ \frac{3}{2}\left(\cancel{2}\ \underbrace{\frac{\partial S_{pq}}{\partial S_{ij}}}_{\delta_{ip}\ \delta_{jq}}\ S_{pq}\right) \\
&= \alpha\ n\ \sigma_e^{n-1}\ \frac{3}{2}S_{ij}
\end{aligned} \tag{F-55}$$

F.8
Part 8 - Displacement

Displacements are obtained from integrating the strains, which must be evaluated by considering that elastic contributions close to the crack tip are neglected. Thus, From eq. (F-15), linear strain in r direction is

$$\epsilon_r = \underbrace{\sigma_r - \nu\sigma_\theta}_{\text{neglect}} + \alpha\ \sigma_e^{n-1}\left(\sigma_r + \frac{1}{2}\sigma_\theta\right) \tag{F-56}$$

that substituting stress definitions in eq. (2-49) provides

$$\begin{aligned}\epsilon_r &= \alpha\left(Kr^{s-2}\tilde{\sigma}_e\right)^{n-1}\left[Kr^{s-2}\ (s\ \tilde{\Psi} + \tilde{\Psi}_{,\theta\theta}) - \frac{1}{2}\ Kr^{s-2}\ s(s-1)\tilde{\Psi}\right] \\ &= \alpha\ \tilde{\sigma}_e^{n-1}\ K^{n-1}\ r^{n(s-2)-(s-2)}\ K\ r^{s-2}\left(s\ \tilde{\Psi} + \tilde{\Psi}_{,\theta\theta} - \frac{s(s-1)}{2}\tilde{\Psi}\right) \\ &= \alpha\ K^n\ r^{n(s-2)}\ \tilde{\sigma}_e^{n-1}\left(\frac{s(3-s)}{2}\tilde{\Psi} + \tilde{\Psi}_{,\theta\theta}\right)\end{aligned} \tag{F-57}$$

Radial displacement results from the integration of linear radial strain definition is polar coordinates as

$$\epsilon_r = \frac{\partial u_r}{\partial r} \rightarrow u_r = \int \epsilon_r\ dr \tag{F-58}$$

Thus using F-57 we have

$$u_r = \alpha\ K^n\ r^{n(s-2)+1}\ \tilde{u}_r(\theta) \tag{F-59}$$

Similarly, the displacement in θ direction, strain ϵ_θ is as follows (eq. F-15)

$$\epsilon_\theta = \underbrace{\sigma_\theta - \nu\sigma_r}_{\text{neglect}} + \alpha\ \sigma_e^{n-1}\left(\sigma_\theta - \frac{1}{2}\sigma_r\right) \tag{F-60}$$

substituting stress definitions in eq. (2-49) results

$$\begin{aligned}\epsilon_\theta &= \alpha\left(Kr^{s-2}\tilde{\sigma}_e\right)^{n-1}\left[Kr^{s-2}\ s(s-1)\tilde{\Psi} - \frac{1}{2}\ Kr^{s-2}\ (s\ \tilde{\Psi} + \tilde{\Psi}_{,\theta\theta})\right] \\ &= \alpha K^{n-1}\ r^{n(s-2)-(s-2)}\ \tilde{\sigma}_e^{n-1}\ K\ r^{s-2}\left[s(s-1)\tilde{\Psi} - \frac{1}{2}\ (s\ \tilde{\Psi} + \tilde{\Psi}_{,\theta\theta})\right] \\ &= \alpha\ K^n\ r^{n(s-2)}\ \tilde{\sigma}_e^{n-1}\left[s\left(s - \frac{3}{2}\right)\tilde{\Psi} - \frac{\tilde{\Psi}_{,\theta\theta}}{2}\right]\end{aligned} \tag{F-61}$$

In polar coordinates , ϵ_θ is

$$\epsilon_\theta = \frac{u_r}{r} + \frac{1}{r}\ \frac{\partial u_\theta}{\partial\theta} \rightarrow u_{\theta,_\theta} = r\cdot\epsilon_\theta - u_r \tag{F-62}$$

where $u_{\theta,_\theta}$ are as in eqs. (F-61) and (F-57), therefore,

$$
\begin{aligned}
u_{\theta_{,\theta}} &= \alpha\ K^n\ r^{n(s-2)+1}\ \tilde{\sigma}_e^{n-1}\left[s\left(s-\frac{3}{2}\right)\tilde{\Psi}-\frac{\tilde{\Psi}_{,\theta\theta}}{2}\right] \\
&\quad -\frac{\alpha\ K^n\ r^{n(s-2)+1}}{n(s-2)+1}\tilde{\sigma}_e^{n-1}\left(\frac{s(3-s)}{2}\tilde{\Psi}+\tilde{\Psi}_{,\theta\theta}\right) \\
&= \alpha\ K^n\ r^{n(s-2)+1}\ \left\{\tilde{\sigma}_e^{n-1}\left[s\left(s-\frac{3}{2}\right)\tilde{\Psi}-\frac{\tilde{\Psi}_{,\theta\theta}}{2}\right]\right. \\
&\quad \left.\underbrace{-\frac{1}{n(s-2)+1}\tilde{\sigma}_e^{n-1}\left(\frac{s(3-s)}{2}\tilde{\Psi}+\tilde{\Psi}_{,\theta\theta}\right)}_{\tilde{u}_r}\right\} \\
&= \alpha\ K^n\ r^{n(s-2)+1}\ \underbrace{\left\{\tilde{\sigma}_e^{n-1}\left[s\left(s-\frac{3}{2}\right)\tilde{\Psi}-\frac{\tilde{\Psi}_{,\theta\theta}}{2}\right]-\tilde{u}_r\right\}}_{\tilde{u}_{\theta_{,\theta}}}
\end{aligned}
\tag{F-63}
$$

Resulting on

$$u_{\theta_{,\theta}} = \alpha\ K^n\ r^{n(s-2)+1}\ \tilde{u}_{\theta_{,\theta}} \tag{F-64}$$

that integrating in θ provides

$$u_{\theta} = \alpha\ K^n\ r^{n(s-2)+1}\ \tilde{u}_{\theta} \tag{F-65}$$

F.9
Part 9 - J integral

After obtaining work in section F.7, the second term of J-integral must be evaluated. From eq. (2-21), J-integral is calculated in the cartesian coordinates. However, in HRR method derivations polar coordinates were employed (see figure 2.5). Thus, in cartesian coordinates, displacements relates to displacements in polar coordinates as

$$\begin{aligned}\boldsymbol{u}^{xy} = \begin{bmatrix} u_x \\ u_y \end{bmatrix} &= R_z(\theta) \cdot \boldsymbol{u}^{r\theta} \\ &= \begin{bmatrix} \cos\theta & -\sin\theta \\ \sin\theta & \cos\theta \end{bmatrix} \cdot \begin{bmatrix} u_r \\ u_\theta \end{bmatrix} \\ &= \begin{bmatrix} u_r\cos\theta - u_\theta\sin\theta \\ u_r\sin\theta + u_\theta\cos\theta \end{bmatrix}\end{aligned} \tag{F-66}$$

and, as a result, displacement derivatives with respect to r and θ may be written as

$$\begin{cases} u_{x,_r} = u_{r,_r}\cos\theta - u_{\theta,_r}\sin\theta \\ u_{x,_\theta} = u_{r,_\theta}\cos\theta - u_r\sin\theta - u_{\theta,_\theta}\sin\theta - u_\theta\cos\theta \\ u_{y,_r} = u_{r,_r}\sin\theta + u_{\theta,_r}\cos\theta \\ u_{y,_\theta} = u_{r,_\theta}\sin\theta + u_r\cos\theta + u_{\theta,_\theta}\cos\theta - u_\theta\sin\theta \end{cases} \tag{F-67}$$

The traction vector in polar coordinates results in

$$\begin{aligned}\boldsymbol{T}^{r\theta} &= \boldsymbol{\sigma}^{r\theta} \cdot \boldsymbol{n} \\ &= \begin{bmatrix} \sigma_{rr} & \sigma_{r\theta} \\ \sigma_{r\theta} & \sigma_{\theta\theta} \end{bmatrix} \cdot \begin{bmatrix} 1 \\ 0 \end{bmatrix} = \begin{bmatrix} \sigma_{rr} \\ \sigma_{r\theta} \end{bmatrix}\end{aligned} \tag{F-68}$$

where the normal vector $\boldsymbol{n}$ is written in a polar coordinate system.

Since the traction vector for the J-integral formula must be written in cartesian coordinate, a rotation transformation is applied

$$\begin{aligned}\boldsymbol{T}^{xy} = \begin{bmatrix} T_x^{xy} \\ T_y^{xy} \end{bmatrix} &= R_z(\theta) \cdot \boldsymbol{T}^{r\theta} \\ &= \begin{bmatrix} \cos\theta & -\sin\theta \\ \sin\theta & \cos\theta \end{bmatrix} \cdot \begin{bmatrix} \sigma_r \\ \sigma_{r\theta} \end{bmatrix} \\ &= \begin{bmatrix} \sigma_r \cos\theta - \sigma_{r\theta}\sin\theta \\ \sigma_r \sin\theta + \sigma_{r\theta}\cos\theta \end{bmatrix}\end{aligned} \tag{F-69}$$

Therefore, the second part of J-integral in eq. (2-21) is

$$T_i u_{i,_x} = T_x^{xy} \cdot u_{x,_x} + T_y^{xy} \cdot u_{y,_x} \tag{F-70}$$

where, by the chain rule it results

$$\begin{cases} u_{x,_x} = \frac{du_x}{dx} = \frac{du_x}{dr}\frac{dr}{dx} + \frac{du_x}{d\theta}\frac{d\theta}{dx} \\ u_{y,_x} = \frac{du_y}{dx} = \frac{du_y}{dr}\frac{dr}{dx} + \frac{du_y}{d\theta}\frac{d\theta}{dx} \end{cases} \tag{F-71}$$

The equations in above are functions of $\frac{dr}{dx}$ and $\frac{d\theta}{dx}$. From polar coordinates, radius is decomposed in x and y, thus

$$\frac{dr}{dx} = \frac{d}{dx}\,(x^2+y^2)^{1/2} = \frac{1}{2}\,(x^2+y^2)^{-1/2}\,2x = \frac{x}{(x^2+y^2)^{1/2}} = \frac{r\cos\theta}{r} = \cos\theta \tag{F-72}$$

while, from trigonometry, θ is defined as

$$\cos\theta = \frac{x}{r} = \frac{x}{\sqrt{(x^2+y^2)^{1/2}}} = x\cdot(x^2+y^2)^{-1/2} \tag{F-73}$$

Taking the derivative if equation in above with respect to θ provides

$$\begin{aligned} -\sin\theta\,\frac{d\theta}{dx} &= (x^2+y^2)^{-1/2} - \frac{1}{2}\,x\,(x^2+y^2)^{-3/2}\,2x \\ &= \frac{1}{r}\left(1-\frac{x^2}{r^2}\right) \\ &= \frac{1}{r}\underbrace{(1-\cos^2\theta)}_{\sin^2\theta}\end{aligned} \tag{F-74}$$

Resulting on

$$\frac{d\theta}{dx} = -\frac{\sin\theta}{r} \tag{F-75}$$

Substituting eqs. (F-72) and (F-75) into eqs. (F-71) provides

$$
\begin{aligned}
u_{x_{,x}} &= \frac{du_x}{dx} = \frac{du_x}{dr}\frac{dr}{dx} + \frac{du_x}{d\theta}\frac{d\theta}{dx} \\
&= (u_{r_{,r}}\cos\theta - u_{\theta_{,r}}\sin\theta)\cos\theta \\
&\qquad - (u_{r_{,\theta}}\cos\theta - u_r\sin\theta - u_{\theta_{,\theta}}\sin\theta - u_\theta\cos\theta)\ r^{-1}\ \sin\theta \\
&= u_{r_{,r}}\cos^2\theta - u_{\theta_{,r}}\sin\theta\cos\theta - r^{-1}\ u_{r_{,\theta}}\cos\theta\sin\theta + r^{-1}\ u_r\sin^2\theta \\
&\qquad\qquad + r^{-1}\ u_{\theta_{,\theta}}\sin^2\theta + r^{-1}\ u_\theta\cos\theta\sin\theta
\end{aligned}
\tag{F-76}
$$

and also

$$
\begin{aligned}
u_{y_{,x}} &= \frac{du_y}{dx} = \frac{du_y}{dr}\frac{dr}{dx} + \frac{du_y}{d\theta}\frac{d\theta}{dx} \\
&= (u_{r_{,r}}\sin\theta + u_{\theta_{,r}}\cos\theta)\cos\theta \\
&\qquad - (u_{r_{,\theta}}\sin\theta + u_r\cos\theta + u_{\theta_{,\theta}}\cos\theta - u_\theta\sin\theta)\ r^{-1}\ \sin\theta \\
&= u_{r_{,r}}\sin\theta\cos\theta + u_{\theta_{,r}}\cos^2\theta - r^{-1}\ u_{r_{,\theta}}\sin^2\theta - r^{-1}\ u_r\cos\theta\sin\theta \\
&\qquad\qquad - r^{-1}\ u_{\theta_{,\theta}}\cos\theta\sin\theta + r^{-1}\ u_\theta\sin^2\theta
\end{aligned}
\tag{F-77}
$$

Therefore, from eqs. (F-69), (F-76) and (F-77), the second part of J-integral is rewritten as following

$$
\begin{aligned}
T_i u_{i,x} &= T_x^{xy} \cdot u_{x,x} + T_y^{xy} \cdot u_{y,x} \\
&= [\sigma_r \cos\theta - \sigma_{r\theta} \sin\theta] \cdot (u_{r,r} \cos^2\theta - u_{\theta,r} \sin\theta\cos\theta - r^{-1}\ u_{r,\theta} \cos\theta \sin\theta \\
&\qquad + r^{-1}\ u_r \sin^2\theta + r^{-1}\ u_{\theta,\theta} \sin^2\theta + r^{-1}\ u_\theta \cos\theta \sin\theta) \\
&\quad + [\sigma_r \sin\theta + \sigma_{r\theta} \cos\theta] \cdot (u_{r,r} \sin\theta\cos\theta + u_{\theta,r} \cos^2\theta - r^{-1}\ u_{r,\theta} \sin^2\theta \\
&\qquad - r^{-1}\ u_r \cos\theta \sin\theta - r^{-1}\ u_{\theta,\theta} \cos\theta \sin\theta + r^{-1}\ u_\theta \sin^2\theta) \\
&= \sigma_r \cos^2\theta\cos\theta\ u_{r,r} - \cancel{\sigma_r \cos^2\theta \sin\theta\ u_{\theta,r}} - r^{-1}\ \sigma_r \cos^2\theta \sin\theta\ u_{r,\theta} \\
&\quad + \cancel{r^{-1}\ \sigma_r \sin^2\theta\cos\theta\ u_r} + \cancel{\sigma_{rr} \sin^2\theta\cos\theta\ u_{\theta,\theta}} + r^{-1}\ \sigma_r \cos^2\theta \sin\theta\ u_\theta \\
&\quad - \cancel{\sigma_{r\theta} \cos^2\theta \sin\theta\ u_{r,r}} + \sigma_{r\theta} \sin^2\theta\cos\theta\ u_{\theta,r} + \cancel{r^{-1}\ \sigma_{r\theta} \sin^2\theta\cos\theta\ u_{r,\theta}} \\
&\quad - r^{-1}\ \sigma_{r\theta} \sin^2\theta \sin\theta\ u_r - r^{-1}\ \sigma_{r\theta} \sin^2\theta \sin\theta\ u_{\theta,\theta} - \cancel{r^{-1}\ \sigma_{r\theta} \sin^2\theta\cos\theta\ u_\theta} \\
&\quad + \sigma_r \sin^2\theta\cos\theta\ u_{r,r} + \cancel{\sigma_r \cos^2\theta \sin\theta\ u_{\theta,r}} - r^{-1}\ \sigma_r \sin^2\theta \sin\theta\ u_{r,\theta} \\
&\quad - \cancel{r^{-1}\ \sigma_r \sin^2\theta\cos\theta\ u_r} - \cancel{r^{-1}\ \sigma_r \sin^2\theta\cos\theta\ u_{\theta,\theta}} + r^{-1}\ \sigma_r \sin^2\theta \sin\theta\ u_\theta \\
&\quad + \cancel{\sigma_{r\theta} \cos^2\theta \sin\theta\ u_{r,r}} + \sigma_{r\theta} \cos^2\theta\cos\theta\ u_{\theta,r} - \cancel{r^{-1}\ \sigma_{r\theta} \sin^2\theta\cos\theta\ u_{r,\theta}} \\
&\quad - r^{-1}\ \sigma_{r\theta} \cos^2\theta \sin\theta\ u_r - r^{-1}\ \sigma_{r\theta} \cos^2\theta \sin\theta\ u_{\theta,\theta} + \cancel{r^{-1}\ \sigma_{r\theta} \sin^2\theta\cos\theta\ u_\theta} \\
&= \sigma_r(\sin^2\theta + \cos^2\theta)\cos\theta\ u_{r,r} - r^{-1}\ \sigma_r(\sin^2\theta + \cos^2\theta)\sin\theta\ u_{r,\theta} \\
&\quad + r^{-1}\ \sigma_r(\sin^2\theta + \cos^2\theta)\sin\theta\ u_\theta + \sigma_{r\theta}(\sin^2\theta + \cos^2\theta)\cos\theta\ u_{\theta,r} \\
&\quad - r^{-1}\ \sigma_{r\theta}(\sin^2\theta + \cos^2\theta)\sin\theta\ u_r - r^{-1}\ \sigma_{r\theta}(\sin^2\theta + \cos^2\theta)\sin\theta\ u_{\theta,\theta} \\
&= \sigma_r \cos\theta\ u_{r,r} - r^{-1}\ \sigma_r \sin\theta\ u_{r,\theta} + r^{-1}\ \sigma_r \sin\theta\ u_\theta + \sigma_{r\theta} \cos\theta\ u_{\theta,r} \\
&\qquad - r^{-1}\ \sigma_{r\theta} \sin\theta\ u_r - r^{-1}\ \sigma_{r\theta} \sin\theta\ u_{\theta,\theta}
\end{aligned}
\tag{F-78}
$$

where

$$
\begin{aligned}
r^{-1}\ \sigma_r \sin\theta\ u_\theta &= r^{-1}\ Kr^{s-2}\tilde{\sigma}_r\ \sin\theta \cdot \alpha K^n r^{n(s-2)+1}\ \tilde{u}_\theta \\
&= \alpha K^{n+1} r^{(n+1)(s-2)} \sin\theta\ \tilde{\sigma}_r\ \tilde{u}_\theta
\end{aligned}
\tag{F-79}
$$

$$
\begin{aligned}
-r^{-1}\ \sigma_r\ \sin\theta\ u_{r,\theta} &= -r^{-1}\ Kr^{s-2}\tilde{\sigma}_r \sin\theta \cdot \alpha K^n r^{n(s-2)+1}\ \tilde{u}_{r,\theta} \\
&= -\alpha K^{n+1} r^{(n+1)(s-2)} \sin\theta\ \tilde{\sigma}_r\ \tilde{u}_{r,\theta}
\end{aligned}
\tag{F-80}
$$

$$
\begin{aligned}
-r^{-1}\ \sigma_{r\theta}\ \sin\theta\ u_{\theta,\theta} &= -r^{-1}\ Kr^{s-2}\tilde{\sigma}_{r\theta}\ \sin\theta \cdot \alpha K^n r^{n(s-2)+1}\ \tilde{u}_{\theta,\theta} \\
&= -\alpha K^{n+1} r^{(n+1)(s-2)} \sin\theta\ \tilde{\sigma}_{r\theta}\ \tilde{u}_{\theta,\theta}
\end{aligned}
\tag{F-81}
$$

$$
\begin{aligned}
-r^{-1}\ \sigma_{r\theta}\ \sin\theta\ u_r &= -r^{-1}\ \ Kr^{s-2}\tilde{\sigma}_{r\theta}\ \sin\theta \cdot \alpha K^n r^{n(s-2)+1}\ \tilde{u}_r \\
&= -\alpha K^{n+1} r^{(n+1)(s-2)} \sin\theta\ \tilde{\sigma}_{r\theta}\ \tilde{u}_r
\end{aligned}
\tag{F-82}
$$

$$\begin{aligned}\sigma_r \cos\theta \; u_{r,r} &= Kr^{s-2}\tilde{\sigma}_r \;\; \cos\theta \cdot \alpha K^n (n(s-2)+1) r^{n(s-2)} \;\; \tilde{u}_r \\ &= \alpha K^{n+1} r^{(n+1)(s-2)} \;\; (n(s-2)+1) \;\; \cos\theta \;\; \tilde{\sigma}_r \;\; \tilde{u}_r\end{aligned} \tag{F-83}$$

$$\begin{aligned}\sigma_{r\theta} \cos\theta \; u_{\theta,r} &= Kr^{s-2}\tilde{\sigma}_{r\theta} \;\; \cos\theta \cdot \alpha K^n (n(s-2)+1) r^{n(s-2)} \;\; \tilde{u}_\theta \\ &= \alpha K^{n+1} r^{(n+1)(s-2)} \;\; (n(s-2)+1) \;\; \cos\theta \;\; \tilde{\sigma}_{r\theta} \;\; \tilde{u}_\theta\end{aligned} \tag{F-84}$$

Finally,

$$\begin{aligned}\sigma_{ij} n_j u_{i,x} = \alpha K^{n+1} r^{(n+1)(s-2)} \{ &\sin\theta [\tilde{\sigma}_r (\tilde{u}_\theta - \tilde{u}_{r,\theta}) - \tilde{\sigma}_{r\theta} (\tilde{u}_r + \tilde{u}_{\theta,\theta})] \\ &+ (n(s-2)+1) \;\; \cos\theta [\tilde{\sigma}_r \tilde{u}_r + \tilde{\sigma}_{r\theta} \tilde{u}_\theta]\end{aligned} \tag{F-85}$$

G
Program Validations

G.1
Simply supported beam under distributed load

This example is intended to verify the element numerical results in material only linear and nonlinear analyses. The fig. G.1 below illustrates the problem of a simply supported rectangular section beam under uniformly distributed transverse loading.

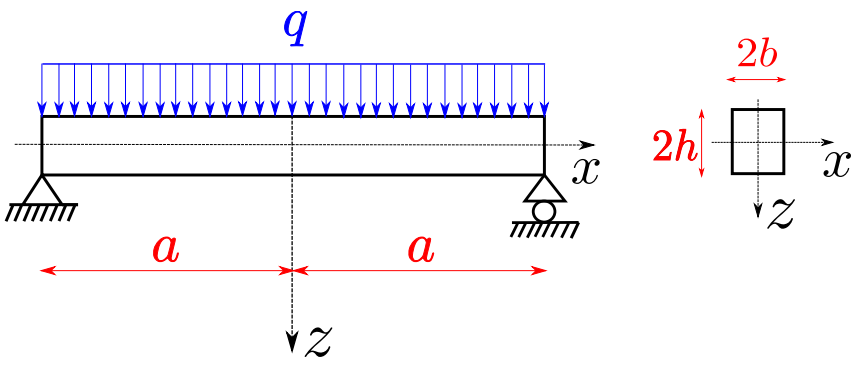

Figure G.1: Simple supported beam

In the simulation the discretization employed a nonlinear parabolic tetrahedron element, T10. This higher order is employed to represent the appropriate displacement distribution over the cross section of the beam due to bending. Due to symmetry to the z-axis, only half of the beam was represented in the model.

Material and geometric parameters employed in the analysies are presented in the table below.
and the obtained displacement field, in the elastic regime, with small displacements, is presented in the fig. G.2.

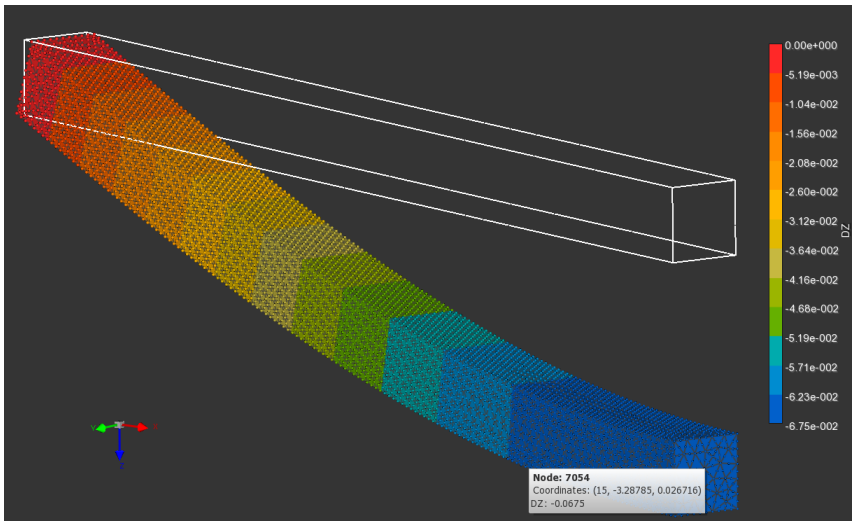

Figure G.2: Displacement field in z-direction from TopSim

where the maximum obtained displacement in z-direction is

$$\delta_{max}^{num} = 0.0675\ m \tag{G-1}$$

while the corresponding analytical solution displacement from [35] gives

$$\delta_{max} = \frac{5qL^4}{384EI} = \frac{5 \cdot 1.116 \cdot 10^5 \cdot 30^4}{384 \cdot 210 \cdot 10^9 \cdot \frac{1}{12}} = 0.0673\ m \tag{G-2}$$

where I is the cross section moment of inertia and a $0,3\%$ of relative error is obtained.

Notice that the analytical solution does not consider transverse shear stresses while it is accounted for in the numerical formulation employed as demonstrated by the larger displacement value obtained in the numerical solution.

In Prager [31] it is proposed an analytical solution using the 2D state of stress and strain model from the Theory of Elasticity, in a perfect plastic material. Two additional parameters

$$\begin{cases} q_0 \coloneqq 4\sqrt{3}\kappa b \\ \rho \coloneqq \frac{q}{q_0}(\frac{a}{h})^2 \end{cases} \tag{G-3}$$

were introduced for algebraic simplification, and the expression, in closed form, for the central deflection is

$$W_0 = \frac{a^2 q_0}{Ebh}\left[\frac{1}{4\sqrt{3\rho}} \cdot \sinh^{-1}\sqrt{\frac{3\rho-2}{3(1-\rho)}} + \frac{\sqrt{1-\rho}}{4\sqrt{3}\rho} + \frac{2\rho^2-1}{8} - \frac{3\rho+1}{\rho} \cdot \sqrt{\frac{\rho(3\rho-2)}{3}}\right] \tag{G-4}$$

indent The deflection, obtained in equation above, is ploted in fig. G.4 varying ρ.

For establishing the dividing surface between plasticity and elasticity a new variable in the z axis was added, ζ. The plastic region for a fixed ρ is bounded with $[-\zeta(x), \zeta(x)]$, where $0 < \zeta \leqslant h$. Notice that ζ varies along coordinate x. Equation (G-5) presents the expression to obtain the plastic surface of the beam as function of ρ.

$$\frac{1}{3}\left(\frac{\zeta}{h}\right)^2 - \rho\left(\frac{x}{a}\right)^2 = 1 - \rho \tag{G-5}$$

Figure G.3 plot eq. (G-5) in a beam with $h = 1.0$ and $a = 1.0$ for different values of ρ. Notice that parameter ρ, related to the load, interferes with the plastic volume in the beam.

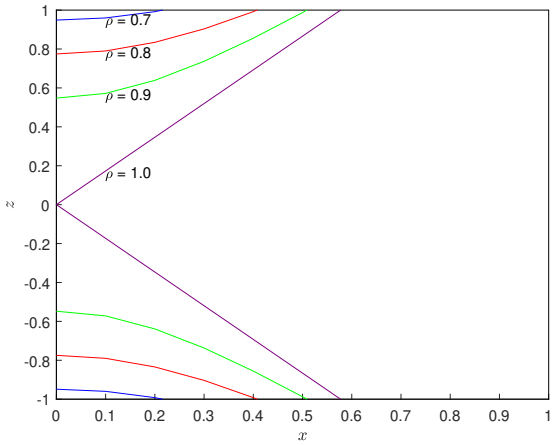

Figure G.3: Plastic evolution as function of ρ

For validation purposes, the analytical central deflection function, presented in eq. (G-4) is compared with the numerical deflection from the FEM program. The geometric, load and material parameters is presented in table below:

For this simulation an incremental-iterative approach on the Newton-Raphson algorithm is adopted. Using 20 increments of load results in 20 respective ρ. Figure G.4 shows the comparison between analytical and Numerical results, where both curves have compatible shape. The numerical solution predicts the analytical solution proposed by Prager.

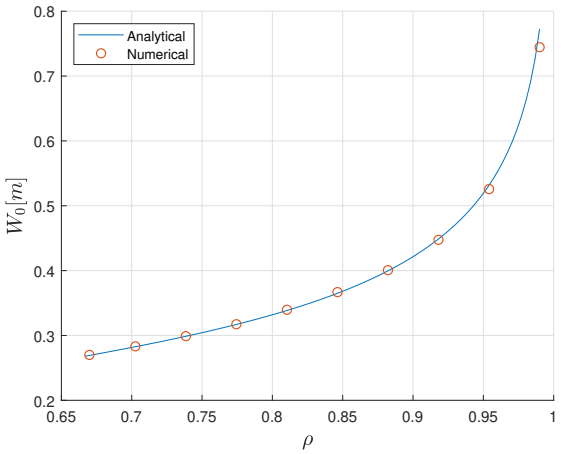

Figure G.4: Central displacement of the beam as function of the plastic variable ρ

To visualize the evolution of the von Mises stress field, 10 increments are present from figure G.5 to figure G.14:

Figure G.5: $t = 0.1s$

Figure G.6: $t = 0.2s$

Figure G.7: $t = 0.3s$

Figure G.8: $t = 0.4s$

Figure G.9: $t = 0.5s$

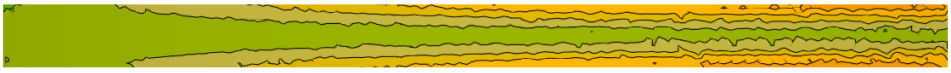

Figure G.10: $t = 0.6s$

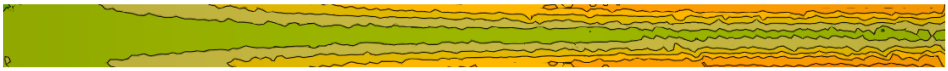

Figure G.11: $t = 0.7s$

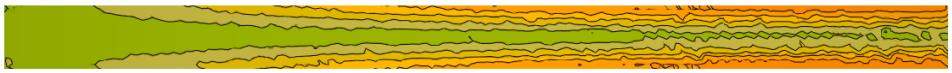

Figure G.12: $t = 0.8s$

Figure G.13: $t = 0.9s$

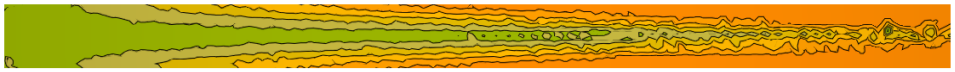

Figure G.14: $t = 1.0s$

G.1.1 Proof

Considering a plane stress state for this formulation and knowing that just plane xx and xz are non-zero:

$$\sigma_z = \sigma_y = \sigma_{yz} = \sigma_{xz} = 0 \tag{G-6}$$

Simplifying the notation:

$$\sigma_x = \sigma \tag{G-7}$$

$$\sigma_{zx} = \tau \tag{G-8}$$

The stress tensor is given by:

$$\boldsymbol{\sigma} = \begin{bmatrix} \sigma_{xx} & \sigma_{xy} & \sigma_{xz} \\ \sigma_{yx} & \sigma_{yy} & \sigma_{yz} \\ \sigma_{zx} & \sigma_{zy} & \sigma_{zz} \end{bmatrix} = \begin{bmatrix} \sigma & 0 & \tau \\ 0 & 0 & 0 \\ \tau & 0 & 0 \end{bmatrix} \tag{G-9}$$

and the pressure, from eq. (3-21)

$$p = \frac{\boldsymbol{\sigma} : \boldsymbol{I}}{3} = \frac{\sigma + 0 + 0}{3} = \frac{\sigma}{3} \tag{G-10}$$

and the deviatoric stress tensor, eq. (3-20):

$$\begin{aligned} \boldsymbol{S} &= \boldsymbol{\sigma} - p \cdot \boldsymbol{I} \\ &= \begin{bmatrix} \sigma & - & \tau \\ 0 & 0 & 0 \\ \tau & 0 & 0 \end{bmatrix} - \begin{bmatrix} \frac{\sigma}{3} & 0 & 0 \\ 0 & \frac{\sigma}{3} & 0 \\ 0 & 0 & \frac{\sigma}{3} \end{bmatrix} \\ &= \begin{bmatrix} \frac{2\sigma}{3} & 0 & \tau \\ 0 & -\frac{\sigma}{3} & 0 \\ \tau & 0 & -\frac{\sigma}{3} \end{bmatrix} \end{aligned} \tag{G-11}$$

In a plastic problem a yield surface must be adopted, in this case, a von Mises formulation is considered. Thus, the yield function Φ is defined as:

$$\Phi^2 = J_2 - \kappa^2 \tag{G-12}$$

From the definition of J_2:

$$\begin{aligned} \Phi^2 = 0 &= J_2 - \kappa^2 \\ &= \frac{1}{2}\left[\left(\frac{2\sigma}{3}\right)^2 + \frac{\sigma^2}{9} + \frac{\sigma^2}{9} + 2\tau^2\right] - \kappa^2 \end{aligned} \tag{G-13}$$

So:

$$\sigma^2 + 3\tau^2 = 3\kappa^2 \tag{G-14}$$

Assuming that the shear stress is small in comparison to the normal stress, the eq. (G-14) can be rewritten as:

$$\sigma^2 = 3\kappa^2 \tag{G-15}$$

or

$$|\sigma| = \kappa\sqrt{3} \tag{G-16}$$

As previously defined, $\pm\zeta(x)$ are the dividing surface between the elastic and plastic domains. In an elastoplastic cross-section, the upper and lower portions of the beam behave plastically while the center elastically. the plastic region presents a constant value of stress, since perfect plasticity is imposed, while the elastic region, from beam theory, a linear decrease reaching zero at the neutral fiber. Thus

$$\sigma = \begin{cases} -\kappa\sqrt{3}, & \text{for } -h \leqslant z \leqslant -\zeta \\ \frac{\kappa z\sqrt{3}}{\zeta}, & \text{for } -\zeta \leqslant z \leqslant \zeta \\ \kappa\sqrt{3}, & \text{for } \zeta \leqslant z \leqslant h \end{cases} \tag{G-17}$$

Figure G.15 above describes the elastoplastic stress distribution at the cross section

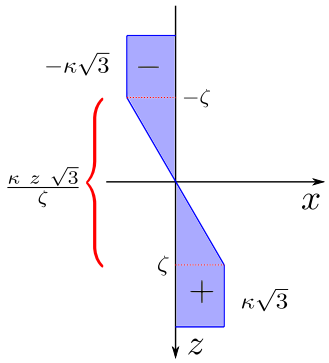

Figure G.15: Elastoplastic cross section

The internal moment at cross section x is given by eq. (G-18). Figure G.16 illustrate stress σ acting at cross section.

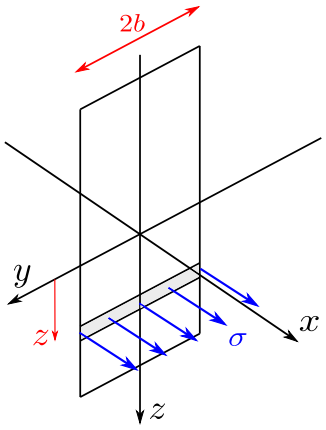

Figure G.16: Moment calculation at cross section

$$M(x) = \int_{-h}^{h} z\ \sigma(x,z)\ 2b\ dz = 4b\int_{0}^{h} z\ \sigma(x,z)\ dz \tag{G-18}$$

Considering elastic and plastic regions, eq. (G-18) may be rewritten as:

$$M(x) = \overbrace{4b\int_{0}^{\zeta} z\ \underbrace{\sigma(x,z)}_{\frac{\kappa z\sqrt{3}}{\zeta}}\ dz}^{\text{elastic}} + \overbrace{4b\int_{\zeta}^{h} z\ \underbrace{\sigma(x,z)}_{\kappa\sqrt{3}}\ dz}^{\text{plastic}} \tag{G-19}$$

resulting in

$$
\begin{aligned}
M(x) &= \frac{4b\kappa\sqrt{3}}{\zeta}\int_0^{\zeta} z^2\, dz + 4b\kappa\sqrt{3}\int_{\zeta}^{h} z\, dz \\
&= \frac{4b\kappa\sqrt{3}}{\cancel{\zeta}}\cdot\frac{\zeta^{\cancel{2}}}{3} + 4b\kappa\sqrt{3}\left(\frac{h^2}{2} - \frac{\zeta^2}{2}\right) \\
&= \frac{2b\kappa\sqrt{3}}{3}(3h^2 - \zeta^2)
\end{aligned}
\tag{G-20}
$$

Alternatively, the moment from the external load can also be calculated. First, the reaction must be computed (see figure G.17).

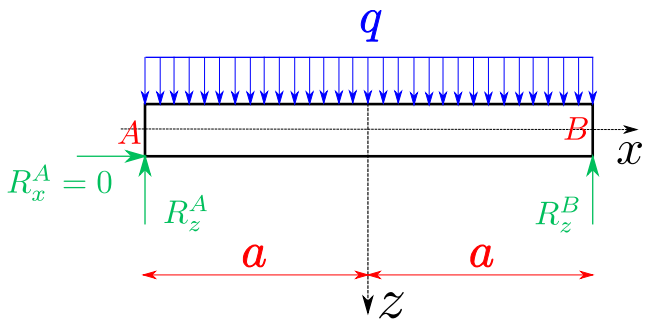

Figure G.17: Beam reactions

Considering resultant force in z direction being zero:

$$\sum F_z = 0 \rightarrow R_z^A + R_z^B = q \cdot 2a \tag{G-21}$$

and the resultant moment at point A also being zero:

$$\sum M_A = 0 \rightarrow -q \cdot \cancel{2}a \cdot a + R_z^B \cdot \cancel{2}a = 0 \tag{G-22}$$

$$R_z^B = qa \tag{G-23}$$

Substituting eq. (G-23) into eq. (G-21) provides:

$$R_z^A = qa \tag{G-24}$$

With R_z^A and R_z^B found, the moment at cross section x is obtained as illustrated in figure G.18.

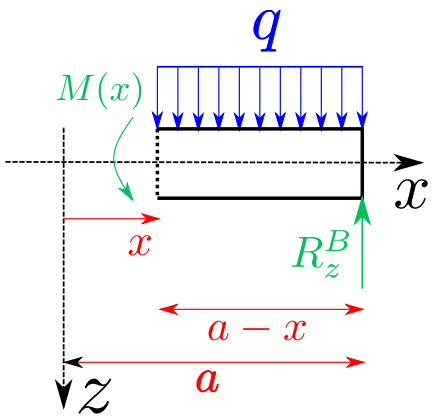

Figure G.18: Moment at cross section

Thus,

$$\begin{aligned} M(x) &= -q(a-x)\cdot\frac{a-x}{2} + qa(a-x) \\ &= \frac{q}{2}(a^2-x^2) \end{aligned} \tag{G-25}$$

For the beam be in equilibrium the internal moment, eq. (G-20), and external moment, eq. (G-25), must be equal. As a result:

$$\frac{2b\kappa\sqrt{3}}{3}(3h^2-\zeta^2) = \frac{q}{2}(a^2-x^2) \tag{G-26}$$

Defying variables q_0 and ρ as

$$\begin{cases} q_0 \coloneqq 4\sqrt{3}\kappa b \\ \rho \coloneqq \frac{q}{q_0}(\frac{a}{h})^2 \end{cases} \tag{G-27}$$

eq. (G-26) is rewritten as:

$$\underbrace{\frac{2\sqrt{3}\kappa b}{q_0/2}}\cdot h^2 - \underbrace{\frac{2\sqrt{3}\kappa b}{3}}_{q_0/6}\cdot\zeta^2 = \frac{q}{2}(a^2-x^2) \tag{G-28}$$

Multiplying for $2/q_0$ and rearranging

$$\frac{q_0}{q_0}1\left[1-\frac{1}{3}\left(\frac{\zeta}{h}\right)^2\right] = \underbrace{\frac{q}{q_0}\left(\frac{a}{h}\right)^2}_{\rho} - \underbrace{\frac{q}{q_0}\left(\frac{x}{h}\right)^2}_{\rho(\frac{x}{a})^2} \tag{G-29}$$

Thus,

$$\frac{1}{3}\left(\frac{\zeta}{h}\right)^2 - \rho\left(\frac{x}{a}\right)^2 = 1-\rho \tag{G-30}$$

The equation above (G-30) defines the boundary surface between elasticity and plasticity. This formulation considers perfect plasticity, an indeterminate problem, for a given stress in the hardening curve the correspondent

strain is not unique. For this reason, the following problem only has a solution because elasticity is a unique problem and restricts plasticity. In the case of having fully perfect plasticity in the beam, there is no solution.

As a result, our model has load limitations, since the cross section can not be under fully plasticity. From eq. (G-30) and fig. G.3 the plastic region is more intense near $x = 0$, the critical cross section for this limitation.

In the case of fully elastic beam $\zeta = h$ and for $x = 0$, critical cross section, from eq. (G-30)

$$\rho = \frac{2}{3} \tag{G-31}$$

while for fully plasticity $\zeta = 0$, so:

$$\rho = 1 \tag{G-32}$$

Consequently, ρ must be a value between both parameters above to be under elastoplastic behavior and have a solution.

$$\frac{2}{3} < \rho < 1 \tag{G-33}$$

Usually, elastoplastic problem is coupling between elastic and plastic regions. However in the case of perfect plasticity, due to hardening indetermination, there is no plastic strain restriction and how determines the strain is the elastic behavior of the beam.

By this reason, the elastic region only depends on itself. From elasticity:

$$\sigma = -Ez\frac{d^2W}{dx^2} \tag{G-34}$$

where in a elastoplastic cross section, the elastic stress from eq. (G-17) provides:

$$\frac{\kappa \not{z} \sqrt{3}}{\zeta} = -E\not{z}\frac{d^2W}{dx^2} \rightarrow \frac{d^2W}{dx^2} = -\frac{\kappa\sqrt{3}}{E\zeta} \tag{G-35}$$

and for fully elastic cross section:

$$\frac{d^2W}{dx^2} = -\frac{M}{EI} \tag{G-36}$$

where $M(x)$ is defined in eq. (G-25) and moment of inertia for a rectangular section is

$$I = \frac{(2b)(2h)^3}{12} \tag{G-37}$$

The next step is to combine both the elastoplastic and elastic differential equations for the whole length of the beam. Figure G.19 illustrates in x axis which formulation must be applied, where x^* is the point that divides both theories.

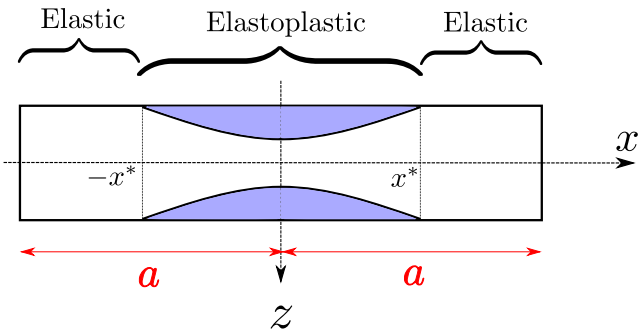

Figure G.19: Elastoplastic and elastic behavior in the beam

To determine x^*, eq. (G-30) must be applied. Note that in the following cross section $\zeta = h$. So:

$$\frac{1}{3}\cancel{\left(\frac{h}{h}\right)^2} - \rho\left(\frac{x^*}{a}\right)^2 = 1 - \rho \tag{G-38}$$

isolation x^*:

$$x^{*^2} = a^2\left(1 - \frac{2}{3\rho}\right) = a^2\left(\frac{3\rho - 2}{3\rho}\right) \rightarrow x^* = \frac{1}{\sqrt{3}}\underbrace{\frac{a}{\sqrt{\rho}}}_{\frac{\alpha}{\sqrt{1-\rho}}}\sqrt{3\rho - 2} \tag{G-39}$$

defying α as:

$$\alpha := \frac{a\sqrt{1-\rho}}{\sqrt{\rho}} \tag{G-40}$$

x^* is rewritten as:

$$x^* = \alpha\sqrt{\frac{3\rho - 2}{3(1-\rho)}} \tag{G-41}$$

Isolation ζ from eq. (G-30) provides:

$$\zeta = \sqrt{3}h\sqrt{1 - \rho + \rho\frac{x^2}{a^2}} \tag{G-42}$$

substituting the equation in above into the elastoplastic differential eq. (G-35) gives

$$\frac{d^2W}{dx^2} = -\frac{\kappa}{Eh}\frac{1}{\sqrt{1 - \rho + \rho\frac{x^2}{a^2}}} \tag{G-43}$$

The box bellow presents the analytical solution of an irrational integral. Note that our second order differential equation can be integrated to reduce the order by using the integral bellow that fits into eq. (G-43).

$$R = \sqrt{ax^2 + bx + c} \tag{G-44}$$

$$\int \frac{dx}{R} = \frac{1}{\sqrt{a}} \sinh^{-1} \frac{2ax + b}{\sqrt{4ac - b^2}} \tag{G-45}$$

for $a > 0$ and $4ac - b^2 > 0$ (non-zero denominator).

Defying a, b and c to adjust the general integral into our problem. So:

$$\begin{cases} a = \frac{\rho}{a^2} \\ b = 0 \\ c = 1 - \rho \end{cases} \tag{G-46}$$

Integrating

$$\begin{aligned} \frac{dW}{dx} &= -\frac{\kappa}{Eh} \frac{a}{\sqrt{\rho}} \sinh^{-1} \frac{2\frac{\rho}{a^2}x}{\sqrt{4\frac{\rho}{a^2}(1-\rho)}} + C_1 \\ &= -\frac{\kappa}{Eh} \frac{a}{\sqrt{\rho}} \sinh^{-1} \frac{2\frac{\rho}{a^2}x}{2\sqrt{\rho(1-\rho)}} + C_1 \\ &= -\frac{\kappa}{Eh} \frac{a}{\sqrt{\rho}} \sinh^{-1} \frac{\sqrt{\rho}\sqrt{\rho}x}{a\sqrt{\rho}\sqrt{(1-\rho)}} + C_1 \\ &= -\frac{\kappa}{Eh} \frac{a}{\sqrt{\rho}} \cdot \underbrace{\frac{\alpha\sqrt{\rho}}{a\sqrt{1-\rho}}}_{1} \cdot \sinh^{-1} \underbrace{\frac{\sqrt{\rho}}{a\sqrt{1-\rho}}}_{1/\alpha} x + C_1 \end{aligned} \tag{G-47}$$

From symmetry, the derivative of the deflection with respect to x must be zero in $x = 0$. As a result of this fact,

$$C_1 = 0 \tag{G-48}$$

Thus,

$$\frac{dW}{dx} = -\frac{\kappa}{Eh} \frac{\alpha}{\sqrt{1-\rho}} \sinh^{-1} \frac{x}{\alpha} \tag{G-49}$$

To obtain the deflection, eq. (G-49) must be integrate.

$$\int_{W_0}^{W(x)} dW = -\frac{\alpha\kappa}{Eh\sqrt{1-\rho}} \int_0^x \sinh^{-1} \frac{x}{\alpha}\, dx \tag{G-50}$$

The box bellow presents a general analytical solution.

$$\int \sinh^{-1} z dz = z \sinh^{-1} z - \sqrt{1 + z^2} + C \tag{G-51}$$

Letting z be:

$$z = \frac{x}{\alpha} \rightarrow dz = \frac{1}{\alpha} dx \therefore dx = \alpha dz \tag{G-52}$$

and changing the integral coordinate gives

$$W - W_0 = -\frac{\alpha^2 \kappa}{Eh\sqrt{1-\rho}} \int_{z_0}^{z_f} \sinh^{-1} z \; dz \tag{G-53}$$

So, substituting result from eq. (G-51) gives:

$$\begin{aligned} W - W_0 &= -\frac{\alpha^2 \kappa}{Eh\sqrt{1-\rho}} \left[\frac{x}{\alpha} \sinh^{-1} \frac{x}{\alpha} - \sqrt{1 + \left(\frac{x}{\alpha}\right)^2} \right]_{x=0}^{x=x} \\ &= -\frac{\alpha^2 \kappa}{Eh\sqrt{1-\rho}} \left[\frac{x}{\alpha} \sinh^{-1} \frac{x}{\alpha} - \sqrt{1 + \left(\frac{x}{\alpha}\right)^2} + 1 \right] \end{aligned} \tag{G-54}$$

From compatibility, the deflection and the derivative of the elastoplastic and elastic solution in the interface point x^* needs to be equal. The deflection in x^* is

$$W(x^*) - W_0 = -\frac{\alpha^2 \kappa}{Eh\sqrt{1-\rho}} \left[\sqrt{\frac{3\rho - 2}{3(1-\rho)}} \sinh^{-1} \sqrt{\frac{3\rho - 2}{3(1-\rho)}} - \sqrt{\frac{1}{3(1-\rho)}} + 1 \right] \tag{G-55}$$

while the derivative from eq. (G-49) at point x^* is

$$\left.\frac{dW}{dx}\right|_{x=x^*} = -\frac{\alpha\kappa}{Eh\sqrt{1-\rho}} \sinh^{-1} \sqrt{\frac{3\rho - 2}{3(1-\rho)}} \tag{G-56}$$

Considering the elastic differential eq. (G-36) and substituting the definition of the moment of inertia for rectangular cross section, eq. (G-37) and the moment expression, on eq. (G-25), gives:

$$\frac{d^2W}{dx^2} = -\frac{3}{8} \frac{q(a^2 - x^2)}{Ebh^3} \tag{G-57}$$

Integrating the differential equation in above for the domain $x^* \leqslant x \leqslant a$:

$$\left.\frac{dW}{dx}\right|_{x} - \left.\frac{dW}{dx}\right|_{x=x^*} = -\frac{3qa^2x}{8Ebh^3} + \frac{qx^3}{8Ebh^3} + C_2 \tag{G-58}$$

and substituting the value of $\left.\frac{dW}{dx}\right|_{x=x^*}$ from the elastoplastic eq. (G-56):

$$\frac{dW}{dx} = -\frac{3qa^2x}{8Ebh^3} + \frac{qx^3}{8Ebh^3} - \frac{\alpha\kappa}{Eh\sqrt{1-\rho}} \sinh^{-1} \sqrt{\frac{1}{3(1-\rho)}} + C_2 \tag{G-59}$$

Moreover, the derivative of the deflection with respect to x must also be equal to eq. (G-56) in the lower bound, point $x = x^*$. So, equalling equation in above with (G-56):

$$-\cancel{\frac{\alpha\kappa}{Eh\sqrt{1-\rho}}\sinh^{-1}\sqrt{\frac{3\rho-2}{3(1-\rho)}}} = -\frac{3q}{8Ebh^3}\cdot\overbrace{a^2}^{\frac{\alpha^2\rho}{1-\rho}}\cdot\alpha\sqrt{\frac{3\rho-2}{3(1-\rho)}}$$
$$+\frac{q}{8Ebh^3}\underbrace{\alpha^3\sqrt{\frac{3\rho-2}{3(1-\rho)}}\frac{3\rho-2}{3(1-\rho)}}_{x^{*3}} - \cancel{\frac{\alpha\kappa}{Eh\sqrt{1-\rho}}\sinh^{-1}\sqrt{\frac{3\rho-2}{3(1-\rho)}}} + C_2 \quad \text{(G-60)}$$

From equation above, the constant C_2 is defined as being:

$$\begin{aligned} C_2 &= -\frac{3q}{8Ebh^3}\frac{\alpha^2\rho}{1-\rho}\alpha\sqrt{\frac{3\rho-2}{3(1-\rho)}} - \frac{q\alpha^3}{8Ebh^3}\frac{3\rho-2}{3(1-\rho)}\sqrt{\frac{3\rho-2}{3(1-\rho)}} \\ &= \frac{\alpha}{Eh\sqrt{1-\rho}}\cdot\frac{q\alpha^2}{8bh^2}\sqrt{\frac{3\rho-2}{3}}\left(\frac{3\rho}{1-\rho}-\frac{3\rho-2}{3(1-\rho)}\right) \\ &= \frac{\alpha}{Eh\sqrt{1-\rho}}\cdot\frac{q\alpha^2}{8bh^2}\sqrt{\frac{3\rho-2}{3}}\cdot\frac{2(3\rho+1)}{3(1-\rho)} \\ &= \frac{\alpha}{Eh\sqrt{1-\rho}}\cdot\frac{q\alpha^2}{12bh^2}\sqrt{\frac{3\rho-2}{3}}\cdot\frac{3\rho+1}{1-\rho} \end{aligned} \quad \text{(G-61)}$$

With the definition of constant C_2 eq. (G-59) is fully determined. Integration the following equation, the deflection of the beam is obtained as:

$$W(x) - W_0 = -\frac{3qa^2x^2}{16Ebh^3} + \frac{qx^4}{32Ebh^3} + \left(\left.\frac{dW}{dx}\right|_{x=x^*} + C_2\right)x + C_3 \quad \text{(G-62)}$$

where C_3 is a constant that needs to be found. As previously presented, by compatibility the deflection at point x^*, domain of both elastoplastic and elastic differential equations must have equal deflection at this interface. Rewriting eq. (G-62) above for x^* :

$$W(x^*) - W_0 = -\frac{3qa^2}{16Ebh^3}\,\alpha^2\,\frac{3\rho-2}{3(1-\rho)} + \frac{q}{32Ebh^3}\,\alpha^4\left(\frac{3\rho-2}{3(1-\rho)}\right)^2$$
$$-\frac{\alpha}{EH\sqrt{1-\rho}}\left[k\sinh^{-1}\sqrt{\frac{3\rho-2}{3(1-\rho)}} - \frac{\rho\alpha^2}{12bh^2}\sqrt{\frac{3\rho-2}{3}}\frac{3\rho+1}{1-\rho}\right]\underbrace{\alpha\sqrt{\frac{3\rho-2}{3(1-\rho)}}}_{x^*} + C_3 \quad \text{(G-63)}$$

From boundary condition, the initial displacement for the elastic differential equation must be the final displacement from the elastoplastic differential equation. As a result, equation in above must be equal to eq. (G-55). Thus:

$$-\frac{3q}{16Ebh^3}\overbrace{a^2}^{\frac{\alpha^2\rho}{1-\rho}}\alpha^2\frac{3\rho-2}{3(1-\rho)}+\frac{q}{32Ebh^3}\alpha^4\left(\frac{3\rho-2}{3(1-\rho)}\right)^2$$
$$-\frac{\alpha^2}{Eh\sqrt{1-\rho}}\sqrt{\frac{3\rho-2}{3(1-\rho)}}\left[\cancel{k\sinh^{-1}\sqrt{\frac{3\rho-2}{3(1-\rho)}}}-\frac{\rho\alpha^2}{12bh^2}\sqrt{\frac{3\rho-2}{3}}\frac{3\rho+1}{1-\rho}\right]+C_3$$
$$=-\frac{\alpha^2\kappa}{Eh\sqrt{1-\rho}}\left[\cancel{\sqrt{\frac{3\rho-2}{3(1-\rho)}}\sinh^{-1}\sqrt{\frac{3\rho-2}{3(1-\rho)}}}-\sqrt{\frac{1}{3(1-\rho)}}+1\right] \quad \text{(G-64)}$$

Isolating constant C_3

$$C_3=\frac{q\alpha^4}{Ebh^3}\cdot\frac{\cancel{3}}{16}\cdot\frac{1}{\cancel{3}}\cdot\frac{\rho(3\rho-2)}{(1-\rho)^2}-\frac{q\alpha^4}{32\cdot3^2\cdot Ebh^3}\frac{9\rho^2-12\rho+4}{(1-\rho)^2}$$
$$-\frac{\alpha^2}{Eh}\frac{q\alpha^2}{12bh^2}\left(\frac{1}{\sqrt{1-\rho}}\right)^2\left(\sqrt{\frac{3\rho-2}{3}}\right)^2\frac{3\rho+1}{1-\rho}+\frac{\alpha^2\kappa}{Eh\sqrt{1-\rho}}\left[\sqrt{\frac{1}{3(1-\rho)}}-1\right] \quad \text{(G-65)}$$

rearranging equation in above

$$C_3=\frac{q\alpha^4}{Ebh^3}\overbrace{\left[\frac{3\rho^2-2\rho}{16(1-\rho)^2}-\frac{9\rho^2-12\rho+4}{16\cdot2\cdot9\cdot(1-\rho)^2}-\frac{(3\rho-2)(3\rho+1)}{12\cdot3\cdot(1-\rho)^2}\right]}^{-\frac{9\rho^2-4}{96(1-\rho)^2}}$$
$$+\frac{\alpha^2\kappa}{Eh\sqrt{1-\rho}}\left[\sqrt{\frac{1}{3(1-\rho)}}-1\right] \quad \text{(G-66)}$$

so the constant C_3 is defined as

$$C_3=\frac{\alpha^2\kappa}{Eh\sqrt{1-\rho}}\left[\sqrt{\frac{1}{3(1-\rho)}}-1\right]-\frac{q\alpha^4}{96Ebh^3}\cdot\frac{9\rho^2-4}{(1-\rho)^2} \quad \text{(G-67)}$$

Substituting all constants from eqs. (G-56), (G-61) and (G-67) into eq. (G-62) provides the displacement in the elastic portion of the beam

$$W(x)-W_0=-\frac{3}{16}\frac{q}{Ebh^3}\left(\frac{\alpha^2\rho}{1-\rho}x^2-\frac{x^4}{6}\right)-\frac{\alpha x}{Eh\sqrt{1-\rho}}\left[\kappa\sinh^{-1}\sqrt{\frac{3\rho-2}{3(1-\rho)}}\right.$$
$$\left.-\frac{1}{12}\frac{q\alpha^2}{bh^2}\frac{3\rho+1}{1-\rho}\sqrt{\frac{3\rho-2}{3}}\right]+\frac{\alpha^2\kappa}{Eh\sqrt{1-\rho}}\left[\sqrt{\frac{1}{3(1-\rho)}}-1\right]-\frac{q\alpha^4}{96Ebh^3}\cdot\frac{9\rho^2-4}{(1-\rho)^2} \quad \text{(G-68)}$$

valid for $x^* \leqslant x \leqslant a$.

In a differential equation for the complete solution two boundary condition needs to be imposed. Previously, the derivative of the displacement with respect to axis x in initial point x^* provided the definition of constant C_3. The next step is to consider the final point a. In this problem, the deflection of the beam in the support is zero. As a result,

$$W(x = a) = 0 \tag{G-69}$$

Substituting the boundary condition above at point a in eq. (G-68):

$$\underbrace{W(a)}_{0} - W_0 = -\frac{3}{16}\frac{q}{Ebh^3}\overbrace{\left(\underbrace{\frac{\alpha^2\rho}{1-\rho}}_{a^2}a^2 - \frac{a^4}{6}\right)}^{\frac{5a^4}{6}} - \frac{\alpha a}{Eh\sqrt{1-\rho}}\left[\kappa \sinh^{-1}\sqrt{\frac{3\rho-2}{3(1-\rho)}}\right.$$
$$\left. - \frac{1}{12}\frac{q\alpha^2}{bh^2}\frac{3\rho+1}{1-\rho}\sqrt{\frac{3\rho-2}{3}}\right] + \frac{\alpha^2\kappa}{Eh\sqrt{1-\rho}}\left[\sqrt{\frac{1}{3(1-\rho)}} - 1\right] - \frac{q\alpha^4}{96Ebh^3}\cdot\frac{9\rho^2-4}{(1-\rho)^2} \tag{G-70}$$

Applying the definition of α, from eq. (G-40) and multiplying q_0 and dividing by itself or the definition of q_0, from eq. (G-27) gives

$$W_0 = \frac{\cancel{3}}{16}\frac{q}{Ebh^3}\frac{5a^4}{\cancel{3}\cdot 2}\overbrace{\frac{q_0}{q_0}}^{1} + \overbrace{\frac{a\sqrt{\cancel{1-\rho}}}{\sqrt{\rho}}}^{\alpha}\cdot\frac{a}{Eh\sqrt{\cancel{1-\rho}}}\left[\cancel{\kappa}\cdot\overbrace{\frac{q_0}{4\sqrt{3}\cancel{\kappa}b}}^{1}\sinh^{-1}\sqrt{\frac{3\rho-2}{3(1-\rho)}}\right.$$
$$\left. - \frac{1}{12}\frac{q}{bh^2}\cdot\underbrace{\frac{\alpha^2}{\frac{a^2(1-\rho)}{\rho}}}\cdot\underbrace{\frac{q_0}{q_0}}_{1}\frac{3\rho+1}{1-\rho}\sqrt{\frac{3\rho-2}{3}}\right]$$
$$- \frac{\cancel{\kappa}}{Eh\sqrt{1-\rho}}\underbrace{\frac{\alpha^2}{\frac{a^2(1-\rho)}{\rho}}}\cdot\underbrace{\frac{q_0}{4\sqrt{3}\cancel{\kappa}b}}_{1}\cdot\left[\sqrt{\frac{1}{3(1-\rho)}} - 1\right]$$
$$+ \frac{q}{96Ebh^3}\cdot\underbrace{\frac{q_0}{q_0}}_{1}\cdot\underbrace{\frac{\alpha^4}{\frac{a^4\cancel{(1-\rho)^2}}{\rho^2}}}\cdot\frac{9\rho^2-4}{\cancel{(1-\rho)^2}} \tag{G-71}$$

where from the definition of ρ (in eq. G-27) and algebraic manipulation:

$$W_0 = \frac{5}{32}\overbrace{\frac{q}{q_0}\left(\frac{a}{h}\right)^2}^{\rho}\frac{a^2}{Ebh}q_0 + \frac{a^2}{Eh\sqrt{\rho}}\frac{q_0}{4\sqrt{3}}\sinh^{-1}\sqrt{\frac{3\rho-2}{3(1-\rho)}} - \frac{1}{12Ebh}\underbrace{\frac{q}{q_0}\left(\frac{a}{h}\right)^2}_{\rho}\frac{1}{\sqrt{\rho}}\frac{a^2\cancel{(1-\rho)}}{\rho}q_0\frac{3\rho+1}{\cancel{(1-\rho)}}\sqrt{\frac{3\rho-2}{3}} - \frac{q_0}{4Eh}\frac{a^2\cancel{(1-\rho)}}{\rho}\left(\sqrt{\frac{1}{3\cancel{(1-\rho)}}}\right)^2 + \frac{q_0}{Eh4\sqrt{3}\sqrt{1-\rho}}\frac{a^2(1-\rho)}{\rho} + \underbrace{\frac{q}{q_0}\left(\frac{a}{h}\right)^2}_{\not{\rho}}\frac{a^2q_0}{96Ebh}\frac{9\rho^2-4}{\rho^{\not{2}}} \quad \text{(G-72)}$$

so,

$$W_0 = \frac{a^2q_0}{Ebh}\cdot\frac{5}{32}\rho + \frac{a^2q_0}{Ebh}\cdot\frac{1}{4\sqrt{3\rho}}\cdot\sinh^{-1}\sqrt{\frac{3\rho-2}{3(1-\rho)}} - \frac{a^2q_0}{Ebh}\cdot\sqrt{\rho}\cdot\cancel{\sqrt{\rho}}\cdot\frac{3\rho+1}{12\rho\cancel{\sqrt{\rho}}}\sqrt{\frac{3\rho-2}{3}} - \frac{a^2q_0}{Ebh}\cdot\frac{1}{12\rho} + \frac{a^2q_0}{Ebh}\cdot\frac{\sqrt{1-\rho}}{4\sqrt{3}\rho} + \frac{a^2q_0}{Ebh}\cdot\frac{9\rho^2-4}{96\rho} \quad \text{(G-73)}$$

Rearranging

$$W_0 = \frac{a^2q_0}{Ebh}\overbrace{\left[\frac{5}{32}\rho - \frac{1}{12\rho} + \frac{9\rho^2-4}{96\rho}\right]}^{\frac{2\rho^2-1}{8}} + \frac{a^2q_0}{Ebh}\cdot\frac{1}{4\sqrt{3\rho}}\cdot\sinh^{-1}\sqrt{\frac{3\rho-2}{3(1-\rho)}} + \frac{a^2q_0}{Ebh}\cdot\frac{\sqrt{1-\rho}}{4\sqrt{3}\rho} - \frac{a^2q_0}{Ebh}\cdot\frac{3\rho+1}{12\rho}\sqrt{\frac{\rho(3\rho-2)}{3}} \quad \text{(G-74)}$$

As a result, W_0 can be defined as

$$W_0 = \frac{a^2q_0}{Ebh}\left[\frac{1}{4\sqrt{3\rho}}\cdot\sinh^{-1}\sqrt{\frac{3\rho-2}{3(1-\rho)}} + \frac{\sqrt{1-\rho}}{4\sqrt{3}\rho} + \frac{2\rho^2-1}{8} - \frac{3\rho+1}{12\rho}\sqrt{\frac{\rho(3\rho-2)}{3}}\right] \quad \text{(G-75)}$$

Equation in above presents the analytical solution for the deflection of the beam on his center. For considering the full x axis domain eq. (G-54) must be use for the elastoplastic regime where $0 \leqslant x \leqslant x^*$ and eq. (G-68) for the elastic regime with $x^* \leqslant x \leqslant a$.

G.2
Multilinear isotropic hardening plasticity under a bar with axial load

In this section, a bar under axial load and unload is performed using elastoplastic simulation with multilinear isotropic hardening. Since this problem can only be solved numerically, the commercial software *Abaqus* is used as a reference.

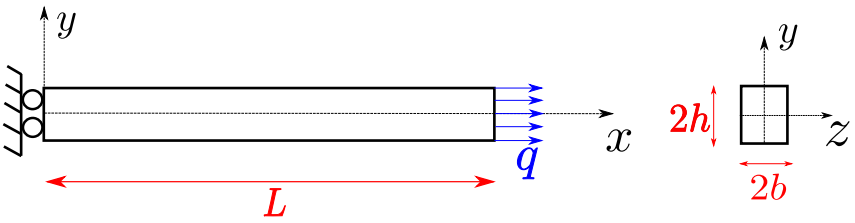

In plasticity, the unload is quite different from the load and requires additional features in the FEM algorithm. To verify residual plastic strain in the problem a variable load q is assumed as expressed in graph G.20.

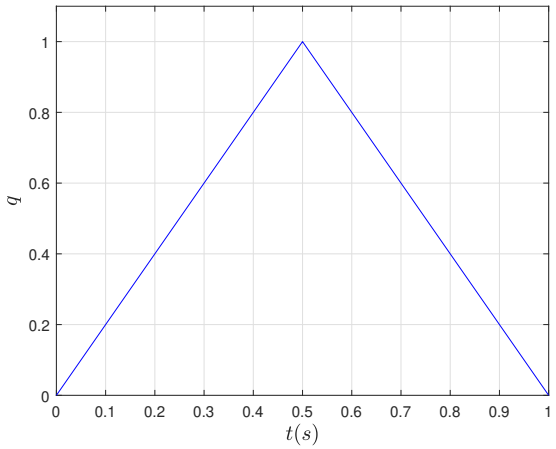

Figure G.20: Variable axial load as function of time

For modeling strain hardening, the yield stress is defined as a function of the total strain ϵ^p as

$$\sigma_y = H_0 + H_1 \cdot \epsilon^p + (H_\infty - H_0) \cdot (1 - \exp(-b \cdot \epsilon^p)) \qquad \text{(G-76)}$$

In this simulation, the geometric, material and load condition is presented in the table below

Parameters		
Parameter	**Value**	**Unit**
Young's Modulus (E)	$210 \cdot 10^9$	Pa

Continuation of table G.1

Parameters		
Yield stress (σ_y)	$300 \cdot 10^6$	Pa
H_0	$300 \cdot 10^6$	Pa
H_1	$30 \cdot 10^9$	Pa
H_∞	$390 \cdot 10^6$	Pa
b	$2 \cdot 10^3$	-
q	$500 \cdot 10^6$	Pa/m^2
b	0.5	m
h	0.5	m
a	10	m

Table G.1: Material, geometric and load parameters for the bar under axial load simulation

Usually, in an elastoplastic FEM problem, the input of the strain curve is not a function of the total strain ϵ, but a function of the plastic strain ϵ^p, case of TopSim and *Abaqus*, making the use of eq. (G-76) convenient since is a function of the plastic strain. For this problem, the curve below presents the points used as input in the simulation.

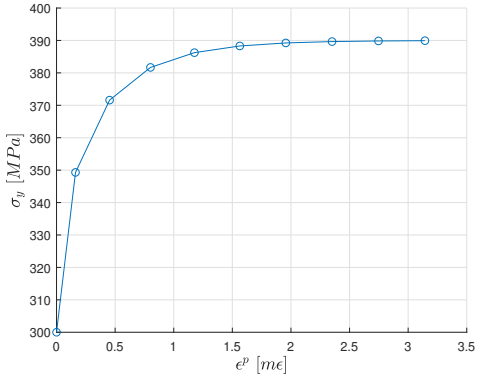

Figure G.21: Yield stress vs. plastic strain

For this simulation the element Brick with 8 nodes is adopted, where the mesh is illustrated in the figure below

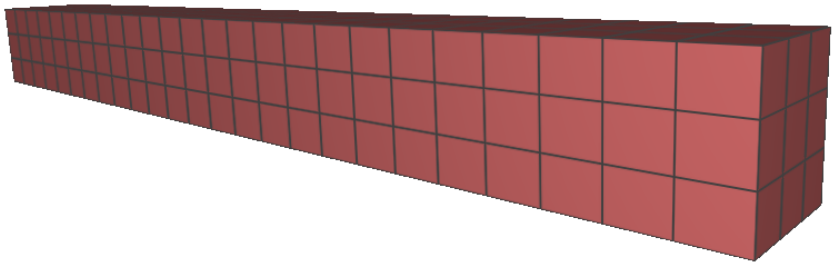

Figure G.22: Mesh of the bar

Due to symmetry, all points in FEM model's domain are subjected to the same history of load. As a consequence, any path plot in the domain remains constant, alternatively figs. G.23 to G.26 presents the value of the stress and strain field of a random gauss point in the model using TopSim simulator. Similarly, figs. G.27 to G.30 also shows the stress and strain field provided by *Abaqus*.

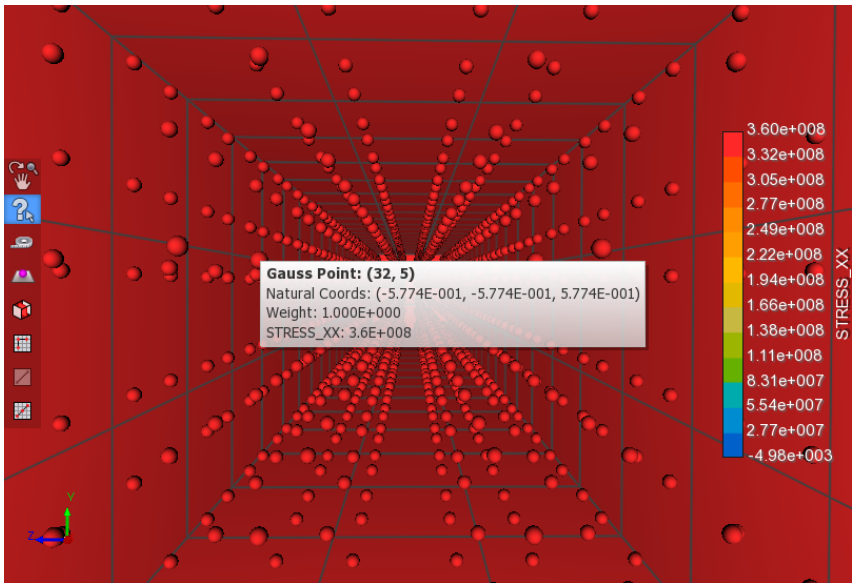

Figure G.23: σ_{xx} field at time $t = 0.5$ in the cross section of the bar from TopSim

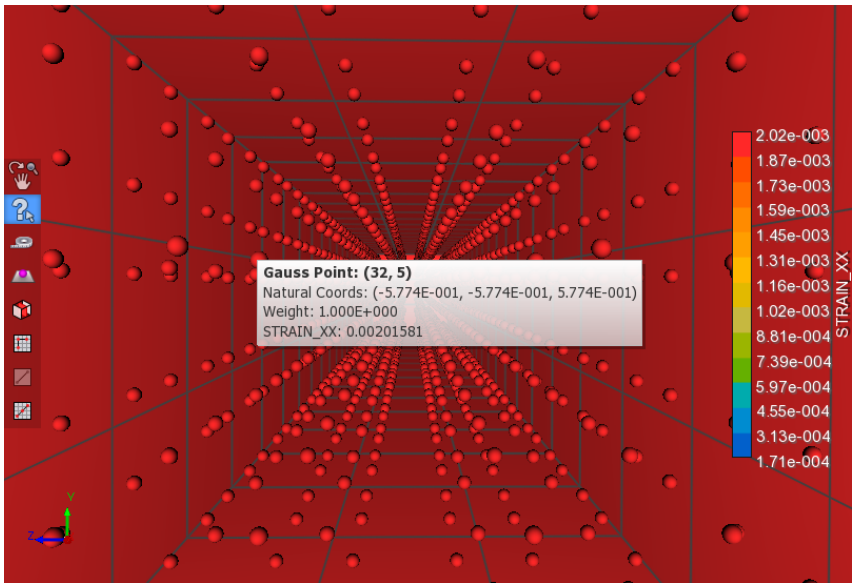

Figure G.24: ϵ_{xx} field at time $t = 0.5$ in the cross section of the bar from TopSim

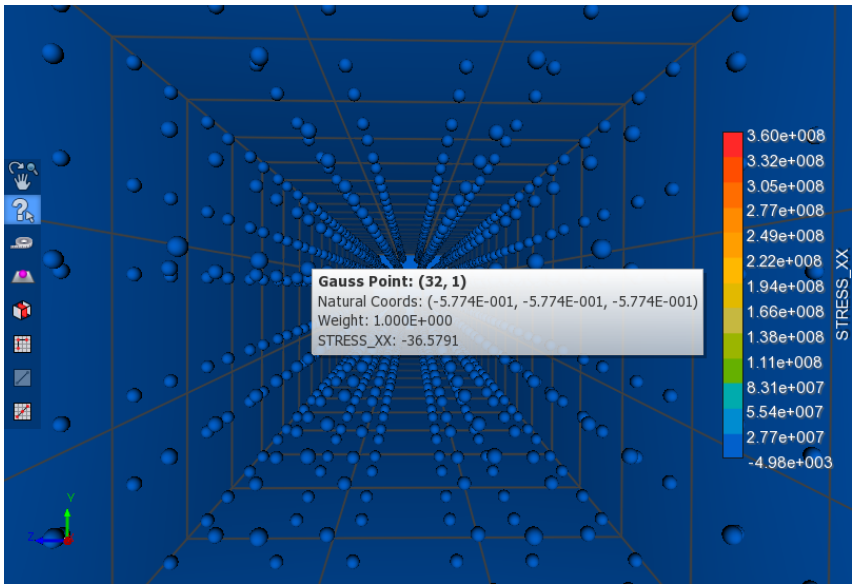

Figure G.25: σ_{xx} field at time $t = 1.0$ in the cross section of the bar from TopSim

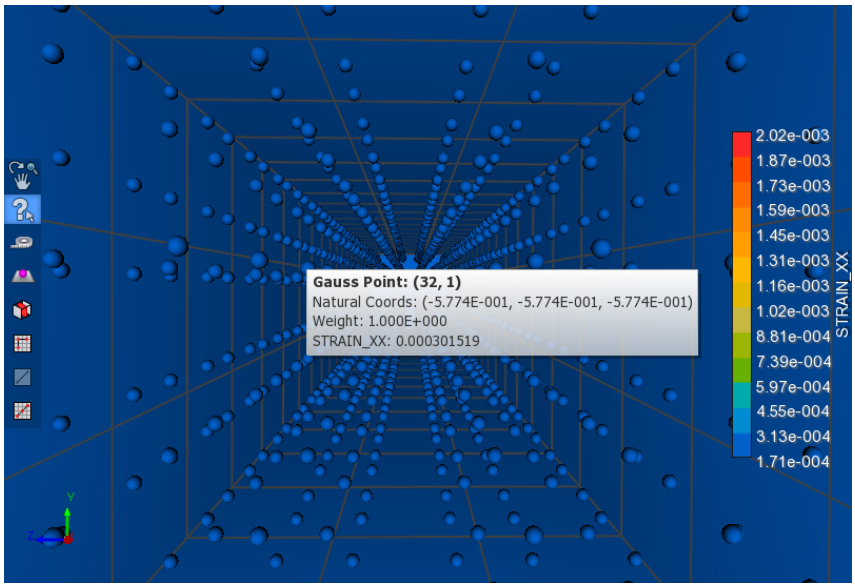

Figure G.26: ϵ_{xx} field at time $t = 1.0$ in the cross section of the bar from TopSim

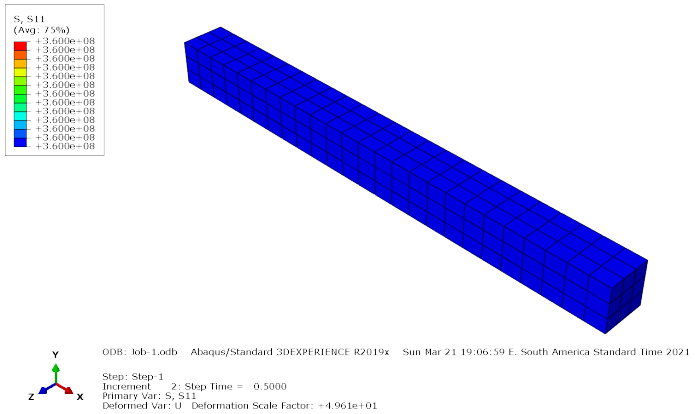

Figure G.27: σ_{xx} field at time $t = 0.5$ in the cross section of the bar from *Abaqus*

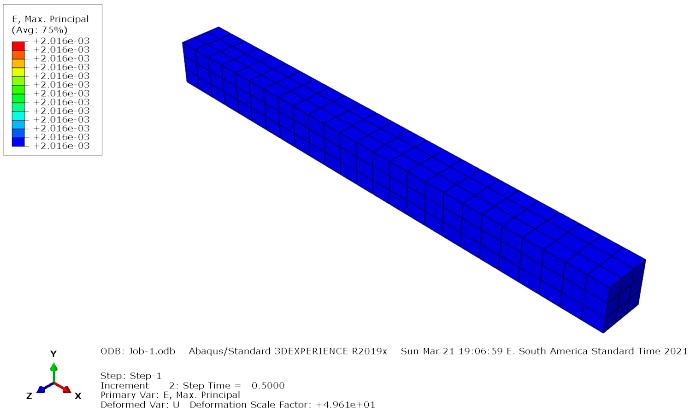

Figure G.28: ϵ_{xx} field at time $t = 0.5$ in the cross section of the bar from *Abaqus*

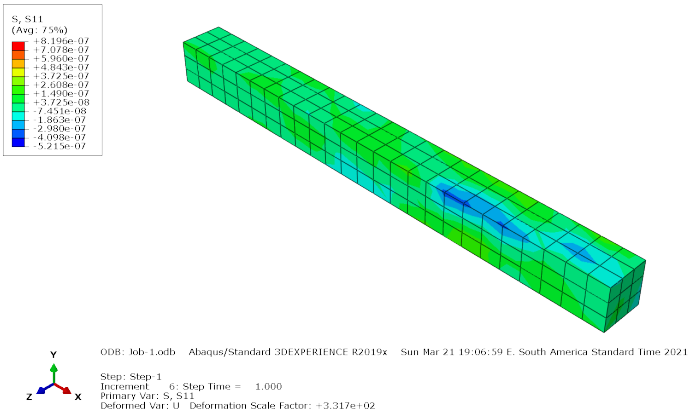

Figure G.29: σ_{xx} field at time $t = 1.0$ in the cross section of the bar from *Abaqus*

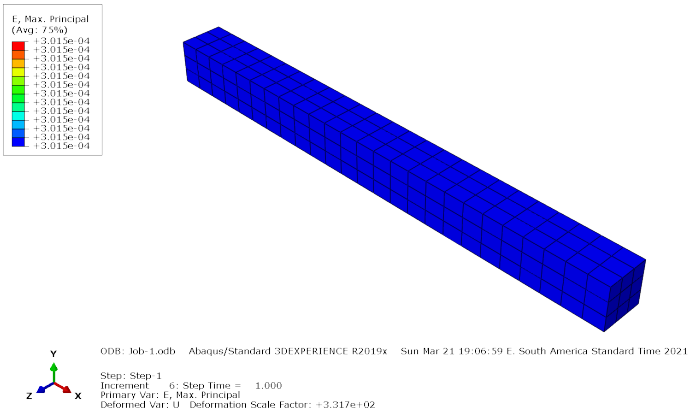

Figure G.30: ϵ_{xx} field at time $t = 1.0$ in the cross section of the bar from *Abaqus*

From the previous figures above, TopSim prediction is numerically equal to *Abaqus* when comparing to load and unload condition.

G.3
Plate with centered hole

In this section, a numerical elastoplastic solution for a centered hole plate is presented. In this case, there is no analytical procedure for comparison, alternatively, the commercial software *Abaqus* is used as reference.

Figure G.31 above illustrate the geometric, load and boundary condition imposed in the following problem.

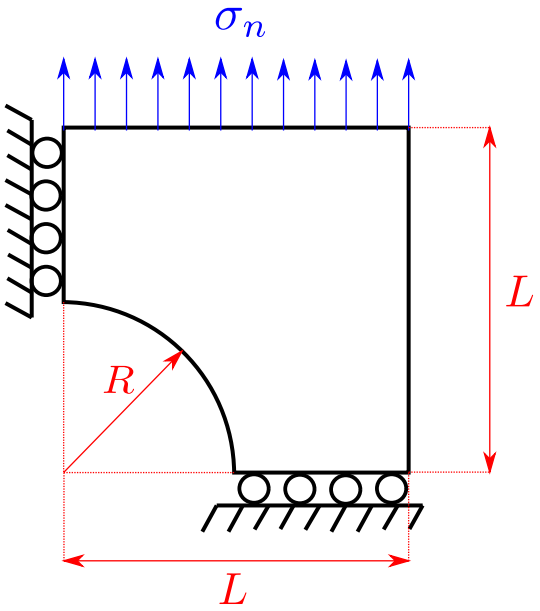

Figure G.31: Geometric dimensions and boundary conditions

For the strain hardening, the yield stress is defined as a function of the total strain ϵ^p as

$$\sigma_y = H_0 + H_1 \cdot \epsilon^p + (H_\infty - H_0) \cdot (1 - \exp(-b \cdot \epsilon^p)) \qquad \text{(G-77)}$$

where the numerical value considered in this problem is presented in the table above:

Parameters		
Parameter	**Value**	**Unit**
Nominal stress (σ_n)	$100 \cdot 10^6$	Pa
Young's Modulus (E)	$210 \cdot 10^9$	Pa
Yield stress (σ_y)	$300 \cdot 10^6$	Pa
α	$0.02 \cdot 10^9$	Pa
n	13	–
Radius (R)	0.25	m

Continuation of table G.2

Parameters		
Length (L)	0.5	m
Thickness (t)	0.1	m

Table G.2: Material, geometric and load parameters for the centered hole simulation

For the FEM, the element Brick of 8 nodes is adopted for this simulation, which the mesh used is presented in the figure G.32 below.

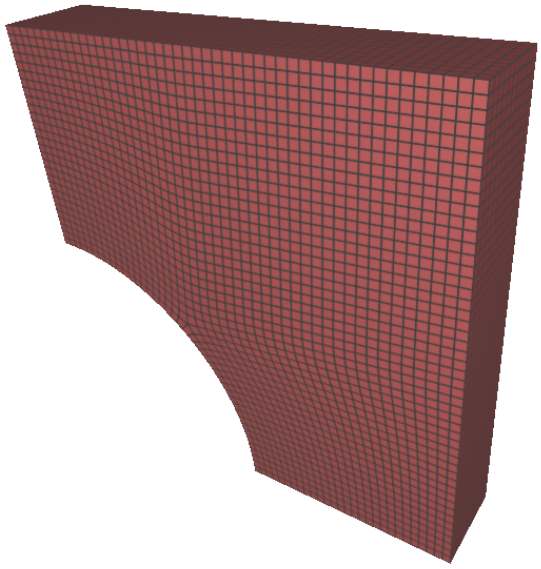

Figure G.32: Mesh for centered hole in a plate

For the comparison between TopSim and *Abaqus*, two paths were added in the Pos-processor for obtaining the stress distribution. The figure below presents path 1 and 2, as well as the local coordinate system used in which of them.

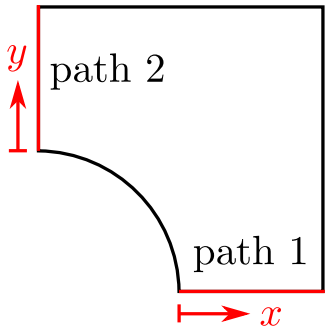

Figure G.33: Coordinates of path 1 and 2

Figure G.34, presents the distribution of stress σ_{yy} in path 1.

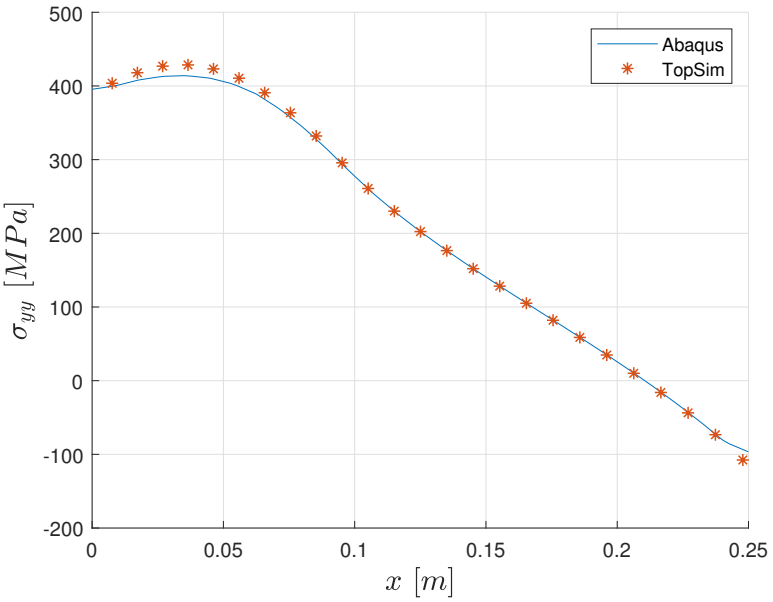

Figure G.34: σ_{yy} comparison in path 1

while, in the case of the stress σ_{xx} along path 2 we have

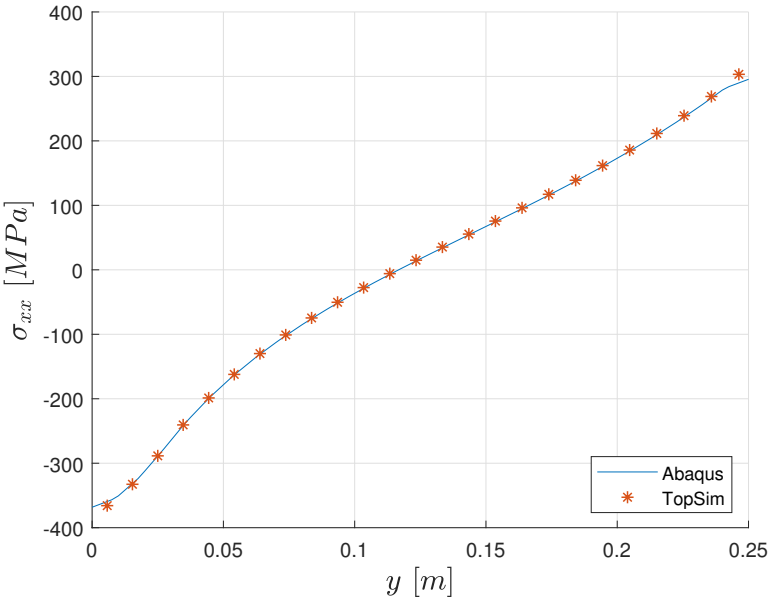

Figure G.35: σ_{xx} comparison in path 2

From both graphs, we can infer the TopSim is compatible with the prediction from *Abaqus*, since the distribution in graphs G.34 and G.35 are quite similar.

H
Table of SIF

H.1
Infinite plate with a crack of size $2a$ perpendicular to the normal stress σ (mode I), analytical solution [16]

$$K_I = \sigma \sqrt{\pi a} \tag{H-1}$$

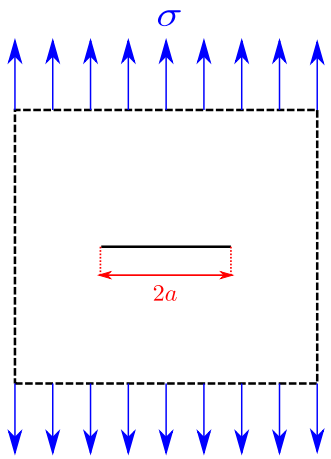

Figure H.1: Infinite plate with a crack of size $2a$ perpendicular to the normal stress σ (mode I), analytical solution [16]

I
Table of J integral

I.1
Tensioned bar with a central crack, plane-σ, [22]

$$J_{pl} = \frac{a(w-a)}{wH^{1/h}} \left(\frac{PS_Y}{P_0} \right)^{\frac{1+h}{h}} h_1 \tag{I-1}$$

$$V_{pl} = a \left(\frac{S_Y}{H} \frac{P}{P_0} \right)^{\frac{1}{h}} h_2 \tag{I-2}$$

$$\Delta_{pl} = a \left(\frac{S_Y}{H} \frac{P}{P_0} \right)^{\frac{1}{h}} h_3 \tag{I-3}$$

$$P_0 = 2t(w-a)S_Y \tag{I-4}$$

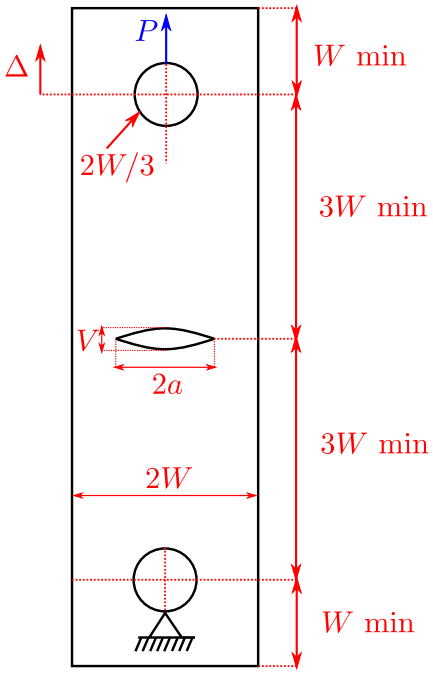

Figure I.1: Tensioned bar with a central crack, plane-σ, [22]

		h							
pl-σ	a/w	0.500	0.333	0.200	0.143	0.100	0.077	0.063	0.050
	0.125	3.57	4.01	4.47	4.65	4.62	4.41	4.13	3.72
	0.250	2.97	3.14	3.20	3.11	2.86	2.65	2.47	2.20
	0.375	2.53	2.52	2.35	2.17	1.95	1.77	1.61	1.43
h_1	0.500	2.20	2.06	1.81	1.63	1.43	1.30	1.17	1.00
	0.625	1.91	1.69	1.41	1.22	1.01	0.853	0.712	0.573
	0.750	1.71	1.46	1.21	1.08	0.867	0.745	0.646	0.532
	0.875	1.57	1.31	1.08	0.972	0.862	0.778	0.715	0.630
	0.125	4.09	4.43	4.74	4.79	4.63	4.33	4.00	3.55
	0.250	3.29	3.30	3.15	2.93	2.56	2.29	2.08	1.81
	0.375	2.62	2.41	2.03	1.75	1.47	1.28	1.13	0.988
h_2	0.500	2.01	1.70	1.30	1.07	0.871	0.757	0.666	0.557
	0.625	1.46	1.13	0.785	0.617	0.474	0.383	0.313	0.256
	0.750	0.970	0.685	0.452	0.361	0.262	0.216	0.183	0.148
	0.875	0.485	0.310	0.196	0.157	0.127	0.109	0.0971	0.0842
	0.125	0.661	0.997	1.55	2.05	2.56	2.83	2.95	2.92
	0.250	1.01	1.35	1.83	2.08	2.19	2.12	2.01	1.79
	0.375	1.20	1.43	1.59	1.57	1.43	1.27	1.13	0.994
h_3	0.500	1.19	1.26	1.18	1.04	0.867	0.758	0.668	0.560
	0.625	1.05	0.970	0.763	0.620	0.478	0.386	0.318	0.273
	0.750	0.802	0.642	0.450	0.361	0.263	0.216	0.183	0.149
	0.875	0.452	0.313	0.198	0.157	0.127	0.109	0.0973	0.0842

J
Coupling

In this appendix, the coupling between two body with different Young's Modulus will be studied. Let's consider two bodies are bonded under x and y direction loadings in a rigid plate connected to the material. The picture bellow illustrates the problem.

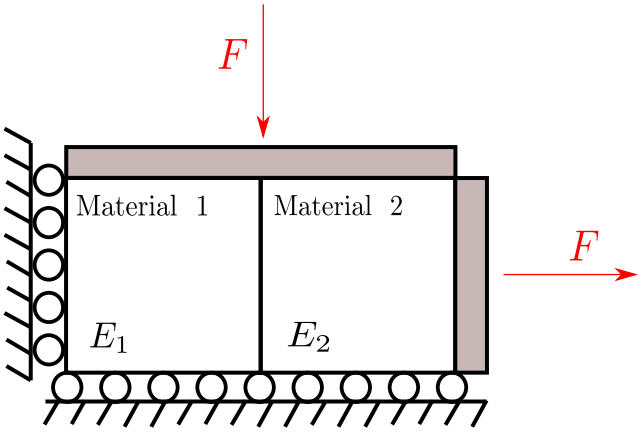

Figure J.1: Coupling problem

To solve the problem, let's expose internal forces by doing the free-body-diagram (FBD) in body 1:

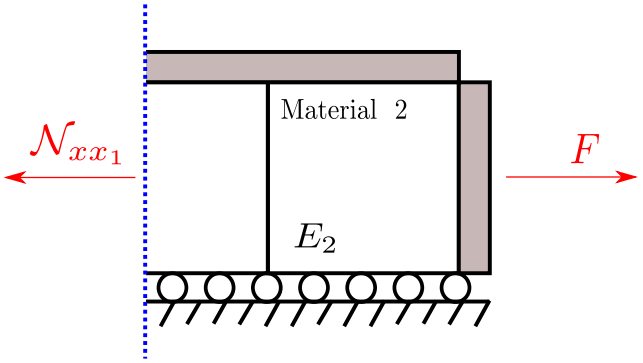

Figure J.2: FBD on material 1

From applying the resultant in y-direction equal to zero:

$$\sigma_{yy_1} = \frac{F}{A} \tag{J-1}$$

analogously, for body 2:

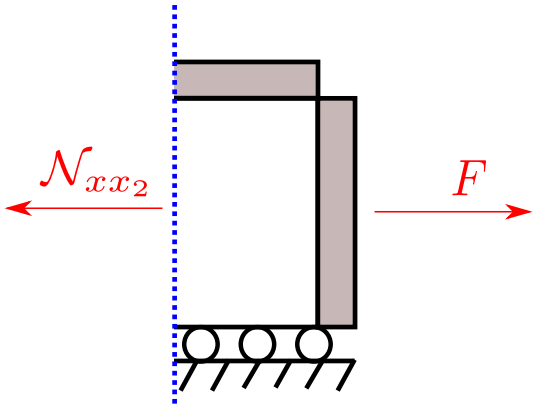

Figure J.3: FBD on material 2

$$\sigma_{yy_2} = \frac{F}{A} \tag{J-2}$$

Strain in y-direction is given by:

$$\epsilon_{yy} = \frac{\sigma_{yy}}{E} - \frac{\nu}{E}\sigma_{xx} - \frac{\nu}{E}\sigma_{zz} \tag{J-3}$$

so, for body number 1:

$$\epsilon_{yy_1} = \frac{\sigma_{yy_1}}{E_1} - \frac{\nu}{E_1}\sigma_{xx_1} \tag{J-4}$$

so, for body number 2:

$$\epsilon_{yy_2} = \frac{\sigma_{yy_2}}{E_2} - \frac{\nu}{E_2}\sigma_{xx_2} \tag{J-5}$$

Next step is critical to understand why coupling occurs. When applying the compatibility condition

$$\epsilon_{yy_1} = \epsilon_{yy_2} \tag{J-6}$$

$$\frac{\sigma_{yy_1}}{E_1} = \frac{\sigma_{yy_2}}{E_2} \tag{J-7}$$

Considering the free-body-diagram (FBD) in y-direction:

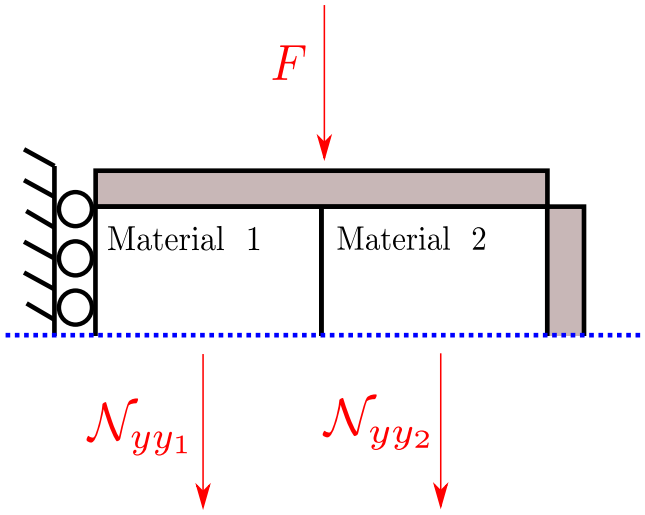

Figure J.4: FBD on material 1 and 2

$$F + \sigma_{yy_1} \cdot A + \sigma_{yy_2} \cdot A = 0 \tag{J-8}$$

substituting the result from eq. (J-7) into equation in above

$$\sigma_{yy_1} = \frac{F}{A\left(1 + \frac{E_2}{E_1}\right)} \tag{J-9}$$

Considering a elastic problem the relation between stress and strain in y-direction is linear, so:

$$\begin{aligned} \sigma_{yy_1} &= E_{y_1} \cdot \epsilon_{yy_1} \\ &= E_{y_1} \cdot \left(\frac{\sigma_{yy_1}}{E_1} - \frac{\nu}{E_1}\sigma_{xx_1}\right) \\ &= E_{y_1} \cdot \left(\frac{1}{E_1}\frac{F}{A\left(1 + \frac{E_2}{E_1}\right)} - \frac{\nu}{E_1}\frac{F}{A}\right) \\ &= E_{y_1} \cdot \frac{F}{E_1 A}\left(\frac{1}{1 + \frac{E_2}{E_1}} - \nu\right) \end{aligned} \tag{J-10}$$

$$E_{y_1} = \frac{\sigma_{yy_1}}{\frac{F}{E_1 A}\left(\frac{1}{1+\frac{E_2}{E_1}} - \nu\right)} \tag{J-11}$$

The equation above shows that relation between σ_{yy_1} and ϵ_{yy_1}, given by E_{y1} is dependable in both material properties (E_1 and E_2).